DEVELOPING A FOREST GAP MODEL TO BE APPLIED TO A WATERSHED-SCALED LANDSCAPE IN THE CROSS TIMBERS ECOREGION USING A TOPOGRAPHIC WETNESS INDEX

Heinrich Goetz, B.S., M.S.

Dissertation Prepared for the Degree of

DOCTOR OF PHILOSOPHY

UNIVERSITY OF NORTH TEXAS

August 2014

APPROVED:

Miguel Acevedo, Major Professor
Pinliang Dong, Committee Member
Paul Hudak, Committee Member
Feifei Pan, Committee Member
Sam Atkinson, Committee Member and Chair of the Department of Biological Sciences
Mark Wardell, Dean of Toulouse Graduate School

Goetz, Heinrich. *Developing a Forest Gap Model to be Applied to a Watershed-Scaled Landscape in the Cross Timbers Ecoregion Using a Topographic Wetness Index*. Doctor of Philosophy (Environmental Science), August 2014, 325 pp., 26 tables, 98 figures, references, 89 titles.

A method was developed for extending a fine-scaled forest gap model to a watershed-scaled landscape, using the Eastern Cross Timbers ecoregion as a case study for the method. A topographic wetness index calculated from digital elevation data was used as a measure of hydrologic across the modeled landscape, and the gap model modified to have with a topographically-based hydrologic input parameter. The model was parameterized by terrain type units that were defined using combinations of USDA soil series and classes of the topographic wetness index.

A number of issues regarding the sources, grid resolutions, and processing methods of the digital elevation data are addressed in this application of the topographic wetness index. Three different grid sizes, 5, 10, and 29 meter, from both LiDAR-derived and contour-derived elevation grids were used, and the grids were processed using both single-directional flow algorithm and bi-directional flow algorithm. The result of these different grids were compared and analyzed in context of their application in defining terrain types for the forest gap model.

Refinements were made in the timescale of gap model's weather model, converting it into a daily weather generator, in order to incorporate the effects of the new topographic/hydrologic input parameter. The precipitation model was converted to use a Markov model to initiate a sequence of wet and dry days for each month, and then daily precipitation amounts were determined using a gamma distribution. The output of the

new precipitation model was analyzed and compared with a 100-year history of daily weather records at daily, monthly, and annual timescales.

Model assumptions and requirements for biological parameters were thoroughly investigated and questioned. Often these biological parameters are based on little more than assumptions and intuition. An effort to base as many of the model's biological parameters on measured data was made, including a new technique for estimating optimal volumetric growth rate by measuring tree rings. The gap model was set up to simulate various terrain types within the landscape.

ACKNOWLEDGEMENTS

There are many people without whose help I would never have been able to complete this endeavor. I would like to express my deepest appreciation and thanks to Dr. Miguel Acevedo, my major professor and committee chair, for all of his help and the many hours of work he put into writing FACETA code. His extreme patience and understanding in helping me complete this project are unprecedented in my experience. I also would like to thank my committee members for all of their help, understanding, recommendations and suggestions. Thanks to Dr. Pinliang Dong for helping me learn to use GIS, and to Dr. Feifei Pan for increasing my understanding of soil water hydrology, to Dr. Paul Hudak for great classes in environmental geology and groundwater hydrology and all his support through the Geography Department, and thanks to Dr. Sam Atkinson for his help not only as a committee member but also his crucial assistance through his roles as Director of the Institute of Applied Sciences and Chair of the Biology Department. I would also like to thank the many other faculty and staff from the Institute of Applied Sciences for their knowledge and assistance over the years. A special thank you to Dr. Rajan Rijal for his help and use of his Greenbelt field survey data, and to Dr. Wilfredo Franco for teaching me about floodplain forest development and forest surveying methods. Lastly, thank you to my friends and family whose support was unwavering and absolutely essential.

TABLE OF CONTENTS

Page

LIST OF TABLES

Page

LIST OF FIGURES

Page

CHAPTER 1

INTRODUCTION

Tree growth depends on a variety of organism, population, ecosystem, and landscape-level factors. Height, leaf area, competition, light availability, soil nutrients, and soil moisture all affect a tree's growth. Soil nutrient and moisture levels vary with topographic position and the soil's physical properties, which are shaped by the underlying geology and surrounding conditions. Water, sediments, and nutrients move through a watershed along a topographic gradient. Slope and its aspect also impact available solar radiation intensity. In other words, landscape factors such as geologic features and topography affect the spatial distribution of the resources necessary for tree growth. Other landscape factors such as surrounding land cover and forest fragmentation can affect seed dispersal, soil erosion, and surface water runoff. Disturbances such as wildfire, flooding, and stress due to wind occur at landscape scales and affect landscape features.

Many environmental problems impact larger areas covering landscape, regional, and even global scales. Understanding ecological processes at a wide range of spatial scales is important in addressing many of these problems. Ecosystem management, conservation programs, and predicting impacts of environmental stressors are all goals and activities that currently use and can further benefit from environmental models. Achieving this over landscape-scaled areas requires developing broad-scale models that are ecologically relevant. One limitation of developing such models is that much of our knowledge base is fine-scale (Urban, Acevedo, & Garman, 1999). For example, plant physiology has developed a good understanding of how individual trees grow and

respond to environmental factors. As a result, there are many forest models based on the dynamics of individual trees and the understood eco-physiological processes of the tree species present. The extent of the scale of such models is typically an aggregate of a statistically relevant number of plots sized according to the crown area of the largest trees. At larger, landscape-level scales, vegetation is often simulated through abstractions such as plant functional types and land cover types, with dynamics often based on transition probabilities from one land cover type to another. Models from different scales are typically not based on the same empirical data, and often are not even based on the same concept of how plants respond to physical and environmental conditions (Urban et al., 1999). Gap models are a category of spatially fine-scaled forest models that simulate the growth and development of a stand of trees. The term *gap* refers to a canopy gap, such as would occur after a large tree in the forest fell. The earliest forest gap model called JABOWA was developed in the late 1960s, and it has since been modified and extended to accommodate for a range of vegetation modeling applications (Bugmann, 2001; Shugart, 2002). Gap models simulate individual trees from birth to death based on the understood properties of different tree species and competition among individuals for light, water, and nutrients. Weather and soil moisture in gap models are typically simulated on monthly time scales, and tree growth is calculated in annual increments as a function of a growing season's worth of monthly conditions. Model parameters used to define different species' responses to environmental conditions and competition, while ideally based on quantitative measurements, are often based on known relative differences between the species, or

on assumptions and intuition. Gap models were originally designed to simulate small, isolated stands of trees on physiographically homogeneous plots.

This research provides a close examination of the development of a high fidelity forest gap model for the Cross Timbers ecoregion and investigates an approach to extend the plot-scaled forest model to a watershed-scaled landscape. The idea is to take a model that simulates forest growth on homogeneous plots based on the physiological responses of individual trees, improve the fidelity of the model's biological parameters and its hydrological components, and develop a method to extend that model across a landscape with heterogeneous soil and topographical conditions, thereby linking through simulation the fine scale of an individual tree's growth responses to the broad scale of a forested landscape. The model selected for this purpose is a gap model derived from FACET, which is a descendant of JABOWA (Urban, 2000; Urban, Miller, Halpin, & Stephenson 2000). The new model, called FACETA, differs from its FACET predecessor by changing the temporal resolution of the soil moisture and weather simulations from monthly to daily time steps and by including annual soil moisture indices aggregated from daily moisture results.

Another change to FACETA is the introduction of a watershed-level input to simulate the hydrological effects of topography. More specifically, there are two topographic inputs with parameter values based on a topographic index that is calculated across the watershed. The index, often called the topographic wetness index (TWI) but also known by several different names and existing in a few different variants, combines the hydrologic run-on potential of the upstream catchment area together with the accumulation potential of the local slope. It is considered an index of hydrologic

similarity, and has been used in a variety of applications in hydrology, soil science, and plant ecology. FACETA has been adapted to use TWI as an input to simulate the spatially distributed effects of topography on hydrology within the modeled watershed.

Using the Cross Timbers ecoregion, or more completely the Cross Timbers and Prairies ecoregion, as a case study for this application of FACETA is a convenient choice as the University of North Texas is located in the Cross Timbers ecoregion. Additionally, the ecoregion has characteristics that make it a good study area for this extension of FACETA. There are three relatively distinct vegetation patterns within the Cross Timbers and Prairies ecoregion, and the physical properties that drive these differences are topography and soil. Upland areas with fine textured soils develop into grasslands, upland areas with coarse textured soils develop into post oak savannas and woodlands, and floodplains and areas along streams develop into hardwood forests with species composition similar to what is found in bottomlands throughout the Southeast. This mix reflects the fact that the Cross Timbers and Prairies is a transitional ecoregion between Southeastern deciduous forests and Midwestern prairies. Because the distinctive vegetation patterns within the Cross Timbers are linked so closely to the watershed-level differences in topographic position and soil type, the ecoregion offers a good case study to test FACETA's ability to simulate the vegetation differences resulting from these landscape characteristics.

A number of secondary research objectives are encompassed in the overall objective of developing a method to extend FACETA. These objectives can be grouped into three categories: landscape and terrain, modeling and simulation, and silvics. While

the categories overlap, it is useful to discuss the categories and the research questions related to each separately.

Landscape and terrain category of objectives starts with determining the landscape factors that are most relevant to vegetation dynamics in the study area. Broadly, these landscape factors are soil and topography, with the primary topographic factors being those that drive hydrological processes. A method for partitioning the modeled landscape into smaller terrain type units that are based on those landscape factors is developed, and the landscape is partitioned into model-ready units. The forest gap model is modified to incorporate a hydrological input from the landscape and terrain types, and the model parameters for the terrain types are estimated. A number of research questions are embedded into these objectives:

1. What topographic features, measurements, or indices that can be determined from elevation data can be used to represent hydrological characteristics in a forest gap model?

2. Do elevation data derived from different sources, for example contour-derived versus light detection and ranging (LiDAR) derived data, affect the topographic feature used to define terrain types, or the terrain type definitions and boundaries?

3. Does the spatial grid resolution of the elevation data affect the topographic feature used to define terrain types, or the terrain type definitions and boundaries?

4. Does using different elevation grid processing algorithms affect the topographic feature used to define terrain types, or the terrain type definitions and boundaries?

5. How do the soil-related components of the terrain types differ if taken from a broad-scaled source such as a USDA county soil survey compared with if they are measured directly from in the study area, and do these differences impact forest model output?

Objectives in the modeling and simulation category include implementing a number of changes to the gap model FACETA in order to simulate the differences in the terrain types. The driver behind all the model changes is the need to implement a mechanism for modeling the spatially distributed hydrological effect of topography without creating a full, spatially distributed hydrology model. The reasons for avoiding a spatially distributed hydrological modeling approach can be summed up as a desire to keep it as simple and generic as possible. The type of hydrological processes that drive vegetation patterns are very complex, and are linked as much or even more to subsurface water dynamics than surface water flow captured by traditional hydrological models. Soil moisture dynamics at the catchment level scale are such that changes occur at time scales of days rather than months, so increasing the fidelity of the soil-moisture component of the model and changing the temporal resolution from what had been monthly time steps to daily ones is another modeling objective. This then necessitates changing the temporal resolution of the weather simulation component of the model from monthly to daily time steps. Research questions addressing these objectives are:

1. Does the TWI represent hydrological similarity and differences well for a forest gap model?

2. Does the FACETA daily weather simulator capture daily, monthly, annual, and long-term weather and climate patterns of the modeled study area?

3. How does an increased temporal scale for soil moisture modeling contribute to a better implementation of tree and soil model relationships?

The silvics category of objectives primarily lies in developing a set of model parameters that are estimated as much as possible from quantitative measurements. One of the problems with any modeling of natural systems is that many aspects of the

modeled system may not be knowable or are not quantitatively measurable, so these aspects are approximated based on assumptions, intuition, or qualitative descriptions. A general goal of this research is to base FACETA's silvics components on quantitative measurements whenever possible, which requires making measurements of the geometry and growth characteristics of trees. In addition to the physical measurements made on trees, this category of objectives also often includes trying to bridge between physical measurements and the assumptions behind a model's parameters. Silvics research questions include:

1. What are the best approaches to estimating silvics model parameters, both ones that can be measured for directly and those that cannot?
2. How well do the tree measurements fit the model assumptions?
3. How can you successfully model tree responses to soil moisture conditions?

Soil and topographical inputs are used to define the model terrain types (Fig. 1.1). Research objectives contained within this group include developing a way to determine the terrain types from spatial elevation data, and investigating how different spatial resolutions and sources of that elevation data and different algorithms used to process that data impact the terrain types. Terrain type, biological, and climatic components are input into the gap model FACETA, which simulates forest growth. A number of research objectives are contained within these categories of model inputs and modeling. Specific model objectives include implementing changes to the temporal resolution for weather and soil moisture simulation, adding tree responses to daily moisture conditions, and implementing a way to simulate hydrologic similarity among terrain types. Estimating model parameters, investigating relationships between tree

measurements and model assumptions and parameters, and investigating differences in the model's soil parameters estimated from a coarse scale soil survey versus from local field measurement are all model input objectives. FACETA can then be used to generate simulated forest cover maps for selected terrain types within the watershed.

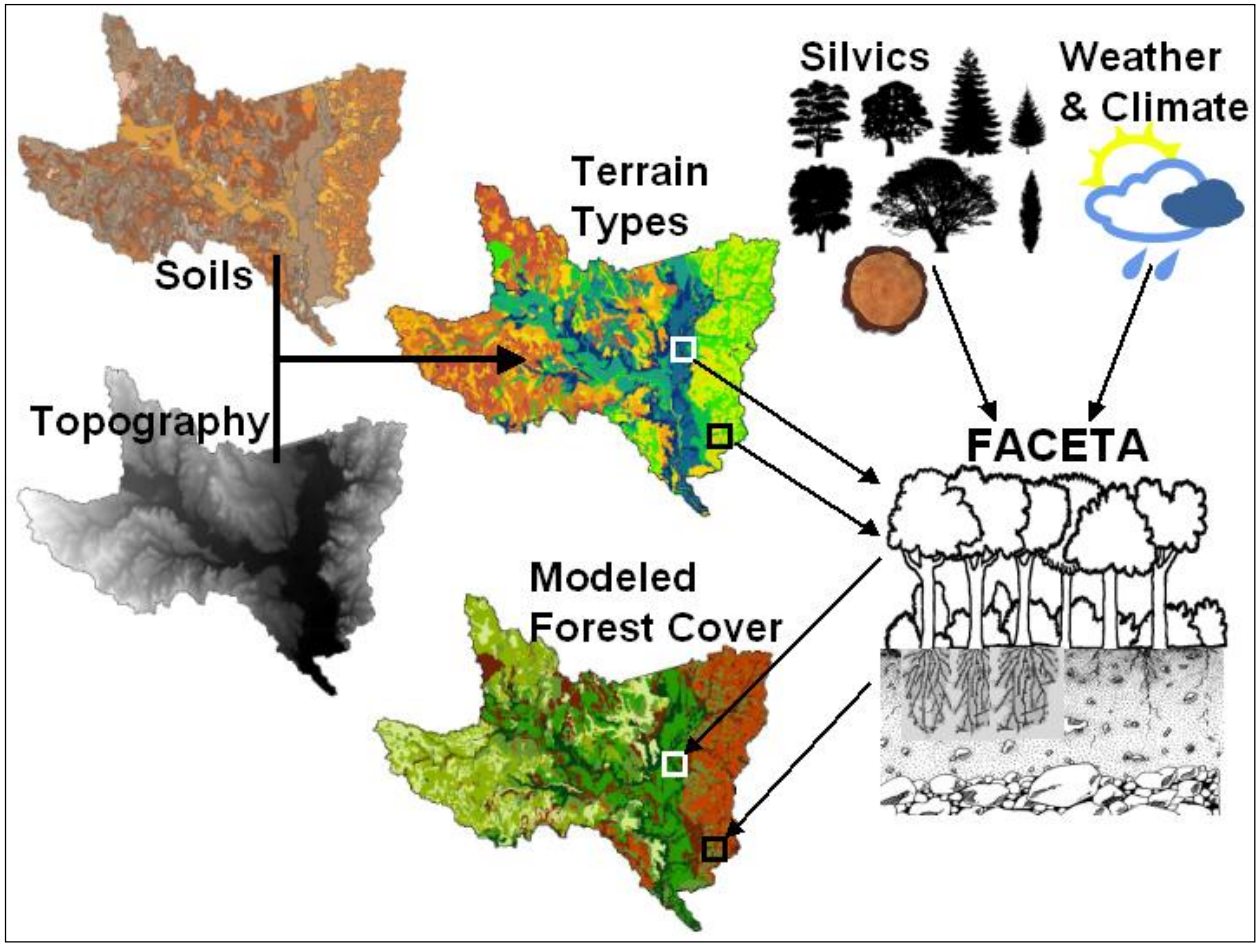

Figure 1.1. Research objectives conceptual flow. This figure provides a conceptual summary of the approach taken in this research. Starting at the top-left side of the figure and moving clockwise: Soil and topographical inputs define the model terrain types. Research objectives within these include developing a way to determine the terrain types from spatial elevation data, and investigating how different spatial resolutions and sources of that elevation data and different algorithms used to process that data impact the terrain types. Terrain type, biological, and climatic components are input into the gap model FACETA, which simulates forest growth. Research objectives within this group include implementing model changes to the temporal resolution for weather and soil moisture simulation, adding tree responses to daily moisture conditions, implementing a way to simulate hydrologic similarity among terrain types, estimating model parameters, investigating relationships between tree measurements and model assumptions and parameters, and investigating differences in model soil parameters estimated from a coarse scale soil survey versus local field measurement. FACETA is then used to generate simulated forest cover maps for different terrain types within the watershed.

This research approach contributes to the knowledge base in a number of different topics. The use of topographic indices is not new in ecological applications or even in context of gap models (Urban, 2000); however, FACETA may be the only example of using a topographic index as a hydrological input in a gap model. There are studies that examine the impact that various sources of digital elevation data, different grid resolutions, or grid processing algorithms have on topographical or hydrological interpretations made using the elevation data, and there are even some that examine the impact on ecological interpretations (Kopecký & Čížková, 2010). However, studies examining the impact these choices have on ecological interpretation are limited, and none examine it in context of a forest model.

Variability of soil conditions over relatively small spatial distances as well as the inaccuracies that can occur in interpreting a 1:24000 scale soil map and survey, too, literally are well known, but soil surveys are a common source of information and data for many applications including models such as FACETA. Measuring soil properties directly from samples taken in the field may be more accurate, but in most cases, it is too costly for determining soil model parameters for an entire watershed. This study looks at how big of a difference there can be in soil parameters for a gap model if estimated from a soil survey compared with parameters estimated from field samples, and whether those differences impact the output of the gap model.

Weather simulation is an important component of many modeling applications, from agricultural to impacts of climate change, and in most applications weather is simulated in daily time steps. However, there are some general problems with daily weather simulators. They often do not capture the real world year-to-year variability of

weather, and they have a tendency to capture the statistical properties of rainfall totals at temporal resolution–daily, monthly, or annual–but not the other two (Srikanthan & McMahon, 2001). The FACETA daily weather simulator compares real weather data for annual variability, statistical properties of rainfall totals at these different time steps, and the ability to simulate dry periods or floods.

Towards the objective of basing as many of the model's silvics parameters as possible on actual measurements rather than on qualitative descriptions and intuition, this research improves the understanding of the silvics of tree species native to the area, some of which are not commercially important or well studied. Specifically, this research highlights the use of tree ring data to improve the estimation of growth rate, which is a sensitive parameter that is difficult to measure directly.

In general, this research examines the structure and assumptions of a gap model, examines a method for scaling the gap model up to a watershed-level landscape, and provides a detailed map for developing a gap model for that landscape.

CHAPTER 2

LITERATURE REVIEW

Introduction

Landscape ecology takes a broad-scale, landscape approach to understanding problems in biology and ecology. Driven by a need to understand ecological and biological impacts of changes in the environment occurring across a range of spatial scales, landscape ecology is being applied to a rapidly growing number of topics and problems (Turner, Gardner, & O'Neill, 2001). Landscape ecology studies the effects of spatial configuration on ecological processes across landscapes, which typically cover spatial extents that are larger than what is usually focused on in ecology. Sanderson and Harris (2000) give a definition of a landscape simply as being two or more ecosystems in close proximity. Turner et al. (2001) define a landscape as “an area that is spatially heterogeneous in at least one factor of interest.” Forman and Godron (1986) require “a heterogeneous land area composed of a cluster of interacting ecosystems that is repeated in similar form throughout.” The notion of repeated spatial patterns is important for many definitions of landscape. Robert Ruhe, one of the first American geomorphologists to study soil-landscape processes at larger regional and watershed-sized scales, defines a landscape as a collection of spatially related landforms that usually can be seen in a single view (Grunwald, 2006; Ruhe, 1969). Haber (as cited in Farina, 2006) offers another visual perspective of a landscape as “a piece of land which we perceive comprehensively around us, without looking closely at single components, and which looks familiar to us.” These last two definitions rely on a view or visual perception of a landscape. Indeed, it is the perception of the organisms living within a

landscape that defines the extent of the landscape. While landscapes are generally thought of as being large geographic areas, the definition is not size dependent, and landscape ecological concepts can be applied to areas ranging in extent from meters to hundreds of kilometers. The scale used depends on the organisms and phenomenon of interest. As Wiens and Milne (1989) point out, a human perceives a much larger landscape than a beetle. If the phenomenon of interest is the dynamics of a forest stand, then an appropriate landscape extent from the *perception* of the stand must be considered. Landscapes are complex systems nested within larger systems, while at the same time composed of smaller subsystems (Farina, 2006). Landscapes have the fractal property of self-similarity of patterns that exist nested at different scales. It is therefore useful to consider landscapes through a hierarchical framework when trying to understand how components at different spatial and temporal scales interact with each other (Urban, O'Neill, & Shugart, 1987; Farina 2006).

Watersheds are also hierarchical systems, being composed of sub-basins that are composed of even smaller order sub-basins. While hydrologic sub-basins form a natural decomposition of a watershed, it can also be partitioned into a mosaic of different landforms, landscape positions, moisture regimes, plant communities, or soil types. The terms watershed and landscape are far from synonymous; e.g., the Mississippi River watershed contains many landscapes while the watershed of a small ephemeral stream may be only one of many features within a human-perceived landscape. However, the watersheds of many lower order streams have a spatial extent similar to what we often think of for landscapes. These landscape-sized watersheds come to mind from the description of a watershed given by the American geologist and

explorer, John Wesley Powell, as being "that area of land, a bounded hydrologic system, within which all living things are inextricably linked by their common water course and where, as humans settled, simple logic demanded that they become part of a community" (United States Environmental Protection Agency [US EPA], 2009). Forest stands within a watershed share resources, and these stands may interact with each other through processes such as seed dispersal (Urban et al., 1987). Therefore, an appropriate landscape extent to consider in understanding forest stand dynamics may be a watershed. Urban et al. describe four levels of forest hierarchy based on functional scale: gap, stand, watershed, and landscape. A gap is defined as the area covered by the crown of a large, canopy-dominant tree. At the gap level, individual trees interact frequently in competition for resources. Fine-scale disturbances such as a single tree falling can significantly affect other trees within the gap but not individuals outside of it. Gaps within a stand share similar but not identical characteristics, and while interactions such as the movement of water and seed dispersal occur among gaps within a stand, the interactions are not as frequent or significant as those within a gap are. Similarly, stands within a watershed interact through the movement of nutrients and seeds but not as frequently as the interaction between gaps within a stand. The watershed level contains many of the processes that affect vegetation distribution. However, some processes such as weather patterns, species movement, and disturbances such as fire may not be contained within a watershed and a larger landscape must be considered.

Forest Gap Models

Models of forest dynamics at the gap-sized scale have been developed and used for several decades. While the term *gap model* was not used until 1980, the first such

model, JABOWA, was developed for the Hubbard Brook Forest in 1969 (Botkin, Janak, & Wallis, 1972; Bugmann, 2001; Shugart 2002). Since then numerous gap models have been developed for other forests and conditions, and eventually for other ecosystems such as grasslands and savannas (Shugart, 2002). Forest gap models belong to a more general family of models called individual-based models (IBMs). As computing resources became more available to ecologists in the 1960s, a variety of models simulating the behavior of individual organisms has been developed. Some of the earliest applications of IBMs included studies of the effects of individual animal behavior within population models, and foresters interested in predicting timber yields from stands of trees. As the models developed, larger numbers of individuals started being simulated resulting in models of community interactions and ecosystem dynamics. Given that early forest IBMs were applied towards predicting timber yields, it is not surprising that they focused on individual tree size, the number of trees in the stand, and how the two relate. Understanding how the growth of individual trees relates to the number of trees within a stand had long been a focus in forestry, making the application of IBMs in understanding forest stand dynamics a somewhat natural development. The earliest forest IBMs were based on stand yield tables, which are tools that have long been used to predict yields in forestry. Yield tables are based on height and diameter growth data taken from study plots, and they are therefore calibrated to particular species growing in specific densities and growing conditions. This poses a problem when trying to apply a yield table calibrated to different soil conditions, stand densities, or species. A crucial difference between JABOWA and these earlier forest IBMs is that the growth of individual trees is simulated using a set of equations based on species-

specific growth properties and environmental tolerances, interactions between individuals in competition for resources, and environmental conditions of the stand. Growth of a tree is based on a growth equation that yields an optimum increment of diameter growth based on the current diameter. Optimal diameter growth is decremented using a set of equations that reduce the growth according to less than optimal environmental conditions or competition for resources. The growth equation is based on two assumptions: as a tree matures and grows, it adds leaf area, thus increasing its photosynthetic capacity and subsequently its growth rate; at the same time, the increased size of a tree requires more respiration and has higher maintenance costs, resulting in a decreased growth rate as the tree ages. While there are a number of different formulations for the growth equation, many adhere to these assumptions resulting in somewhat parabolic shapes with increasing growth rates during the first part of a tree's life, followed by decreasing growth as the tree ages. Both the growth equation and the equations that reduce the growth from optimum are parameterized according to species.

Many gap models originating from the original JABOWA model have stuck closely to the original structure, but others have also diverged from it (Shugart, 2002). The models have been applied to many different kinds of forests around the world in applications ranging from forest management to understanding the impacts of climate change. Some of the assumptions and simplifications contained in JABOWA that made simulating numerous individual trees of different ages and species possible at a time when computing capabilities were limited have also lead to some strongly criticized weaknesses (Bugmann, 2001). While these assumptions and simplifications continued

in many subsequent gap models, some more recent models have tried to address some of the weaknesses by eliminating assumptions, increasing complexity and fidelity of tree responses to environmental conditions and competition for resources, increasing fidelity of the environmental conditions, or developing spatial context and relationships both within and between plots. JABOWA was designed with the assumption that plots are horizontally homogenous and the locations of individual trees within the plot are not tracked, which results in the assumption that the crowns of all trees within the plot cover the entire area of the plot. This produces shading biases. An example is between two small trees that realistically would have little or even no interaction. Another assumption that produces a strong bias in shading relationships is that all of the leaf area exists in a single horizontal layer at the top of each tree, so a tree even a centimeter shorter than another tree will be completely underneath the taller tree. The problem of asymmetry in shading is addressed in Leemans and Prentice's (1989) FORSKA model, which introduced a cylindrical crown. Some other gap models have since adopted a cylindrical crown. The cylinder was first applied in conifer forests, but it has been used generically as the crown geometry for deciduous trees as well. Other geometries such as spheres could be used as a further refinement. The model SORTIE represents a greater refinement in modeling light competition by using a three-dimensional crown, modeling crown transmissivity, and by abandoning the horizontal homogeneity assumption and assigning locations for individual trees. Another one of JABOWA's original assumptions is that there are no interactions between modeled plots. This limitation was first addressed by Urban et al.'s (1999) model ZELIG, which incorporated some interactions between plots. For example, shading can occur across adjacent plots. ZELIG originally

used the two-dimensional disc crown geometry but later incorporated the cylindrical crown. A later version of ZELIG adjusted the climatic variables according to topographic position. First applied to mountainous terrain of the Pacific Northwest, slope, aspect, and elevation were used as the important topographic variables. A plot of homogeneous slope, aspect, and elevation is referred to as a slope facet, lending the name FACET to this terrain sensitive version of ZELIG. The gap model used in this research was modified from FACET, primarily by incorporating a refined time scale for the soil moisture and weather sub routines. The changes made to the existing FACET model were significant enough to warrant a new name: FACETA. Another valid criticism that has been made generally for gap models is that they often use fairly simple parameterizations rather than modeling the relevant physiological processes mechanistically (Bugmann, 2001). While a large amount of data exits for a few commercially important tree species, the data for high fidelity parameterization simply do not exist for most species important in modeling many forests. Consequently, many parameters are based on groupings such as tolerance classes. A well-studied species might be used to determine the equations, and then parameters are assigned for the different classes by ranking the tolerances of lesser-known species relative to the tolerances of the well-known ones. However, there have been many efforts to base important parameters more on empirical data rather than on observed relative rankings. This version of FACETA attempts some of these refinements by incorporating allometric measurements and tree ring data of the modeled local tree species to determine some of the important growth parameters.

Forest Models and Landscapes

The evolution of IBMs and gap models is an example of applying ecological knowledge across scales. IBMs model the behavior of individuals, but the result is an emergent community, so the knowledge of how individuals respond is being used to simulate a hierarchical level above the individual responses. Understanding how processes at one hierarchical level of living systems affects other levels are important research areas in many ecological and biological fields. An example is how molecular-level changes to DNA can result in cancer or how the toxicological effects of a pesticide can affect an ecosystem. However, the relationships between hierarchical levels are often complex and difficult to predict. Given that ecosystem processes occur at many different scales, understanding the relationships of patterns and processes at different spatial and temporal scales is an important pursuit in ecology. One problem with understanding processes at larger spatial and temporal scales is that it becomes more difficult to collect the relevant data. As the importance of understanding ecological processes at the landscape scale has become more recognized, the variety and applications of landscape-scaled models has grown. Forest landscape models have developed out of a variety of ecological concepts and theories, and have included both empirical and mechanistic approaches (Mladenoff & Baker, 1999). Forest landscape models have been developed as resource management tools used to assess alternative scenarios that cover broad spatial and temporal scales that are often not possible to do in real-world conditions. Many have been applied in the management of real landscapes. Shifley, Thompson, Dijak, and Fan (2007) note the increased use of forest landscape disturbance and succession models in forest management and planning over

the last two decades. They discuss three categories of approaches used for modeling forest landscapes. One approach is to represent the landscape as a mosaic of polygons of homogeneous vegetation patches. Each polygon is in one of a finite number of possible forest states, and the polygons transition between states according to a set of rules. Spatial relations in these kinds of models can be but are not always modeled using neighborhood rules (Barrett, 2001). The second approach described by Shifley et al. (2007) divides the landscape using a regular raster grid. Tree species composition, age classes, and size classes change for each cell according to a set of rules. These models are essentially state transition models like the polygon-based models but with potentially much finer resolutions spatially, temporally, and in the possible states or demographic descriptions. The raster-based models do not simulate individual trees, rather the demography of the cell as a whole. The third approach is to extend individual-based models across landscapes. Individual-based models such as forest gap models were originally designed to model a single stand without any spatial relations simulated. Today, using high-speed computers and parallel processing, multiple stands in different physical settings can be modeled simultaneously along with spatial processes that occur between the stands. In general, these three forest landscape modeling approaches are described in order of increasing complexity, computational load, input requirements, and output options.

Urban et al. (1999) discussed three approaches to extending fine-scale models to cover larger spatial extents. The simplest method was to use a sampling approach across the modeled landscape to develop a different set of parameters for a fine-scale point model at different locations. The landscape was modeled as a conglomeration of

these point models. This approach has the advantage of simplicity but ignores interactions between the point model locations, such as the flow of water, and therefore is not truly spatial. A second approach was described as *brute force* (i.e., build a bigger model that runs on a bigger computer). Such a model necessarily was more complex as it needed to simulate spatial interactions across the landscape such as hydrology and nutrient flow. The third approach described using a fine-scale point model to determine parameters for broad-scaled landscape models that statistically reconstructed the results of the fine-scale model. Urban et al. (1999), Acevedo, Urban, and Ablan (1995, 1996), Acevedo, Ablan, Urban, and Pamarti (2001), and Acevedo, Pamarti, Ablan, Urban, and Mikler (2001) used simulation runs of a plot-scaled forest gap model (ZELIG and FACET) to estimate parameters for a landscape-scaled semi-Markovian patch transition model (MOSAIC) to link models from these two different scales. In an approach such as this, variations in the landscape that affect the forest dynamics should be accounted for within the plot-scaled model. Acevedo et al. (1995) applied this technique to the H. J. Andrews Forest in the Oregon Cascade Mountains and identified temperature and precipitation as affected by elevation as the key variants of the landscape. Gap model simulations were done using parameters representing a number of different elevations, and the results from the gap model runs were used to determine state transition probabilities for different elevations on the mountain landscape.

Urban et al. (2000) and Urban (2000) took the sampling approach and applied the gap model FM, a modified version of FACET, to a Sierra Nevadan landscape with simulated plots representing different positions on the landscape. The landscape contained large ranges in elevation, slope, aspect, and soils. In this Mediterranean-type

climate, almost no precipitation occurred during the summer months, so water was considered a driving factor for vegetation patterns. Supply and demand on water varied spatially, and there were different reasons for the variation at different spatial extents. At the landscape scale, temperature and precipitation, determined primarily by elevation, were the key factors on water balance. At a basin-level scale within any limited range of elevation, topographic position, and aspect largely influenced soil moisture availability and demand from solar radiation respectively. At finer scales within a forest stand, soil depth played a big role in water availability. Field studies were analyzed at multiple scales. Simulation runs of FM were done for numerous possible landscape facets, with the key parameter differences being elevation, slope, aspect, and soil depth, and results were compared with the field studies. An important conclusion reached was that the different physical processes affecting water supply operated at different scales, and forest vegetation patterns were explained by different factors at different scales. While Urban et al. (2000) acknowledged the importance of topography in this application of FM in the Sierra Nevada, the hydrological affects of topography were not simulated or mimicked. However, topography was used as a measure of uncertainty of the model results for specific portions of the modeled landscape.

Seidl, Rammer, Scheller, and Spies (2012) discussed the need for an integrated, multi-scaled modeling approach to forest landscapes. Forests are complex systems with processes and interactions occurring across scales, and in order to make predictions and effectively manage forest resources in a world with changing climatic and environmental conditions, there is a need to understand these multi-scale interactions. Forest ecosystem complexity can be divided into different dimensions such as

structural, functional, or spatial complexity. These different dimensions of complexity have traditionally been modeled using different families of forest models. Forest gap models have been used to simulate forest composition and structure and study structural complexity. Physiological models have been used to get a glimpse into functional complexity by studying ecosystem processes such as photosynthesis, respiration, and nutrient cycling. Spatial complexity of ecosystems across broad landscapes has been modeled using forest landscape models such as the first two types discussed by Shifley et al. (2007). From a complex systems point of view, traditional forest modeling approaches have been reductionist (Seidl et al., 2012). Recently, hybrid approaches have been developed to integrate some of these dimensions. Seidl, Lexer, Jäger, and Hönninger (2005) integrated structural and functional complexity by hybridizing a gap model, PICUS, with a physiological model, 3-PG. In a similar integration, Peng, Liu, Dang, Apps, and Jiang (2002) developed the model TRIPLEX by hybridizing 3-PG with a forest growth and yield model called TREEDYN3. However, integrating the different aspects of ecosystem complexity and incorporating multiple levels of organization in such a way that can be scaled across a large spatial landscape remains a difficult task (Seidl et al., 2012). The model iLand was developed to integrate processes that occur across scales by using a spatially explicit IBM approach for simulating growth, regeneration, and mortality of individual trees. By modeling the availability of light, water, and soil nutrients as continuous fields determined by each individual tree's ability to compete for them, resource availability is spatially dependent within the stand. Computational scalability that allows the simulation to be run across large landscapes is achieved in part by using a modular approach for

light interference patterns of individual trees based on height and crown shape. Light interference patterns are predetermined for a library of different tree species and heights, and these patterns are assigned to individual trees at each time step in the simulation. The approach used in iLand models processes at the individual, community, and landscape levels; integrates aspects of functional, structural, and spatial complexity; and is scalable to larger landscapes. However, it does not incorporate differences in topography or hydrology across the modeled landscape.

FACETA used in this research takes a modeling approach that is similar to the simpler sampling approach discussed by Urban et al. (1999) while still preserving some of the hydrological spatial relationships of the landscape by simulating the effects of topographic position on soil moisture. It integrates aspects of structural and spatial complexity, and it can be extended across a landscape of heterogeneous terrain. In that sense, it is similar to the approach taken with the gap model FM as applied to the Sierra Nevada landscape, but with a factor incorporated to account for the hydrological effects of topography. It shares similarities to the polygon-based forest landscape models described by Shipley et al. (2007) in that the terrain type units the landscape is partitioned into are essentially polygons that are treated as patches with homogeneous conditions. Since the terrain type map is generated from a raster digital elevation model (DEM), there is flexibility with the spatial resolution and the shape of these polygons. The hydrological spatial relations between the terrain units are pseudo-simulated through a hydrologic model parameter based on topographic position. This approach therefore does not result in a true spatial model, but it has the advantage of avoiding the

complexities of the brute force approach while still simulating some of the spatial variability due to topography.

Topography and Topographic Indices

The terrain attributes considered key in the variation of vegetation patterns in this research are topographic position and soil conditions. In general, the topography of a watershed largely affects the hydrology and geomorphological processes, such as soil formation, and impacts biological processes as well (Moore, Grayson, & Ladson 1991). Altitude, slope, aspect, curvature, flow direction, and specific catchment area are all known as primary topographic attributes because they can be calculated directly from elevation data. Altitude can affect temperature and precipitation, in turn affecting vegetation. Aspect affects sun exposure, and slope affects sun exposure and both surface and subsurface water flow. Slope, in combination with soil conditions such as depth to bedrock and drainage, is often used as the primary topographic attribute for classifying land capability. Specific catchment area, a topographic attribute that can be calculated for every contour line segment, is defined as the upslope contributing area draining across a unit width of a contour line (Moore et al., 1991). The specific catchment area at any point within a watershed is a quantification of the potential of surface and shallow subsurface water flowing to that point. Zaslavsky and Sinai (as cited in Moore et al., 1991) found that soil moisture within an experimental catchment was correlated with curvature, and Moore, Burch and Mackenzie (as cited in Moore et al., 1991) found relationships between soil moisture and slope, aspect and specific catchment area. Secondary topographic attributes, also called compound attributes or compound indices, are calculations that combine two or more primary attributes.

Compound indices are often used to characterize variability of specific landscape processes such as soil moisture.

The compound index most used in characterizing soil moisture and hydrology combines specific catchment area together with slope. The compound topographic index was first developed for a terrain-based hydrology and runoff model, TOPMODEL (Lanni, McDonnell, & Rigon, 2011; Sørensen, Zinko, & Seibert, 2006). TOPMODEL is a physically based hydrological model applied at the watershed-level scale that was developed in the 1970s by Bevin and Kirby (1979). It was developed at a time when research trends and increasing computing power were driving models of natural phenomena, including hydrological models, to become more physically based and more complex. However, given the complexity of any individual watershed and the number of parameters required to model its hydrology accurately, increasing the fidelity and physical basis for watershed hydrology models can become exceedingly problematic. These complex hydrology models became difficult to apply objectively and lacked a basis from field measurements (Kirkby, 1997). Some hydrologists felt a need for simpler models that could still be based on physical processes and tied to field observations. The rationale behind the development of TOPMODEL was to create a model that incorporated a physically based spatial structure and aspects of the effects from flow networks and variable contributing areas, while at same time maintaining the simplicity of a lumped parameter model using parameters directly measurable in the watershed.

The concept of variable contributing areas is based on the idea that precipitation within a watershed can produce runoff and discharge with both spatial and temporal variability. There are at least four different ways that runoff might be produced across a

uniform watershed (Beven & Kirkby, 1979). One possibility is for runoff to be generated uniformly throughout the watershed from precipitation that exceeds the surface infiltration rate or soil storage capacity. However, in areas with vegetation cover or with high infiltration capacities, a uniform response is not likely. A second possibility is that, due to spatial variability in infiltration and in soil moisture content, runoff is generated across a variable area dependent on where the soil is at or near saturation. A third way runoff and stream flow is generated is by precipitation falling directly into or on saturated soils near stream channels. A fourth runoff factor is from downslope lateral subsurface flow, either in the unsaturated or saturated zones. This kind of subsurface flow, known as *shallow subsurface storm flow* when occurring in the unsaturated zone, is typically much slower than surface runoff and is more of a factor in stream baseflow than in peak channel flow during or after storms. In general, these runoff processes are called *infiltration-excess overland flow* if generated when the precipitation rate exceeds the instantaneous infiltration rate, or *saturation-excess overland flow* if the runoff is generated from precipitation falling on saturated soils. Saturation-excess overland flow is generally more likely to occur in low-lying areas adjacent to stream channels. TOPMODEL tries to capture the spatial variability of both infiltration-excess and saturation-excess overland flows.

The primary underlying assumption of TOPMODEL is that topography is the dominant factor in the spatial variability of flow. For any segment of the watershed, the size of the upslope contributing area is proportional to the inflow rate, and the outflow rate increases with local slope. Thus, the size of the contributing area and the local slope are assumed to be to two topographic quantities that control the water balance for

that segment. TOPMODEL relies on a few underlying assumptions of the physical conditions and hydrological response of the watershed. One assumption is that the hydraulic gradient is the same as the slope of the land surface (Beven, 1997). Another is that saturated zone dynamics can be approximated by uniform subsurface runoff production across the area and draining through a point. This assumption is interpreted as the steady state per unit area contribution to base flow, or the steady state recharge rate. Through water balance accounting of the total flow coming in to any hillslope segment and the subsurface flow transmitted downslope from that segment, together with the steady state assumption that these two quantities are equal, the compound topographic index used in TOPMODEL can be derived. The basic form of this topographic index is $TI_1 = \ln\left(\frac{A_S}{\tan(\beta)}\right)$, where A is the specific catchment area and $\tan\beta$ is the local surface slope of the watershed segment. This topographic index is assumed to represent the hydrology of different parts of the watershed (i.e., different points having the same topographic index will behave hydrologically similarly).

There are a number of variations of this index, the most common one being the one defined above. It is referred to by a few different names, often called the wetness index, steady-state wetness index, topographic wetness index (TWI), topographic convergence index, compound topographic index (CTI). While many sources use the term CTI to refer specifically to the wetness index, this may create confusion with the generic concept of a compound topographic index being the combination of any topographic attributes, so this index will be referred to as either the wetness index (generically for all formulations) or TWI (for a specific formulation).

The wetness index has been applied in fields ranging from soil science to forestry to human health. A study conducted in the southern part of the California Coast Range physiographic province on a hillside landscape containing a range of soil conditions and topographic positions found strong correlations between the wetness index and soil depth, A-horizon depth, soil organic carbon content, and net primary productivity (NPP; Gessler, Chadwick, Chamran, Althouse, & Holmes, 2000). The wetness index explained between 71%–84% of the variation of soil depth, organic carbon and A-horizon depth, and it accounted for 58% of the variation of NPP. In a study conducted in a forested area of Ohio, soil moisture was measured at a number of locations at various depths over a 2-year period (Iverson, Prasad, & Rebbeck, 2004). Iverson et al. found a significant but weak correlation between soil moisture and the wetness index. Equipment problems noted in the study may in part explain the weak correlation. Soil moisture sampling rate also was low–measured 18 times over two growing seasons–and there was no indication in the study of when the sampling times occurred relative to rain events. A detailed study was conducted in a forested watershed in central Pennsylvania that compared soil moisture measurements with soil type, soil depth, wetness index, slope, precipitation, and stream discharge (Lin, Kogelmann, Walker, and Bruns, 2006). Using a fine-scaled soil type map generated from an Order I soil survey (most USDA soil maps are generated from coarser-scaled Order II surveys, and the coarsest scale is Order V), the study found a very good relationship between the classified soil series and soil moisture. The wetness index worked to separate sites into groups with relatively different surface moisture. The wetness index, slope, and depth to bedrock were all correlated with surface and subsurface soil moisture; however, none of

these variables completely explained soil moisture variation. Taken together, a combination of certain terrain and soil attributes yielded a good predictor of soil moisture both spatially and temporally. Cluster analysis of the wetness index, slope, and depth to bedrock (a numeric variable that to some degree differentiated the soil series) was used to separate 30 monitored sites into four different wetness categories, which accurately reflected differences in moisture measurements at varying depths taken over time. The ways that topography and soil conditions combined to impact soil moisture were complex and difficult to separate. Yang, Chapman, Young, and Gray (2007) used a wetness index map together with a soil type map to delineate soil landscape *facets*, which were then used as the base units for creating land capability and feasibility maps. The term facet in Australian soils science refers to an area of land within a soil landscape, typically less than 5 km^2, which is identified by particular land-formed elements, landscape position, parent material, or natural vegetation community. This process was determined to be an automated, low-cost alternative to facet delineation through field studies and was successful at dividing about 60% of the soil landscape into facets. In applying the gap model FACET (FM) in a Sierra Nevada landscape, Urban et al. (2000) and Urban (2000) computed a wetness index map that was interpreted as a map of hydrologic uncertainty. The model did not simulate the hydrologic contribution from upslope areas, so it underestimated moisture for places on the landscape that received substantial run-on. The map was used to devise a monitoring and sampling plan, with sampling locations chosen from areas in the 80^{th} percentile of wetness index values. In a study done in the boreal forest in Sweden, vascular plant species richness increased with wetness index values up to a point, after

which species richness stayed the same or even declined (Zinko, Seibert, Dynesius, and Nilsson, 2005). This study found that the relationship was sensitive to plot size, and the positive correlation was stronger in larger plots. This sensitivity to plot size may be a reflection of the accuracy of the elevation data used to derive the wetness index. In a human health study conducted in the Kenyan highlands, Cohen et al. (2008, 2010) found that distance of households to areas with high wetness index values was significantly associated with malaria risk. The study found that proximity to high wetness index areas was a better predictor of malaria risk than elevation or satellite-derived land-cover and land-use variables.

The TWI has clearly been useful in a variety of applications involving soil, landscape attributes, and ecology, but strong correlations between the wetness index and soil moisture measurements have not always been found. Several issues related to the derivation and calculation of the wetness index may play a role in this. One problem may be the accuracy and resolution of the digital elevation data used to calculate the wetness index. Much of the available elevation data is at a 30-m grid, or horizontal, resolution, which may be too coarse to identify the microtopographical effects on water flow and collection. Elevation data at 10-m grid resolution is now freely available through the U.S. Geological Survey's National Elevation Dataset (NED) for all of the contiguous United States, and 3-m data are available for limited parts of the country (United States Geological Survey [USGS], n.d.). This is not true for all places; for example, the best resolution data for most of Alaska is 60 meters. One-meter resolution elevation coverage does exist for some places, but not through the NED or other freely distributed source. High-resolution (3 m or better) and moderate-resolution (some 10 m)

digital elevation data are typically derived from either light detection and ranging (LiDAR) data or digital photogrammetry. The bulk of the NED data uses a 10-m grid resolution, but it is derived from cartographic contours and is therefore not considered high or moderate resolution. Vaze, Teng, & Spencer (2010) examined the affects that both grid resolution and vertical accuracy of digital elevation data have on various topographic indices. The study found that digital elevation data derived from LiDAR yields a much better representation of the topographic surface than elevation data generated using cartographic contours. When comparing elevation data derived from LiDAR originally sampled at 1-m resolution and then resampled to 2-m, 5-m, 10-m, and 25-m resolutions, the different grid resolutions yielded hillshade views with essentially no differences. Small differences were found between the different LiDAR-derived grid resolutions in the delineated watersheds stream networks. Comparing hillshade views, watersheds, and stream networks, the differences between the 25-m resampled LiDAR derived data and the 25-m contour derived data were very large and obvious.

Zhang, Wu, Chang, Elliot, and Dun (2009) used six different digital elevation datasets from three different sources (NED, LiDAR, and Shuttle Radar Topography Mission or SRTM) and three different grid resolutions (30, 10 and 4 meter) as input into a hydrology and erosion model (the Water Erosion Prediction Project or WEPP) that was applied to two forested watersheds in Idaho. Model outputs were then compared to field measurements and observations. One of the watersheds was more topographically complex with steeper slopes, and it lay immediately upstream of the other one. Due to the forested cover of the watersheds, which characteristically yielded little surface runoff, model estimates for water discharge differed little between the six different input

elevation datasets. Comparing model estimates of discharge to field measurements, within each watershed the model produced consistent estimates for all six different elevation datasets. However, the upstream watershed consistently resulted in significant overestimates (greater than 65%), and the downstream watershed resulted in small underestimates (about 6%). These differences in discharge were thought to result from model not accounting for groundwater baseflow. There were also large differences in the model estimates for soil erosion from the different elevation datasets. The SRTM 30-m resolution data resulted in a 10-fold overestimate of soil erosion in the more topographically complex watershed, and more than a two-fold overestimate in the smoother one. The 10-m LiDAR data yielded model results of erosion field measurements off by 12% in one watershed and 9% in the other, making it the most accurate across the two watersheds. The 10-m NED produced slightly closer estimates in the more topographically complex watershed, and the 4-m LiDAR produced slightly closer results in the smoother one. Taking into consideration the accuracies in watershed area, number of hillslopes, and number of channels as compared to field observations, the 10-m LiDAR generally yielded the best results for both watersheds. The 4-m LiDAR data yielded similar results; however, they did not improve model accuracy over the 10-m LiDAR and were in fact substantially less accurate for soil erosion in one of the watersheds.

The specific formulation of the wetness index also may have been an issue. The typical formulation of the wetness index had slope in the denominator, which created a calculation error when measured slope was zero. The Terrain Analysis Using Digital Elevation Models (TauDEM) geographic information systems (GIS) toolbox for

analyzing digital elevation data gets around this problem by flipping the ratio and putting slope in the numerator and specific catchment area in the denominator (Tarboton, 2012). In this reciprocal formulation, zero was the lower limit of index values, and decreasing values indicated wetter conditions. This formulation has a different problem in that all areas with measured slope of zero have a wetness index value also equal to zero, regardless of whether the land is a flat spot on top of a hill or flat and at the bottom of a valley. The potential divide-by-zero problem can be avoided if no cells have calculated slopes of zero, and there are DEM processing tools or algorithms that ensure that result. An example of such tool, the PDEM, assigns a slope to a flat area through linear interpolation between the highest and lowest elevations surrounding the area (Pan, Stieglitz, & McKane, 2012). The PDEM tool is used to process DEMs to make them depressionless and to eliminate any flat cells. Making a DEM depressionless is often referred to as filling the sinks. This process ensures that there is a defined flow path out of every cell. There are a number of algorithms available for filling sinks in DEMs; however, the PDEM tool has the added effect that no cells have a zero slope, which is not the case in general for depression filling techniques.

Algorithms used for determining either the slope or the specific catchment area can impact the calculation of the wetness index, and the choice of algorithm used can be another issue to consider. Calculating specific catchment area requires first determining the flow direction (the way water flows from each cell to its neighbors) from the digital elevation data. There are numerous algorithms for determining flow direction, and they yield different results. The most commonly used algorithms are single flow direction in that water flow from each cell is restricted to only one of its neighboring

cells, but numerous multiple flow direction algorithms have been developed. Kopecký and Čížková (2010) analyzed wetness indices calculated using 11 different flow direction algorithms and compared them to more than 500 vegetation plots in three different regions to determine if the algorithm used mattered in applications to plant ecology. They used soil moisture and plant composition measurements to compare the performance of the different wetness indices. While all 11 indices were significantly correlated with soil moisture and plant composition in all three regions, the choice of flow direction algorithm made a considerable difference in the performance of the wetness index. Some algorithms resulted in wetness indices that performed more poorly across all regions, including the one most widely available in most GIS (single-direction D8). One algorithm (multi-direction FD8) performed substantially better than the other algorithms.

As with flow direction, there are also numerous algorithms for calculating slope. Rodriguez and Suárez (2010) compared slopes calculated from 10-m resolution elevation data of a watershed characterized by gullies and steep slopes using nine different mathematical algorithms. Field measurements of slope were taken at 32 points within the watershed, and an error term was calculated between the measured and calculated slopes. The resulting slope maps were not significantly different from one another. However, the error terms calculated for the various slope algorithms were different, particularly for steep slopes greater than 36%. It should be noted that the digital elevation data used in this study were generated from cartographic contours, and error with the elevation data itself is not discussed.

In a comparison of how different flow direction algorithms and slope calculation methods affect calculation, Pan, Peters-Lidard, Sale, and King (2004) examined the performance of six different variations of the TWI. The flow direction algorithms used included a single flow direction (SFD), a bi-flow direction (BFD), and a multiple flow direction (MFD) algorithm. Two different methods were used to calculate slopes in flat areas, the tracking flow direction (TFD) and Wolock and McCabe methods. The calculations were performed on different idealized hillslopes. Three hillslopes with constant slopes – one planar, one convergent, and one divergent – were used. Nine different slope values were tested for the constant-slope idealized hillslopes. Additionally two divergent hillslopes with varying slopes were tested – one concave and one convex. To measure the performance of the different index variants, root-mean-square errors between the calculated and the theoretical topographic index values were determined. Several conclusions were reached: (a) In all cases the MFD flow direction algorithm together with the TFD method for slope calculation in flat areas yielded the smallest error, (b) scenarios with larger slopes resulted in smaller error, and (c) slopes below a certain threshold resulted in no difference in between SFD and BFD.

Sørensen et al. (2006) calculated multiple variations of the wetness index from 20-m resolution elevation data by using different combinations of algorithms and parameters. Using two different algorithms each for specific catchment area, stream delineation, and slope, combined with 6 to 8 different parameter values for each, they computed 2688 different variations of the wetness index. The results were then compared to field studies from two boreal forest watersheds to determine if computation method affects the correlation between the wetness index and four different field-

measured variables: plants species richness, soil pH, groundwater level, and soil moisture. The study sought to determine if calculation method affected correlation, which methods yielded the best correlations, and if there was a best overall method. Different calculation methods yielded high variability in the correlations between wetness index values and the measured variables, so for any one measured variable the calculation method did matter. No single calculation was found to be the best in that no calculation yielded the highest correlation for all four variables in both sites. Certain methods were identified to be generally best overall for all variables, but these methods did not produce the highest correlations for any single variable. In general, the multi-direction flow algorithms produced higher correlations than the single-direction algorithms.

Pei et al. (2010) compared relationships of wetness index values calculated using a common single-direction flow algorithm with those from a multi-direction flow algorithm to soil organic matter. Soil organic matter was measured at 54 locations in various topographic positions in a low relief study area, and the data were compared to both the multi- and single-direction wetness index values generated from 10-m resolution, contour-derived elevation data. The multi-direction wetness index correlated better with soil organic matter than the single-direction. Soil organic matter maps were generated from the study area using ordinary kriging and three other kriging methods that incorporate wetness index values as a secondary variable. Two of these kriging methods were somewhat incompatible with the both sets of wetness index values, and the ordinary kriging map outperformed the maps produced by them. The third method, called collocated cokriging, benefited from the use of the wetness index as a secondary

variable. The soil organic matter map produced using collocated cokriging and the single-direction wetness index outperformed the ordinary kriging map, and the collocated cokriging, multi-direction map outperformed the single-direction one.

Before calculating slope or flow direction, different algorithms can be used in the processing of the elevation data that can lead to differences in the calculation of topographic indices. One of the requirements to calculate flow direction is that the *sinks* in the elevation data must be *filled*; that is, depressions and flat areas must be adjusted so that a flow path from each cell can be calculated. Sinks in elevation data may be artifactual, errors in the data, or representations of true depressions. Nevertheless, they must be filled to allow the calculation of flow direction. If the TWI is to be calculated, flat grid cells with zero slopes must also be adjusted to avoid division by zero. There are numerous algorithms and techniques to fill sinks, but they all can be problematic or introduce uncertainty in some circumstances (Pan et al., 2012). The algorithm to fill sinks in the most commonly used GIS software is the Jenson and Dominque (JD) method, which tends to produce unrealistic parallel flow patterns in flat and flow accumulation areas. Pan et al. proposed a new algorithm, PDEM, using linear interpolation to fill sinks in a DEM in a way that avoids many of the problems that can arise in hydrological modeling. By using linear interpolation between the high and low elevation cells around the sides of a sink, the technique ensured that all cells have at least one downward slope in the outflow direction. The algorithm was applied to two virtual landscapes and one real one, and the results were compared with those using the JD method and with another common method called TOPAZ. In the two virtual landscapes, PDEM produced more hydrologically coherent drainage patterns through

the flat accumulation areas then either of the other two methods. In the real landscape (an area within the Big Swamp watershed in North Carolina), PDEM produced more realistic flow accumulation patterns than the JD method. The stream channel network produced using the PDEM method matched the stream network indicated on the USGS topographic map more closely than TOPAZ, and the stream network produced by the JD method was less consistent with the USGS topographic map than with both PDEM and TOPAZ.

Other variations of the wetness index have been formulated to improve its predictive power for soil moisture, wetlands, species richness, or other important variables. One common variant of the wetness index includes a soil transmissivity factor (Moore et al., 1991; Kirkby, 1997). This factor causes the wetness index value to increase as saturated hydraulic conductivity decreases, for example with depth. Goodwin (2003) discussed a wetness index developed to account for the effects that urbanization in a forested watershed has on the spatial distribution of soil moisture. Urbanization increases impervious surface area, which decreases soil infiltration, groundwater recharge, and stream baseflow. Reduction in baseflow can reduce the length of perennial streams. On the other hand, removal of forest or other vegetation can decrease evapotranspiration and the loss of soil moisture. This index is similar to the common wetness index in that it includes the ratio of specific catchment area and slope, but it also includes terms for steady-state recharge rate and soil transmissivity. Recharge rate increases the index value while transmissivity decreases it. Applying this index to a suburban Atlanta watershed as a model of soil saturation and perennial stream flow yielded the prediction that 19% impervious surface area in the formerly

forested watershed reduced saturation extent and stream length by 15%. Field verification of this model result was not done.

A number of variations of quasi-dynamic and dynamic wetness indices have been developed, as compared with the steady state or static wetness index discussed so far. The wetness index is based upon several underlying assumptions. These assumptions include that soil hydrology is dominated by lateral subsurface flow, and that this subsurface flow is in a steady state (Grayson, Western, Chiew, and Blöschl, 1997). This steady state assumption is manifested in the wetness index in that it uses the entire upslope contributing area, implying that the soil moisture at any point in the watershed is affected by that entire area. In wet climates, wet seasons, or during prolonged periods of rainfall this steady state assumption might be realistic. However, in dry climates or during dry times of the year lateral flow may become nonexistent, and when precipitation does occur the moisture will soak into the soil and subsequently be removed through evapotranspiration. To ease this steady state assumption, Barling, Moore, and Grayson (1994) developed a quasi-dynamic wetness index. The quasi-dynamic index was time-dependent in that it uses an *effective* specific catchment area, where the effective size of the upslope contributing area depended on the duration of a rainfall event as well as soil properties. In wet conditions, the specific catchment area and the effective specific catchment area were the same. The interesting conclusion in the Grayson et al. (1997) study was that the hydrologic state of the soil could switch from a state dominated by lateral flow to a state dominated by vertical fluxes, and vice versa, quite suddenly. The implication to this was that two different wetness indices should be used, one for wet times when lateral flow dominated and one for dry times. A

two-index modeling approach would also require criteria or a mechanism to switch between the two states.

Another assumption of the steady-state wetness index is that the hydraulic gradient is parallel to the surface slope. In order to ease this assumption of parallelism, Lanni et al. (2001) developed an index that took the quasi-dynamic wetness index developed by Barling et al. (1994) and replaced the local slope term in the equation with a downslope wetness index (DWI). Comparing this and five other wetness index variants calculated from 2-m, LiDAR-derived, high-resolution elevation data to the results of a process-based hydrologic model, Lanni et al. (2011) found this index produced the best results for patterns of soil moisture deficit for rainfalls lasting up to three hours. However, using the DWI instead of local slope reduced the index's ability to predict groundwater levels, and the other indices outperformed this index in longer duration rainfalls. Additionally, because the DWI depended on a parameter based on the micro-topographic relief of the watershed, Lanni et al. found the DWI difficult to apply. Another index examined in this study took the quasi-dynamic wetness index and ran it through a 3x3 low-pass filter in order to smooth out the effects of local topography. The smoothed quasi-dynamic wetness index was generally performed the best in this study, and the smoothing was found to be important when using a high-resolution grid.

Fully dynamic wetness indices have also been developed in order to address some of the limitations of the static wetness index. Kim and Jung (2003) proposed extending the quasi-dynamic wetness index to a fully dynamic index by integrating the convolution of the upslope contributing area with the time series of effective rainfall, yielding a model of spatial and temporal patterns of soil moisture. In cases where

meteorological and hydrological data were available, Grabs, Seibert, Bishop, and Laudon (2009) developed a technique of using dynamic simulations of a distributed hydrological model to derive a model-based wetness index (MWI). The intent of the MWI was to account for the dynamic influence of both upslope and downslope conditions, whereas the traditional wetness index only accounted for static upslope and local conditions.

The choice of topographic index and the algorithms used to calculate them all matter when it comes to interpreting hydrological, ecological, or pedologic information from elevation data. In some situations, an entirely different topographic index may be more appropriate. For example, in certain mountainous terrains, slope aspect and insulation may play a much greater role in soil moisture than upslope contributing area does. Generally, the use of multi-direction flow algorithms seems to be gaining preference over single-direction ones, and the use of dynamic and quasi-dynamic variations of the wetness index are becoming more common. These variations have all been developed to overcome valid criticisms and limitations of the steady state TWI and the algorithms used to derive them. However, there are a number of variations and parameterizations of all these indices, and usefulness of any topographic index depends on the application and the physical terrain to which it is applied. While a certain variant of the wetness index may have greater predictive ability in certain situations, it may not in others. More investigation into the differences can help bring about better utilization of geographic information system tools to ecological applications. The grid resolution of the elevation data is also important. One might generally conclude that finer resolution, when accurate, is desired. However, this may not be the case. The best

resolution to use depends upon the scale of the process of interest and the scale of topographic variation within the terrain.

Gap Models and Weather

Forest gap models typically incorporate stochastic weather generators to input variables such as temperature and precipitation used in tree growth response. In many models such as FACET, weather is simulated with monthly time steps (i.e., total monthly precipitation and average monthly temperature are generated for each simulated month, and tree growth is modeled using annual time steps). Weather is then scaled down to sub-monthly steps using linear interpolation. Tree growth response to the simulated weather is based on an aggregate of weather generated during the growing season for the entire year. Modeling weather and soil water balance using time steps greater than a day makes it difficult to account for water infiltration and surface runoff during rain events. In hot climates and sandy soils, moisture from the upper layers can be depleted through evapotranspiration in a matter of a few days after being soaked. Using coarse time scales for weather and soil moisture simulation may not fully capture stress caused from short-term dry spells. Forest gap models have been criticized for not always accurately simulating the impacts of droughts (Bugmann & Cramer, 1998). To improve the performance of the gap model FORCLIM (Bugmann, 1996) in predicting the impact of droughts to species composition, Bugmann and Cramer (1998) considered increasing the accuracy of the drought tolerance parameters of the modeled tree species and increasing the fidelity of the soil water balance model. They found that with both these refinements together the model performance did improve along a drought gradient. They did not investigate refining the temporal scale of

the weather or soil moisture simulations, and most gap models still use monthly time steps for these. The forest landscape model iLand did incorporate refined time scales using daily time steps for both its soil water balance calculations and its tree growth environmental response functions (Seidl et al., 2012). While iLand was not technically a forest gap model, it shared similarities in how it models individual tree growth. However, iLand did not use a weather generator for simulated weather; rather as input, it used a time series taken from real daily weather data. The weather generator and soil water balance subroutine were refined for the gap model FM when it was applied to a landscape where soil moisture was deemed a critical factor in vegetation patterns (Urban, 2000; Urban et al., 2000). The soil water subroutine was changed to a daily time step, and the precipitation portion of the weather generator was altered to produce precipitation amounts on a daily timescale. However, the weather generator was described as being based on both monthly and daily timescales. The model used average monthly total precipitation amounts and generated precipitation events on daily time steps. Precipitation event amounts and frequencies were based on long-term data. While details on the daily precipitation model, how it was connected with the monthly total precipitation amount, or an analysis of its performance were not included, presumably it followed the interpolation scheme of FACET. Similarly, one of the refinements implemented in FACETA to improve the fidelity of the hydrological response was to change the time scale of the soil moisture subroutine to a daily time step, which in turn necessitated changing the weather generation time scale to daily.

Weather Generators

Weather generators are algorithms that use random number generators based on probability distributions to generate time series of artificial weather variables. Probability distributions are selected and parameterized to match observed weather data. Weather generators are used in applications of agriculture, hydrologic engineering, climate change simulations, and ecological models (Wilks & Wilby, 1999). While it is not the case with forest gap models, daily weather generators are commonly used in most applications. The greatest effort in developing weather generators has been given to simulating precipitation. In part, this is because precipitation is a key variable in many applications. Simulating precipitation patterns probabilistically poses some difficulties. Many days will have zero precipitation, and on days when precipitation occurs, the amount can range from a trace to a deluge. This results in a discontinuity in the probability distribution for precipitation on dry days and rainy days. Depending on the climate, the distribution of precipitation amounts on rainy days are usually strongly skewed right, with many days having small amounts of rain and very large amounts occurring on a small number of days. One pattern that is fundamental to weather generators is that dry days and rainy days tend to have a degree of serial autocorrelation. Most weather generators use a two-part process for simulating precipitation, with the first part determining whether precipitation occurred, and the second part determining the amount of precipitation, if it did occur.

Gabriel and Neumann are often attributed to developing the first stochastic daily rainfall model in 1962. In their model, they used a first-order Markov chain to simulate the sequence of wet and dry days. With a Markov chain model, the probability that it

rains on any given day is conditioned on whether or not it rained on the previous day. Being a first-order Markov chain means that the probability of precipitation is conditioned only on the previous day's precipitation state and not on any days prior to that. Determining the conditional probabilities from daily weather data for this kind of model is straightforward, the resulting model simulates the persistent patterns of wet and dry days well, and it produces long-run relative frequencies of wet and dry days that match the fitted data. However, it has been noted that in some climates it may not produce enough long dry spells. One possible refinement is to use a higher-order Markov chain, where the probability of precipitation on any given day is conditioned on the previous two, three, or more days.

Another approach that has been used is to generate a sequence of spell-lengths (i.e., lengths of consecutive dry days or wet days). If a geometric probability distribution is used to generate the spell lengths, this approach is equivalent to using a Markov chain. In climates where the first-order Markov chain does not produce sufficiently long dry spells, distributions other than geometric can be used to generate spell lengths with improved results. The second part is the precipitation amount that occurs on wet days. For most climates, the distribution is very right skewed. Various distributions including the exponential distribution have been used for precipitation amounts, but the most common has been to use the gamma distribution. The exponential and to a lesser degree the gamma distribution sometimes underestimate the frequencies of large precipitation events. A mixed exponential distribution, which is a combination of two exponential distributions, sometimes improves simulating the large amount events; however, this approach has been used infrequently. Other weather variables often

simulated are daily high and low temperatures and solar radiation. These variables are often conditioned on whether or not precipitation occurred. Temperature variables are often modeled using a normal distribution, but other distributions have also been used. Parameters for all the weather variables are typically determined for each month, but not always.

In a semi-arid climate in southern Arizona where rainfall patterns exhibited a large amount of spatial and temporal variability, Hsieh, Stone, Guertin, and Slack (2003) found that using semi-monthly rather than monthly periods to determine the wet day and dry day Markov chain transition probabilities was more appropriate. To address the spatial variability throughout the watershed of rain events, the authors incorporated an interesting approach. On wet days, a spatial distribution model was used to determine location of storm center, rainfall depth at center, size and shape of storm, and a calculation of rainfall depth throughout the storm area based on the depth at the center. Simulating this kind of spatial variability of rainfall events may be important in distributed hydrologic modeling, especially in semi-arid climates, but horizontal spatial variability of weather is not commonly incorporated into forest models. One general problem with weather generators is that the interannual variability of the simulated weather tends to be smaller than in the real observed weather data.

Most models do not take into account strings of consecutive wet or dry years (Srikanthan & McMahon, 2001). One approach to incorporate interannual variation is to use a two-stage model similar to daily rainfall generation with the first stage being a Markov chain determining if each given year is wet or dry. The second stage determines the total annual rainfall from a normal distribution with a different mean depending on if

the year is wet or dry. To incorporate interannual variation with this kind of approach into a daily rainfall generator, the daily model has to be coupled with the annual model. Another general problem for daily rainfall generators is that when the synthetic daily amounts are summed into monthly and annual totals, these totals often do not preserve the statistical properties of the real world monthly and annual totals (Piantadosi, Boland, & Howlett 2009; Srikanthan & McMahon, 2001; Wang & Nathan, 2007). Wang and Nathan (2007) proposed a model that produced two time series, one at the daily scale and the other at the monthly scale, with each preserving the statistical real world properties of their respective scales. The daily time series was then adjusted to fit the monthly time series. This produced results that matched the data well at the daily and monthly time scales, and preserved some of the annual statistical properties. Piantadosi et al. (2009) proposed an approach that coupled all three timescales. Annual rainfall total was first generated using one of two normal distributions depending on if the year was wet or dry. For each year, many monthly total time series were generated, and the monthly time series that best matched the annual total generated was chosen. A similar process was then incorporated at the daily timescale, with many daily time series being generated for each month, and the one that matched the monthly total best was chosen. This method, while a bit convoluted and computationally costly, produced results that matched statistically across all three timescales

Cross Timbers as a Case Study

Using the Cross Timbers ecoregion as a case study for FACETA is a somewhat natural choice as the University of North Texas campus and much of the City of Denton are located within it. Conditions in the Cross Timbers are also ideal for testing FACETA,

the intent of which is to predict how hydrology, soil, and topography impact forest growth. While often thought of as a post oak forest, the Cross Timbers ecoregion is a mix of post oak forests, woodlands and savannas, bottomland hardwood forests, and patches of prairie (Francaviglia, 2000). Positioned between the temperate deciduous forest and humid climate of the East and the tall grass prairies and semiarid climate of the Midwest, the Cross Timbers is a transition zone between the two. It has long been recognized that the underlying geology and subsequent soil that develops from it plays a critical role in the development of either post oak forests or prairies, and topography is the driver between bottomland hardwood forest and upland forest or prairie. Robert Hill (1887), sometimes referred to as the father of Texas geology, documented in an early description of the Cross Timbers within Texas how closely the vegetation patterns were linked to the geology and topography. The Greenbelt, a protected area of land located within the Cross Timbers, is the site of a number of research studies by faculty and students from the University of North Texas and is at the center of the landscape used in this case study. In a phytosociological description of the Greenbelt, tree surveys were conducted in 128 plots, and forest composition was analyzed (Barry & Kroll, 1999). In a study on avian communities, Barry (2000) conducted tree surveys, forest structure and composition analysis, and habitat evaluations in 62 plots. In an historical and ecological examination of the area, Holcomb (2001) included a characterization of the forest and parameterized the gap model ZELIG for parts of the Greenbelt. Komperad (2009) conducted a study examining relationships between climate and flooding and tree growth, which included tree ring analysis of numerous green ash (*Fraxinus pennsylvanica*) trees from the Greenbelt. Rijal (2011) examined the relationship

between forest composition, soil, and topography through the analysis of tree surveys and 2-m deep soil cores from 30 plots located at different topographic positions within the Greenbelt. Soil moisture data at various locations and soil depths and weather data were collected in the Greenbelt as part of the ongoing Texas Environmental Observatory project (Texas Environmental Observatory, 2012). Vegetation and soil data from the Greenbelt from these previous studies are valuable resources in estimating and calibrating parameters and validating FACETA results.

CHAPTER 3

METHODOLOGICAL OVERVIEW

The underlying research objective is to develop a method of extending the plot-scale forest gap model FACETA to a watershed-scaled landscape. This objective acts as an umbrella to a number of finer but interesting objectives that branch into a few distinct directions, for example topography and hydrology, silvics, and weather simulation. A brief overview of the methodological approach used in some of these different objectives is provided here. Specific methods pertaining to each of these branches are discussed in the subsequent chapters covering them.

Defining the study area to be modeled was the first step necessary. For this research, a nearby state park containing a relatively large area of bottomland forest within a floodplain, as well as small areas of upland forest and grassland, offered a good starting point. As the modeled study area covered a hydrologically based landscape, watershed delineation was performed to define the boundary of the watershed containing the state park. This watershed defined the study area landscape. The watershed delineation as well as all the topographical and hydrological analysis was done using digital elevation models (DEMs) and geographic information systems (GIS). GIS was also used for soil type mapping, delineation of terrain types, and for visual analysis of aerial photographs and other remote sensing data. Each of the different parts of this research started with a review of existing literature and of previous approaches taken. The range of topics covered and knowledge needed to achieve the research objectives was quite broad; therefore, gathering information and applying ideas from previous research and approaches was an important component to the

methodologies behind them all. The idea of applying a particular topographic index as a hydrological input to a forest gap model came out of the review of literature, mostly in the context of hydrological and soil modeling. A review of literature revealed some examples of such topographic indices being used in plant studies and within the context of applying a forest gap model, but not as a hydrological input to a gap model. With the idea planted to try to implement a topographical index as an input to represent hydrology in a scaled-up gap model, the remaining pieces of the research included defining landscape terrain types for the gap model, incorporating necessary model changes, and estimating model parameters. The methods used in defining the landscape terrain types primarily involve GIS. For the topographic component of defining terrain types, digital elevation data were obtained from two sources and with multiple grid resolutions, and were then processed using different algorithms. Delineating the soil type component of the terrain types was also done using GIS and the digital version of the USDA soil survey. Both a review of the historical vegetation of the Cross Timbers ecoregion as well as tree surveys conducted within the study area were used in determining the tree species to be included in the model. Determining values for all of the biological model parameters started with a survey of published information, but silvics information can be quite variable and is often more qualitative than quantitative. Therefore, measurements on local trees were included as much as possible in estimating these parameters. Parameters involving tree geometry were determined exclusively from local measurements, and growth rate parameters were estimated using a combination of local measurements and published information that was largely qualitative. Some of the biological parameters such as tolerances to drought

or flooding were difficult to measure for, and for those it became necessary to extrapolate model parameters from qualitative descriptions. Required environmental model parameters included ones for soil conditions and for weather simulation. Soil parameters were determined using two methods. In one method, parameters were estimated from the soil series descriptions in the USDA soil survey. This was done for all of the soil series included in the model. For some of the soil series, model parameters were also estimated from soil samples taken from the Greenbelt and analyzed. Weather parameters were determined using statistical techniques applied to an approximate 100-year record of daily weather. FACETA simulation was performed on selected terrain types that were representative of the range of different soil and topographic conditions found within the study area.

Each of the subsequent chapters covers a thematically grouped set of objectives, with the methodologies and results for each group of objectives included within the chapter. The process of defining the landscape terrain types through a combination of soil and topographic position is described in Chapter 4. Chapter 5 discusses the measurements and estimates of FACETA biological parameters. Environmental parameters for FACETA, which include weather, soil and topographic parameters, are covered in Chapter 6. Chapters 7 and 8 discuss the model results and final research conclusions, respectively. A description of the study area is provided before going into each of these chapters.

The study area used for terrain analysis and application of the forest model FACETA was the Ray Roberts Lake and Lake Lewisville Greenbelt Corridor in Denton County, TX, referred to from here on simply as the Greenbelt. The Greenbelt was a

state park, part of the Texas Parks and Wildlife system, located within a watershed of the Elm Fork Trinity River, which flowed from Ray Roberts Lake to Lake Lewisville. For the purposes of determining the relevant landscape factors and defining terrain types, the study area was extended to the entire watershed; however, parameterization and simulation of FACETA was limited to the Greenbelt (Fig. 3-1).

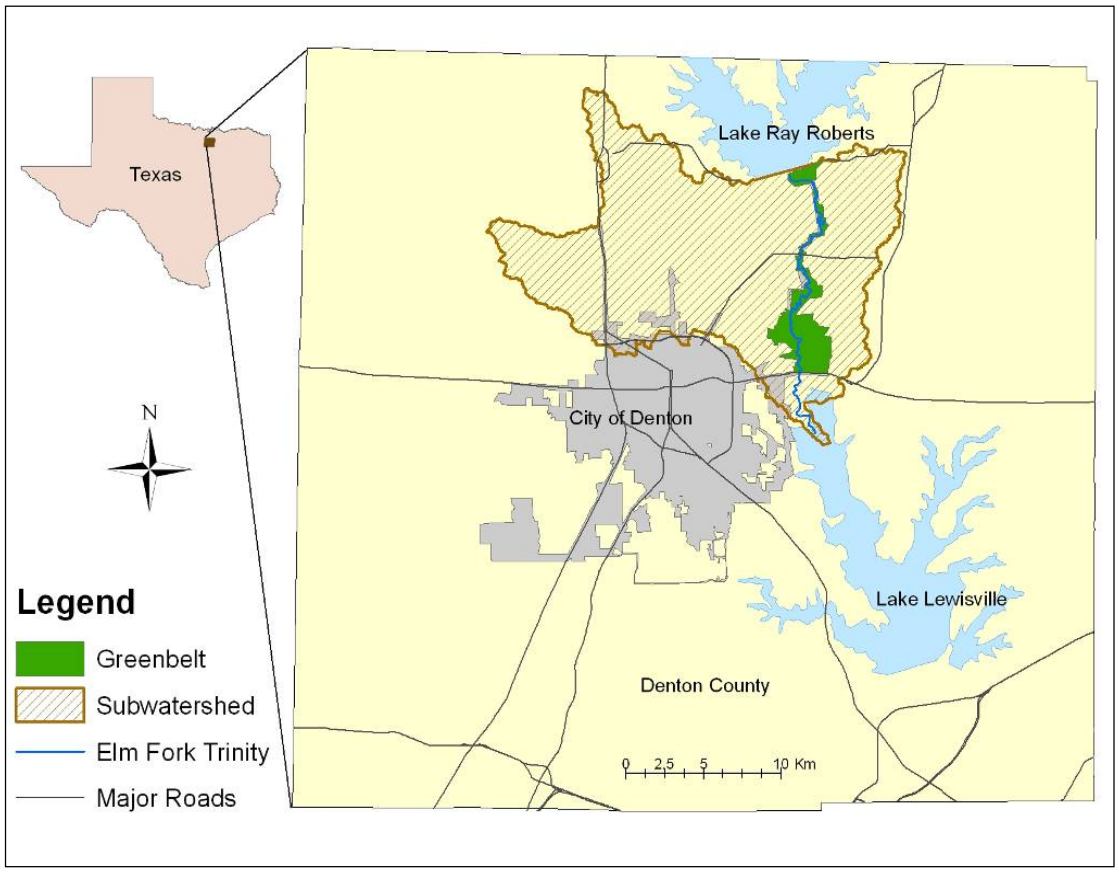

Figure 3.1. The study area location. The Greenbelt runs along the Elm Fork Trinity River from the Lake Ray Roberts dam to the headwaters of Lake Lewisville. Landscape factors and terrain types for FACETA are determined from the Elm Fork Trinity watershed; however, FACETA simulation is limited to terrain types found within the Greenbelt.

Denton County lies within the Prairie Parkland subtropical ecological province, an area composed of a mix of prairies and savannas (Fig. 3.2; Bailey, 1995). Low rainfall and probably wildfire historically have kept the natural vegetation in this province dominated by grasses and a few drought tolerant tree species, with soil being a key

factor in vegetation distribution. Fine textured soils have supported grasslands while savannas and woodlands have developed on coarser soils.

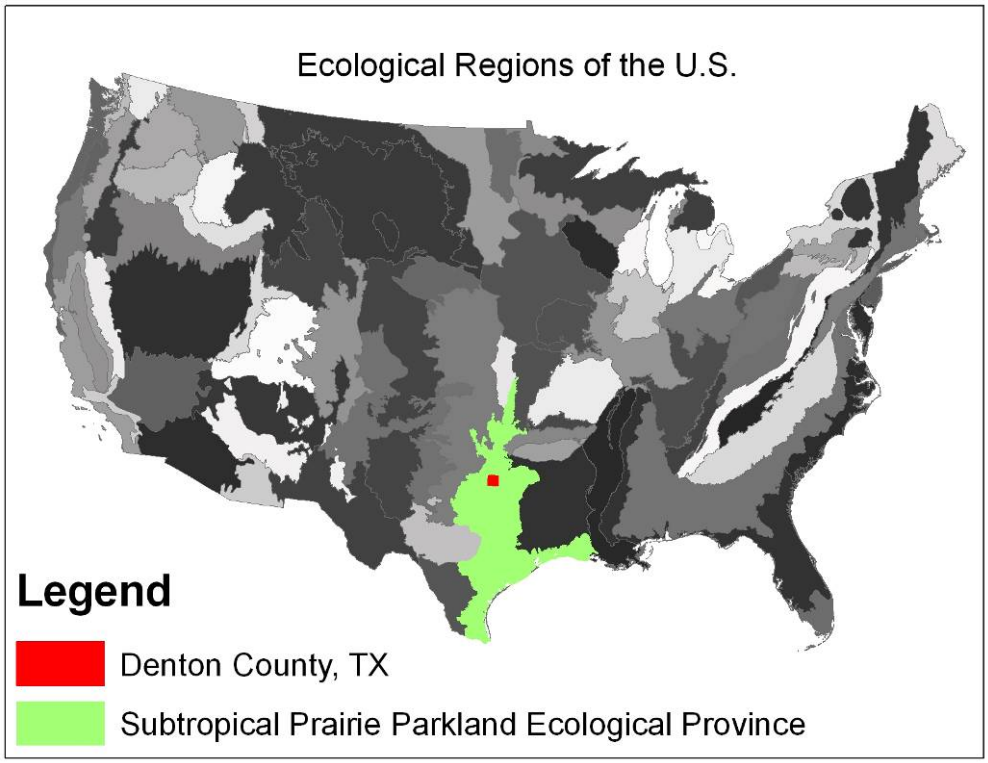

Figure 3.2. Denton County within its ecological province. Denton County and the study area watershed lie within the Subtropical Prairie and Parkland Ecological Province, a grassland-forest transition area. Provinces make up Level II in the Environmental Protection Agency's (EPA) hierarchy in the ecological classification of different regions. The Prairie Parkland province contains a mix of prairies and savannas. The ecoregion base map is from the EPA (Griffith et al., 2004).

The western portion of Denton County lay in the ecological subregion known as the Cross Timbers and Prairies, which contained a mixture of prairies and upland oak woodlands and savannas (Fig. 3.3). The eastern side of the county lay in the Texas Blackland Prairie ecological subregion. Under the EPA ecoregion hierarchy scheme, these two ecoregions were designated as Level III ecoregions.

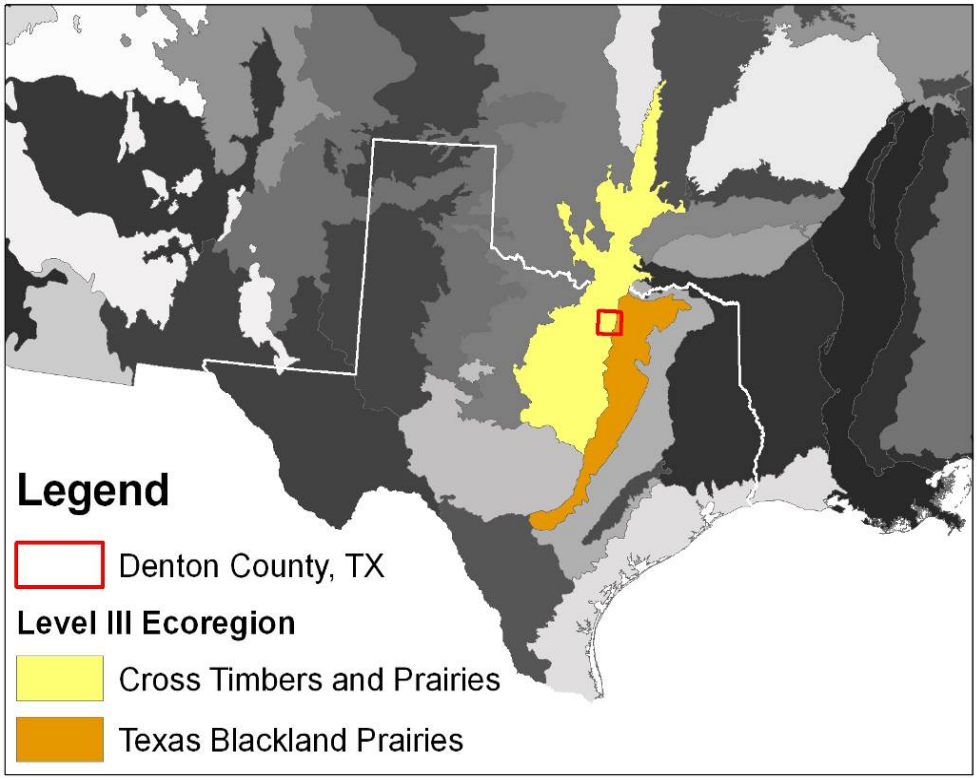

Figure 3.3. Denton County within its level III ecoregions. At the Level III Ecoregion scale, Denton County is split between the Cross Timbers and Prairies ecoregion and the Texas Blackland Prairies ecoregion. Grasslands historically dominated the Texas Blackland Prairies vegetation, and the Cross Timbers and Prairies was a mix of grasslands and post oak dominated woodlands and savannas. These two ecoregions are a part of the Prairie and Parkland ecological province. The ecoregion base map is from the EPA (Griffith et al., 2004).

At Level IV of the ecological classification hierarchy, the western half of the county was in the Grand Prairie subregion of the Cross Timbers and Prairies, and a strip down the middle of the county ranging from 10 to 20 km wide belonged to the Eastern Cross Timbers subregion (Fig. 3.4; Griffith et al., 2004). Three natural vegetation types found in the county were tallgrass prairies, upland oak woodlands, and bottomland hardwood forest. The Cross Timbers have been often described as a post oak savanna ecosystem, and the original character likely was a mosaic of savannas, grasslands, oak thickets, and dense woodlands shaped by frequent fires on a landscape having a combination of fire-prone topographic features and natural fire barriers (Engle, 1997). At the time of this study, few undisturbed large tracts of Eastern

Cross Timbers vegetation remained, and more suitable land had been cleared for pasture, cropland, and in recent decades rapid development. This together with wildfire suppression have resulted in the remaining natural wooded Cross Timbers vegetation in Denton County to be small and more like oak thickets or dense woodlands than open savannas. The upland areas of the Grand Prairie ecoregion part of Denton County have been characterized as naturally developing into grasslands and having deep, dark clayey soils overlying calcareous clay, marl, and limestone (Ford & Pauls, 1980).

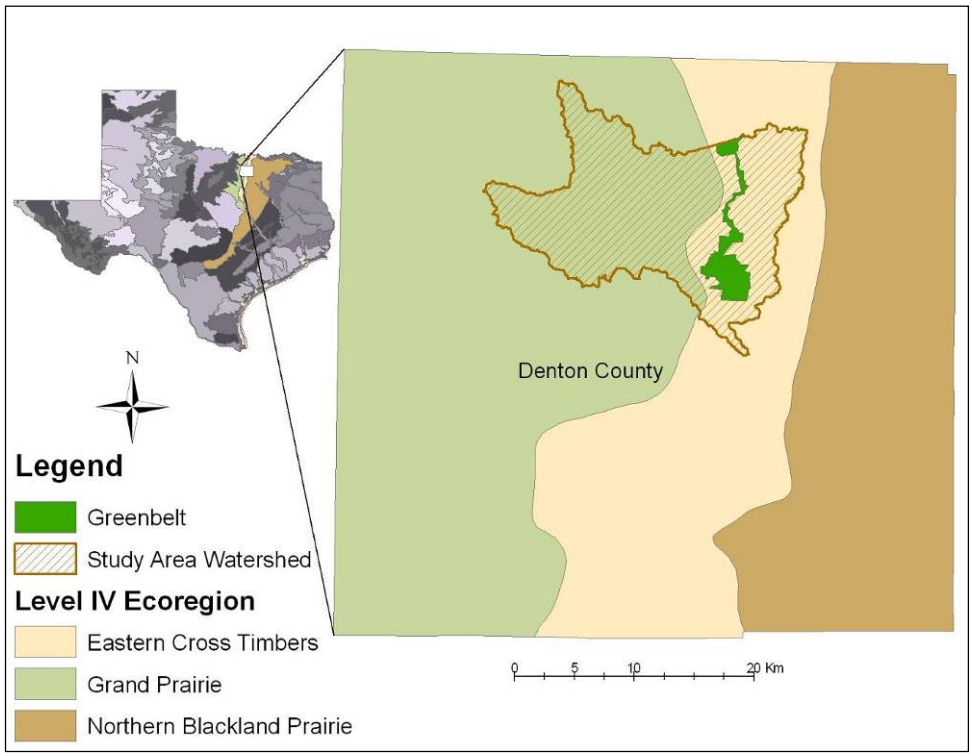

Figure 3.4. The study area within Texas ecoregions. The Greenbelt lies within the Eastern Cross Timbers Level IV ecoregion. While primarily a floodplain of the Elm Fork Trinity River, bottomland hardwood forest, wet shrubland, upland oak forest, and upland prairie vegetation types can all be found within the Greenbelt. The study area watershed is within both the Grand Prairie and Eastern Cross Timbers ecoregions. The ecoregion base map is from the Environmental Protection Agency (Griffith et al., 2004).

Topography was mostly level with some moderately steep slopes. The Cross Timbers ecoregion consisted of upland areas having deep sandy loam to shallow, rocky, sandy loam soils with clayey lower layers and sandstone bedrock. The topography was rolling

with some steep slopes. Bottomland hardwood forests occurred along the floodplains of rivers and creeks with soils of deep clay or silty clay to sandy loam, with nearly level topography.

The study area watershed was over 28,000 ha lying within the Grand Prairie and Eastern Cross Timber ecoregions. The Greenbelt was just under 2000 ha and was contained within the Eastern Cross Timbers; however, all three vegetation types were present. Much of the Greenbelt was within the floodplain of the Elm Fork Trinity River, and approximately 500 ha of it consisted of bottomland hardwood forest (Barry, 2000). While much smaller in area, the Greenbelt also contained areas of upland oak forest and upland prairie. Most of the remaining Greenbelt consisted of frequently flooded shrubland used as part of the flood control pool for Lake Lewisville and an old-field that was converting back to either forest or prairie. Not long ago much of the Greenbelt was privately owned and was used for grazing and crops. In the 1980s, prior to the construction of Ray Roberts Lake, the U.S. Army Corps of Engineers began purchasing the land to manage lake levels and flood control for Ray Roberts and Lewisville Lakes. At the time of this study, the Texas Parks and Wildlife Department managed the land, and the areas once used for agriculture were returning to a natural vegetation cover. In addition to flood control, the Greenbelt was used for recreation such as canoeing and trails for walking, bicycling, and horseback riding. Some parts of the Greenbelt were still grazed by cattle coming from adjacent private land.

CHAPTER 4

LANDSCAPE TERRAIN TYPES

A primary objective of this research was to develop a method of partitioning the study area into smaller terrain type units that were suitable for FACETA parameterization and simulation. Topographic parameters for slope and upstream catchment area were added to FACETA to incorporate the effects of the flow of water across the landscape onto simulated plots. This movement of water, together with soil conditions that influenced the storage of water, differentiated upland positions from hardwood forest development in the bottomland positions. The most important factor for differences in vegetation types within the upland areas of the Cross Timbers and Prairies ecoregion was the soil type. Oak woodlands or savannas were found on sandy upland sites, while grasslands occur on clayey upland soils. Therefore, the terrain features considered for partitioning the landscape were topographic position, represented by upstream catchment area and slope, and soil type.

Methods: Soils and Terrain Types

A soil survey of Denton County, TX, provided by the U.S. Department of Agriculture's Soil Conservation Service, together with its current electronic version available from the Natural Resources Conservation Service (NRCS), formed the basis of soil information in the study area (Ford & Pauls, 1980; NRCS, 2006). The system used to classify soils had six hierarchical categories. Soil order was the broadest category, which differentiated the dominant soil formation processes and the degree of formation. Soil series, which consisted of soils having similar soil horizons in their profile, was the finest category. Since FACETA required soil parameters for depth,

fertility, infiltration rates, and hydraulic properties, the soil series classification level was used to differentiate between soil types in the study area. The soil survey map was used in defining terrain type boundaries within the study area. Denton County soil data were prepared from an Order II soil survey and mapped at a scale of 1:24000. Using this level of soil survey data to derive hydraulic properties for hydrological modeling may have produced unrealistic soil moisture pattern results (Lin et al., 2006). Therefore, some locations within the study area were parameterized using higher fidelity soil core data collected from within the Greenbelt. Soil core data were collected from different topographic and soil conditions within the Greenbelt in a study by Rijal (2011) which looked at relationships between topography, soil, and forest development. Both the derived soil parameters and model results for the high fidelity plots were compared with the corresponding information derived from the Denton County soil survey. Soil model parameters are discussed in Chapter 6.

Results: Soils and Terrain Types

There were 44 different soil map types within the study area watershed (Fig. 4.1). Soil map type as used here was not the same as a soil series. While most map types in the Denton County soil survey represented a single soil series, some map types were complexes of two or more soil series contained within an area too small for the scale of the soil survey map to represent individually. For example, a soil map polygon labeled as Birome-Aubrey-Rayex complex may have consisted of soils classified in all three of these soil series. Other map types were associations of two or more soil series, where the soils were grouped together because the present or anticipated land use made it impractical or unnecessary to map them separately. Still other map types were

undifferentiated groups of two or more soil series that were not separated because the soil properties for the anticipated land use were considered similar enough not to require separation. Other map types, such as water and arents, did not represent a soil series at all.

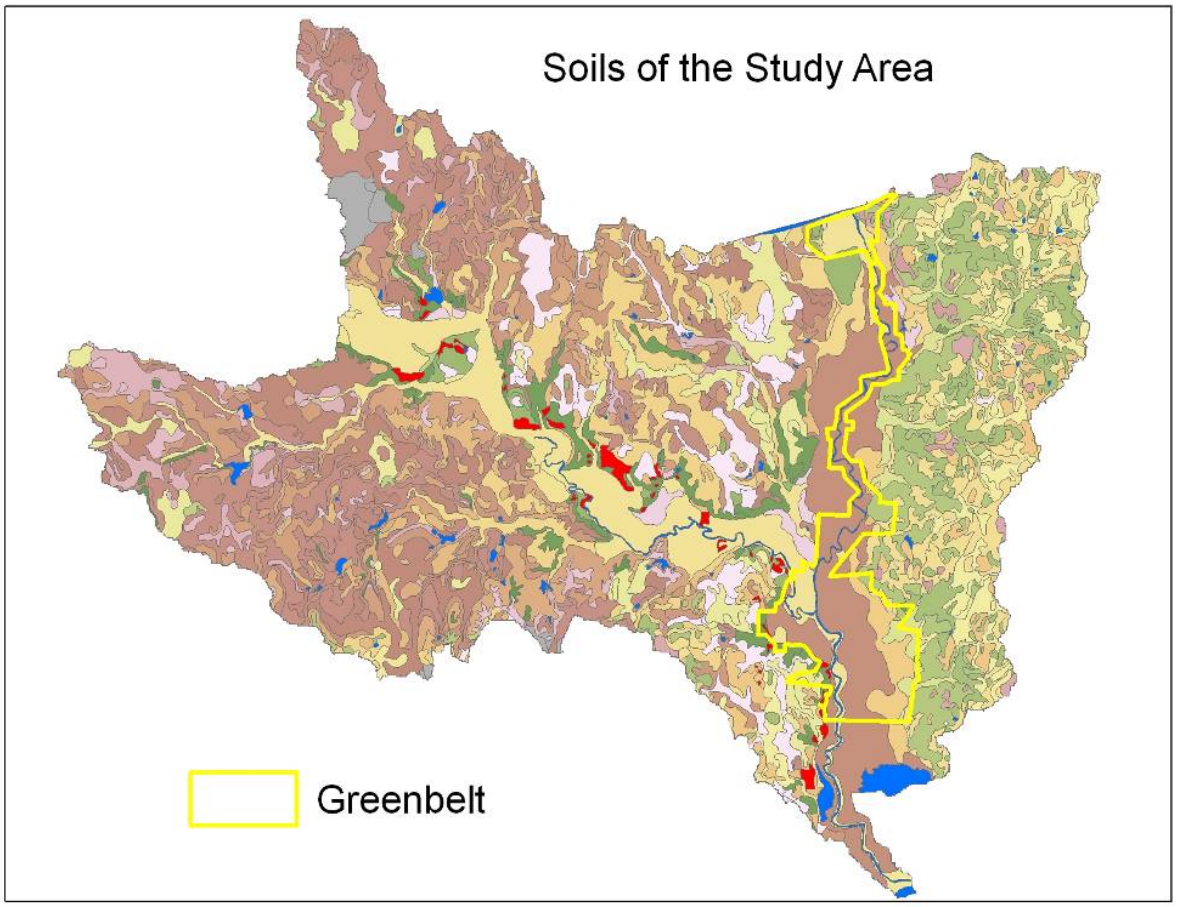

Figure 4.1. Soils of the **s**tudy **a**rea **s**ub-watershed**.** There were 44 soil map types indicated in the study area, but some such as *Arents* (colored red) and *water* (blue) do not represent a soil series. The urban land complexes (gray) were soils with substantial urban development and were not appropriate terrain for FACETA simulation. The soil base map was from the NRCS **(**2006).

Arents were soils that had been deeply disturbed by plowing, mining, or other human activity, and thereby were variable in physical characteristics and did not possess a diagnostic horizon. A more descriptive name used by some is anthroposols, but arents is the official term used in the U.S. soil taxonomic system. Arents found within the Greenbelt were primarily former sand and gravel pits. There were also soil map types

classified as urban land complexes. These areas comprised one or more soil series that had a concentration of human development on the surface. At its most detailed level, the Denton County soil survey partitioned these soil map type polygons into smaller polygons defined by a combination of a map type and a range of slopes. For example, a map unit labeled *Altoga silty clay, 5% to 8% slopes* consisted of soils classified in the Altoga series with surface slopes ranging from 5% to 8%. The Altoga series was also grouped into other slope ranges of 3% to 5% and 5% to 12%. For this study, all soils of the same type were grouped together, regardless of the slope range. The reasons for this were twofold: (a) The detail level needed to parameterize the FACETA soil survey did not give any different information about the soil types in different slope ranges, and (b) slope was already used in FACETA as a topographic parameter that was determined from digital elevation data.

In this research, FACETA simulations were limited to terrain types found within the Greenbelt, so those soils found within its boundaries were given focus. The Greenbelt contained 21 different soil map types, including water, Arents, an undifferentiated group, and a soil complex (Fig. 4.2). Areas of water and arents were not considered for FACETA simulation. Areas identified as arents within the Greenbelt were in fact becoming reforested; however, the Denton County soil survey did not have any soil property information for these areas, so it was not possible to determine FACETA parameters from it.

Soil complexes, associations, and undifferentiated groups contained mixtures of soil series, and each generated different FACETA parameters if considered separately. In this case, that was determined to be unnecessary.

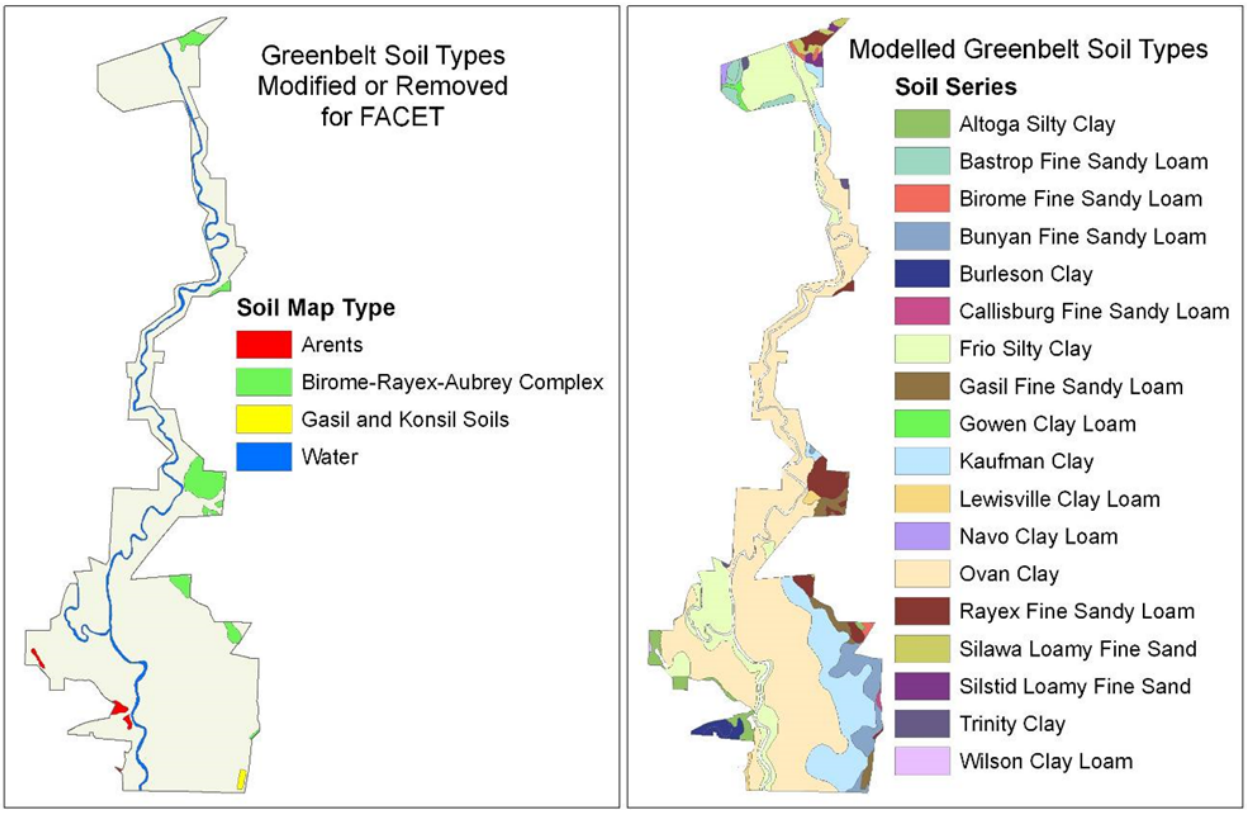

Figure 4.2. Soil types of the Greenbelt corridor. Soil types were identified using the USDA soil survey. Identified categories within the Greenbelt corridor included 21 soil map types, including water. Water and Arents were omitted, the Gasil and Konsil group was lumped together with Gasil, and the Birome-Rayex-Aubrey Complex was parameterized as Rayex, leaving 18 soil types for FACET simulation. The soil base map was from the NRCS (2006).

The Greenbelt contained one small, approximately 3.5-ha area of the Gasil and Konsil soils undifferentiated group. In general, soils belonging to an undifferentiated group had similar properties. This particular area of Gasil and Konsil soils was adjacent to and downslope of a larger area of Gasil soils and was not adjacent to any Konsil soils; therefore, it was lumped with and parameterized as Gasil. No other areas of only Konsil soils occurred within the Greenbelt. The soil complex found within the Greenbelt was Birome-Rayex-Aubrey. This complex was described as typically being composed of roughly equal parts of each of the three soil series, with the soils so intricately mixed making separation impractical at the scale mapped. They occurred on sandstone outcrops with Rayex developing on convex benches, with Aubrey forming above and

Birome forming below the Rayex. Rayex was rockier than either Birome or Aubrey and was shallow, while Birome and Aubrey were both moderately deep. The largest Birome-Rayex-Aubrey polygon within the Greenbelt was in a sandstone hill area locally referred to as Wildcat Hill. Much of this hill area was quite rocky. As part of a soil-forest survey done in 2007, an attempt to sample a soil core using an auger was made at several different spots on the top of Wildcat Hill, but due to the amount rocks in the soil, no core was removed. Within this same soil map polygon but on the slope towards the bottom of Wildcat Hill, a soil core was successfully removed. At this site, the soil was much less rocky and deeper, with gravel appearing at about 1.5 m depth. Of the three soil series, the area on the top of the hill best fit the description of Rayex, while on the slope where a core was removed the soil was more like Birome. There were several other polygons of Birome-Rayex-Aubrey complex within the Greenbelt, but they were all much smaller and were not field surveyed for this research. Because of the seemingly rocky and shallow nature of much of the largest polygon, the entire complex was treated as Rayex soils. However, as seen in the differences between the soil on top of Wildcat Hill and towards the bottom of its slope, there was no doubt that areas within these Birome-Rayex-Aubrey complex polygons would more appropriately be treated as Birome or Aubrey. There were no polygons of pure Rayex or Aubrey soils within the Greenbelt, but there were some small areas of Birome soils. With this reassignment of the complex, two of the three soil series in the complex were still simulated in FACETA. The reassignments resulted in 18 soil series for which FACETA parameters were determined.

A large majority of the Greenbelt was covered with bottomland soils; however, the 18 soil series selected for FACETA parameterization represented the range of different soil types and associated vegetation covers found throughout the study area watershed. Together they made up approximately 55% of the total area of the watershed, and they included the soils of its larger floodplains as well as several upland post oak, savanna, and prairie grassland soil types (Fig. 4.3).

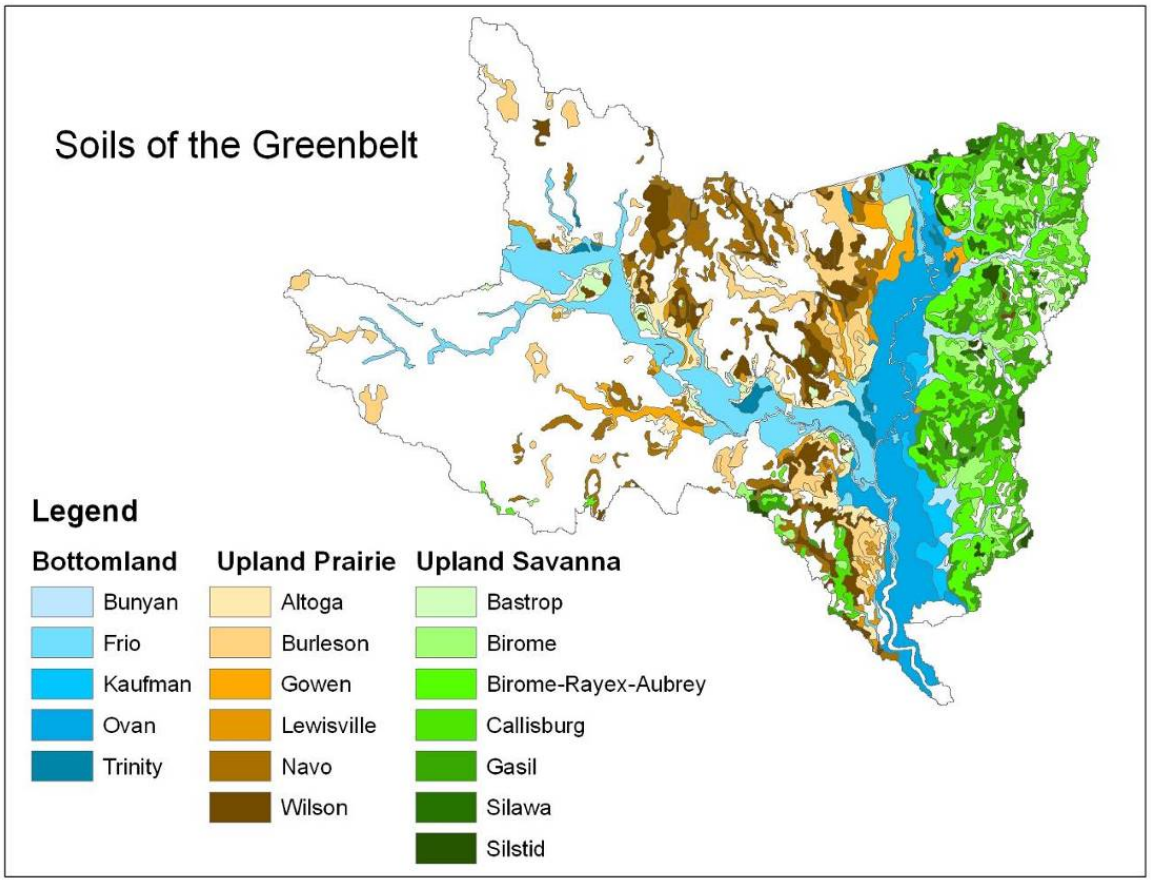

Figure 4.3. Soils of the Greenbelt. The 18 soil types selected for FACETA parameterization covered approximately 55% of the study area sub-watershed and were a good representation of all the different soil types it contains. The soil base map was from the NRCS, (2006).

A question that arose at this point was why parameterize a forest model for soil and topographic characteristics that in the real world were associated with prairie grasslands. Historically fire plays a large role on maintaining the prairie grasslands, and

in the absence of fire, the grasslands start to be taken over by certain tree species. Additionally, FACETA is not programmed to simulate grasses, only trees. If parameterized correctly, then FACETA simulations on these prairie terrain types should result in forests filled with small trees of species that are both drought tolerant and tolerant to clay soils. Some of the general properties of the soil series modeled in the Greenbelt are summarized in Table 4.1. Details of the FACETA parameters estimated from both the soil types described in the county soil survey as well as from the measurements made on soil cores sampled from the Greenbelt are discussed in the section on FACETA soil parameters in Chapter 6.

The digital version of the USDA's soil survey map for Denton County was used to delineate the soil component of the FACETA terrain types (USDA, 2010). With over 40 different USDA soil types found within the study area watershed, FACETA terrain type definition was limited to the 21 soil map units found within the Greenbelt. Most of these soil map units represented a single soil series, and the two map units that included groups of soil series were each interpreted to be one of the soil series in the group based on context of their locations within the Greenbelt. The two non-soil series map units, arents and water, were removed from the soil component of the FACETA terrain type map. With the restrictions, reassignments, and removals, 18 different USDA soil series were used in defining terrain types and estimating model parameters. These 18 soil series together made up approximately 55% of the study area watershed and fully represented soils associated with all three of the Cross Timbers vegetation cover types–sandy upland post oak woodlands, clayey upland grasslands, and alluvial soils that produced bottomland hardwood forests.

Table 4.1

Characteristics of Soils in the Greenbelt

Soil Series	General Description	Topography	Ecological Site Name; Historic Climax Plant Community
Altoga silty clay (Al)	Deep soils on upland prairies	Sloping to strongly sloping, on old, high terraces of major streams	CLAY LOAM 28-40'' PZ; Fire-influence tallgrass prairie sparsely interspersed with pecan, hackberry, elm, oak, sumac
Bastrop fine sandy loam (Ba)	Deep loamy soils on upland savannas	Gently sloping, on high stream terraces above flood plains of major streams	SANDY LOAM 32-40'' PZ; Post oak, blackjack oak savanna
Birome fine sandy loam (Bi)	Moderately deep soils on upland savannas	Gently sloping, on convex ridges and lower side slopes	SANDY LOAM 32-40'' PZ; Post oak, blackjack oak savanna
Bunyan fine sandy loam (Bun)	Deep soils on bottomlands	Nearly level, on narrow floodplains of streams draining sandy and loamy soils	LOAMY BOTTOMLAND 32-40'' PZ; No plant community data available
Burleson clay (Bur)	Deep soils on upland prairies	Nearly level to gently sloping, on ancient upland terraces, edges of terraces and valley fills	BLACKLAND 28-40'' PZ; Fire-influence tallgrass prairie interspersed with occasional forbs and woody species
Callisburg fine sandy loam (Ca)	Deep soils on upland savannas	Gently sloping, on sides of ridges, foot slopes and valley fills of uplands	SANDY LOAM 32-40'' PZ; Post oak, blackjack oak savanna
Frio silty clay (Fr)	Deep soils on bottomlands	Nearly level, on floodplains of major streams	LOAMY BOTTOMLAND 30-38'' PZ; Fire-influenced tallgrass prairie with few shrubs and trees
Gasil fine sandy loam (Ga)	Deep soils on upland savannas	Gently sloping to sloping, on convex ridges and side slopes	SANDY LOAM 32-40'' PZ; Post oak, blackjack oak savanna
Gowen clay loam (Go)	Deep soils on bottomlands	Nearly level, on floodplains of major streams	LOAMY BOTTOMLAND 30-38'' PZ; Fire-influenced tallgrass prairie with few shrubs and trees
Kaufman clay (Ka)	Deep soils on bottomlands	Gently sloping, on plane to convex high terraces of major streams	CLAY LOAM 30-38" PZ; Fire-influenced tallgrass prairie with very few shrubs and trees

(table continues)

Table 4.1 *(continued)*

Soil Series	General Description	Topography	Ecological Site Name; Historic Climax Plant Community
Lewisville clay loam (Le)	Deep soils on upland prairies	Nearly level, on outer edges of floodplains of major streams draining from clayey areas	CLAYEY BOTTOMLAND 28-40'' PZ; Fire-influenced tallgrass/hardwood savanna interspersed with occasional forbs, dense woodlands in the absence of fire
Navo clay loam (Na)	Deep soils on upland prairies	Nearly level to gently sloping, in valley fills, terraces, and on side slopes along and above drains and low hills	CLAYPAN PRAIRIE 28-40" PZ; Fire-influence tallgrass prairie interspersed with occasional forbs and woody species
Ovan clay (Ov)	Deep soils on bottomlands	Nearly level, on floodplains of major streams	CLAYEY BOTTOMLAND 28-40'' PZ; Fire-influenced tallgrass/hardwood savanna interspersed with occasional forbs, dense woodlands in the absence of fire
Rayex fine sandy loam	Shallow soils on upland savannas	Gently sloping to moderately steep, on convex benches of sandstone outcrops	SANDSTONE HILL 32-40''; Savanna
Silawa loamy fine sand (Sila)	Deep soils on upland savannas	Gently sloping, on high convex ridges	LOAMY SAND 32-40" PZ; Post oak, blackjack oak savanna
Silstid loamy fine sand (Sils)	Deep soils on upland savannas	Gently sloping, on gently undulating ridges and sides of ridges	SANDY 32-40" PZ; Post oak, blackjack oak savanna
Trinity clay (Tr)	Deep soils on bottomlands	Nearly level, on low floodplains of major streams	CLAYEY BOTTOMLAND 28-40'' PZ; Fire-influenced tallgrass/hardwood savanna interspersed with occasional forbs, dense woodlands in the absence of fire
Wilson clay loam (Wi)	Deep soils on upland prairies	Nearly level to gently sloping, on low part of landscape along drainage ways, in concave areas and side slopes	CLAYPAN PRAIRIE 28-40" PZ; Fire-influence tallgrass prairie interspersed with occasional forbs and woody species

Note. The table is derived from the hardcopy soil survey (Ford & Pauls, 1980), the Soil Survey Geographic database SSURGO (NRCS, 2010) and the Web Soil Survey (NRCS, 2012). The "ecological site" classification system has replaced the "range site" system used in the 1980 soil survey. Ecological site descriptions are not all complete (e.g., LOAMY BOTTOMLAND 32-40'' PZ, SANDSTONE HILL 32-40'' PZ), and information on them differs some between the various soil survey resources. Ecological sites are defined by soil and physical characteristics that produce distinctive vegetation patterns and disturbance responses. Vegetation patterns are thought of as dynamic with various states and transitions between them. In contrast, the range site system characterized sites as a single climax vegetation community with a focus on grazing. Ecological site names are formal, and in the case of Texas, the naming format includes a soil description and annual precipitation range ("PZ" stands for precipitation

zone). The 2- to 4-letter abbreviations in parentheses after the soil series names are used to identify soil series in the graph in Fig. 4.40.

Methods: Topographic Position and Terrain Types

Topographic position was the second component of defining terrain types for FACETA. The topographic parameters used by FACETA were elevation, aspect, slope, and flow accumulation. Flow accumulation, a geographic information systems (GIS) calculation that counts the number of upstream cells in a raster elevation map that drains onto a cell, was used to calculate the upslope contributing area. Specific catchment area was a topographic measurement defined to be the area of land upslope of a width of a contour line, divided by that contour width. With digital elevation data in a raster format of grid cells rather than contour lines, the specific catchment area for any one cell was calculated as its upslope contributing area divided by the width of the grid cell. Flow accumulation was dependent on the flow direction output, and subsequently the specific catchment area depended on flow direction. Therefore, the results for specific catchment area and the topographic wetness index (TWI) were dependent on the choice of algorithm used to determine the flow direction. A digital elevation model (DEM) was a GIS-ready digital grid of cells representing the topography of an area of land, with the value assigned to each cell representing the elevation at the center of the cell. DEMs determine values for slope, aspect, flow accumulation, and many other topographic parameters. This section discusses how DEMs of the study area were used to determine the topographic characteristics that, together with soil types, defined the landscape terrain types. Determining the parameter values for the terrain types used in the forest model is discussed in Chapter 6 in the section on FACETA landscape and terrain parameters.

Elevation can impact floristic composition through its effect on temperature and rainfall, and impacts can be dramatic in mountainous terrain. In this study area, the highest and lowest points were 247 m and 155 m above sea level, respectively. With a total difference of less than 100 m, elevation was not considered a factor in species composition within the study area, and therefore was not used in the determination of terrain types. Aspect can play an important role in species composition in hilly terrains where differences in aspect lead to differences in insulation, shading, or rainfall. However, the terrain of much of the study area was generally flat, and it was located at approximately 33.2º N latitude, which was not high enough for aspect to become a large factor in insulation. Thus, for this research aspect was not assumed to have a significant effect on species composition and therefore was not considered in terrain type definition. Both topographic parameters were still required as input for FACETA, but they remained constant for the simulation of all terrain types.

The two other topographic parameters required by FACETA were slope and flow accumulation. One possible approach to partitioning the landscape into terrain types that used both of these topographic parameters was to use combinations of different slope classes, flow accumulation classes, and soil types. Using this approach for the Greenbelt, with the landscape partitioned into only three slope classes and three flow accumulation classes, would result in possibly as many as 3 x 3 x 18 = 162 different terrain types. In addition to the large number of terrain types the three factors yielded, there were problems using flow accumulation to categorize the landscape. Flow accumulation by itself and likewise specific catchment area would work well for delineating stream networks but not so well for predicting soil moisture patterns.

Different versions of TWI, which combined some quantification of run-on potential together with accumulation or runoff potential, correlate with soil moisture and vegetation patterns, albeit with varying strengths depending on the landscape, elevation data, topographic index, and the computer algorithm used to generate it. The approach taken in this research used TWI together with the soil series to partition the landscape into different terrain types.

Results: Topographic Position and Terrain Types

Topographic terrain analysis using GIS was a multi-step process that started with a DEM. A DEM could be derived from a variety of sources such as aerial photographs, contour maps, and light detection and ranging (LiDAR). Regardless of what kind of terrain analysis was to be done on a DEM, there were some initial processing steps required. Once the DEM was processed, it could be analyzed for slope, flow accumulation, or any other topographic feature or measurement. In this research, the final product of the terrain analysis was TWI. The results of the topographic terrain analysis are described for each of the steps of DEM processing.

Digital Elevation Model

All topographic analysis starts with a base DEM. Both the source data for deriving a DEM and the grid resolution can impact the accuracy and the output from the calculations of topographic indices. This research examined DEMs with three different grid resolutions, derived from two different sources. Two DEMs, a national elevation dataset (NED) 1 arc second and a NED $^1/_3$ arc second, were downloaded from the United States Geological Survey (USGS, n.d.) National Map Seamless Data Distribution

System. Both were derived from cartographic contours. The seamless system was retired in July 2012, and the NED was transferred to the National Map Viewer system.

The NED is assembled by the USGS from a variety of source DEMs and is updated on a bimonthly basis. At each update cycle, the *best available* DEMS are pieced together to obtain national coverage, where best available is described as being the most detailed and current data that can be freely distributed. The grid size in meters is a little less than 29 m for the 1 arc second and 10 m for the $^{1}/_{3}$ arc second DEMs, respectively. Vertical accuracy is required to be within +/- 7 to 15 meters for the 29-m DEM, and +/- 7 meters for the 10-m DEM; however, the actual accuracy varies with the source DEM (USGS, n.d.). While the 10-m DEM has better vertical accuracy *specifications* than the 29-m DEM, it is not clear how much more accurate, if at all, it is. When comparing the two sources, more than 90% of the cells differ by less than 1 meter, the median difference is approximately 13 cm, and the mean difference is just under 29 cm. Additionally, it must be kept in mind that elevation can change over a 30-m horizontal distance, or even over a 10-m distance, so it is difficult to say just exactly what vertical accuracy means.

LiDAR-derived DEMs have yielded better results regardless of grid resolution (Vaze et al., 2010). Three LiDAR-derived DEMs were examined and compared to those derived from cartographic contours. All three DEMs were derived from the same LiDAR dataset, but with different grid resolutions: approximately 29 m, 10 m, and 5 m. The exact grid resolutions for all of these DEMs, both the LiDAR-derived and the contour-derived ones from the NED, were actually a little smaller than the rounded whole numbers just stated. For example, the grid resolution for the NED 29-m DEM was

actually 28.75 m, and it was 28.79 m for the LiDAR-derived DEM. The grid resolutions of the two DEMs from the NED were already set in the downloaded product. For simplicity, the resolutions were referred to by the rounded up whole numbers. The grid resolutions of the 10-m and 29-m LiDAR-derived DEMs were set to match the two corresponding contour derived resolutions; however, the final grid sizes differed slightly. With differences of less than 1%, further resampling to force the grid sizes to match exactly was determined unnecessary. The point spacing of this LiDAR data, where point spacing was the average horizontal resolution of the LiDAR data points, was between 0.5 m and 1 m. The grid resolution used in relationship to the LiDAR point spacing was important. If the cell size were too small, there would be cells containing no measured elevation points resulting in holes of missing data within the DEM. This could potentially be rectified through interpolation, but that would introduce more uncertainty and error. However, larger grid sizes may contain multiple measured elevation points, with the number of points increasing with cell size, and the result would be a loss of detail through the averaging of those multiple points. A good guideline followed for minimum grid size when converting LiDAR data to a DEM was multiplying the cell width by four times the point spacing. Since portions of the LiDAR dataset used had an average point spacing of 1 m, the grid size should have been no smaller than 4 m by that guideline.

Vertical accuracy of 1 m LiDAR data is typically within 10 cm; however, once the LiDAR data are converted to the grid format of a DEM, accuracy can again become questionable. Elevation can change by more than 10 cm over even small horizontal distances. While it may seem on the surface obvious that a finer grid resolution would yield better results, this may not always be the case. For some applications, a coarser

resolution may perform better (Zhang et al., 2009). The most appropriate grid resolution depends on the complexity of the topography and the spatial scale of the processes of interest. Another issue related to grid resolution is resampling. Resampling refers to the process of creating a new grid from an existing one, often to increase or decrease the grid resolution or when performing map algebra with two grids. There are multiple methods for resampling grid data; e.g., nearest neighbor or bilinear interpolation. In the case of continuous data such as elevation, some resampling methods result in a smoother surface while others reveal artifacts such as periodic lines. Resampling was required in this research for converting LiDAR point data into an elevation grid. A 10-m resolution, all five contour-derived DEMs obtained from NED appeared the same, and from a broad perspective, there was little difference between them (Fig. 4.4).

When comparing distributions of elevations, the three LiDAR-derived DEMs were nearly identical. Since all three LiDAR DEMs were derived from the same data source, that was expected. The distributions of elevations of the two contour-derived DEMs were also very similar to each other. They may also have been derived from the same source data; however, it was not possible to determine that from the information provided through the NED. The distributions of elevation values of the contour-derived DEMs differed a little from those of the LiDAR-derived DEMs (Fig. 4.5).

Summary statistics of elevation values from the five base DEMs are given in Table 4.2. The contour-derived DEMs had a larger range of elevation values than the LiDAR-derived DEMs, including having substantially smaller minimum and slightly higher maximum values. There was very little difference in quartile values between the three LiDAR DEMs or the two contour-derived DEMs.

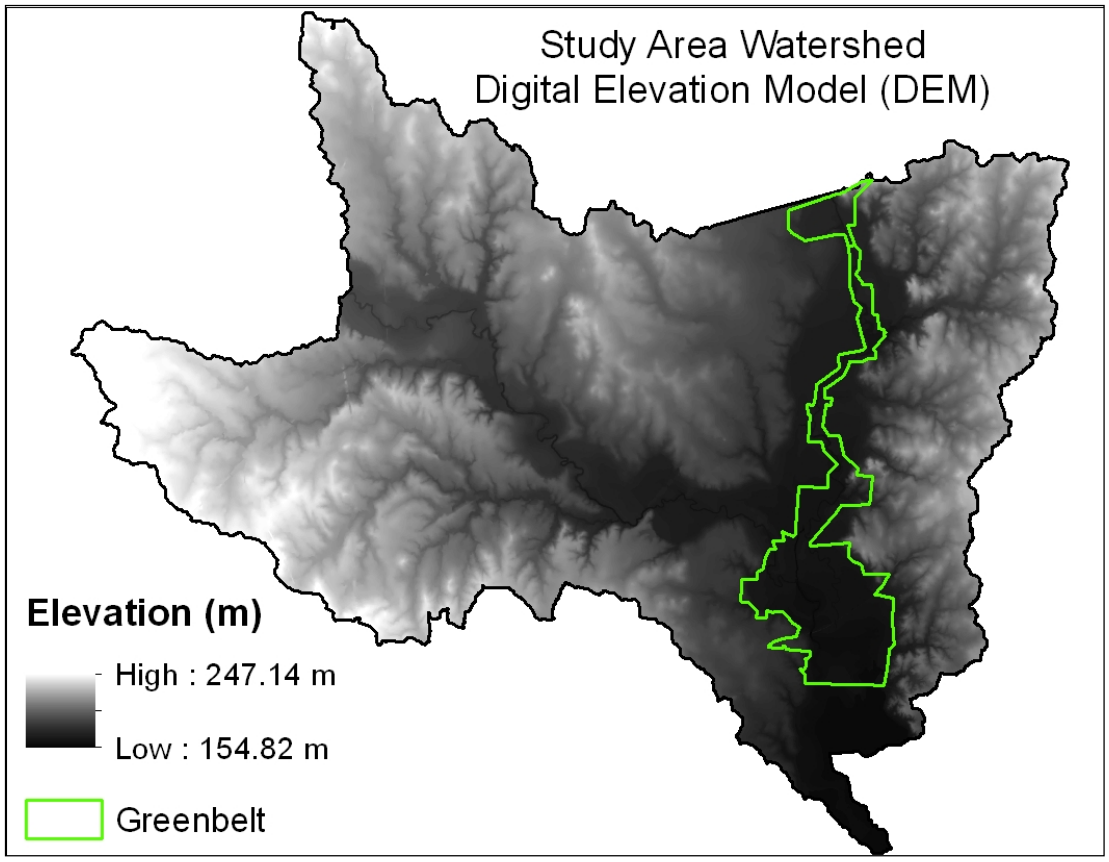

Figure 4.4. DEM of study area watershed. Elevations of a continuous surface are represented by square grid cells, or pixels, with value of each cell representing the elevation of the land contained in it. The cell value is typically interpreted as the elevation of the center of the cell; however, depending on how the data was generated, that may not be the case. This particular DEM has grid cells with a 10 m horizontal resolution, and was derived from cartographic contours and obtained from the NED.

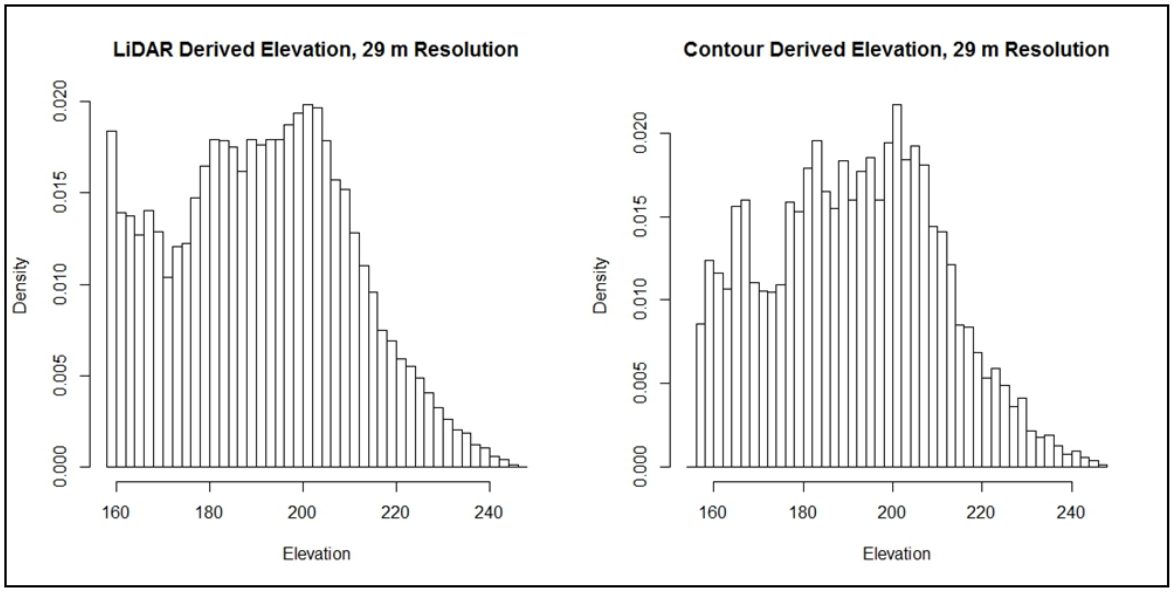

Figure 4.5. Distribution of elevations for LiDAR and contour-derived DEMs. Histograms of elevation values differed slightly between the contour- and LiDAR-derived DEMs, with the LiDAR DEMs having a

smaller range in elevation values and a larger proportion of its cells with lower elevations. These examples were from the two 29-m resolution DEMs, but there was little difference in the distributions between the different grid sizes within the same DEM source.

Table 4.2

Summary Statistics of the Elevations from the Five Base DEMs

DEM Source	Grid Size (meters)	Five Number Summary of Elevations					Average Elevation
		Min.	1st Qu.	Median	3rd Qu.	Max.	
LiDAR	5	158.0	176.7	191.3	204.6	246.8	191.1
LiDAR	10	158.1	176.7	191.3	204.6	246.7	191.1
LiDAR	29	158.3	176.7	191.3	204.6	246.6	191.1
Contour	10	154.8	176.9	191.7	204.9	247.2	191.3
Contour	29	155.5	177.0	191.7	204.9	247.2	191.3

Note. Five number summary and average elevation values from the five different base DEMs: LiDAR-derived with 5-m, 10-m, and 29-m grid resolutions, and contour-derived with 10-m and 29-m grid resolutions. There is very little difference in the distributions of the three LiDAR-derived DEMs, and very little difference between the two contour-derived DEMs. Elevations are in meters above mean sea level.

Filling Sinks

Terrain analysis with digital elevation data requires generating a series of new data grids, ultimately calculated or derived from the DEM. When doing hydrological analysis with the DEM, it must first undergo a procedure known as *filling the sinks* in order to create a depressionless DEM. Sinks in a DEM are any cell or group of cells out of which a hydrological flow direction cannot be calculated. Filling the sinks ensures that in the context of hydrological modeling with the DEM, water in any one cell will flow to another cell. Sinks within a DEM may be from errors in the data or artifacts from the derivation of the DEM. However, there are also true sinks in the real world (e.g., lakes, ponds, or depressions, which show up as sinks in a DEM). There are methods for selectively filling sinks to avoid filling true ones, but any sinks, whether real or from data errors, will prevent calculating flow direction for those cells. Almost all topographic and

hydrological calculations that can be done on a DEM require flow direction, so not filling sinks will result in incomplete grids and could potentially isolate portions of the grid.

The method for filling sinks in the DEMs used here was a flooding approach that raised the elevation of sink cells to the minimum elevation of the neighboring cells with an outflow direction. The specific algorithm, Pit Removal procedure implemented in the Terrain Analysis Using Digital Elevation Models (TauDEM) version 5.1.2 toolbox, was adapted from the Planchon-Darboux algorithm. Many different algorithms are available for filling sinks, but these were not compared or examined in this research. All base DEMs underwent the sink-filling process, and the filled DEMs were then used for all further terrain analysis. Since calculating flow direction was required before finding the sinks and comparing the output from two different flow direction algorithms was one of the research objectives, each of the depressionless DEMs was processed using the same flow direction algorithm that was used again later for the hydrologic terrain analysis (Fig. 4.6).

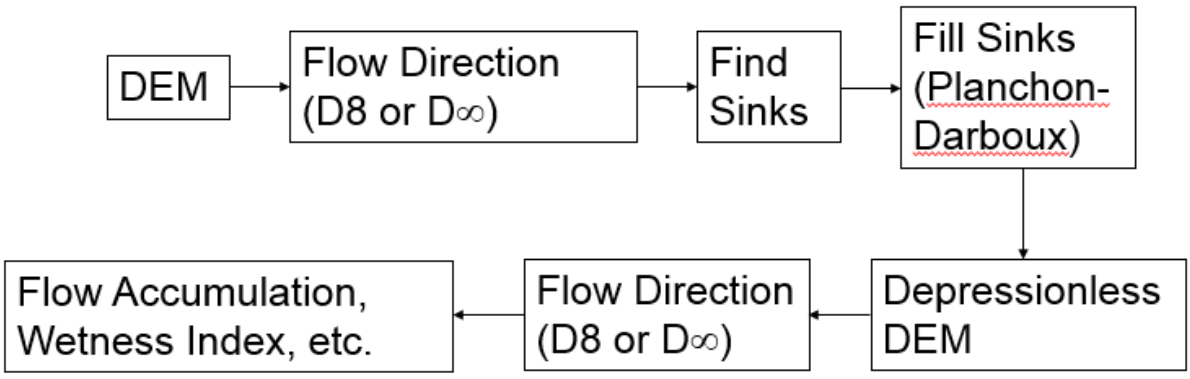

Figure 4.6. Flow for processing DEMs for terrain analysis. Prior to any hydrologic analysis of a DEM, the DEM is typically processed to fill in any depressions and ensure that hydrologic flow can be modeled throughout the DEM. While different algorithms and methods exist for generating a depressionless DEM, they all follow the same basic flow: Flow Direction is calculated, Sinks are found, and then Sinks are filled. The second flow direction grid calculated from the depressionless DEM is then used in further terrain analysis. In this research, the two flow direction algorithms used are D8 and D∞, and the sink filling method was adapted from the Planchon-Darboux algorithm, all as are implemented in the TauDEM version 5.1.2 toolbox.

Flow Direction

A flow direction grid, derived from a DEM, is a raster grid in which the value of each cell indicates the direction of water flow (i.e., which neighboring cell or cells that running surface water would move to). While the flow direction grid is not directly useful, it is an important precursor to all other hydrological GIS calculations and operations such as upslope contributing area and delineating stream networks, as well as any secondary calculations that rely on them such as the TWI. There are numerous algorithms for determining flow direction, all resulting in somewhat different outcomes. The choice of flow direction algorithm has been found to affect the performance of the wetness index in ecological applications (e.g., Kopecký and Čížková 2010). Performance may also depend upon the ecological application and characteristics of the terrain. Flow direction algorithms are broadly grouped into two categories: single-direction (SDF) and multi-direction (MDF). The number of directions refers to the number of different neighboring cells into which water could flow. Any cell has eight immediate neighboring cells, and an SDF algorithm restricts flow from any cell to only one of its neighbors (Fig. 4.7). Sometimes the MDF group of algorithms is split into two subgroups: bi-directional (BDF) algorithms, where the flow is restricted to no more than two neighboring cells, and true MDF algorithms.

This research examined two flow direction algorithms: deterministic-eight (D8) and deterministic-infinity (D∞; Fig. 4.8). The D8 algorithm was an SDF, was probably the most commonly used algorithm, and was the one implemented in the most popular commercial GIS software product. The *eight* in the name referred to the flow going to exactly one of the eight neighboring cells. The flow direction was towards the cell with

the steepest descent, which was calculated as the slope between the centers of the cells. The D∞ algorithm was an MDF, but with the flow from any cell limited to no more than two contiguous neighboring cells; more, specifically it was a BDF algorithm.

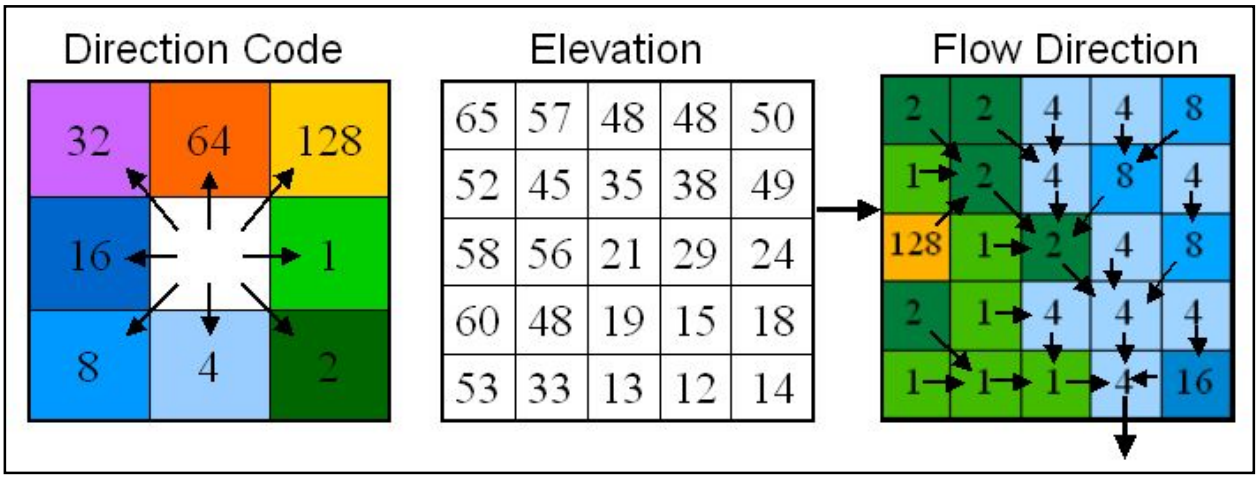

Figure 4.7. Single directional flow. SDF algorithms such as the deterministic 8 (D8) restrict flow from each cell to only one of its eight neighboring cells. This algorithm calculates the slope of the line segments connecting the centers of the cells and then assigns the flow direction to be in the direction of the steepest slope. *Left*: Numbers assigned to the eight different directions are successive powers of 2, starting with 2^0=1 towards the east direction and then going clockwise to 2^7=128 towards the northeast direction. *Center and right*: An example of an elevation grid and the resulting D8 flow direction grid.

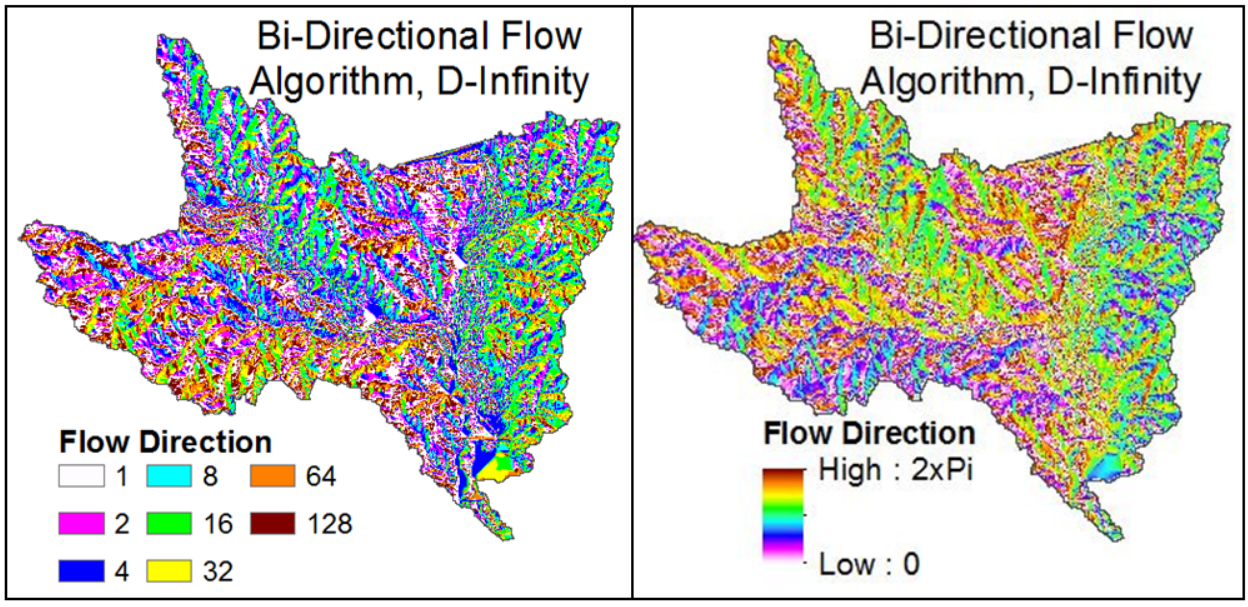

Figure 4.8. SDF and BDF flow directions. Results from two different flow direction algorithms: the SDF D8 algorithm (left) and the BDF D∞ algorithm (right). Differences in the flow direction results were carried over through all the remaining GIS hydrological calculations. Both these examples were calculated from the 29-m resolution LiDAR derived DEM.

Infinity referred to the infinite number of values between 0 and 2π the calculation can take on. The value represented the angle of the direction of steepest descent from the center of the cell. If the steepest descent line lay exactly on a cardinal or ordinal direction, then that line went into exactly one of the cell's immediate neighbors, and all of the flow was assigned to that one neighboring cell. Otherwise, the steepest descent line passed through exactly two of its neighbor cells, and the flow was assigned proportionately between these two adjacent cells, with the proportioning based on the angle. There are many other SDF and BDF algorithms, and there are MDF algorithms that allow for flow to as many as all eight adjacent cells. For example, a cell that represents the top of a hill could have flow that diverges down all sides of the hill, and some algorithms attempt to capture this. In this research, the DEMs were processed using the D8 and D∞ flow direction algorithms, and the impacts the algorithms had on the resulting grids were compared and analyzed to determine which of these two was most appropriate for application to FACETA terrain types.

Slope

Slope is a required input parameter for FACETA; however, in its current implementation, slope is not used by the model for hydrologic purposes. FACETA only uses the input for slope, together with aspect, in the solar radiation component of the model. Slope is of course important to hydrology and needs to play a role in the terrain analysis and in defining the FACETA terrain types. In order to incorporate slope into the hydrological and terrain aspects of FACETA, it is used in the calculation of the TWI, which is used in defining FACETA terrain types. Slope is one of the few topographic or hydrologic characteristics that can be calculated from a DEM without first filling the

sinks; however, in this case the slope grids were all calculated from the depressionless DEMs. Since filling the sinks required first determining a flow direction, each of the slope grids was associated with one of the two flow direction algorithms. Grid size and DEM source were the other two variables behind the different slope grids. The ranges and distributions of slope values generated from the different DEM grid resolutions, sources, and flow direction algorithms were compared (Table 4.3).

One expected trend that was apparent in the different slope calculations was that finer grid resolutions lead to higher slope values. This trend held true for every quartile when compared within a DEM source and a flow direction algorithm.

Table 4.3

Five Number Summaries of Slopes from Different DEMs

DEM Source	Grid Size (meters)	Flow Direction	Five Number Summary of Slopes (in %)				
			Min.	1st Qu.	Median	3rd Qu.	Max.
LiDAR	29	D8	0.00	0.92	1.99	3.73	38.37
LiDAR	29	D∞	0.00	0.92	2.08	4.00	49.91
Contour	29	D8	0.00	0.87	1.96	3.85	40.40
Contour	29	D∞	0.00	0.81	1.97	4.09	55.19
LiDAR	10	D8	0.00	1.03	2.23	4.34	65.15
LiDAR	10	D∞	0.00	0.99	2.29	4.57	71.25
Contour	10	D8	0.00	0.86	2.00	4.11	77.30
Contour	10	D∞	0.00	0.83	2.00	4.18	107.70
LiDAR	5	D8	0.00	1.07	2.35	4.67	81.30
LiDAR	5	D∞	0.00	1.03	2.42	4.90	138.04

Note: Five number summaries for slopes were derived from different DEM sources, grid resolutions and flow direction algorithms. While the distributions for all these slope grids were similar, they differed some at the largest slope values. General trends across these slope grids included finer grid resolutions leading to higher slope values, within a DEM source and a grid resolution the D∞ algorithm resulting in a larger maximum and third quartile values than the D8 algorithm, and within a grid size and a flow direction algorithm the contour-derived DEMs had higher maximum slopes than the LiDAR derived DEMs.

This result was expected because increasing the grid size had the effect of smoothing out the microtopography of elevation changes occurring within a grid cell. Smaller grid cells captured finer resolutions of microtopography, thereby capturing a larger range of slopes. Another trend when comparing a DEM source and a grid resolution was that the D∞ algorithm resulted in a larger maximum, third quartile, and in most cases median slope value than the D8 algorithm. Within a grid size and a flow direction algorithm, the contour-derived DEMs had higher maximum slopes than the LiDAR-derived DEMs; however, that trend did not hold true in general for the other quartiles (Fig. 4.9 and Fig. 4.10). At this broad perspective, the maps and distributions of the different slope variations looked similar with the main difference being the *tail* length of the histograms.

Two areas chosen within the study area visually examined slope differences from a closer perspective, with each area containing different topography (Fig. 4.10). Area A was in the uplands with hills and a large variation in slopes. A large part of the area was dominated by a hilltop, but it also included some smaller hills, the hillslope down to the Elm Fork Trinity River, and some smaller drainage channels from the hills down to the river. Area B was in the heart of the bottomland floodplain and was mostly flat. The larges slopes within area B occurred along the banks of the Elm Fork.

Examining area A closer revealed more differences in the various slope maps (Fig. 4.11; Fig. 4.13). Comparing the four contour-derived slopes with each other (Fig. 4.11), the D8 algorithm generated a smaller range of slopes and produced a smoother map with fewer contrasting differences in slopes.

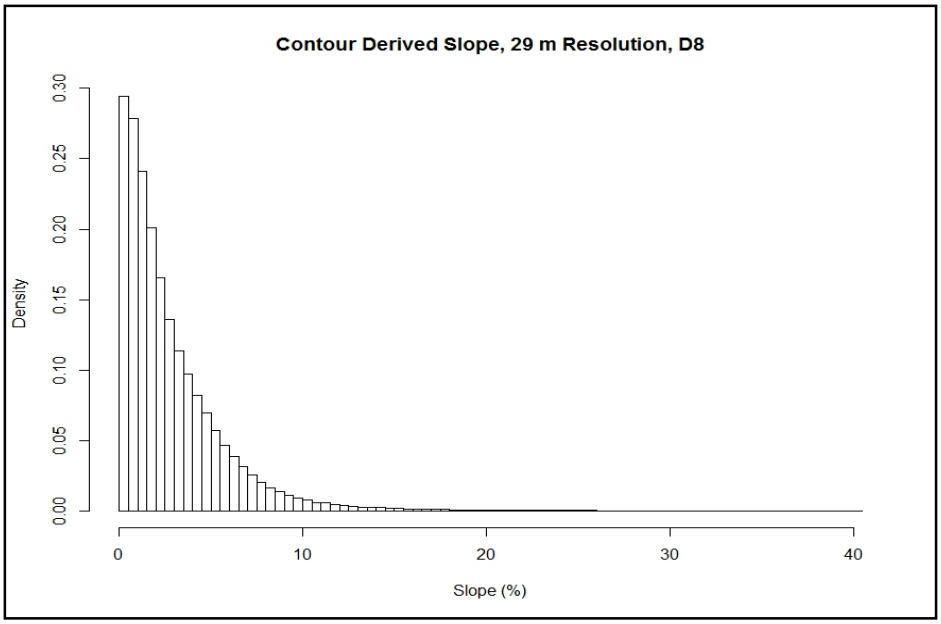

Figure 4.9 Greenbelt study area slope histogram. Distribution of slope values from the Greenbelt study area watershed as calculated from the contour-derived, 29-m resolution, D8 flow direction grid. The distribution for all the slope variants had similar shapes, with the only apparent difference being in the length of the tails of high slope values.

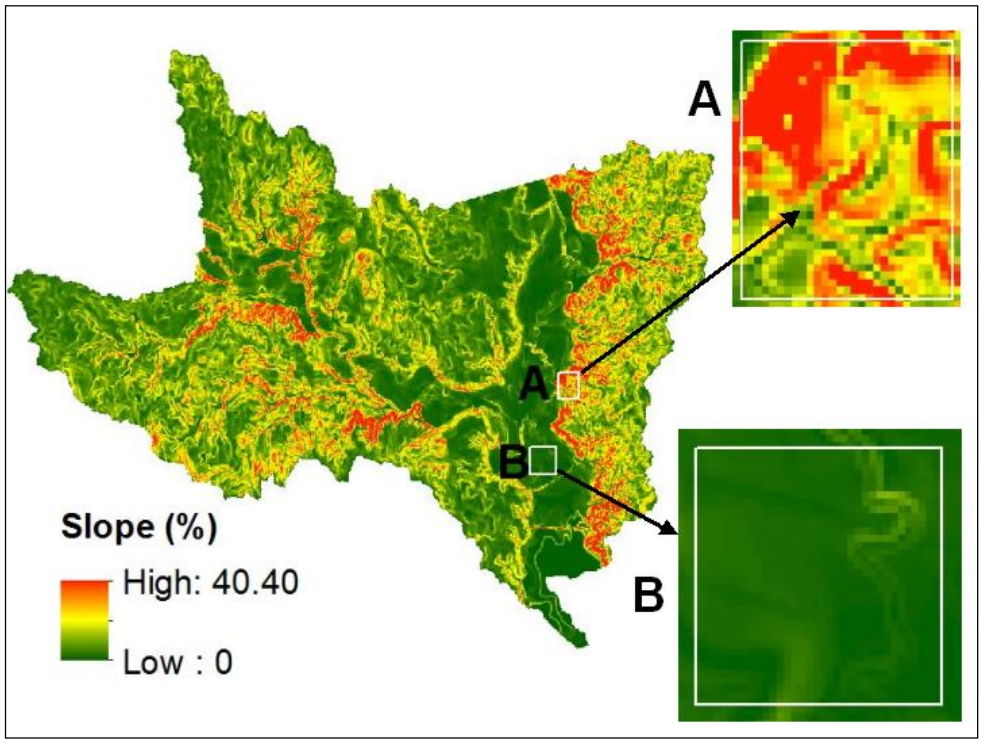

Figure 4.10. Greenbelt study area slopes. Slope map resulting from the 29 m, contour-derived DEM processed using the D8 flow direction algorithm. At this perspective, all slope maps and distributions looked similar, with the only apparent difference being the maximum slopes. Areas A and B were chosen to visually examine differences in the variants of slope more closely. Area A was in a hilly upland location, while area B was in the mostly flat floodplain.

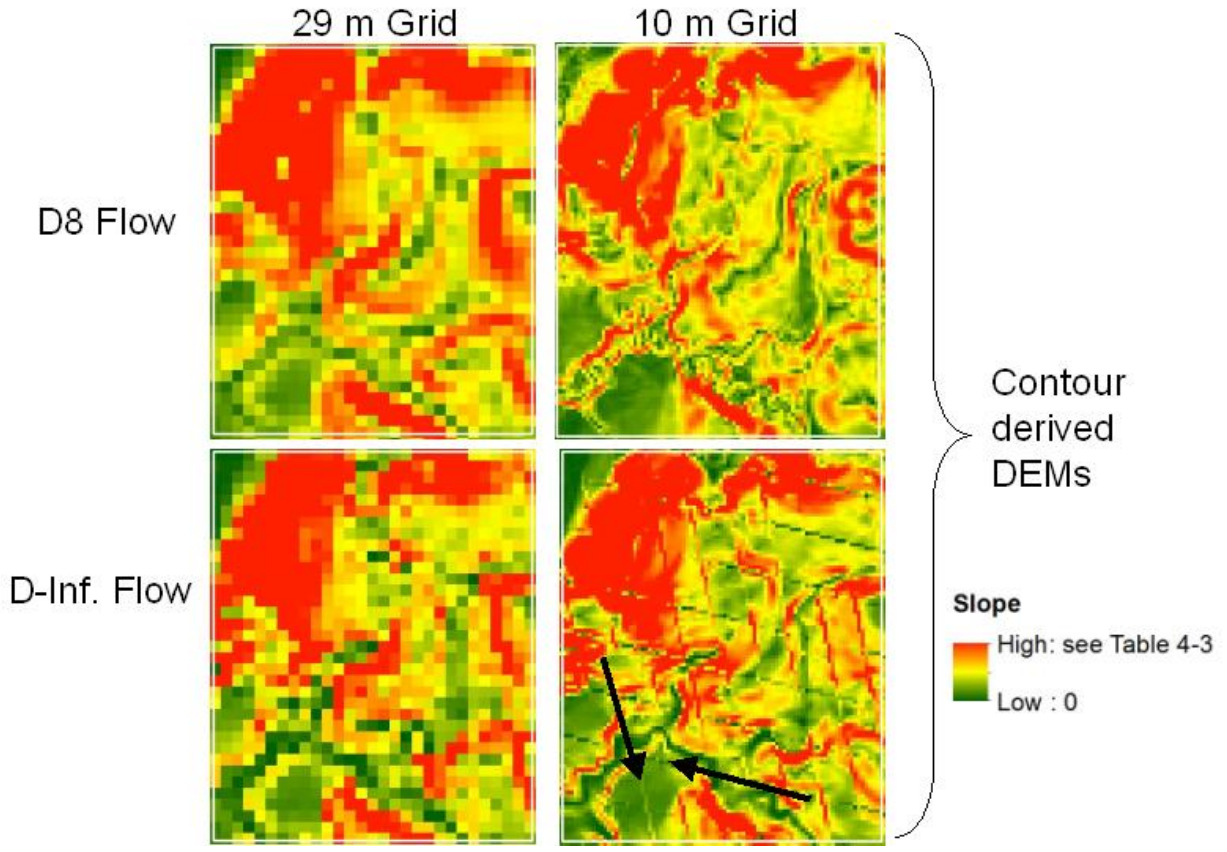

Figure 4.11. Slope maps of upland area A from contour-derived DEMs. Each of the images is a close-up of the slope map generated from one of the contour-derived DEMs of the hilly upland area A. The images are arranged by columns for grid size and rows for flow direction algorithm. The color scale is the same for all four maps in that it goes from the low slope of 0 displayed in green to the highest slopes displayed in red, but the highest slope values differ for the maps. The high slope values can be seen in Table 4.3. For both grid sizes, the D8 algorithm generated a smaller range of slopes and produced a smoother map with less sharp contrasts. The 10-m grid, D∞ derived slope revealed a series of parallelogram-forming lines that crisscrossed the map (as indicated by the black arrows on the image). These lines were striping artifacts, which were systematic and spatially structured errors known to result from certain DEM production methods such as deriving DEMs from contour maps.

While not visible in the 29-m grid or the D8-derived slope maps of area A, the 10-m grid, D∞ derived slope map revealed a very unnatural series of parallelogram-forming lines that crisscrossed the map. These lines were striping artifacts, which were systematic and spatially structured errors that were known to result from certain DEM production methods such as deriving DEMs from contour maps. There are filters for removing such artifacts (Albani & Klinkenberg, 2003), but no such filters were investigated as part of this research.

Artifacts were not apparent in the 10-m, D8-derived slope map of area A. However, the error was not in the flow direction algorithm; rather it lay hidden within the DEM, and the algorithm simply made it visible. In the flatter, bottomland area B, striping artifacts were visible in both the D8 and D∞ generated, 10-m slope maps (Fig. 4.12). Left unfiltered, these artifacts may have made the 10-m, contour-derived DEM unacceptable for defining a terrain type map. While not apparent in these two particular areas, striping artifacts were visible in other parts of the contour-derived, 29-m grid slope map, more so in the D∞ derived slope map than the D8-derived slope map. Striping artifacts existed in all contour-derived DEMs, but they were more apparent in the 10-m grids than the 29-m grids and became more apparent through application of the D∞ flow direction algorithm than the D8 algorithm.

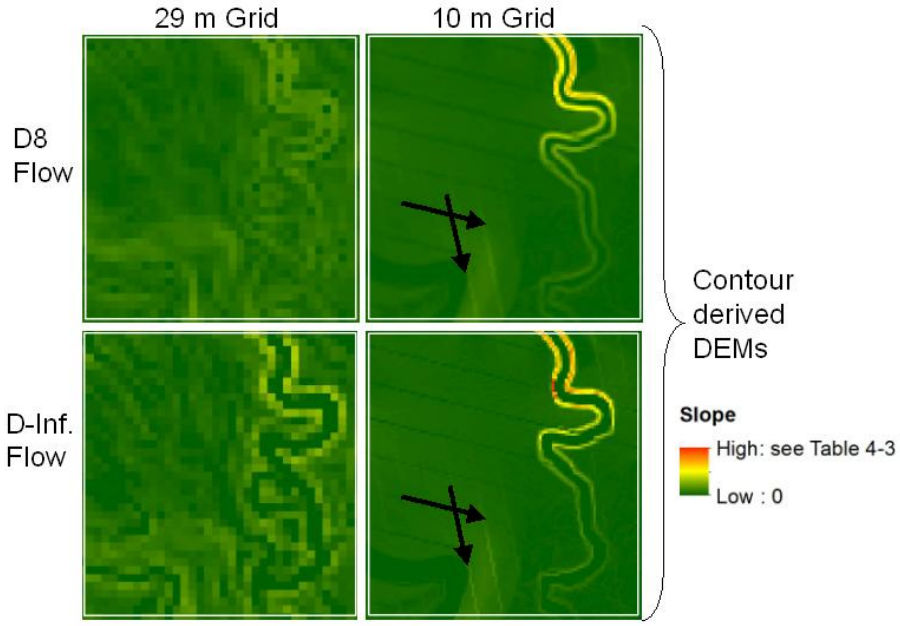

Figure 4.12. Slope maps of bottomland area B from contour-derived DEMs. Each image is a close-up of the slope map generated from one of the contour derived DEMs of the flat bottomland area B. The images are arranged by columns for grid size and rows for flow direction algorithm. The color scale is the same for all four maps in that it goes from the low slope of 0 displayed in green to the highest slopes displayed in red, but the highest slope values differed for the maps. The high slope values can be seen in Table 4.3. As with area A, the D8 algorithm generated a smaller range of slopes and produced a smoother map with fewer contrasts in slopes. Striping artifacts are revealed in area B in both 10-m slope grids, as indicated by the black arrows on the image**.**

Some differences were also seen in the different LiDAR-derived DEMs (Fig. 4.13; Fig. 4.14). Consistent with the difference noted in the contour-derived DEMs, both smaller grid resolutions and the D∞ flow direction algorithm resulted in a larger range of slopes. With the LiDAR DEMs, the differences that resulted from the different flow direction algorithms were more subtle as the striping artifacts were not an issue with the LiDAR DEMs. In some cases, it appeared the D∞ algorithm captured a more realistic image of the topography, including the two small streams (one flowing down the hill towards the southwest, and the other flowing towards the southeast; Fig. 4.13) These streams had steep banks and steep gradients. These differences were more apparent in the larger grid size DEMs.

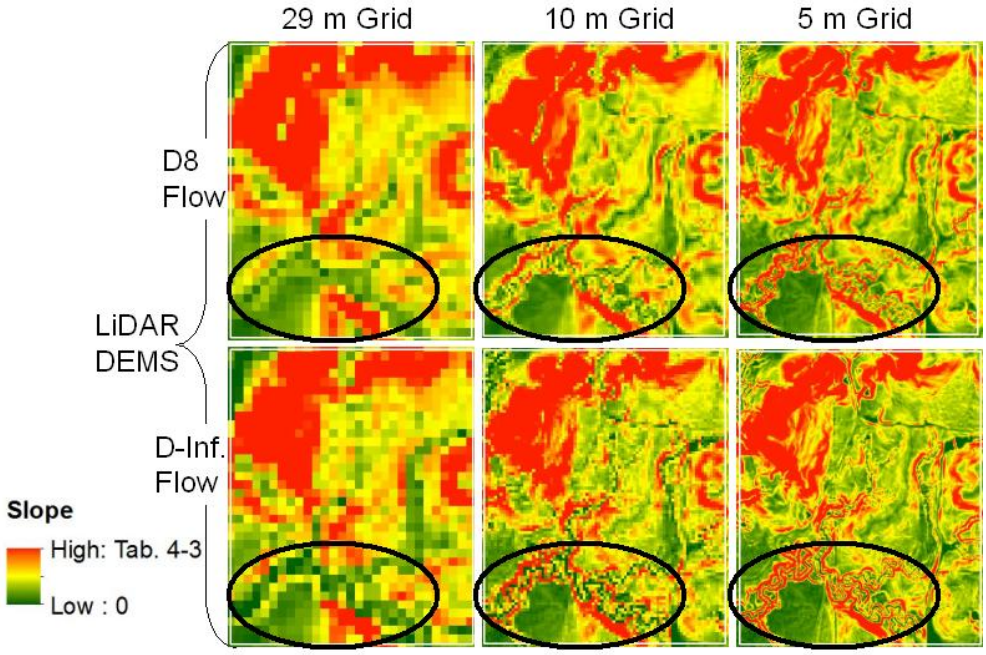

Figure 4.13: Slope maps of upland area A from LiDAR-derived DEMs. Each image is a closeup of the slope map generated from one of the LiDAR-derived DEMs of the hilly upland area A. The images are arranged by columns for grid size and rows for flow direction algorithm. The color scale is the same for all four maps in that it goes from the low slope of 0 displayed in green to the highest slopes displayed in red, but the highest slope values differed for the maps. These high slope values can be seen in Table 4.3. For all grid sizes, the D8 algorithm generated a smaller range of slopes than the D∞ algorithm. The D∞ algorithm appeared to highlight changes in slope more realistically, as with the two small streams within the black ovals. The striping artifacts apparent in the contour-derived DEMs were not present in the LiDAR-derived DEMs.

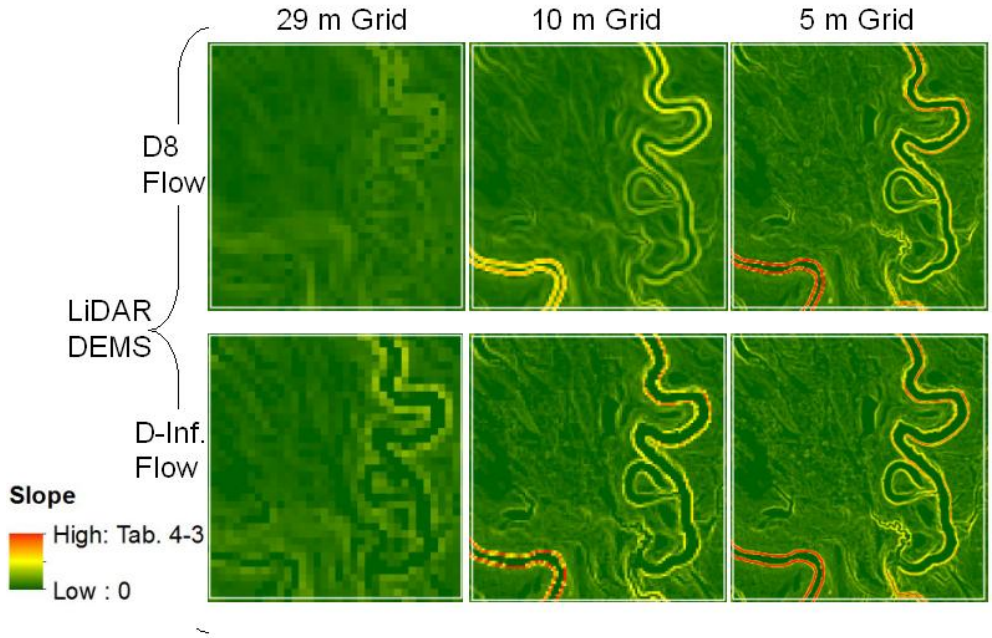

Figure 4.14. Slope maps of bottomland area B from LiDAR-derived DEMs. Each of the images is a close-up of the slope map generated from one of the LiDAR-derived DEMs of the flat bottomland area B. The images are arranged by columns for grid size and rows for flow direction algorithm. The color scale is the same for all four maps in that it goes from the low slope of 0 displayed in green to the highest slopes displayed in red, but the highest slope values differ for the maps. These high slope values can be seen in Table 4.3. For all the grid sizes, the D8 algorithm generated a smaller range of slopes than the D∞ algorithm. The D∞ algorithm appeared to highlight changes in slope more realistically, as with the two small streams seen within the black ovals. The striping artifacts apparent in the contour-derived DEMs were not present in the LiDAR-derived DEMs.

Within area B, differences in slopes resulting from the different LiDAR-derived grid resolutions were most notable along the stream channels where the slopes were greatest. Particularly notable in area B was the stream channel in the southwest corner (bottom-left) of the area. This channel was almost imperceptible in the 29-m slope grids, but became very visible with apparently very steep channel walls.

There were some general differences in the slope maps resulting from the various DEMs within the context of different topographic conditions. These included the expected difference that a finer grid resolution leads to a larger range in slope values, higher maximum slopes, and a more detailed impression of the changes in topography

over smaller spatial scales. The increased accuracy that the LiDAR-derived DEMs provided over the contour-derived ones yielded slope maps with more topographical changes as well, although this was more apparent in the 10-m grid than the 29-m grid. A major difference seen between the LiDAR- and contour-derived DEMs was the appearance of striping artifacts in the contour DEMs. While the striping artifacts existed in all four contour DEMs, they were more apparent in the 10-m grid than the 29-m grid, were highlighted more by the D∞ than the D8 flow direction algorithm, and were more apparent in the flat bottomland topography than in the hilly upland terrain.

Aspect

Aspect impacts the incident solar radiation, or insulation, received at any location. Aspect is used in FACETA to calculate the incident solar radiation and is a required topographic input parameter. In certain terrains, such as in mountainous areas at high latitudes, aspect may be one of the most important factors in plant growth. In some hot, dry climates, a sun-facing aspect can have much drier soil. The Greenbelt study area was located on subtropical latitude of approximately 33˚ N, and most slopes within the study area were less than 5%. As can be seen from the maximum slopes in Table 4.3, places in the study area had steep slopes, but the slope lengths were typically not very long. Because of the hot, dry summers, aspect undoubtedly was a significant factor in tree growth rates in the study area with steep south-facing slopes. Personal observations suggested that aspect did not play a significant role in the composition of tree species found in the study area or in the development of the three different vegetation patterns of the Cross Timbers ecoregion. Because of these observations of the study area together with the focus on the hydrological aspects of

topography, the assumption was made that aspect was not a significant factor in forest development in the study area and thus was not included as a factor in defining terrain types. However, it should be emphasized that this was an untested assumption that was made in order to simplify the number and complexity of the landscape terrain types. Although not used as an input parameter, differences in aspect resulting from the different DEMs were explored (Fig. 4.15).

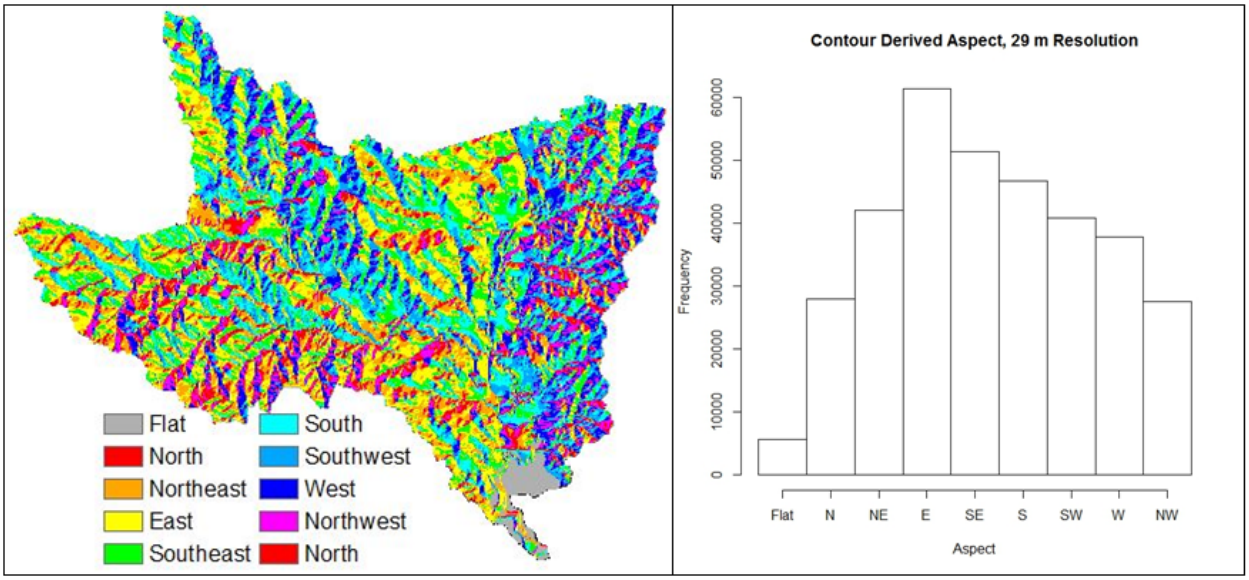

Figure 4.15: Aspect of the study area. Only rudimentary differences in aspect maps resulting from the different DEM grid sizes and sources were examined. The basic spatial patterns and distributions of aspects between the four DEMs were very similar. One difference was that the contour-derived DEMs resulted in a significant proportion of the watershed with a flat aspect, whereas the 29-m LiDAR DEM had no flat aspects, and the 10-m LiDAR DEM had only a very small proportion. The example shown here was derived from the contour-derived 29-m grid DEM.

Aspect was calculated for the unfilled DEMs from both LiDAR and contour sources at both 29-m and 10-m grid resolution. There was little difference in both distribution of values and the maps of aspect from these four DEMs. One difference of note was that both of the contour-derived DEMs resulted in a significant number of cells with aspect determined as flat (Fig. 4.15), while the 2- m LiDAR DEM had zero cells calculated as flat, and the 10-m LiDAR DEM had only a very small proportion of such

cells. Between the two grid resolutions examined, the differences in aspect were limited to differences in the granularity. The overall pattern and distribution of aspect values differed little with grid size.

Flow Accumulation and Specific Catchment Area

The specific catchment area, A_s, was defined as the ratio of the upslope contributing area to the length of the contour line segment that area drained to it: $A_S = A/l$. When using a raster DEM, the contour length was assumed equal to the raster cell width. Flow accumulation (FA) in a GIS was defined for any raster cell to be the number of cells that eventually drain onto it, and therefore, it was affected by flow direction. Flow accumulation was used to estimate the size of A_s for a cell by calculating the product of the cell's width with the flow accumulation plus one: $A_s = (cell\ width)$ x $(FA+1)$. To clarify a subtle GIS point, multi-directional flow (MDF) direction algorithms such as D∞ may bypass calculating flow accumulation and calculate specific catchment area directly. Since the D∞ algorithm used a proportional assignment in flow direction, counting flow accumulation cells amounted to counting and adding together parts of cells. In those cases, the language of catchment area fit better than speaking of number of cells. However, the difference was semantic and the two concepts were considered interchangeable. Flow accumulation, and subsequently specific catchment area, was itself not a good predictor of soil moisture. The vast majority of cells within a DEM had very small flow accumulation values (Fig. 4.16). A very small number of cells had a very large flow accumulation. These cells with large flow accumulation values were typically interpreted as belonging to a stream channel, and in fact, flow accumulation was useful in determining stream channel networks. Similarly, slope alone was not a good predictor

of soil moisture by itself. Because of the interactive effects of slope and specific catchment area on the flow and collection of water, hydrologists and soil scientists have combined the two attributes into a compound TWI. The output map of the flow accumulation calculation, and subsequently the wetness index, depends on the flow direction algorithm used.

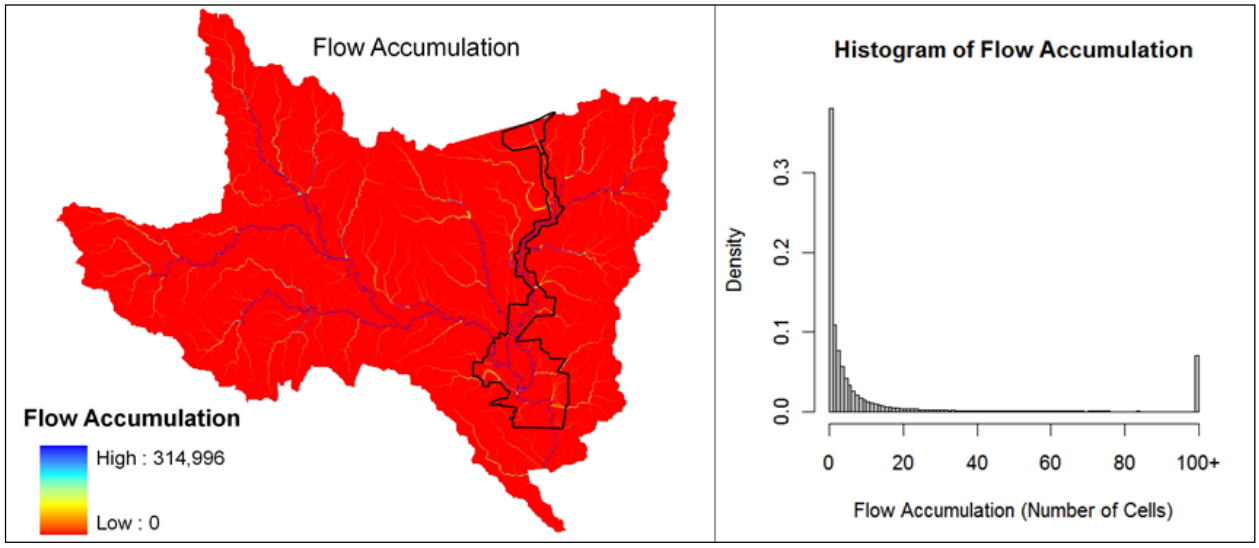

Figure 4.16. Flow accumulation for the Greenbelt study area. This example of flow accumulation is from the contour-derived, 29-m grid, D8 flow direction DEM. The distribution of values for all the flow accumulation variations was similar. Most DEM cells had small flow accumulation values. In this example, the 35th percentile was 1, meaning no other cells drained onto those cells. The median value was 3. Cells with high values (usually in the 10^2 order of magnitude) were interpreted as belonging to a stream channel. The highest values in this example belonged to the watershed's two largest streams and their tributaries, which all came together in the southern part of the Greenbelt State Park (boundary drawn on map), which consisted mostly of floodplain of these streams.

The various flow accumulation results from the different DEM sources, grid resolutions, and flow direction algorithms were compared. Since most of the watershed consisted of cells with very small flow accumulation values, the best areas to compare different flow accumulation results, at least visually, were where these accumulation numbers were highest. Two areas were selected to compare flow direction (Fig. 4.17). Area C contained the confluence of the Elm Fork Trinity River and Clear Creek. This area had a

large amount of flow accumulation but was mostly concentrated within the stream channels, making a good location to compare how well the different flow accumulations identified stream channels. Area D was in the lowest part of the Greenbelt floodplain where a lot of flow accumulated, but it was spread out over the low, flat plain. Flow direction algorithms typically have great difficulty accurately depicting flow in these kinds of low, flat areas, and flow accumulation output can be unreliable in them, which is why area D was selected for comparing flow accumulation results.

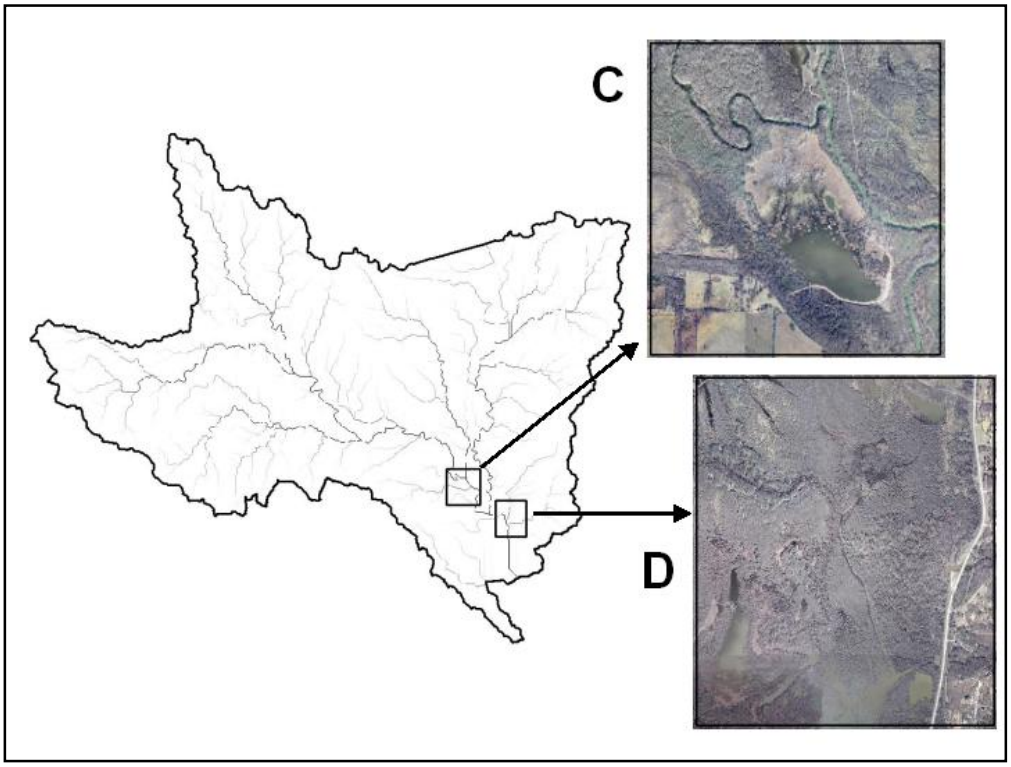

Figure 4.17. Areas for closer examination of flow accumulation. In order to examine differences in flow accumulation resulting from the different DEMs, two areas were selected to zoom in on. Area C contained convergence of the two largest streams in the watershed. Area D included the lowest part of the floodplain consisting of very flat land.

Flow accumulation maps calculated from the various DEMs were compared within each area to a high-resolution aerial image taken in the winter of 2005 (Fig. 4.18). Areas with standing water bodies, stream channels, sloughs, and wetlands that could

be identified in the aerial image were compared with the flow accumulation outputs. Some specific issues of note occurred in the flow accumulation outputs from the two flow direction algorithms applied to the contour derived, 29-m grid DEM (Fig. 4.18).

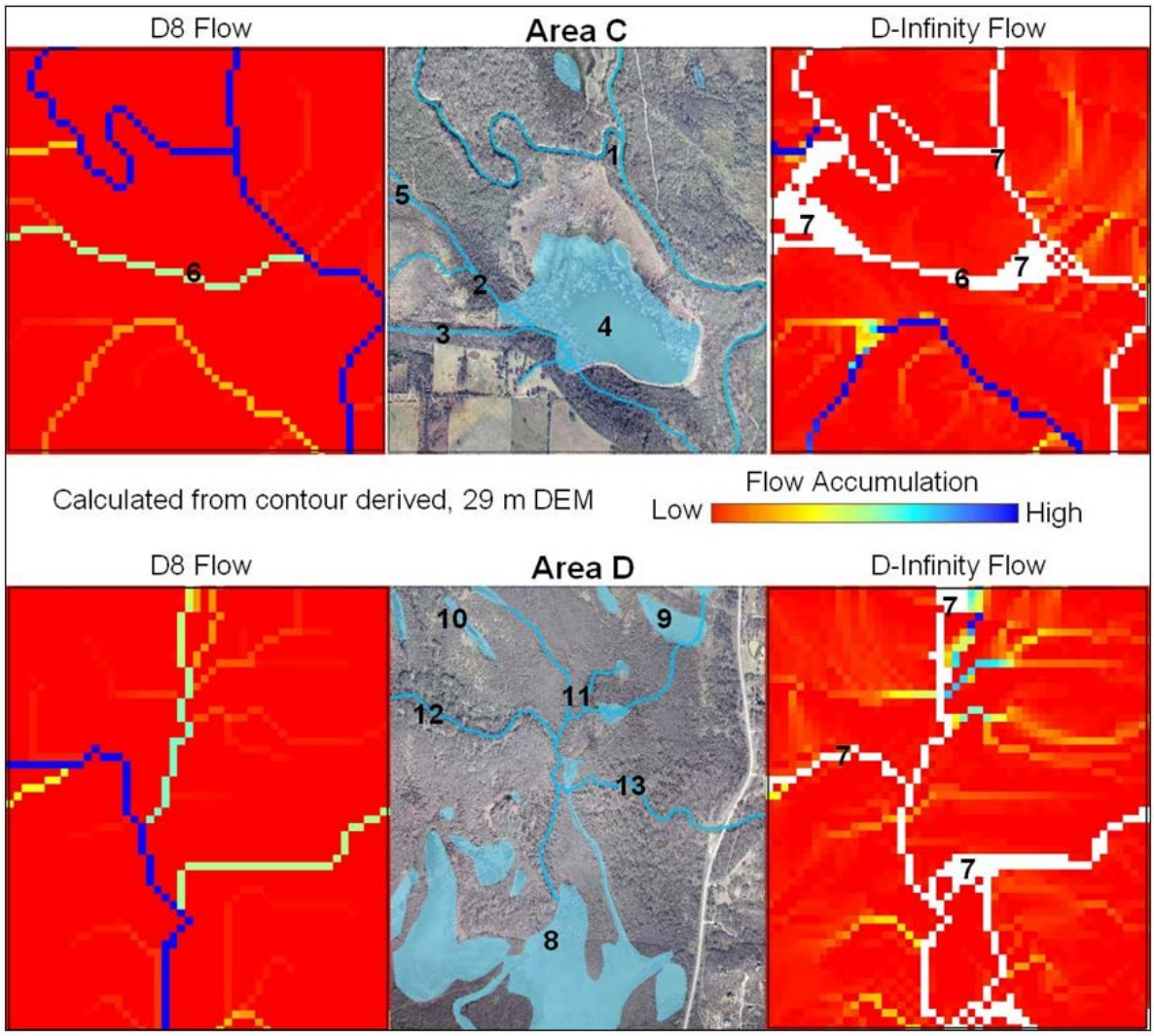

Figure 4.18. Flow accumulation using contour-derived, 29-m grid DEMs. Flow accumulations were calculated from contour-derived, 29-m DEMs using both the D8 (left column) and D∞ (right column) flow direction algorithms. The center column is an aerial image of the areas taken in the winter in 2005. Stream channels, sloughs, wetlands, and areas with visible standing water are highlighted in blue on the aerial images. Area C (top row) includes the confluence of the two largest streams in the watershed, and area D (bottom row) is in a flat, low-lying part of the floodplain. The two streams are Elm Fork, which is the main stream that flows from the top of the image to the bottom, and Clear Creek, which comes into the image on the top-left side and joins Elm Fork. Locations of note within area C are: (1) Both algorithms defined the shape of the two main streams fairly well, although they both missed at times, such as the small bend just before the confluence. (2) Neither algorithm did a good job detecting the upper part of this small stream, but both algorithms picked it up a little further down. (3) This small tributary was detected more clearly by the D∞ algorithm and was only barely detectable under the D8 algorithm. (4) The wetland

was constructed and replenished in part from diversion from the little stream (#2) with a berm and from the westward flow of water downslope towards the river. (5) Both algorithms picked up the two little streams coming together, but neither detected that the stream then continued southeast towards the constructed wetland. (6) Rather, both algorithms detected that flow as going westward in what appeared as stream channels, but there was not a channel along that path. (7) From the shapes displayed in the flow accumulation maps, the D∞ algorithm appeared to resemble the surface hydrology a little better. However, there was a problem with the D∞ output. While the shapes looked similar to the stream channels, grid cells colored white in the image were actually cells with no data (i.e., the algorithm failed to calculate values for these cells). These no data cells were also seen in the D∞ flow accumulation output within area D. The complexity of the flow paths in flat topography such as within area D made accurate hydrological calculations difficult. Locations of note within area D are: (8) Flow accumulation was not a good tool to detect wetlands (e.g., the vast majority grid cells within this wetland area had a flow accumulation value of zero for both flow direction algorithms). However, the D∞ algorithm gave a better indication of the accumulated water being spread over a wider area. (9 and 10) D∞ picked up the accumulation in these wetlands better. (k) Both algorithms picked up this stream network, but it was clearer with D∞. (11) Neither algorithm picked up this cannel, but both picked up the general flow accumulation occurring around it.

Generally, both algorithms applied to the 29-m, contour-derived DEM did a good but not perfect job defining the shape of the two largest streams, Clear Creek and Elm Fork (Fig. 4.18). Detecting smaller stream channels was hit or miss, but in general, the D∞ algorithm did a better job detecting these. Both algorithms did poorly in flat areas and tended to concentrate the flow accumulation into what appeared as channels, when in reality the flow was spread over a wider area, with the D8 algorithm having a stronger tendency to do so than the D∞ algorithm. Neither algorithm was good at outlining or detecting wetlands, but D∞ was a little better in that some wetlands showed up as a cluster of channels. In general, D∞ located more channels throughout the watershed. Striping artifacts did not show in the flow accumulation maps calculated through either flow algorithm in the 29-m contour-derived DEM. The biggest problem occurred with the D∞ algorithm where a number of cells were not successfully assigned a value, resulting in gaps of missing values within the map. Missing data values occurred all around the outer perimeter of the watershed and in the interior of the watershed in areas of high flow accumulation, particularly in stream channels (Fig. 4.19).

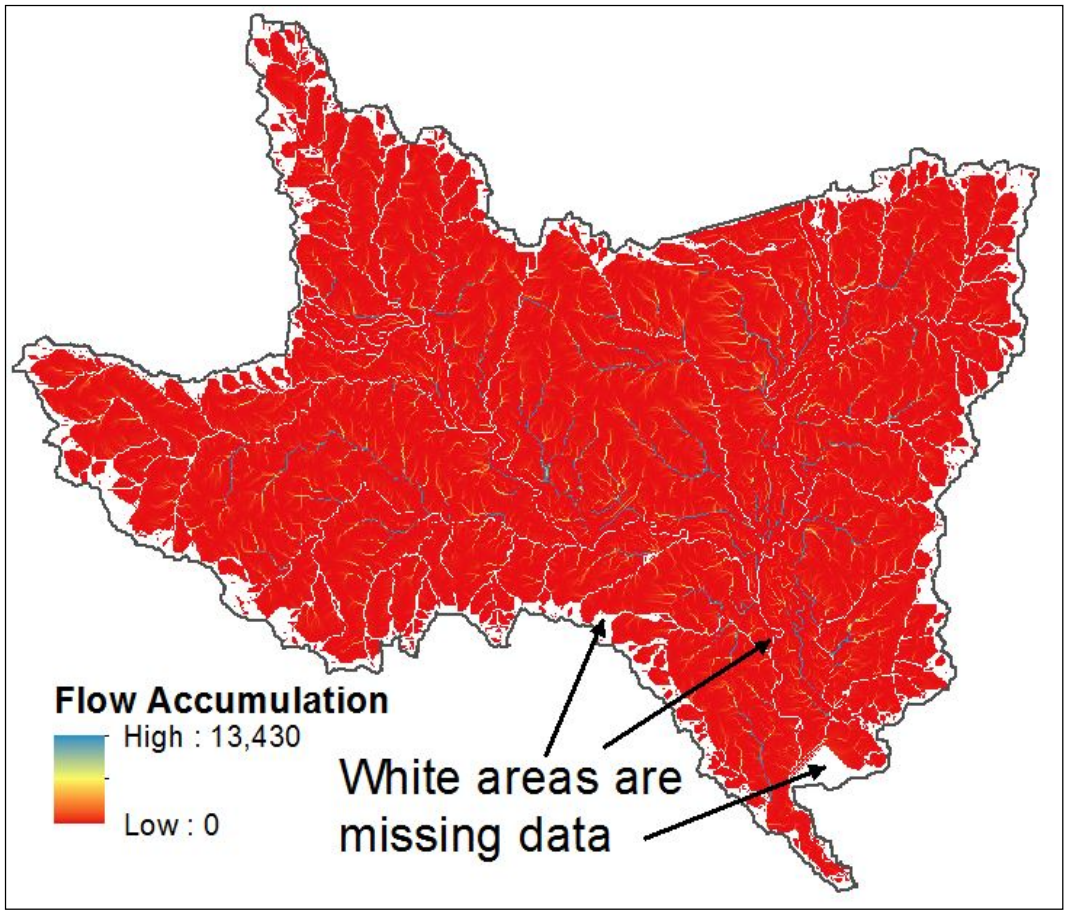

Figure 4.19. Missing data cells on D∞ specific catchment area. Cells around the perimeter and in areas of high flow accumulation resulted in missing data when calculating specific catchment area using the D∞ algorithm implemented in the TauDEM version 5.1.2 extension under ArcMap version 10.2.1. In the interior of the watershed, missing data cells primarily occurred in stream channels.

Larger channels in the D∞ flow accumulation grid eventually become no data as the accumulation increased going down the stream. Missing data cells did not occur in either the D∞ flow direction or slope maps. The specific implementation of the D∞ algorithm and corresponding flow accumulation algorithm used here was the TauDEM version 5.1.2 extension running under ArcGIS version 10.2.1. It was not clear what caused the error. Previously, missing data cells occurred using TauDEM version 3.x and ArcGIS 9.x on the same 29-m and 10-m contour-derived DEMs but in a small enough number to be almost imperceptible. It was not believed the error resulted from the D∞ flow direction algorithm in general, so the use of the algorithm in determining the

TWI for FACETA terrain types was still evaluated. However, missing data cells in the flow accumulation map were also missing data cells in the TWI map and subsequently in the terrain type maps. For purposes of this research, it was considered a problem, but not one so severe to prevent proceeding with the maps produced by the D∞ algorithm.

One surprising finding was that between the flow accumulation map, produced through the D8 algorithm from the 29-m LiDAR DEM, and the flow accumulation map calculated from the 29-m contour DEM, the LiDAR-derived map looked worse (Fig. 4.20). Clear Creek was barely visible in this map. In general, the shape of the stream channels were simplified, straightened, and fit poorly to the true locations of the streams; at least this was the case for the two areas zoomed in on. When zooming out and comparing the two flow accumulation maps across the entire watershed, that comparison was not true in general. Neither of the 29-m, D8-produced flow accumulation maps accurately located small stream channels, and both were poor in very flat terrain. However, the contour-derived map was for some reason more accurate in locating this part of these two major streams, Elm Fork and Clear Creek. Comparing the D∞ 29-m LiDAR and D∞ 29-m contour flow accumulation maps, the map derived from LiDAR was generally an improvement. Stream channels were located more accurately, and the output resulted in fewer no data cells. Between the two 29-m LiDAR derived maps, D∞ located more small channels and did a much better job locating the position of Elm Fork and Clear Creek going through the Greenbelt than did the D8.

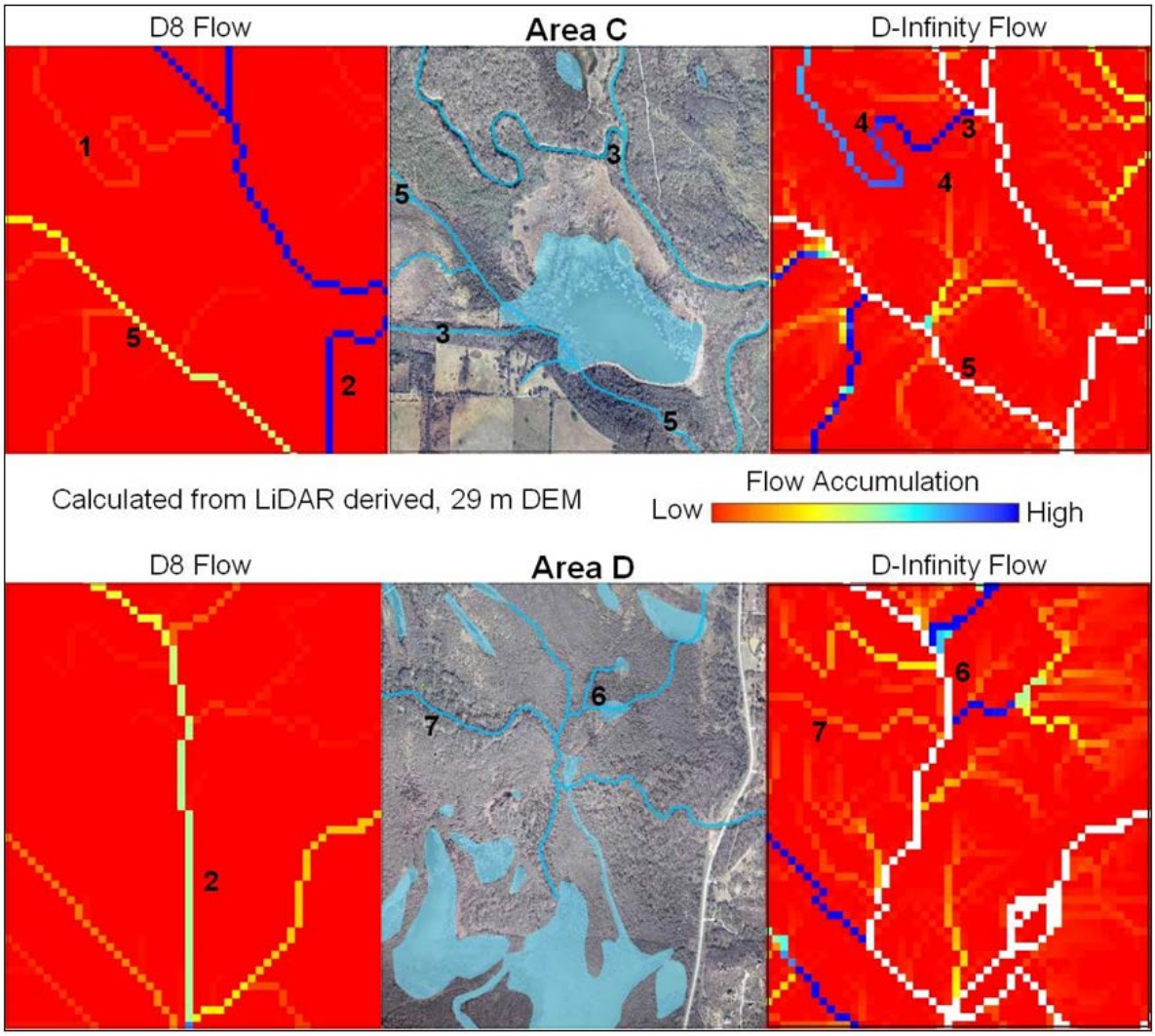

Figure 4.20. Flow accumulation using LiDAR-derived, 29-m grid DEMs. Flow accumulations were calculated from LiDAR-derived, 29-m DEMs using both the D8 (left column) and D∞ (right column) flow direction algorithms. The center column is an aerial image of the areas taken in the winter in 2005. Stream channels, sloughs, wetlands, and areas with visible standing water are highlighted in blue on the aerial images. The D8 algorithm produced a worse flow accumulation map from the LiDAR DEM than it did from the 29-m, contour DEM, whereas the D∞ map was an improvement over its contour-derived counterpart. Locations of note: (1) Clear Creek was barely visible under the D8 algorithm. (2) The D8 algorithm, especially in flat areas, artificially straightened the flow accumulation paths. (3) The D∞ algorithm applied to LiDAR DEM did a better job finding the bend in Clear Creek than it did with the contour DEM. (4) Compared to the contour DEM, the D∞ algorithm resulted in fewer no data cells (e.g., Clear Creek). (5) The small stream was better detected with this DEM than with the contour DEM under both algorithms. (6) The channel network was better detected from the LiDAR DEM under the D∞ algorithm. (7) With the LiDAR DEM, the small channel was picked up by the D∞ algorithm.

Comparing the 10-m flow accumulation maps to their 29-m contour-derived counterparts, the increased grid resolution did not improve the result by much (Fig. 4.21). Stream channel positions were nearly identical between the two D8-derived

flow accumulation maps, although there were some minor improvements in locations of bends and smaller channels. Generally, that was the case in comparing D∞ produced output from the 10-m contour DEM with 29-m contour DEM. Comparing two 10-m flow accumulation maps, the D∞ produced map found more small channels, located the position of the channels slightly better, but again had the problem of missing data cells.

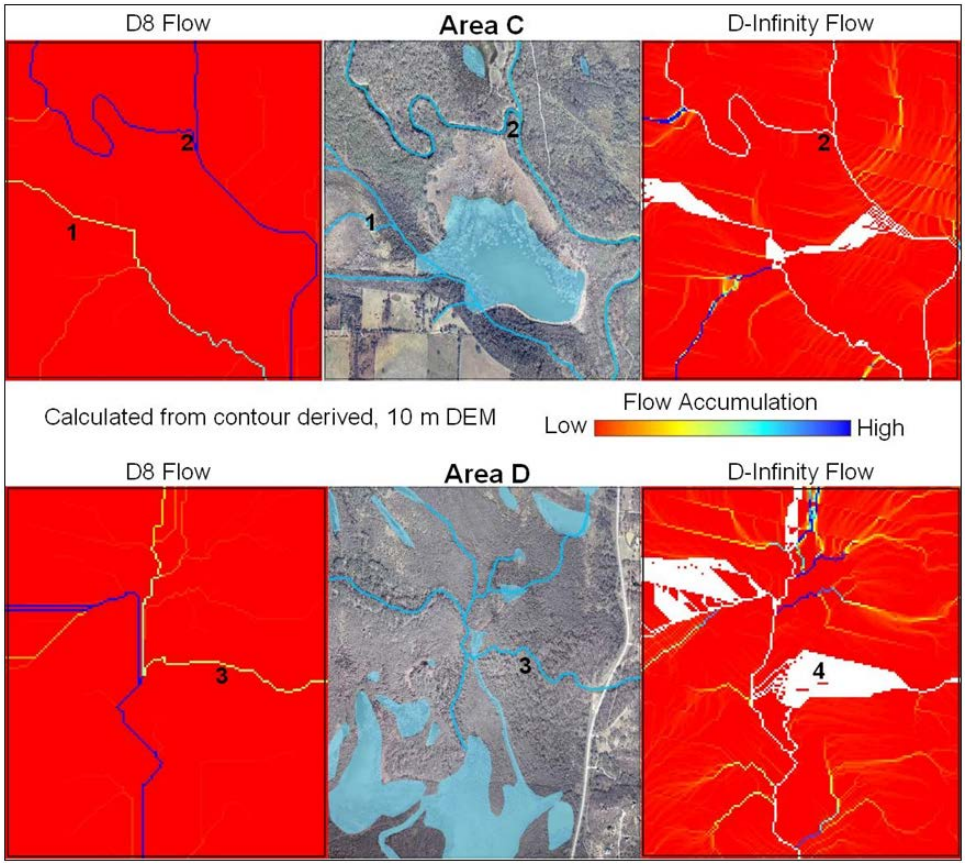

Figure 4.21. Flow accumulation using contour-derived, 10-m grid DEMs. Flow accumulations were calculated from contour-derived, 10-m DEMs using both the D8 (left column) and D∞ (right column) flow direction algorithms. The center column is an aerial image of the areas taken in the winter in 2005. Stream channels, sloughs, wetlands, and areas with visible standing water are highlighted in blue on the aerial images. Comparing the 10-m flow accumulation maps to their 29-m contour-derived counterparts, the increased grid resolution did not improve the result by much. While some of the stream channels appeared a little closer to the actual paths, most of the patterns between the two grid resolutions were very similar. Some differences included: (a) The small stream and flow about the constructed wetland improved a little under the D8 algorithm. (b) Both algorithms started to pick up the bend in Clear Creek, but not very well. (c) The path of the small bottomland stream fit the real path a little closer than it did in the 29-m grid. (d) The bottomland no data areas enlarged under the D∞ algorithm compared with the 29-m DEM.

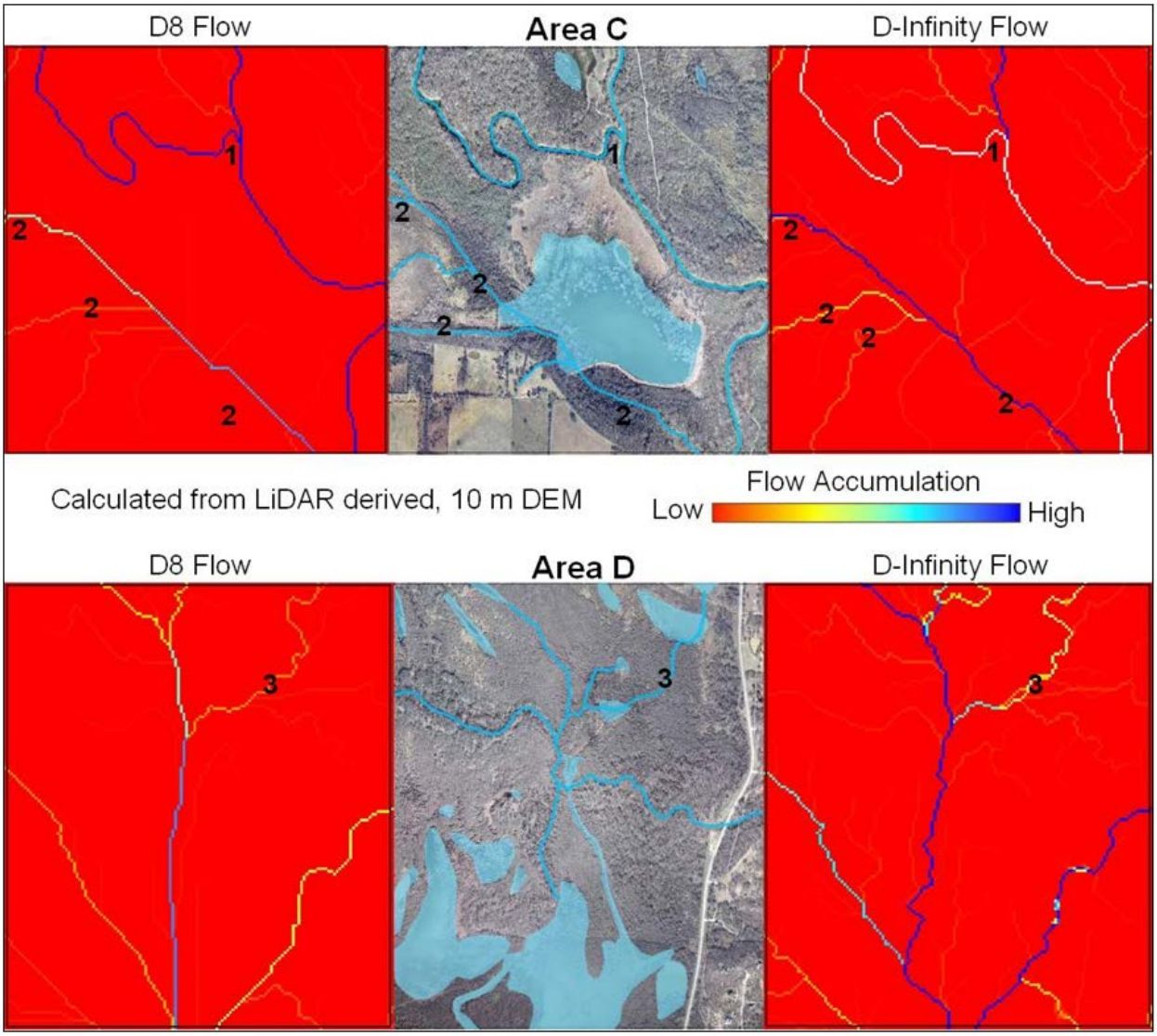

Figure 4.22: Flow accumulation using LiDAR-derived, 10-m grid DEMs. Flow accumulations were calculated from LiDAR-derived, 10-m DEMs using both the D8 (left column) and D∞ (right column) flow direction algorithms. The center column is an aerial image of the areas taken in the winter in 2005. Stream channels, sloughs, wetlands, and areas with visible standing water are highlighted in blue on the aerial images. Regarding accuracy of stream channel locations and shapes, the 10-m LiDAR derived DEM was mostly an improvement over both 29-m DEMs and the 10-m contour-derived DEM. Locations of note include: (1) Both algorithms detected the bend in Clear Creek with this DEM. (2) The network of small channels was detected better using this DEM. (3) The small channel in the flat bottomland came out better with the contour-derived DEMs than with this LiDAR DEM.

Compared to the 10-m LiDAR-derived DEM, the 5-m DEM did not improve the accuracy when using the D8 algorithm (Fig. 4.23). Most of the channel positions were the same when comparing the two 5-m accumulation maps with their respective 10-m counterparts. There were some minor improvements in locating some of the smaller

channels using D∞; however, surprisingly the areas of missing data were larger with the 5-m grid than the 10-m grid, and most of the missing data areas around the perimeter of the watershed returned.

To summarize the flow accumulation results, differences in flow accumulation outputs from five different DEMS and two flow direction algorithms were examined and the outputs were compared with surface water features as detected from an aerial image. The general shape and position of large streams was accurate for most of these outputs, but accuracy improved with resolution, source (LiDAR-derived was more accurate than contour-derived), and flow direction algorithm (D∞ was more accurate than D8). There were some exceptions to this general statement. For example, the 29-m LiDAR-derived D8 map was no better than the 29-m contour-derived D8 map. Additionally, there were some caveats. The D∞ algorithm resulted in cells without any data. Within a particular grid resolution, there were more missing data cells resulting from the contour-derived DEMs than from the LiDAR-derived DEMs, and for both DEM sources, there were far fewer missing data in the 10-m grids than in the 29-m grids. The 5-m grid surprisingly had more missing cells. Accuracy did not improve with the 5-m flow accumulation grids as compared to their 10-m LiDAR counterparts. The striping artifacts seen in the contour-derived slope maps were not become apparent in any of the flow accumulation maps.

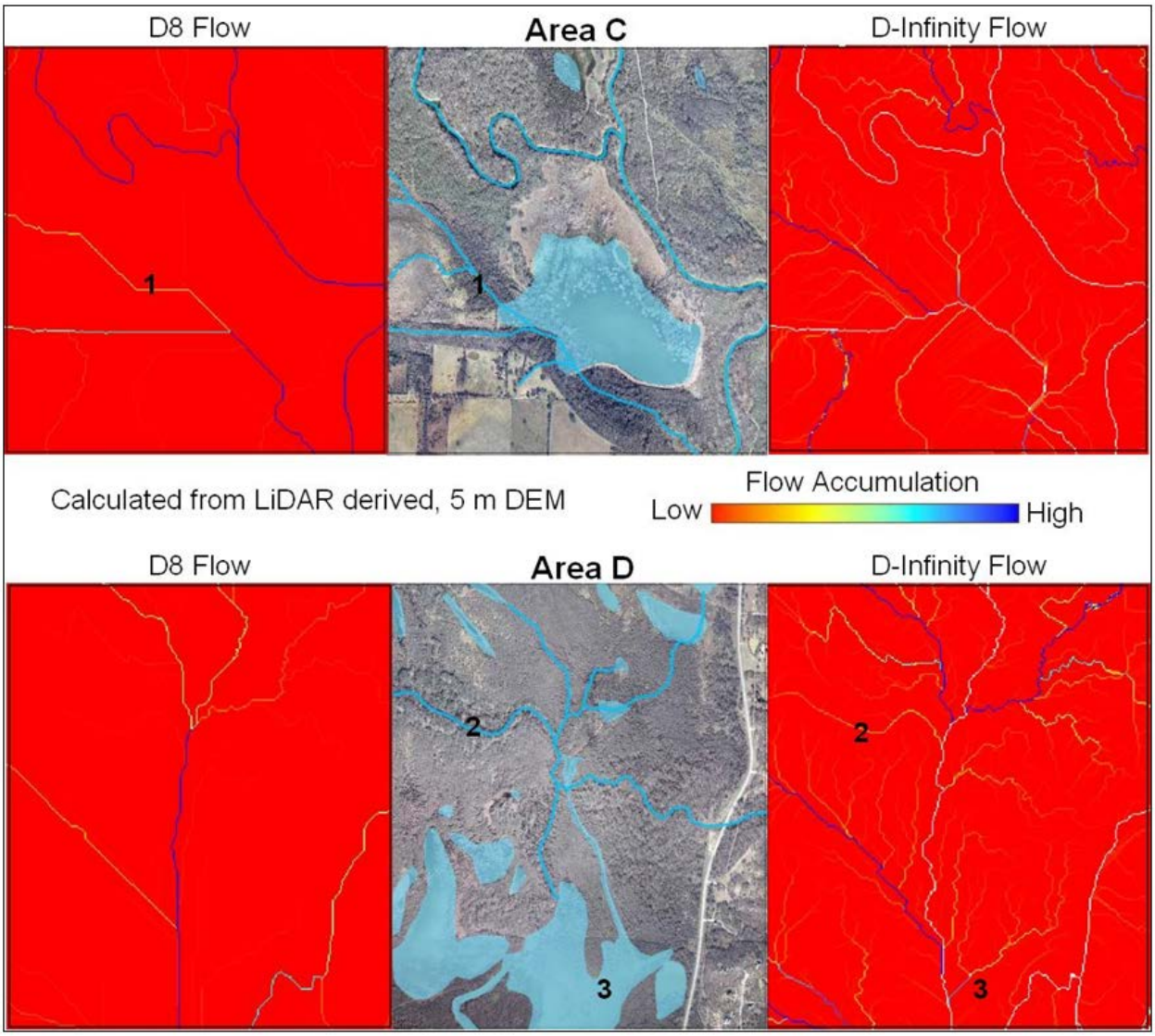

Figure 4.23: Flow accumulation using LiDAR-derived, 5-m grid DEMs. Flow accumulations were calculated from LiDAR-derived, 5-m DEMs using both the D8 (left column) and D∞ (right column) flow direction algorithms. The center column is an aerial image of the areas taken in the winter in 2005. Stream channels, sloughs, wetlands, and areas with visible standing water are highlighted in blue on the aerial images. Compared to the 10-m LiDAR-derived DEM, the 5-m DEM did not improve accuracy when using the D8 algorithm; however, it did improve some with the D∞. Of note: (a) the path of the small stream was less accurate using the 5-m DEM than the 10-m LiDAR DEM with the D8 algorithm, (b) the small channel in the flat bottomland was detected in the 5-m DEM using D∞, and (c) when using the finer grid resolution, the accumulation in the flat wetland area became more spread out.

Most of the cells were either on the perimeter of the watershed or in channels with high flow accumulation, so this was not considered a problem bad enough to prevent the algorithms' use in determining terrain types. Between the increased accuracy of the bi-directional flow algorithm over the single directional algorithm and the missing data

problem resulting from the D∞ algorithm, a recommendation and potential future improvement would be to compare these results with output generated with a true MDF algorithm.

Topographic Wetness Index

Slope and specific catchment area are both primary topographic attributes. These two attributes interacting together, along with soil depth and texture, significantly impact soil moisture patterns. Specific catchment area impacts the potential for upslope water contribution, and slope impacts accumulation and the flow of water. However, neither topographic attribute by itself makes a good predictor of soil moisture. By combining the two primary attributes, the TWI is a better predictor of soil moisture. Although it has limitations, the TWI is often used as a measure of hydrological similarity within a watershed. In FACETA's current formulation, there are input parameters for flow accumulation and slope, and a third parameter referred to as the run-on coefficient is a multiplicative coefficient applied to flow accumulation. Flow accumulation together with the run-on coefficient is encoded in the model to simulate run-on water from the upslope portion of the surrounding watershed. Slope is currently not implemented into the hydrological component of the model. By using the TWI to define terrain types for FACETA parameters, the goal is to incorporate the combined hydrological component of both slope and upslope catchment area into the terrain units and then calibrate the run-on coefficient to the terrain units. The issues involved in TWI implementation considered here included the specific TWI formulation to be used, DEM source, DEM grid size, and flow direction algorithm.

Many different formula variations are used for calculating a wetness index from slope and contributing area, two of which are examined here:

$$TWI_1 = \ln\left(\frac{A_S}{\tan(\beta)}\right), \text{ and } TWI_2 = \frac{\tan(\beta)}{A_S}.$$

The angle of the local slope is β, so $\tan(\beta)$ is the local slope expressed as a ratio of the change in elevation to the change in horizontal distance. The problem with the formula most often used, TWI_1, is that a slope of zero is mathematically undefined. Especially within the topography of a floodplain, having land so flat that a GIS determines it to have a slope of zero is likely. The second formula gets around this problem by putting the non-zero specific catchment area term in the denominator of the fraction. While the two formulations highlight similar features, they are very different (Fig. 4.24).

A major difference between the two indices was that their interpretations were inverses of each other. Higher values of the first index corresponded to wetter terrain, while higher values in the second index corresponded to drier terrain. While it avoids the divide-by-zero problem, the second formula had the problem that any slope of zero ended up with a TWI of zero regardless catchment area size. Because any cell with a small slope would result in an index value of almost zero, there was much more clustering around zero in the frequency distribution of TWI_2 (Fig. 4.24). While both distributions were positively skewed, the skew was much greater for the second formula. This seemed to imply that the results of the two formulas were very different, and numerically they were. However, with an appropriately chosen display method, the two results were more equivalent than they might seem.

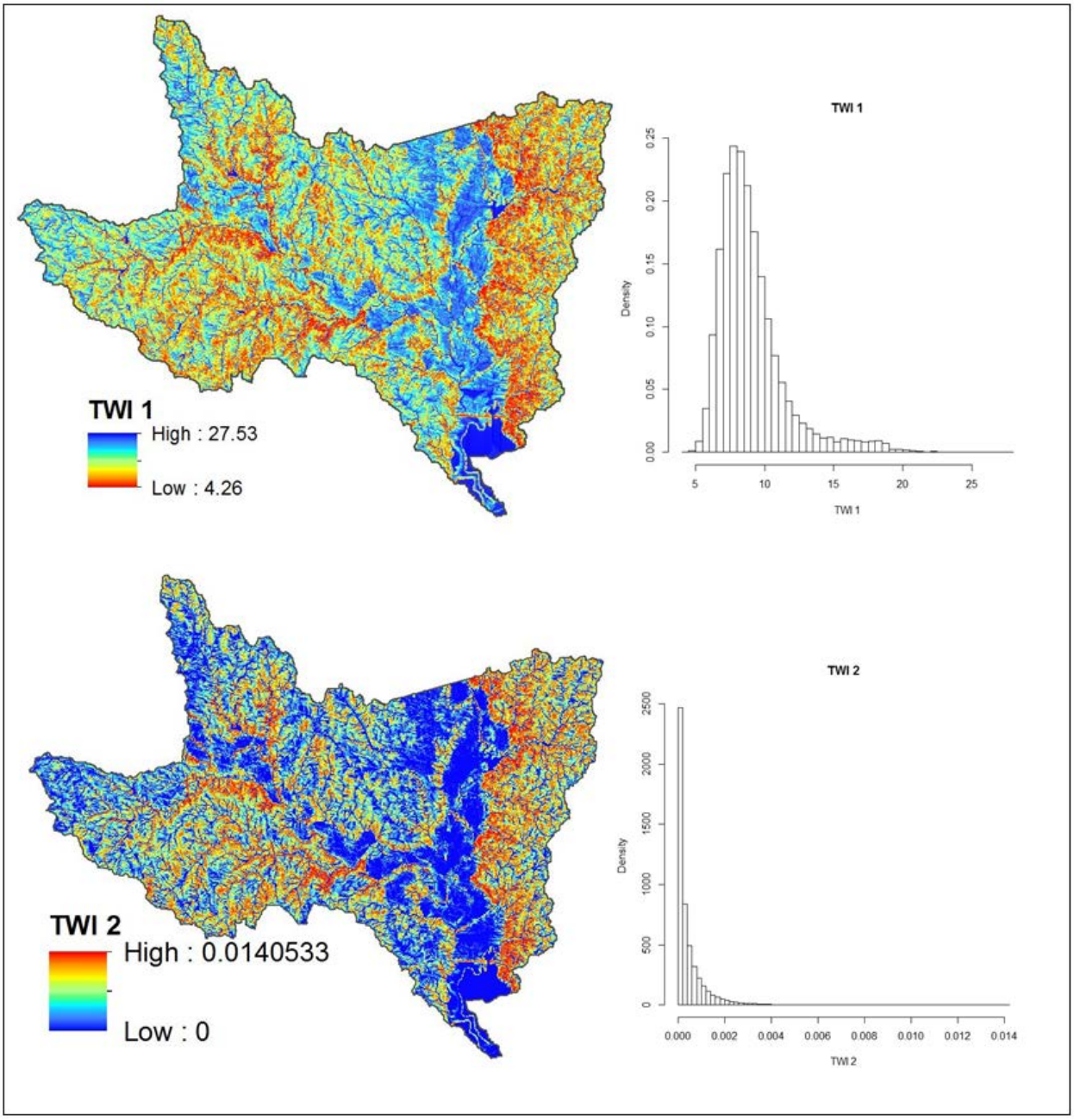

Figure 4.24. Results from two different TWI formulas. The results across the study area watershed using the formula $TWI_1 = \ln(A_S / \tan(\beta))$ are on the top row, and the results from the formula $TWI_2 = \tan(\beta) / A_S$ are on the bottom row. The first formula can have the problem of dividing by zero on flat terrain. The second formula avoids this problem by inverting the fraction, but it results in a clustering of values close to zero and is not capable of differentiating between flat upland and bottomland sites. These examples were calculated from the 29-m, contour-derived DEM processed with the D8 flow direction algorithm.

A histogram equalization method was used, which is a good method to use when a large number of cell values are clustered close together. However, the clustering made mathematically differentiating cells into groups a bit more complex. Additionally, one of the general known problems with the wetness index was that it became less able to differentiate soil moisture in flat landscapes with low topographic relief, and it seemed that the second formula had the potential to highlight that problem. This could potentially have been a problem using TWI_2 in flat and dry upland areas, but it could have been a benefit within a flat floodplain. This research used a variation of TWI_1, but further investigation using TWI_2 to define terrain types should be considered as a next step.

The TWI formula used here was modified by adding a small constant to the slope in the denominator, thus avoiding division by zero:

$$TWI = \ln\left(A_S / \left(\tan\left(\beta\right) + 0.00001\right)\right).$$

While the vast majority of the landscape had a non-zero slope in all of the DEMs, there were still a significant number of cells with a zero slope, particularly within the bottomland areas. For example, there were thousands of grid cells just within the bottomland Ovan clay soil series with a calculated slope of zero. Adding a number to the calculated slope in the denominator was not the best solution, and the number added was in some ways an arbitrary choice. The value was chosen simply because it was small. Adding this number to the denominator amounted to adding .0001% to the slope of each cell as determined from the DEM, which was equivalent to a vertical change of one meter over a horizontal distance of 100 km.

Another way to avoid division by zero when calculating the wetness index was to ensure no cells had with a calculated slope of zero. There are algorithms that eliminate

flat slopes from the DEM. PDEM uses an iterative process of linear interpolation across sinks and flat areas between the high elevation cells and low elevation cells that surround the flat area (Pan et al., 2012). This algorithm results in a DEM that is both depressionless and has no zero slope cells. Algorithms eliminating flat areas were not examined in this research; however, they should be as a follow up to this study.

To get a sense of the landscape surface features that the TWI highlights, three areas were selected to zoom in on (Fig. 4.25). Two of the areas, C and D, were the same as those used in the examination of the flow accumulation maps. Area E was added to include an upland location with post oak forest.

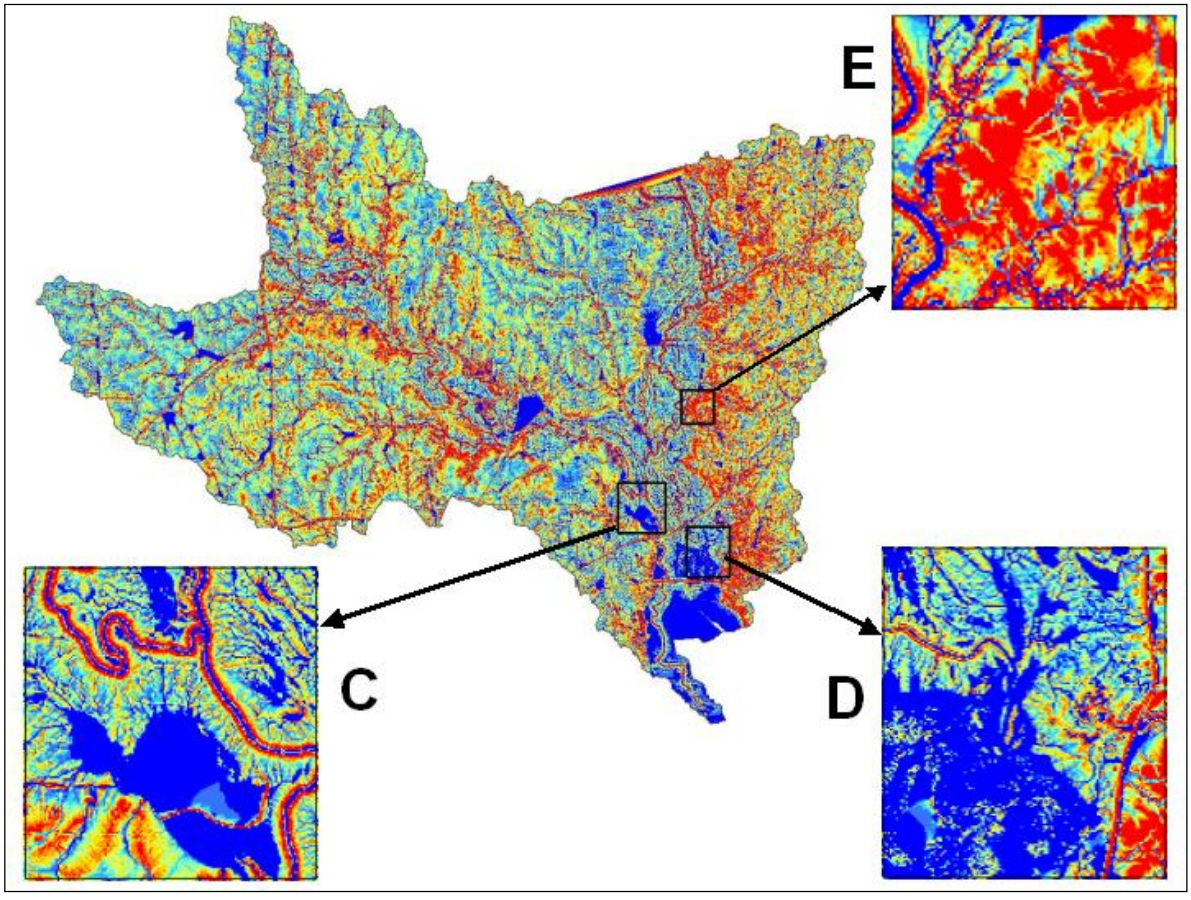

Figure 4.25. Areas for **c**loser **e**xamination of TWI**.** To examine the TWI maps closer**,** three areas were chosen to focus in on. Areas C and D **we**re the same as those used in the examination of the flow accumulation maps. Area E was added to include a distinctly upland location. Area E **wa**s just an enlargement of area A used in comparing slope outputs. The area was enlarged to include the transition from upland to bottomland forest.

This area was almost the same as area A that was used in comparing the slope maps, but it was enlarged to include the transition from upland to bottomland forest (Fig. 4.26, Fig. 4.27, & Fig. 4.28). The color scale in the TWI maps had the lowest values represented with red and the highest represented by blue, with yellow in the middle. This particular TWI map was calculated from the 10-m grid LiDAR-derived DEM that was processed using the D∞ flow direction algorithm, but all of the TWI maps highlighted similar surface features to varying degrees.

Area C included the confluence of Clear Creek and Elm Fork (Fig. 4.26). Similarities were seen between the TWI patterns and surface hydrological features.

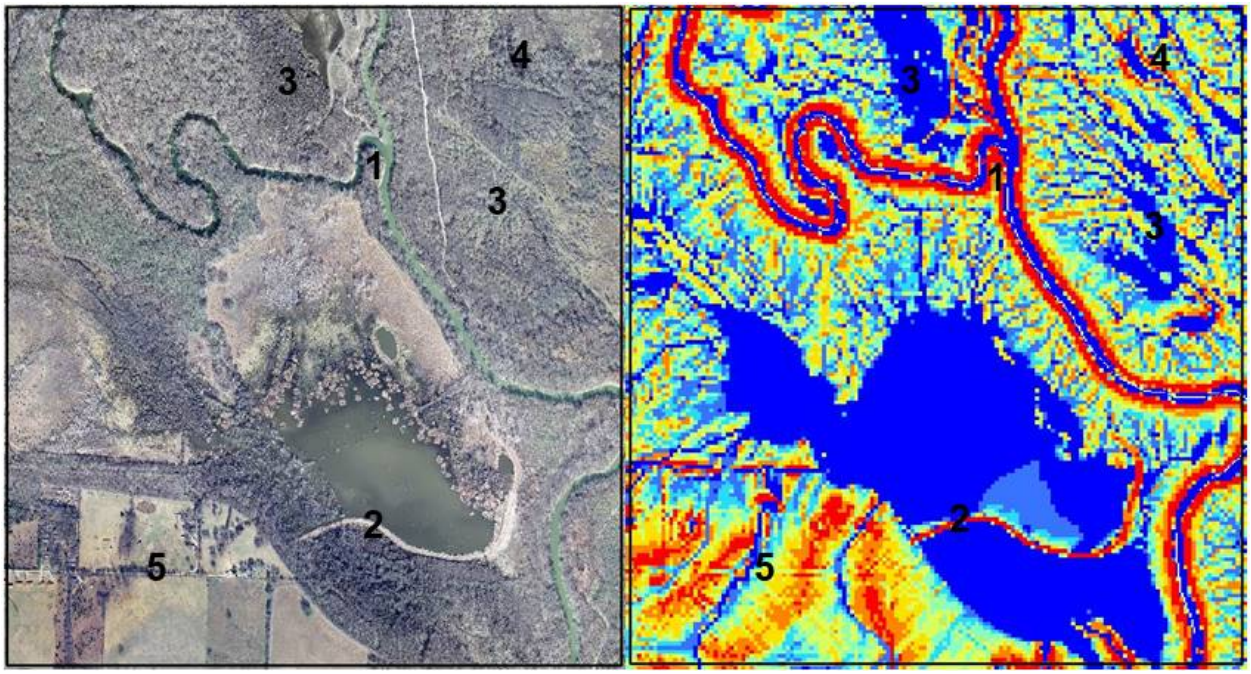

Figure 4.26. Area C aerial image and TWI map. Area C shows the confluence of Clear Creek and Elm Fork. The TWI was calculated from the 10-m grid LiDAR-derived DEM that was processed using the D∞ flow direction algorithm. The color scale of the TWI map was set with red representing low values and blue representing high values. Note that in the TWI map, the shape of the major stream channels included their banks (1) as well as the constructed wetland and its berm (2). The TWI map also picked up the floodplain wetlands located between the two streams and to the east of Elm Fork (3). The small pool in that wetland area was clearly visible (4). The area with low TWI values in the southwest corner, which is now covered in residential properties and agricultural land, was an upland area with soils associated with grassland vegetation, while most of the remainder of the frame would historically be covered in bottomland hardwood forest.

The shape of the major stream channels including their bends and banks were visible in the TWI map. The constructed wetland could be seen, and its artificial berm was clearly visible. While difficult to see in the image at this zoom, wetland areas in the floodplain between the two streams and to the east of Elm Fork were visible in the TWI map. The area in the southwest, or bottom-left, corner map with the high TWI values, covered in residential properties and agricultural land, was an upland area with soils associated with grassland vegetation. Most of the land to the northeast of that corner was historically covered in bottomland hardwood forest.

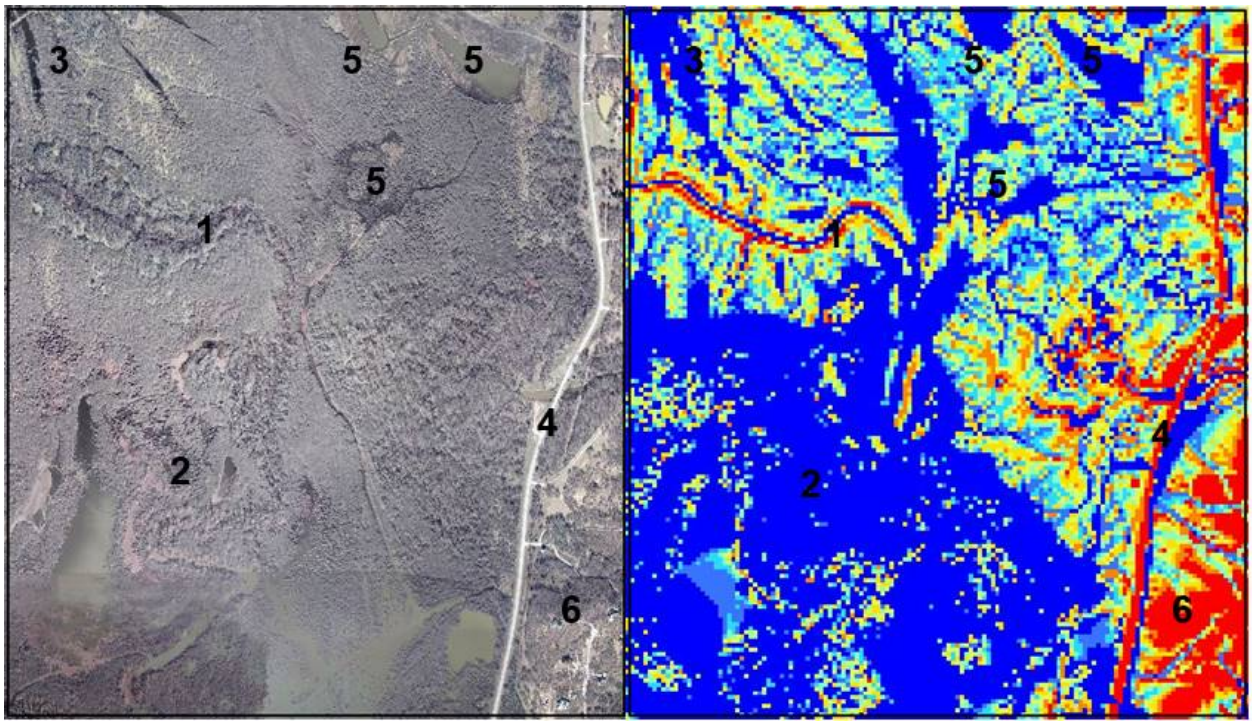

Figure 4.27. Area D aerial image and TWI map. Area D shows the flat, bottom floodplain of Elm Fork. The TWI was calculated from the 10-m grid LiDAR-derived DEM that was processed using the D∞ flow direction algorithm. The color scale of the TWI map is set with red representing low values and blue representing high values. The TWI map correctly shows the shape of the little stream channel coming in from the west side of the image (1). The entire southwestern section of the map (2), which is dense with high values of TWI, is a wetland. The wetlands or sloughs in the northwest corner are also visible in the TWI map (3). The north-south road on the east side of the frame shows up as a bright red line of low TWI values (4). The wetland areas and ponds that are in the northeastern portion of the frame fit well to the shapes of high TWI values (5). The southeastern corner of low TWI values, along with all the land immediately to the east of the road, is an area of upland post oak forest (6).

The TWI map (Fig. 4.27), which was a close up of the flat floodplain area D, correctly showed the shape of the little stream channel coming in from the west side of the image. The entire southwestern swath of the map was a wetland, and that area was covered in high values in the TWI. The wetlands or sloughs in the northwest corner, none of which were visible in the flow accumulation maps, were visible in the TWI map. A road running north-south road along the east side of the frame showed up as a line of low TWI values. The wetland areas and ponds in the northeastern portion of the frame fit the shapes of the blue areas with high TWI values nicely. The southeastern corner of low TWI values, along with all the land immediately to the east of the road, was an area of upland post oak forest.

Area E was mostly composed of an upland, post oak forest hill, but it also included a transition down into bottomland forest closer to the river (Fig. 4.28). The large stream channel on the east side of the image is Elm Fork, and it along with its banks is clearly visible in the TWI map. All of the red area in the eastern portion of the TWI map corresponds to hilly upland covered historically by post oak forest. Small streams are often easier to see in the TWI map than they are in the aerial image. In addition to stream channels, the TWI map can pick up places with evidence of sheet flow and surface runoff. Roads show up as lines of low TWI values, while ponds show up as spots of high TWI.

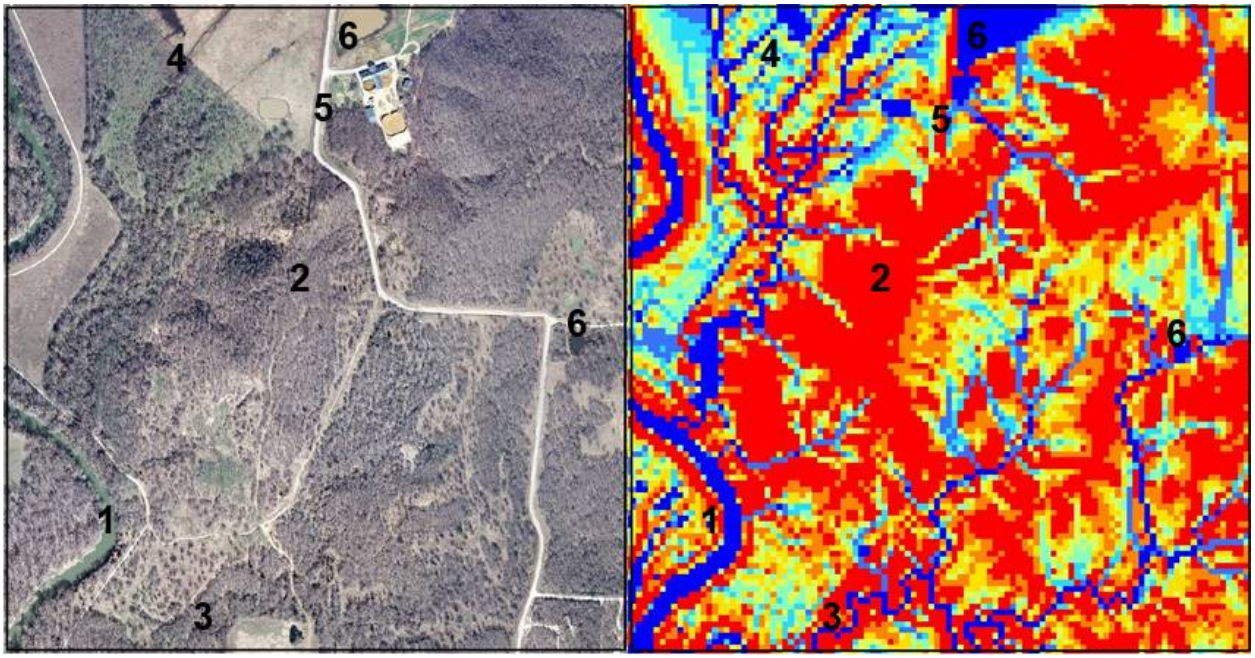

Figure 4.28: Area E aerial image and TWI map. Area E was mostly composed of an upland, post oak forest hill but also included a transition down into bottomland forest closer to the river. The TWI was calculated from the 10-m grid LiDAR-derived DEM that was processed using the D∞ flow direction algorithm. The color scale of the TWI map is set with red representing low values and blue representing high values. The large stream channel on the east (left) side of the frame, which is Elm Fork, is clearly visible in the TWI map along with its banks (1). All of the red area in the eastern portion of the map is hilly upland covered historically by post oak forest (2). The little stream channels coming down the hills are easier to discern in the TWI map than in the aerial image (3). The evidence of surface runoff and sheet flow going towards the stream channel at the top of the frame is also picked up in the TWI map (4). Some of the roads in the image appear as lines of low TWI values (5). Ponds in the image show up as blue spots of high TWI values (6).

It is clear that the TWI map can detect or correlate to surface features related to topography and hydrology, which is why it was chosen as the tool to partition the terrain types for FACETA. Before discussing how that was done, the most appropriate version of the TWI map for this task was determined. To accomplish this, the impacts that different DEM sources, grid resolutions, and flow direction algorithms have on the TWI map and its ability to determine terrain types were examined. The general spatial pattern of values was similar across the different TWI maps, at least at a broad perspective. The frequency distribution of values across the versions was also similar (Fig. 4.29). Frequency distributions from two different TWI maps were examined, using

the two most different versions as examples – those calculated from the 29-m grid contour-derived, D8 flow algorithm processed DEM and the 5-m grid LiDAR-derived D∞ processed DEM. Their frequency distributions were similar with the only notable difference being the unusual spike in frequency in the 5-m grid map at the TWI value of approximately 13.

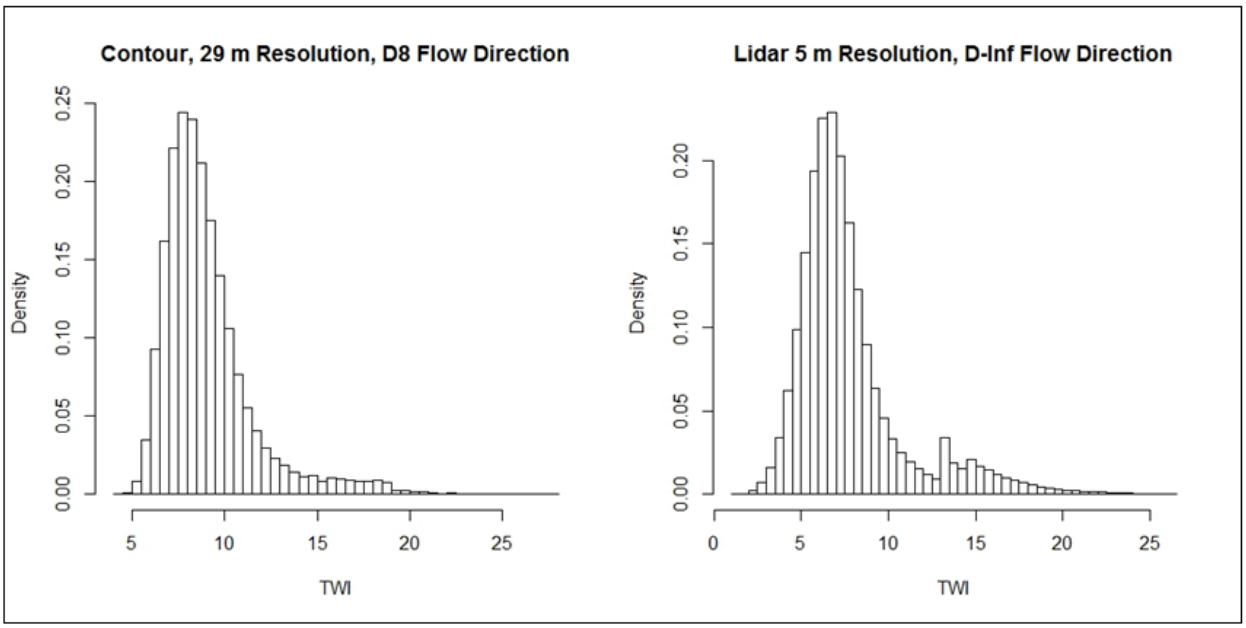

Figure 4.29. Frequency distribution of two TWI maps. The two frequency distributions of values of TWI maps are generated from the 29-m contour-derived DEM using the D8 flow direction algorithm (left) and the 5-m LiDAR-derived DEM using the D∞ flow direction algorithm. These were the two most different TWI maps, but their frequency distributions were still similar. The only notable difference in them was the unusual spike in frequency exhibited in the 5-m grid map at the TWI value of approximately 13.

A broad examination of the summary statistics for the different TWI maps did not reveal any striking differences or trends (Table 4.4). There were no noticeable trends across DEM sources or flow direction algorithms. There was a trend across grid sizes in that the smaller the grid, the smaller the minimum and first quartile values of TWI were. However, this trend was just a consequence of the fact that approximately the first quartile of flow accumulation was typically zero, resulting in a specific catchment area equal to the width of a grid cell. Therefore, the smaller the grid resolution, the smaller

the minimum and first quartile would be. There were spatial differences between the various TWI grids that were not detectable in either the summary statistics or frequency distributions of values. Visual examinations of the TWI maps zoomed into the three focus areas were used to investigate those spatial differences.

Table 4.4

Five Number Summaries of TWI from Different DEMs

DEM Source	Grid Size (meters)	Flow Direction	Five Number Summary of TWI					Mean TWI
			Min.	1st Qu.	Median	3rd Qu.	Max.	
LiDAR	29	D8	4.39	7.43	8.35	9.65	27.57	8.98
LiDAR	29	D∞	4.09	7.33	8.28	8.94	24.38	9.61
Contour	29	D8	4.27	7.46	8.49	9.06	27.53	9.88
Contour	29	D∞	4.00	7.38	8.47	9.01	24.34	9.91
LiDAR	10	D8	2.90	6.43	7.40	8.05	28.61	8.72
LiDAR	10	D∞	2.71	6.58	7.62	8.49	27.58	9.11
Contour	10	D8	2.55	6.73	7.83	8.32	28.63	9.18
Contour	10	D∞	2.18	6.90	8.04	8.49	25.44	9.44
LiDAR	5	D8	1.90	5.69	6.71	7.45	29.31	8.16
LiDAR	5	D∞	1.29	5.86	6.98	7.78	26.13	8.51
Contour	29 Resampled	D∞	3.96	7.55	8.67	10.18	27.52	9.34

Note. Five number summaries and arithmetic mean for TWI derived from different DEM sources, grid resolutions and flow direction algorithms. The distribution of values and summary statistics for all the different TWI grids are similar, and there are no clear trends across DEM source or flow direction algorithm. One trend across grid sizes is that the smaller the grid the smaller the minimum and 1st quartile values of TWI are, but this trend is just a consequence of the fact that approximately the 1st quartile of flow accumulation is zero, resulting in a specific catchment area equal to the width of a grid cell. There are spatial differences between the various TWI grids that cannot be seen in the summary statistics or distribution of values. The last grid listed in the table is generated from a 29-m grid that was resampled from the 10-m contour-derived DEM.

TWI maps of area C were derived from the two contour-derived 29-m resolution DEMs (Fig. 4.30). One map was processed with the D8 flow algorithm, and one map on was processed using D∞. The spatial pattern of the two TWI maps was very similar. The D8-generated map had a patchier appearance than the D∞ generated one. The primary difference between the two maps was the missing data values found within the stream channels and through the center of the D∞ generated map. These were the same missing data cells found in the corresponding flow accumulation grid, were a carryover from the flow accumulation grid, and were expected in the TWI map. The missing data cells that fall within stream channels did not cause a problem with defining terrain types, but the missing data cells on land did cause a problem. Without correcting or filling in the missing data, classifying land into terrain types was not possible.

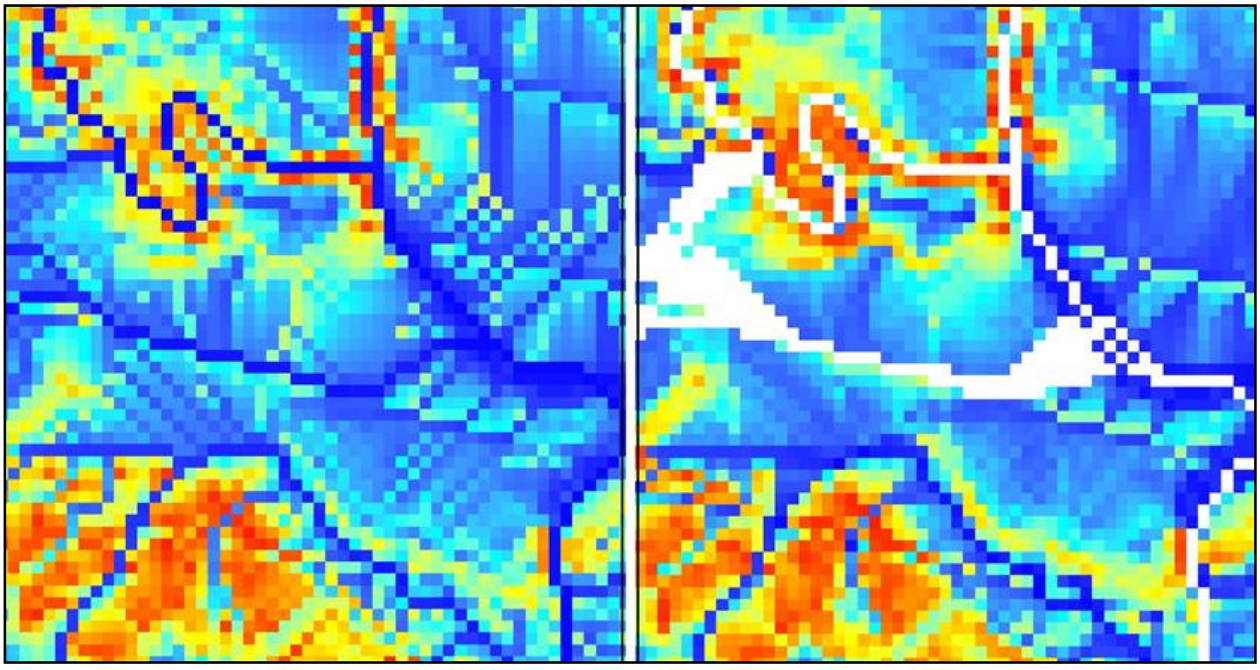

Figure 4.30: TWI maps of area C from contour-derived 29-m DEM. The spatial patterns of the two TWI maps derived from the contour-derived 29-m grid DEM at area C were very similar. The two TWI maps were processed with different flow direction algorithms, with the D8-generated TWI map on the left and the D∞ generated TWI map on the right. There were subtle differences in the values for some cells, and the D8-generated map had a patchier appearance. The only distinct difference between the two was the missing data values found within the stream channels and along a swath through the center of the image in the D∞ generated map. These no data values were carried over from the flow accumulation grid and

were not a surprise. Missing data within the stream channels did not present a problem with defining terrain types, but the missing values on land through the center of this map made classifying the land into terrain types impossible without some correction.

The two same TWI maps also focused on the flat bottomland area D (Fig. 4.31). The two TWI maps compared much the same in area D as in area C. The spatial patterns were much the same between the two maps, the D8 generated map was patchier, and the D∞ map had missing values. However, a characteristic seen in both maps was a pattern of crisscrossing diagonal lines running across the frame, although it was not as easy to see at this zoom. By viewing the maps a little more broadly, the pattern of lines became clear (Fig. 4.32). These striping artifacts were the same artifacts seen in the slope maps calculated from the contour-derived DEMs.

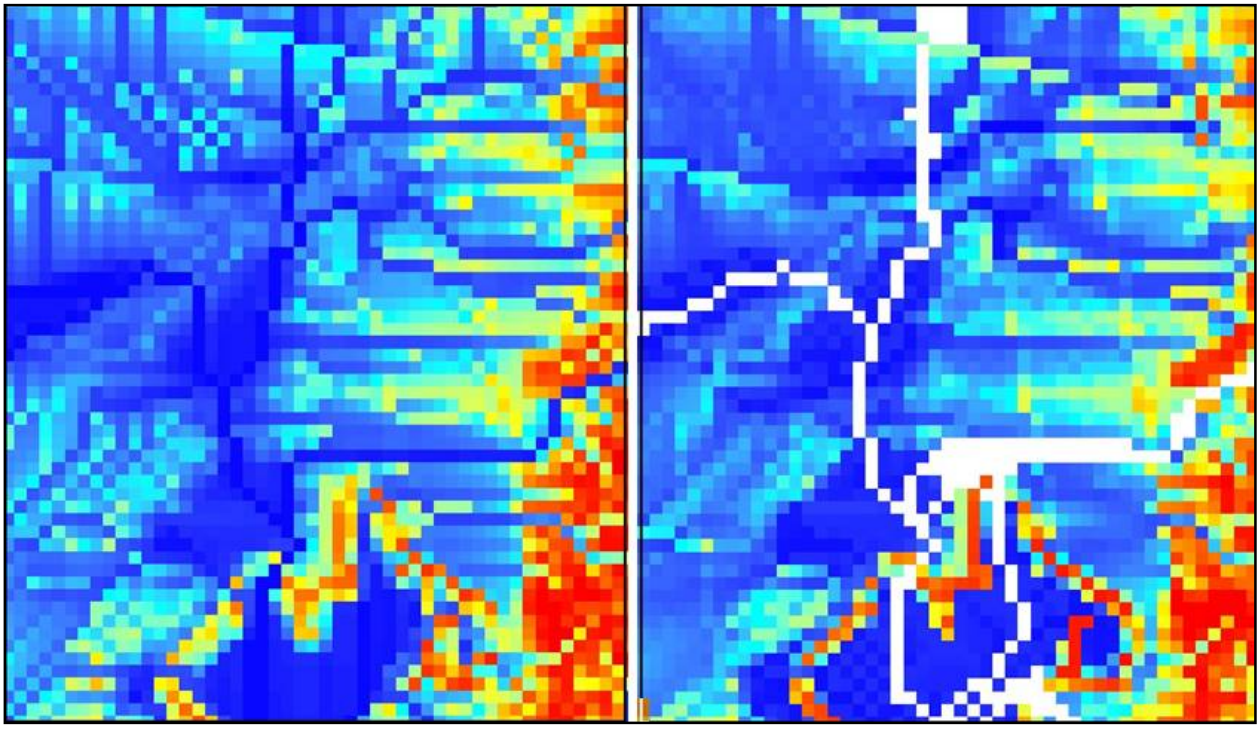

Figure 4.31. TWI maps of area D from contour-derived 29-m DEM. As in area C, the spatial pattern of the two TWI maps derived from the contour-derived 29-m grid DEM at area D were very similar. The difference that the maps were processed with different flow direction algorithms, with the D8-generated TWI map on the left and the D∞ generated TWI map on the right. There were subtle differences in the values for some cells, and the D8-generated map had a patchier appearance. The only distinct difference between the two maps was the missing data values found in areas of high flow accumulation in the D∞ generated map.

In the broader perspective shown, the striping artifacts came out stronger in the D∞ generated TWI map (Fig. 4.32). The striping artifacts were also seen in the slope maps. Once slope was calculated, the error, which started in the elevation grid, was then manifested as subtle errors in slope. The likely explanation of why it appeared worse in the D∞ generated maps was that the algorithm was better at detecting subtle differences in slopes than was the D-8, or perhaps the algorithm overestimated subtle differences in slope. In both the D8 and D∞ maps, the artifacts were worse in the flat areas with low TWI values.

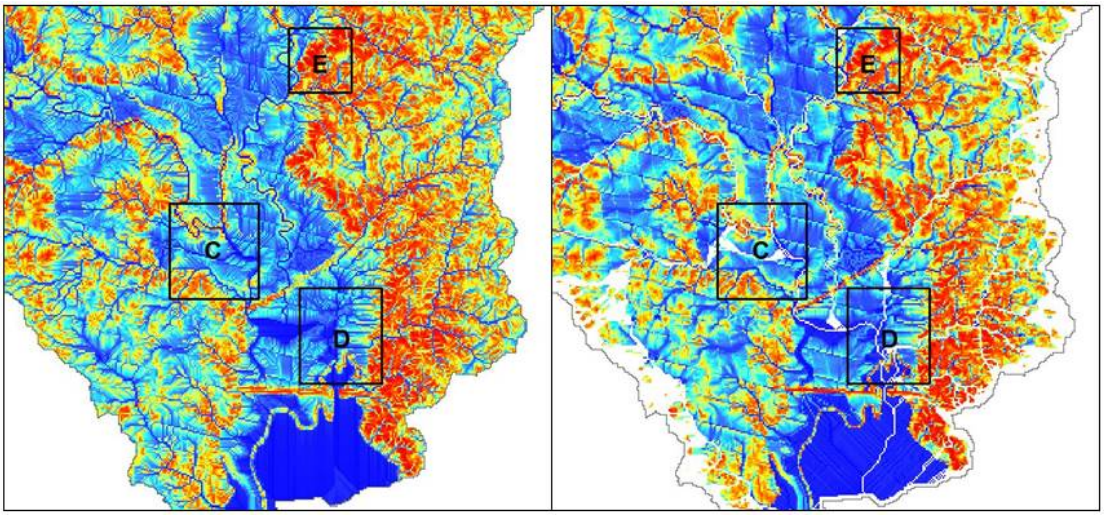

Figure 4.32. Striping artifacts in 29-m contour-derived TWI maps. Striping artifacts were clearly visible in both the D8 and D∞ generated 29-m contour-derived TWI maps. The lines were more prevalent in the D∞ generated map (right) than the D8 map (left).

When viewing continuous raster data, the display setting can make a tremendous difference in the visual interpretation of the data. In order to see how these striping artifacts impacted the delineation of terrain types, the maps needed to be displayed in a way that was meaningful to the terrain type definitions. The way the TWI map was used in terrain type definition in this study was through classification by percentiles. This approach was purposefully simple and should be considered a first try; the method of

partitioning terrain types can be refined in the future. In fact, at this time the cut off points for TWI categories should be considered like a model parameter that needs to be calibrated. The same two TWI maps were evaluated with the display setting set to correspond to terrain type definitions (Fig. 4.33).

This particular classification scheme had three categories with the percentile breaks set at 20% and 80%. The categories were interpreted as being the wettest fifth of the land, the driest fifth, and the 60% majority in the middle. However, these percentile values should be further be calibrated to fit the characteristics of the watershed. While the striping artifacts were not as visible with this setting, they were still visible (Fig. 4.33). For both the 29-m grids and the 10-m grids, the artifacts were more pronounced under the D∞ flow direction algorithm, and they were more pronounced in the 10-m grids than the 29-m grids.

When compared with aerial images and with the LiDAR-sourced TWI maps, it was clear that these lines were artificial and did not correspond to changes in the terrain on the ground. Without filtration or some other means of correcting the contour-derived DEMs, the TWI maps derived from them presented a problem in classifying terrain types that the LiDAR-derived grids did not. With LiDAR-sourced DEMs available for this research, there was no reason to continue the terrain delineation process with these grids. However, LiDAR data were not available for many places, and a contour-derived DEM might be the only available option. A new version of one of these DEMs was introduced at this time as an example of a workaround to the striping artifacts.

Resampling performed on the 10-m contour-derived DEM to change the grid size to match the 29-m DEMs acted as a filter to most if not all of the artifactual lines. The

resampling method used was *nearest neighbor.* This particular grid was processed with the D∞ flow direction algorithm. Close up views of the southern portion of the study area watershed showed both the unclassified grid and the grid classified using the same 20% and 80% cut offs (Fig. 4.34).The striping artifacts were not apparent in either map. Different resampling methods were not tested for this study, and D8 flow direction was not used to process this resampled DEM. For investigation of terrain type delineation, this DEM acted as the sole replacement to the other four contour-derived DEMs.

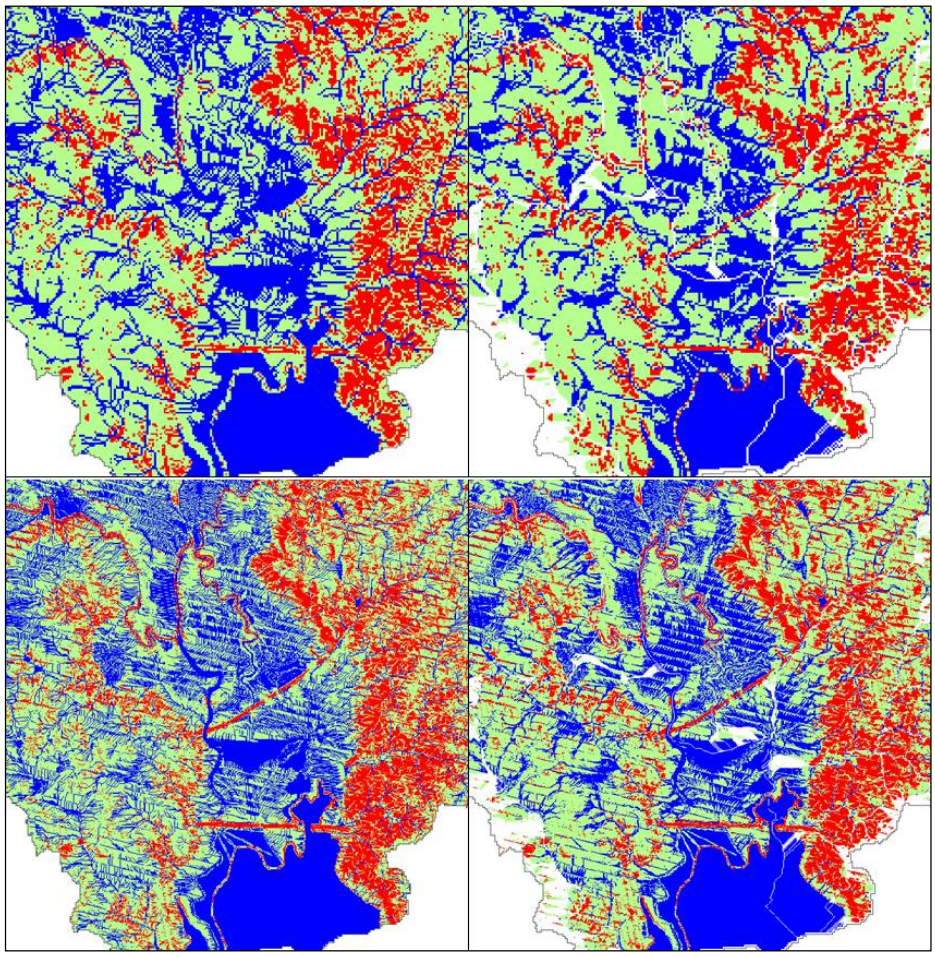

Figure 4-33. Artifacts in contour-derived TWI maps with quintile classification. All four TWI maps from the contour-derived DEMs showed striping artifacts, even after the TWI values were classified by terrain types. In this example, quintiles were used to partition the TWI values with the middle three quintiles grouped together as one category. The artifacts were more pronounced in the D∞ generated maps than the D8 maps for both grid sizes, and they were worse in the 10-m grids than the 29-m grids. Note identity: (*top-left*) 29-m D8-generated TWI classes, (*top-right*) 29-m D∞ generated TWI classes, (*bottom-left*) 10-m D8-generated TWI classes, and (*bottom-right*) 10-m D∞ generated TWI classes.

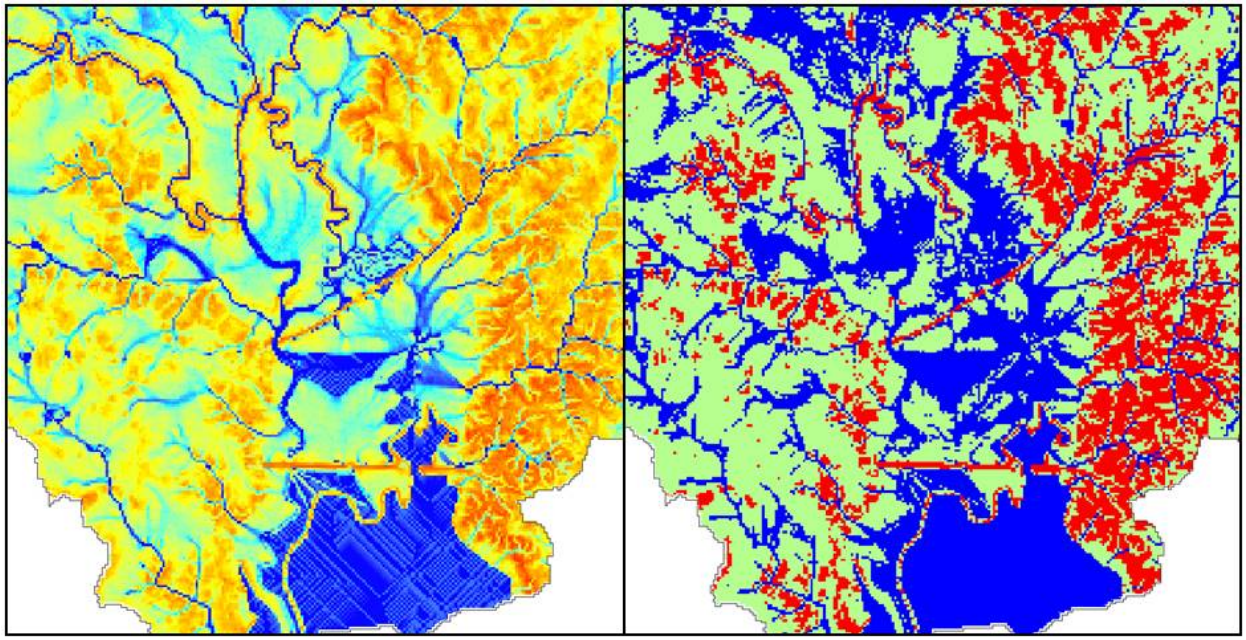

Figure 4.34. TWI from resampled contour-derived DEM. With striping artifacts apparent in the TWI terrain type classes in all four of the contour derived grids, the 10-m grid was resampled to a 29-m resolution using the nearest neighbor resampling method. This resulted in filtering out the artifactual lines. (*Left*) TWI from the resampled grid displayed using a stretched color scheme. (*Right*) TWI from the resampled grid classified into three groups using percentiles, with 20% and 80% used as the cutoff points.

With the rejection of the four contour-derived grids and their replacement with the resampled grid, seven TWI maps evaluated terrain type delineation. The seven maps were compared with each other and surface features were seen in the aerial image in the three areas, C, D, and E. In the comparisons, all of the TWI maps were displayed using a 2.5σ standard deviation stretch. Due to space limitations, a color ramp key was not included in the TWI figures. Figure 4.35 shows the color ramp used for all of the TWI maps. Table 4.4 lists the specific high and low TWI values for any particular TWI map.

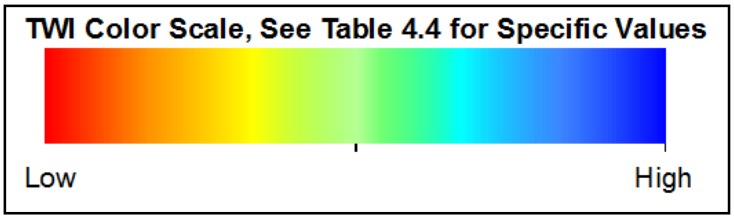

Figure 4.35. Color ramp scale for TWI maps. All of the TWI maps are displayed using a 2.5σ standard deviation stretch with a color ramp going from red for low values to blue for high values. Specific high and low values for each TWI map are listed in Table 4.4.

The three remaining 29-m TWI maps – contour-derived and resample, LiDAR-derived and D8 processed, and LiDAR-derived and D∞ processed – of area C were compared with each other and the aerial image (Fig. 4.36). The general pattern for all three maps was similar, but there were some differences. The LiDAR-derived TWI maps were more accurate in outlining shapes and locating positions of wetlands and surface water, while the contour-derived resampled map had a smoother appearance due to the averaging effect of resampling the DEM. The two LiDAR-derived TWI maps were generally very close to each other, but the D∞ processed map was considerably patchier in the flat areas than the D8 map. There was not much difference between the two LiDAR-derived TWI maps in the more flat upland positions.

The detail level for all four 5-m and 10-m LiDAR-derived TWI maps was much higher than the 29-m grids (Fig. 4.37). In flat areas, both the 10-m and 5-m D∞ processed TWI maps were patchier than the corresponding D8 processed maps, and they contained artificial crisscrossing lines. However, in the upland areas, the D8 processed grids were patchier and more dendritic. The problems of patchiness and artificial lines were generally more pronounced in the smaller grid resolutions. The finer grid size maps showed more detail and changes in relief, but often over areas where the type of terrain and forest coverage did not vary much.

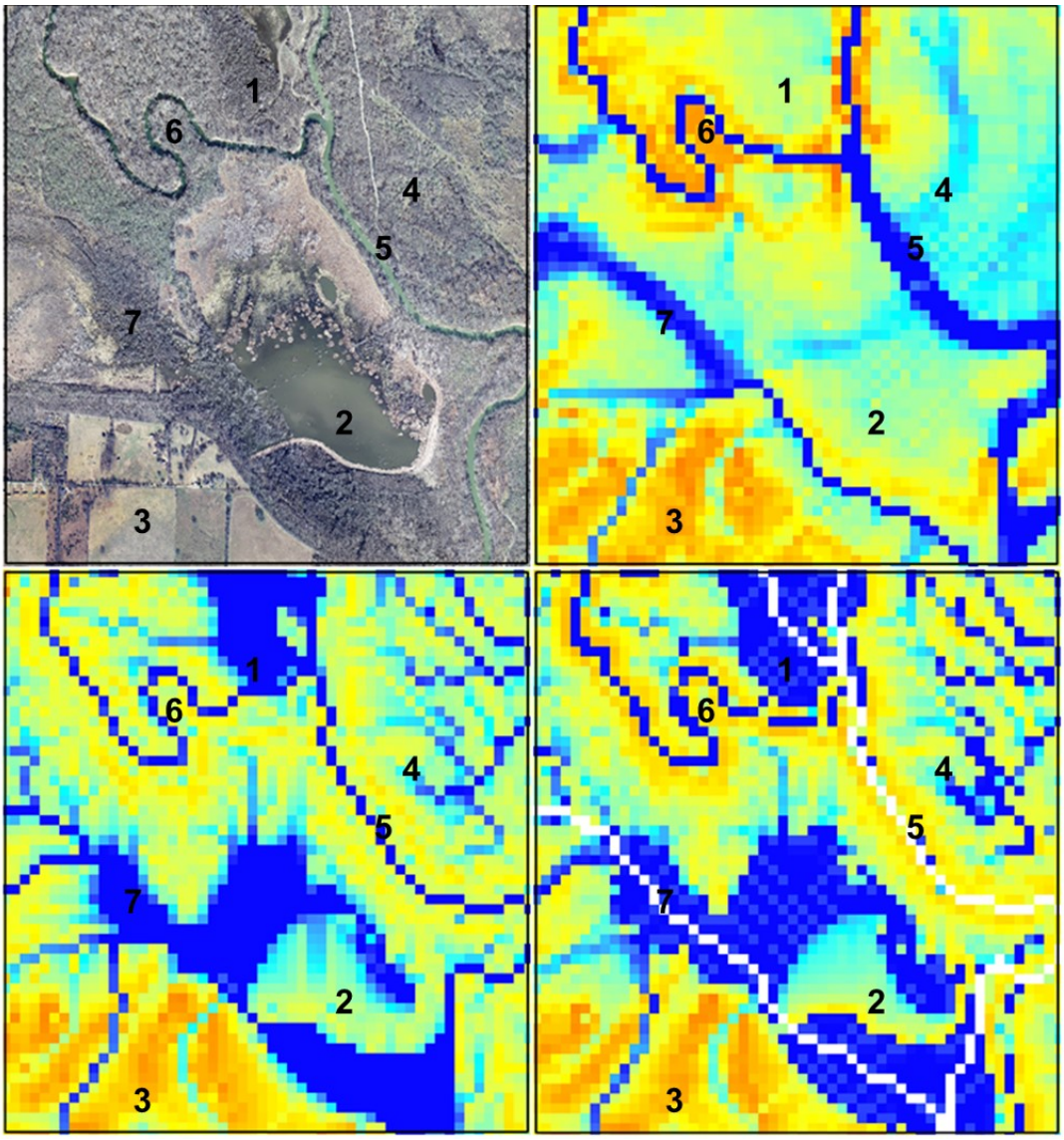

Figure 4.36. TWI calculated from 29-m grid DEMs at area C. TWI maps of area C were calculated from the three remaining 29-m DEMs. (*Top-left*) The aerial image was taken in the winter in 2005. (*Top-right*) Map calculated from the contour-derived DEM that was resampled from 10-m to 29-m due to the striping artifacts. (*Bottom-left*) Map was calculated from 29-m LiDAR-derived DEM processed using the D8 flow algorithm. (*Bottom-right*) Map was calculated from 29-m LiDAR-derived DEM processed using the D∞ flow algorithm. Locations of note: (1) The wetland area between the two streams showed up well in the two LiDAR-derived maps but was not apparent in the resampled contour-derived map. The flat, wet area was patchier in the D∞ derived map than in the D8 derived map. (2) The large constructed wetland did not appear in the resampled TWI map, but it was delineated in both LiDAR-derived TWI maps. Neither matched the surface water pattern as seen in the aerial image, but that may likely have been due to the wetland being constructed with an artificial berm. (3) All three TWI maps identified the upland area in the southwest corner well. (4) The general pattern of wetness found in this area was most apparent in the TWI map from the resampled DEM; however, the two LiDAR DEMs did a better job at detecting sloughs. This was likely due to the averaging effect of the resampling and the improved accuracy of the LiDAR data. (5) The Elm Fork River channel was too wide in the resampled, contour-derived TWI map, while the channel cells were missing in the D∞ derived TWI map. (6) The land within this bend of Clear Creek showed up with too high TWI values in the resampled, contour-derived TWI map, and to a lesser degree in the D∞ derived map. While the land within this bend was slightly higher than some of the surrounding

bottomland, it was still bottomland that was prone to flooding. (7) This wetland area and small stream showed up best in the D8 derived TWI map. The general shape of the area was captured well by both of the LiDAR-derived TWI maps, but was patchier and contained missing data cells in the D∞ map.

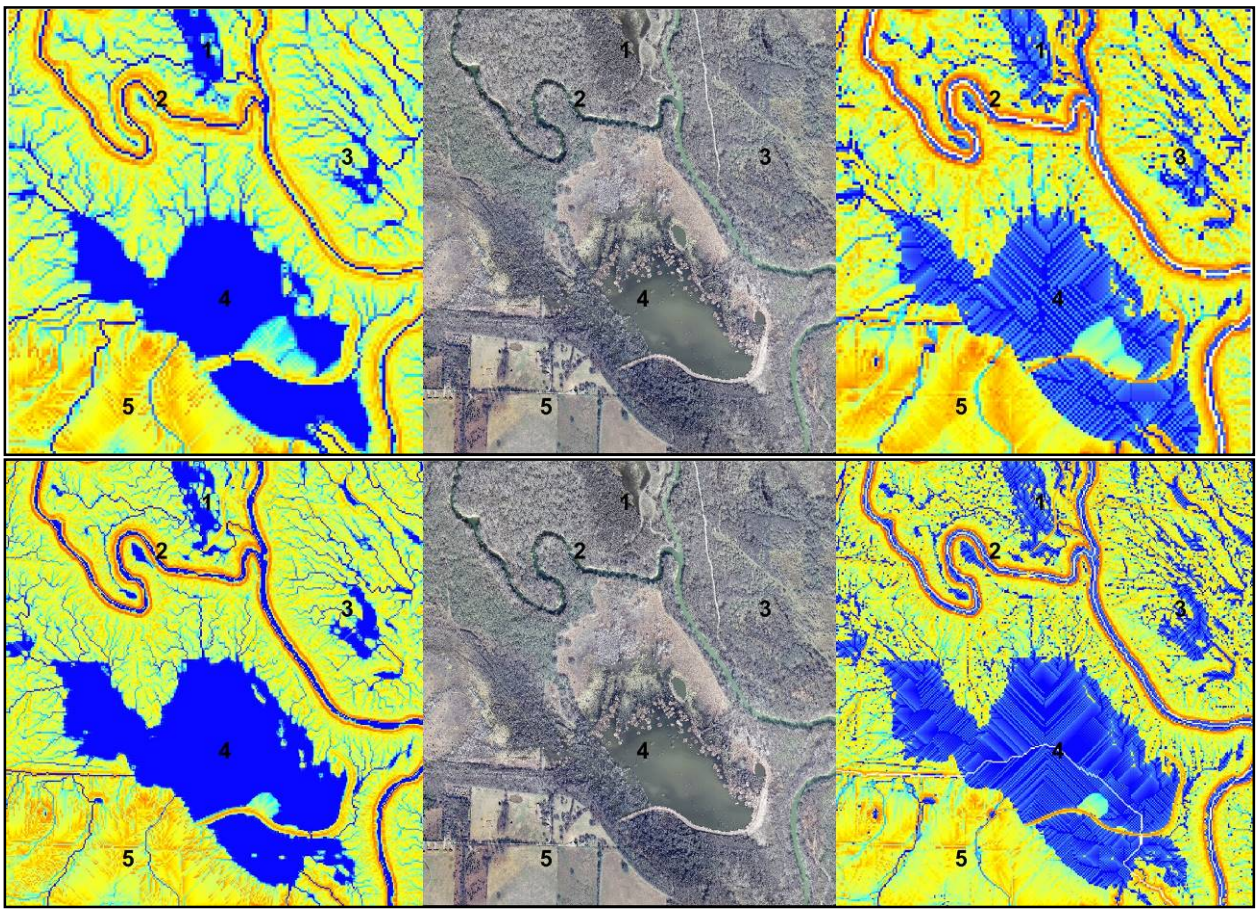

Figure 4.37. TWI calculated from 10-m and 5-m grid DEMs at area C. TWI maps of area C were calculated from the two 10-m and two 5-m LiDAR-derived DEMs. (*Top-left*) TWI map calculated from the10-m D8 processed DEM. (*Top-center*) Aerial image of the area was taken in the winter in 2005. (*Top-right*) Map was calculated from the 10-m D∞ processed DEM. (*Bottom-left*) Map was calculated from the 5-m D8 processed DEM. (*Bottom-center*) Aerial image. (*Bottom-right*) TWI map from the 5-m D∞ processed DEM. Locations of note: (1) The wetland area between the two streams appeared in all four TWI maps; however, there was a patchy, crisscrossed line pattern reminiscent of the striping artifacts seen previously in the contour-derived DEMs. The 5-m D8 processed TWI map showed more detail of possible higher relief within the wetland area. There were changes in relief within this general area; however, all of this was wet bottomland forest. (2) The stream banks and channel walls were identified more as dry terrain in both D∞ processed TWI maps than in the D8 processed maps. They appeared drier in the 5-m D8 map than in the 10-m D8 map, and they appeared equally dry in intensity in the two D∞ processed TWI maps. However, the indicated dry area of the channel banks was wider in the 10-m D∞ map. (3) In this wetland area, both D∞ processed TWI grids were patchier and contained a larger range of values, including more and lower dry TWI values than the corresponding D8 processed grids. The 5-m D8 processed grid was more accurate with surface water and indicated a larger wetland area with a smoother boundary than the 10-m D8 processed grid, but it also contained a larger range of values, greater contrast within the general bottomland area, and cells with lower and drier TWI values. (4) All four TWI maps indicated the location of the large constructed wetland well, but both D∞ processed maps again had the artificial crisscrossing lines in this flat area. (5) This upland area appeared as such in all four grids; however, the pattern was slightly patchier and more dendritic in the D8 processed TWI grids

than in the corresponding D∞ grids. Both 5-m grids were more dendritic in pattern in the upland area than their corresponding 10-m grids. At the same time, the values in the two 10-m grids ranged lower than the two 5-m grids.

These finer grid resolutions made the stream channel banks appear as low TWI value land, implying dry terrain. While certainly there were differences between the banks, flats, and sloughs, having them designated in the driest category of terrain may have presented a problem in the model. While the stream bank areas had lower TWI values in the 29-m grids than in the adjacent bottomlands, the values did not fall into the lowest categories.

In the very flat bottomland area D, the general pattern of values between the two LiDAR-derived 29-m grid TWI maps was quite similar, but it was much different in the resampled contour-derived map (Fig. 4.38). Locations of channels and wetlands were very inaccurate in the contour-derived grid, while both of the LiDAR-derived grids matched the aerial image fairly well. Flat areas and wetlands were patchier and contained lower and drier TWI values in the D∞ processed grid than in the D8 TWI maps. However, in the hilly upland areas, the pattern of values was slightly patchier in the D8 processed grid, but these differences were slight.

In the wetlands of the low, flat bottomland area D, the D∞ processed 10-m and 5-m TWI grids both were very patchy, had artificial crisscrossing lines, and contained cells with values that were too low for their generally flat, wet nature (Fig. 4.39).

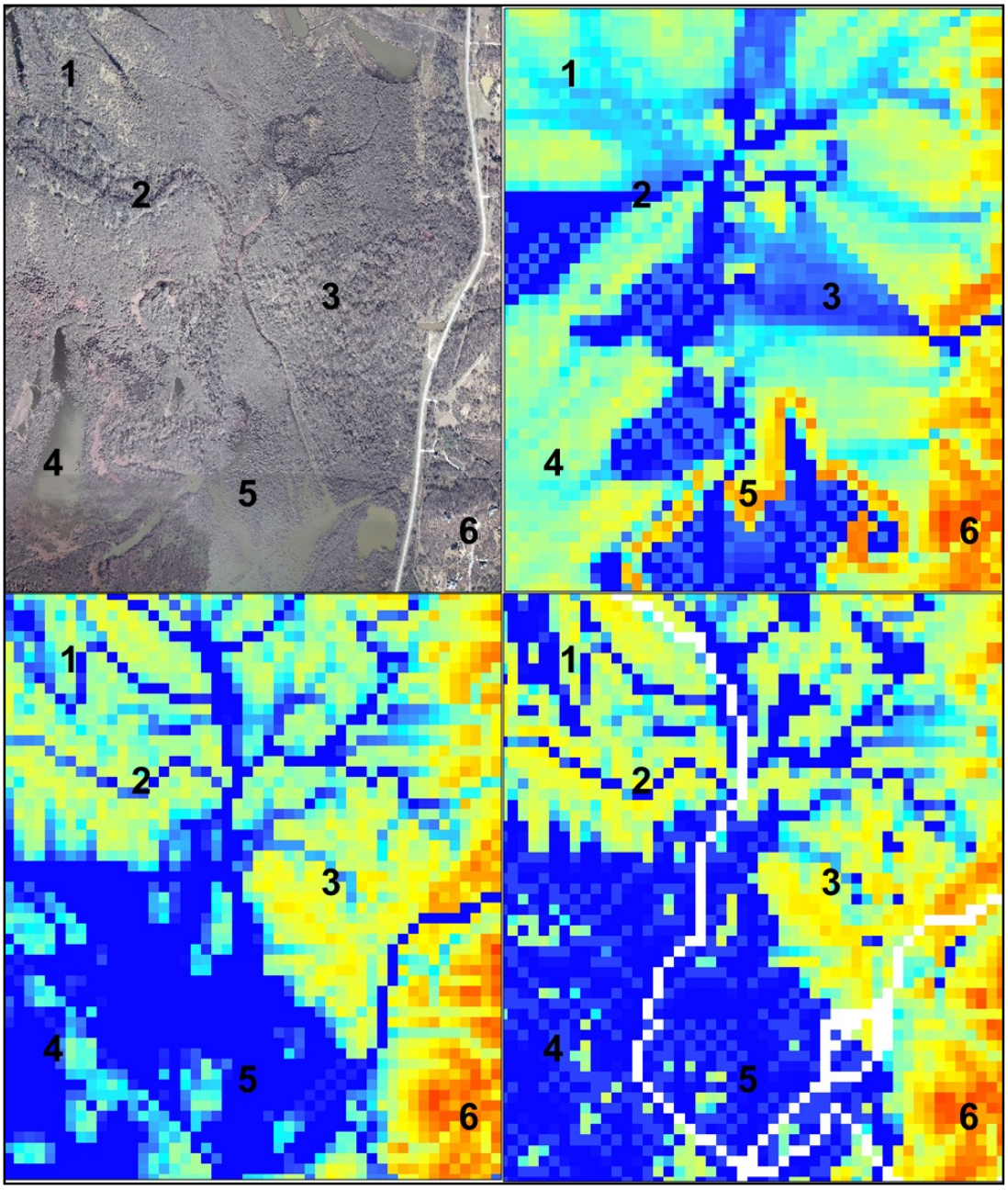

Figure 4.38. TWI calculated from 29-m grid DEMs at area D. TWI maps of the swampy bottomland area D calculated from the three remaining 29-m DEMs. (*Top-left*) Aerial image of the area was taken in the winter in 2005. (*Top-right*) TWI calculated from the contour derived DEM that was resampled from 10-m to 29-m due to the striping artifacts. (*Bottom-left*) TWI from the 29-m LiDAR-derived DEM processed using the D8 flow algorithm. (*Bottom-right*) Map calculated from 29-m LiDAR-derived DEM processed using the D∞ flow algorithm. Locations of note: (1) The two LiDAR-derived maps indicated the sloughs more accurately, while the contour-derived grid gave a more general, averaged wet image of the area. (2 and 3) Small channels such as these are very inaccurately indicated in the contour derived grid as compared to the LiDAR derived grids, probably due to a combination of errors in the source and the averaging that resulted from resampling. (4 and 5) These wetland areas show up as being too dry in the contour derived TWI map. They are patchier and contain lower and drier TWI values in the D∞ processed grid. (6) This hilly upland area shows up well in all three grids; however, the pattern of values is slightly patchier in the D8 processed grid.

Of these four grids, the 10-m D8 processed grid gave the best indication of flat and wetland areas. However, because the 29-m D8 map was less patchy and contained fewer misrepresentative low TWI values, it was better in flat and in wetland areas than the 10-m grid. In the hillier upland areas, the D∞ processed grids yielded a slightly smoother, less patchy pattern of TWI values than the D8 grids, and the 5-m D8 grid was patchier than the 10-m D8 grid.

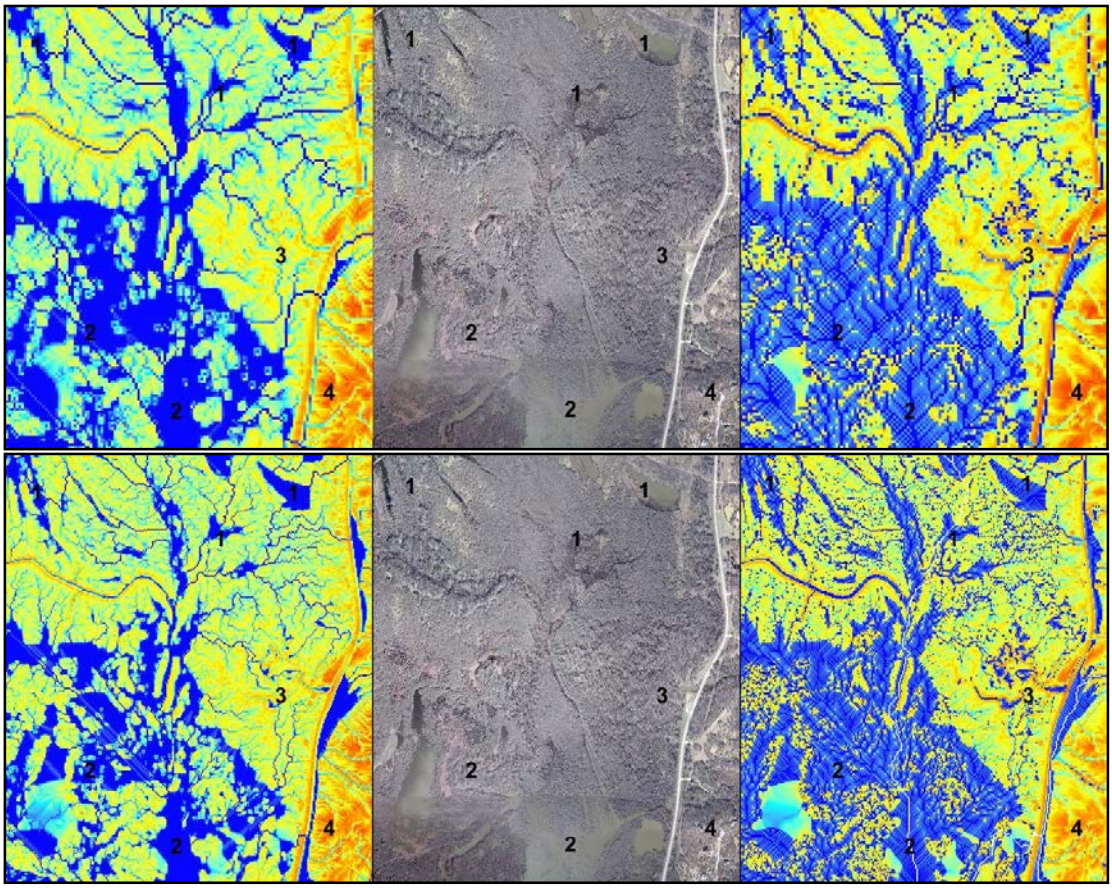

Figure 4.39. TWI calculated from 10-m and 5-m grid DEMs at area D. TWI maps of area D calculated from the two 10-m and two 5-m LiDAR-derived DEMs. (*Top-left*) TWI map calculated from the10-m D8 processed DEM. (*Top-center*) Aerial image of area taken in the winter in 2005. (*Top-right*) Map calculated from 10-m D∞ processed DEM. (*Bottom-left*) Map calculated from 5-m D8 processed DEM. (*Bottom-center*) Aerial image. (*Bottom-right*) TWI map from 5m D∞ processed DEM. Places of note include: (1) Wetland areas were generally well located in all four grids, but D∞ processed grids were patchy and contained artificial lines and values ranging too low. The range in values went lower, and more contrast was indicated in the 5-m D8 processed grid than the 10-m grid; however, the terrain in these areas was all fairly flat and similar. (2) In these lower, wetter bottomland areas, all four grids indicated wet terrain in general; however, they also all contained TWI values that were too low when compared to the terrain. The 10-m D8 processed grid gave the overall best impression of this wetland area out of these four grids. (3) While this area was drier than in location 2, both of the D∞ processed grids yielded values too low for

this generally low lying area. (4) In this hilly upland area, the D∞ processed grids yielded smoother patterns in TWI values than the D8 grids, and the 5-m D8 grid was patchier than the 10-m D8 grid.

All three 29-m grids gave a good general representation of the hilly upland area E (Fig. 4.40). The contour-derived resample grid was the least accurate of the three. There was very little difference between the two LiDAR grids in determining the wettest locations. While the D∞ processed algorithm was a little better than the D8 algorithm at indicating the locations of some of the ponds, it also had some missing data values.

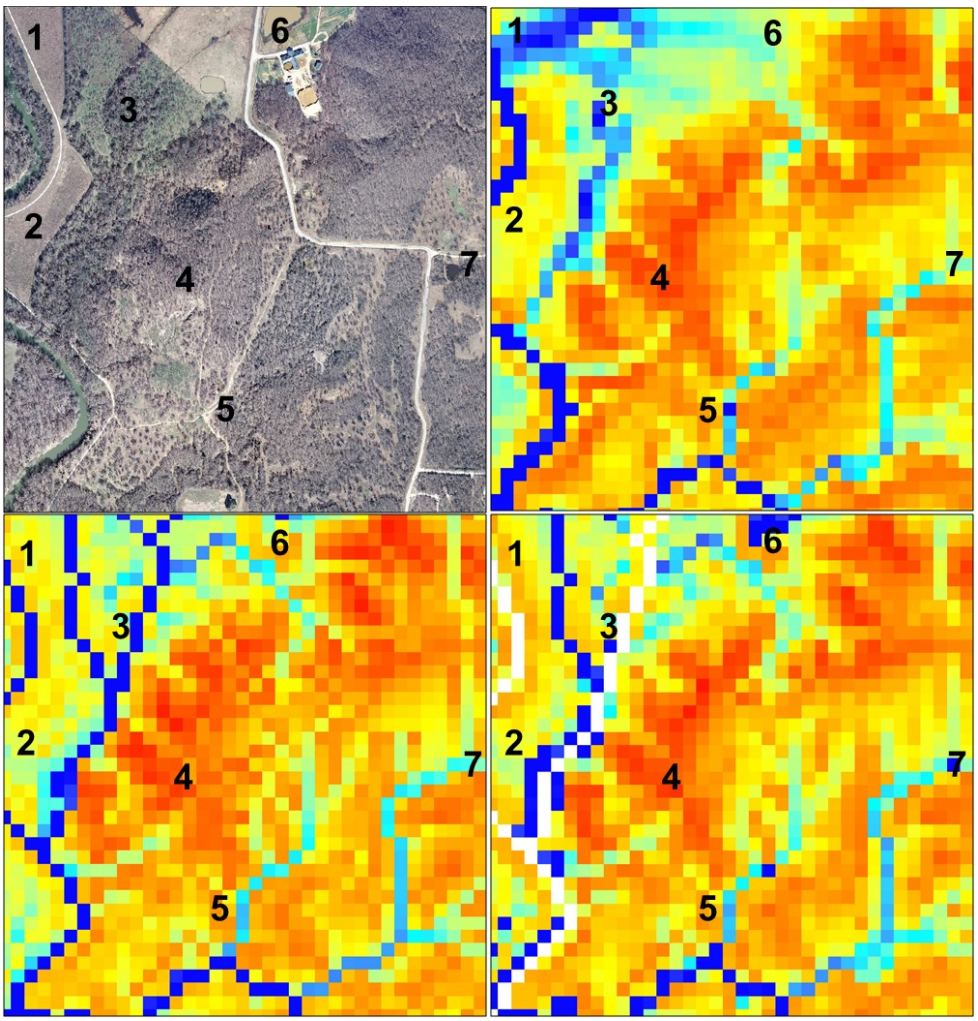

Figure 4.40. TWI calculated from 29-m grid DEMs at area E. TWI maps of the hilly upland area E were calculated from the three remaining 29-m DEMs. (*Top-left*) Aerial image was taken in winter 2005. (*Top-right*) TWI map was calculated from contour-derived DEM resampled from 10-m to 29-m due to striping artifacts. (*Bottom-left*) TWI from the 29-m LiDAR-derived DEM processed using the D8 flow algorithm. (*Bottom-right*) Map calculated from 29-m LiDAR-derived DEM processed using the D∞ flow algorithm. Locations of note: (1 and 2) These flat but somewhat upland areas are old fields that have until now maintained grassland characteristics. They were appropriately indicated with mid-range TWI values with

the exception of the contour-derived grid in location 1, which inaccurately showed wet territory crossing through it. (3) This flat terrace area consisted of very heavy clay soil that stays dry for long periods of time, but that will occasionally get flooded and can remain saturated for extended periods. All three grids appropriately put it into the wetter side of the TWI range, except that the D∞ processed LiDAR- derived grid had missing values in this area. (4) This hilly area known as Wildcat Hill was the driest area within the Greenbelt and was appropriately indicated so with low TWI values in all three grids. (5) An upland post oak forest site, this location was towards the bottom of the Wildcat Hill area and contained soil that was deeper, loamier, and moister than in location 4. There were also small drainage channels that passed through this location. All three grids were a good representation of this location. (6) Only the LiDAR-derived D∞ TWI grid indicated the location of this pond; however, the pond, while fed by natural surface flow, was artificially constructed. (7) All three grids indicated possible water accumulation at this location, but the LiDAR-derived D∞ map again gave the best indication that a pond was located in this spot.

Compared with the 29-m grids, the 10-m and 5-m grids were more accurate in locating surface features (Fig. 4.41). In the flat areas, these finer grids indicated more contrasting differences and a lower range of TWI values than the corresponding 29-m grid. As these differences in TWI occurred over distances too small to see substantial changes in vegetation patterns, they were considered as a negative characteristic for defining FACETA terrain types. As with the other two areas examined, the D8 algorithm yielded less patchy results in flat areas, and D∞ produced less patchy or dendritic results in hilly areas. Smaller grid sizes yielded patchier results in all situations.

After rejecting use of contour-derived DEMs because of the presence of striping artifacts, seven TWI grids were evaluated: the three LiDAR-derived grid resolution processed using either the D8 or D∞flow direction algorithm, and the contour-derived DEM resampled from a 10-m to 29-m grid size. The general spatial patterns of TWI maps were similar, but a number of differences were noted upon closer examination. A general trend under both flow direction algorithms was that the finer grid resolutions produced TWI maps that were more accurately able to predict the location of surface water features such as sloughs, wetlands, and stream channels than coarser grids.

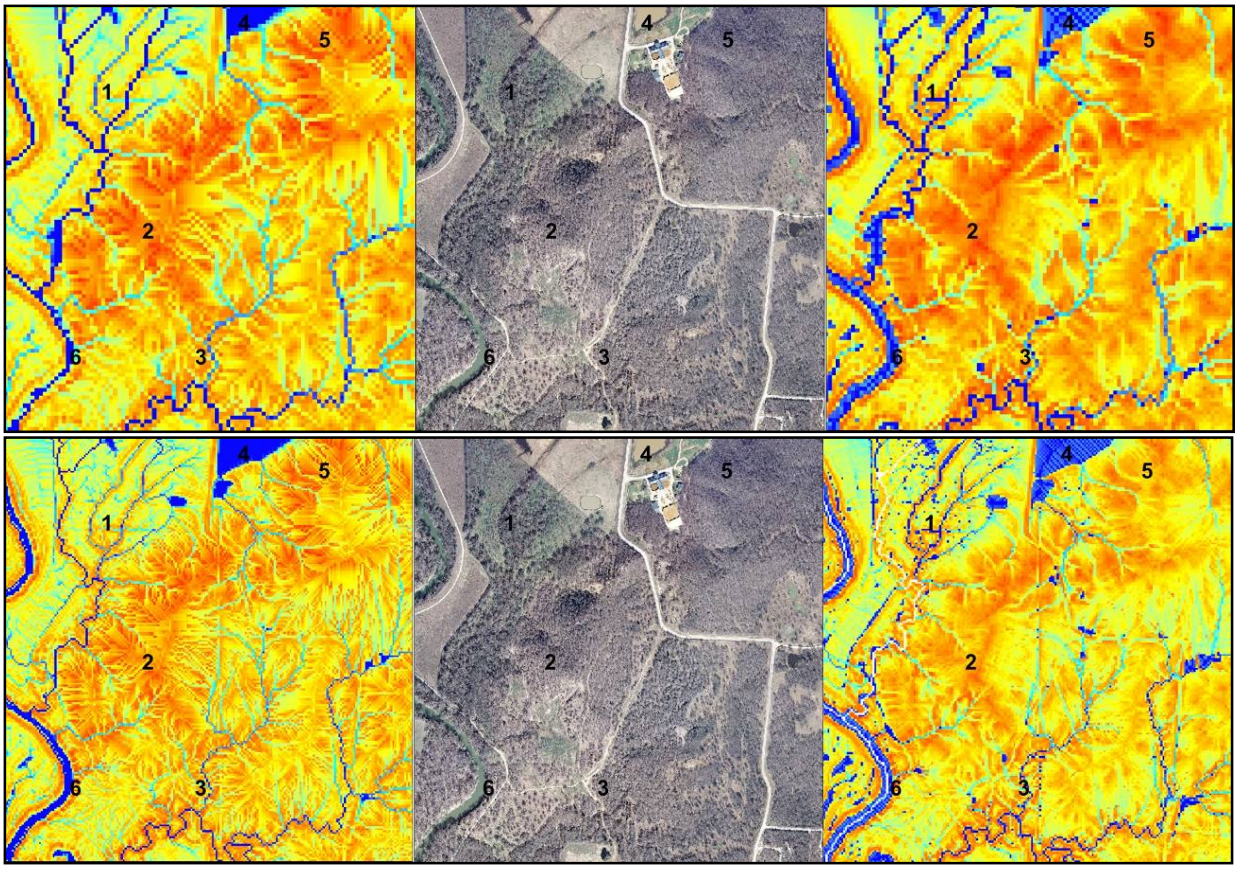

Figure 4.41. TWI calculated from 10-m and 5-m grid DEMs at area E. TWI maps of the hilly upland area E were calculated from the two 10-m and two 5-m LiDAR-derived DEMs. (*Top-left*) TWI map calculated from the10-m D8 processed DEM. (*Top-center*) Aerial image of the area was taken in the winter in 2005. (*Top-right*) Map calculated from the 10-m D∞ processed DEM. (*Bottom-left*) Map calculated from the 5-m D8 processed DEM. (*Bottom-center*) Aerial image. (*Bottom-right*) TWI map from the 5-m D∞ processed DEM. Places of note include: (1) This flat terrace area consisted of very heavy clay soil that can stay dry for long periods of time but occasionally floods and can remain saturated for extended periods. All three grids appropriately put it into the wetter side of the TWI range, except the D∞ processed LiDAR-derived grid had missing values in this area. Compared with the 29-m grids, these finer grids indicated an area with more contrasting differences and lower TWI values than the general nature of this location should have. The D8 processed grids were a little better than the D∞ grids in this location. (2) This hilly area known as Wildcat Hill was the driest area within the Greenbelt. All four grids appropriately indicated this area as being on the dry end of the range; however, the D8 processed grids were patchier and had a more dendritic pattern than the D∞ grids. The 5-m grids were patchier than the 10-m grids. (3) This location towards the bottom of the Wildcat Hill area and contained soil that was deeper, loamier, and moister than in location 2, but it was still an upland post oak site. All four grids represented the slightly moisture area well and captured the presence of the small drainage channels in the vicinity. (4) At these finer grid resolutions, all four grids captured the presence of the small pond. The D∞ grids again had the problems of patchiness and artificial lines. (5) As with location 2, this upland location was best represented by the 10-m D∞ processed grid when compared to the other three grids. (6) All four grids overemphasize the TWI values of the channel banks, with the 10-m D∞ processed grid being the worst of the four.

However, the finer grids also tended to have some common problems making them less desirable to use in FACETA terrain type definition. All of the finer grid resolutions could

result in increased patchiness in the TWI values that did not reflect changes in vegetation and terrain features on the ground. The D∞ processed grids could be very patchy, particularly in flat areas, and they resulted in many isolated pixels and patches with low TWI within the flat bottomland. The D8 processed grids had a tendency to be patchier and had a somewhat dendritic pattern in the hilly areas, resulting in numerous *channels* of higher TWI values within distinctively upland terrain. Under both flow direction algorithms, the finer grids over emphasized the stream channel banks as dry terrain. All of these problems were worse with the 5-m grids than the 10-m grids, and the most likely explanations included the sensitivity of the TWI to changes in slope and problems with both of the flow direction algorithms used. The fact that the two flow direction algorithms seemed to complement each other when comparing hilly areas versus flat ones suggested the possibility of a hybridized flow direction algorithm. The amount of patchiness apparent in any of the TWI grids was reduced if the TWI values were grouped into categories, but with the finer resolution grids, even a coarse grouping of three categories still yielded undesirably patchy areas in the TWI maps.

Among the three 29-m grids, the contour-derived resampled TWI map resulted in too many inaccuracies when comparing locations of high or low TWI with surface features. Its general pattern fit fairly well when viewed from a broad perspective, but on closer examination the inaccuracies in predicting the locations of sloughs or even large wetland areas made this grid unacceptable for application in FACETA terrain types. The other two 29-m TWI grids were relatively similar to each other, and the accuracy in locating surface features for both was good, although they were not as good as their finer grid counterparts. The D∞ processed 29-m grid was patchier than the D8

processed map in flat areas, and it had more isolated pixels of low TWI values scattered within the wetlands. The D∞ processed grid also contained missing data cells in areas of high accumulation. However, the apparent advantage that the finer resolution D∞ processed grids had in the hilly areas over their D8 counterparts was diminished; the 29-m D8 grid was not obviously more dendritic in the hilly areas. Because of its better representation of flat, bottomland areas, the D8 29-m grid was determined to be more appropriate than the D∞ 29-m grid. Due to their patchy and dendritic natures, the finer resolution grids often overemphasized changes in TWI when compared to the terrain and vegetation cover on the ground. Therefore, the 5-m and 10-m grids were less appropriate for this application of FACETA terrain types. From the different DEM sources, grid sizes and flow direction algorithms, the two LiDAR-derived 29-m grids were the only two that were really appropriate for terrain type definition at the spatial scale of interest. Of these two, the D8 processed grid was slightly favored because of problems the D∞ grid had in flat areas.

Terrain Types

One of the objectives of this research was to devise a way to combine soil and topographic characteristics in defining and delineating FACETA terrain types. The USDA soil types are nominal values represented as homogeneous polygons on a map, whereas the TWI is a continuous variable with each raster cell taking on a different value. One possible approach to the continuous TWI values is to partition them into different categories (e.g., high and low). This research devised a way of partitioning the TWI values into categories, combining them with the soil types so the watershed could be partitioned and FACETA parameters could be determined for the resulting terrain

types. The simplest and most logical way to incorporate the USDA soil map was to use the soil type polygons as part of the terrain type definition. The soil type polygons partitioned the landscape, and as discussed in the section on Soils and Terrain Types, the USDA classification level necessary for defining FACETA parameters was the soil series. An obvious problem with this approach was that, unlike the way it was depicted on the soil map, soil conditions were also continuous variables that could change rapidly with respect to horizontal distances. However, without an enhanced, finer resolution soil survey and soil map, the Order II survey supplied by the USDA was the best available source of information to partition the watershed by soil properties.

To bring the TWI into the terrain type delineation, the continuous grid of TWI values first had to be discretized in some way to form categories. In this research, a simple approach was taken, which was to use percentiles to break the TWI values into categories of high, medium, and low. The reasoning behind this simple approach was that from a broad perspective, different areas within a watershed could be thought of as belonging to one of three categories: the relatively wet bottomlands, the relatively dry slopes and hilltops, and valleys and flat terraces with moisture levels somewhere between these other two conditions that make up large parts of many watersheds. For the initial categorization, the lowest 20% of cells made up the low, i.e. dry, category; the highest 20% made up the wet category; and the middle 60% were the medium group. To arrive at the 20% and 80% cutoffs, different values were tried and compared to the aerial images, and these values gave satisfactory representations of the wet bottomlands and dry post oak hills. However, much as any other model parameter,

these cutoff points could themselves be further calibrated to the landscape as well as to output from the forest model to improve performance.

One problem with any systematic way to split the TWI values is that there will be some mixing of cells from different groups (i.e., the patchiness as described in the section discussing the TWI). For example, some stray-looking medium categories appeared in the middle of the bottomland or on top of a dry hill. A potential benefit of using the TWI together with the soil type to partition the landscape was that the soil types might further have separated the topographic wetness groups. To test this idea, the soil type map was intersected with the TWI map, and then summary statistics of TWI values were examined within each soil type (Fig. 4.42).

A Kruskal-Wallis test was performed on TWI values separated by soil type. The resultant TWI values were not from the same distributions ($p<10^{-15}$). Applying a Kruskal-Wallis multiple comparison test yielded differences between distributions of TWI values from most pairs of soil types ($\alpha = 0.05$). The only pairs where the hypothesis of the same distribution could not be rejected were Bastrop/Wilson, Birome/Silstid, Bunyan/Gowen, Gasil/Silstid, Gasil/Silawa, Birome-Rayex-Aubrey/Silstid, and Ovan/Silstid. Most pairs where the distributed TWI values could not be differentiated by the Kruskal-Wallis multiple comparison test were understandable. Birome, Silstid, Gasil, Silawa, and the Birome-Rayex-Aubrey complex were all similar, upland soils with sandy to sandy loam textures. All were associated with post oak and blackjack oak forest or savanna (Table 4.1). Bunyan and Gowen were both loamy bottomland soils associated with bottomland, hardwood forest growth. The two somewhat surprising pairs were Bastrop-Wilson and the far more surprising Ovan-Silstid.

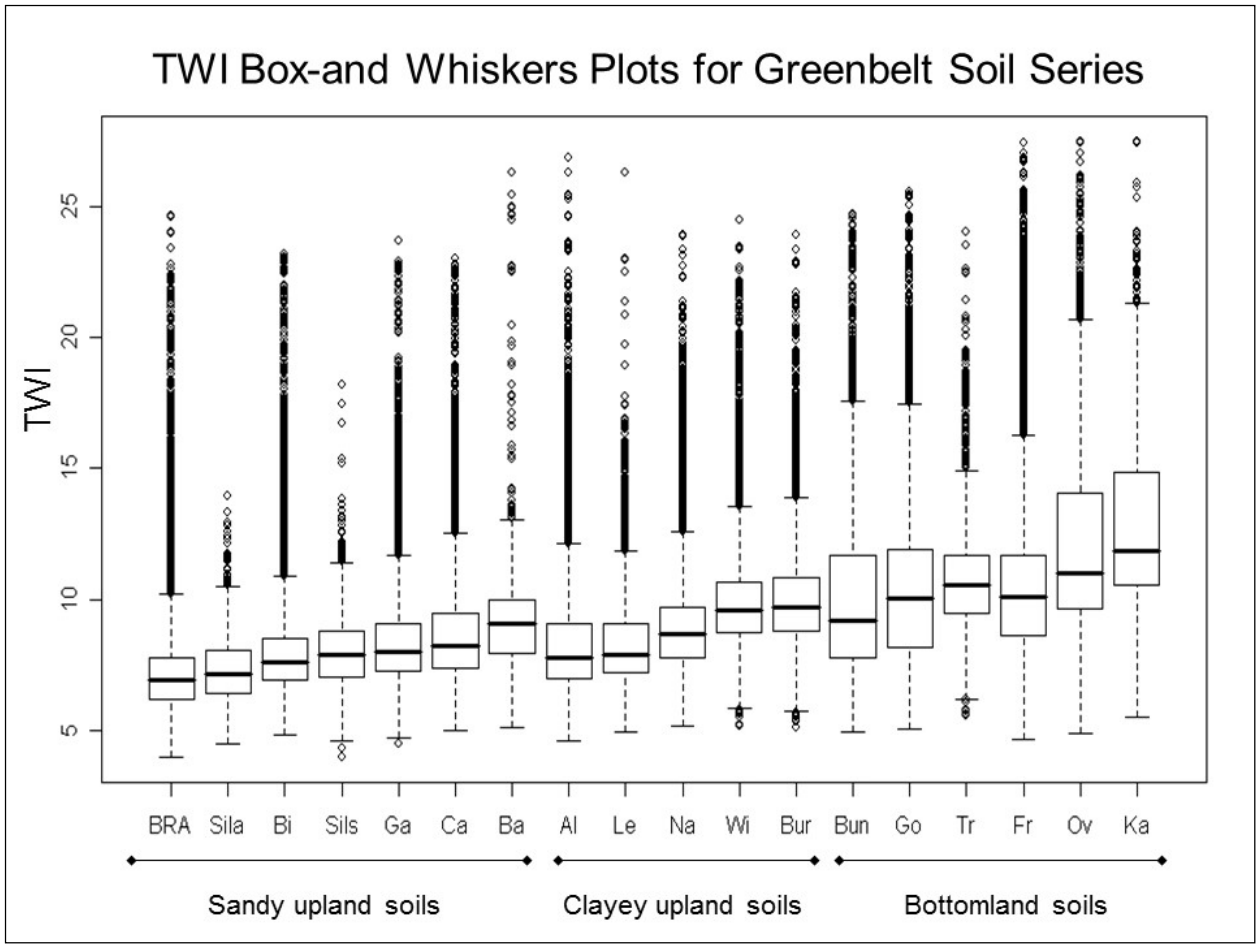

Figure 4.42. TWI box-and-whiskers plots for Greenbelt soil series. The ranges of TWI values for the Greenbelt soil series are graphed in the box-and whiskers format. The horizontal lines of the boxes are the first, second, and third quartiles, and the ends of the *whiskers* are a distance of 1.5 times this interquartile range. Individual points outside of the whiskers can be thought of as outliers. Statistically the distribution of TWI values for each of the soil series was unique (Mann-Whitney U test, $p < 10^{-8}$). The abbreviations used to identify the soil series are used in Table 4.1, except for BRA, which is the Birome-Rayex-Aubrey complex. Information regarding this soil complex can be gleaned from the Birome and Rayex descriptions in Table 4.1. There is no box-and-whiskers plot for Rayex because no pure polygons of this series occurred within the Greenbelt.

While Bastrop was a sandy soil associated with post oak growth and Wilson was a clayey soil associated with grasslands, both found in upland areas. Characteristic topography where these two soil series were found were different, but the range of their TWI values within the study area watershed, as seen in the box-and-whiskers graph, were close (Fig. 4.43). The fact that the Kruskal-Wallis multiple comparison test could not differentiate the TWI values of Ovan and Silstid was bewildering.

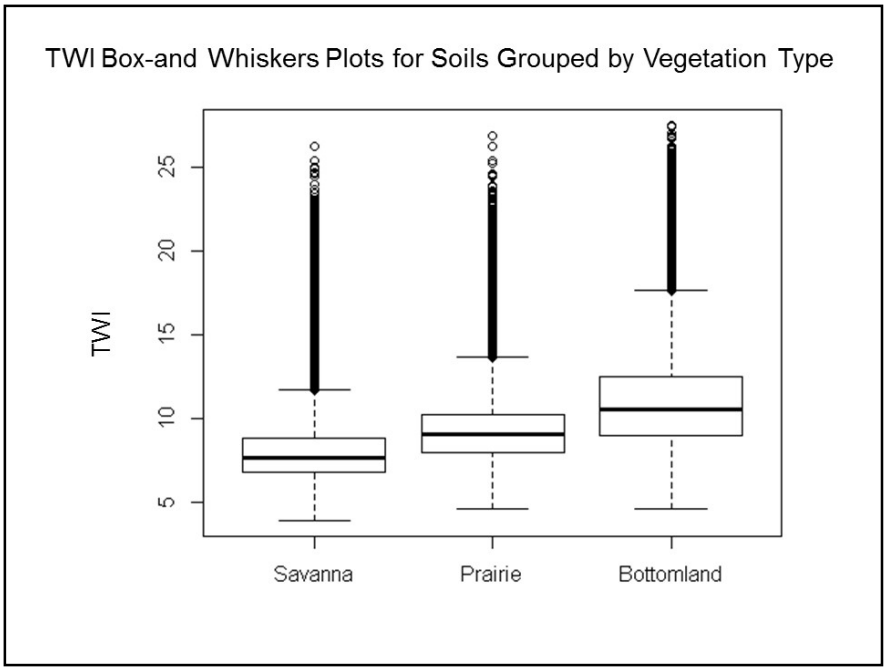

Figure 4.43. TWI box-and-whiskers plot for soils grouped by vegetation type. By grouping soil series of the Greenbelt by associated vegetation covers (upland post oak savanna, upland tallgrass prairie, and bottomland hardwood forest), the difference in the TWI distributions was clear. Bottomland, hardwood forest soils tended to have the highest TWI values, and upland post oak savannas had the lowest.

These two soils were about as different as they can be in terms of topographic position, texture, and associated vegetation, not to mention that the hypothesis of similarity in TWI distribution could confidently be rejected simply by comparing their box-and-whiskers graphs. Using the statistically more powerful one-tailed Mann-Whitney U test to compare these pairs alleviated any concerns. The distribution of TWI values in the Ovan series was shifted positively from that of Silstid ($p < 2.2 \times 10^{-16}$), and Wilson TWI values were shifted positively from those for Bastrop ($p < 2.2 \times 10^{-16}$). Applying the two-tailed Mann-Whitney U test to all of the other pairs resulted in a rejection of the null hypothesis of a zero distribution shift with the largest of the *p*-values from all of these pair-wise tests being less than 10^{-8}. Statistically, at least the soil types helped further separate the TWI values. By grouping the soils together into their associated vegetation types, the differences in the TWI distributions was more clear (Fig. 4.44). This raised the

consideration for another approach at defining terrain types, which was to use the ecological site designations rather than the soil series together with the TWI.

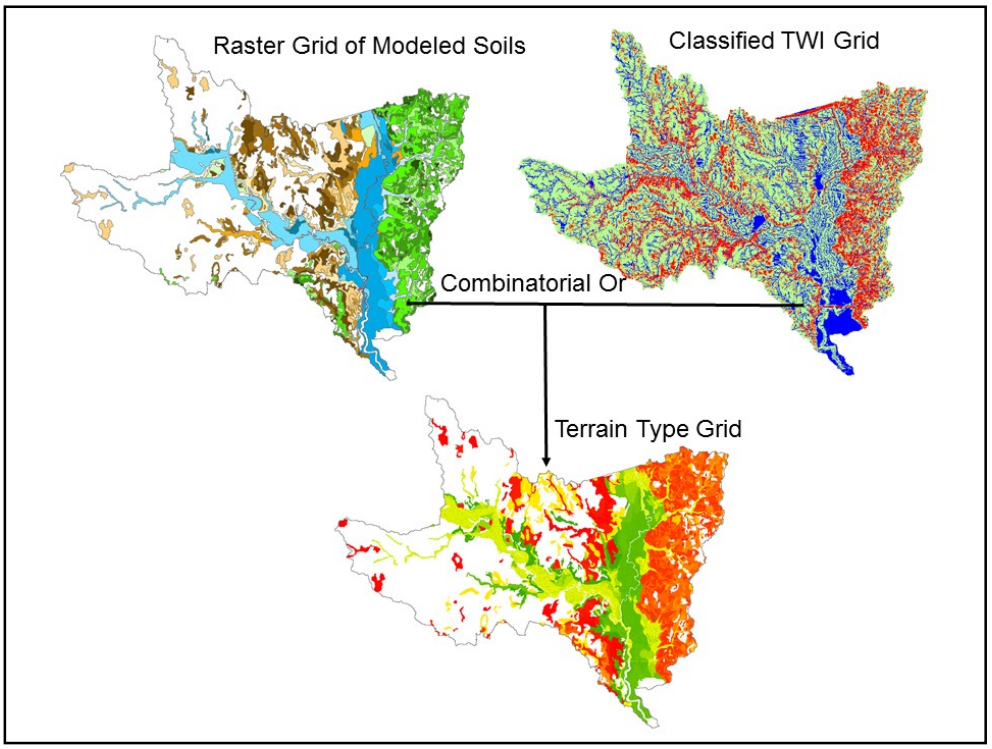

Figure 4.44. FACETA terrain types. This figure shows the conceptual flow for partitioning the study area into terrain types. The soil map was converted to a raster grid, and the TWI map was classified into high, medium, and low categories. In this case, percentiles were used for the classification cutoffs, with low being the bottom 20% and high being the top 80% of TWI values throughout the watershed. The GIS combinatorial or function was used on the two grids to assign a new value to each unique combination of soil type and TWI category. Combining the 18 USDA soil types identified within the Greenbelt together with three TWI classes yielded 54 different terrain types.

The method for partitioning the watershed map into terrain type units was the GIS *combinatorial* or function. This combined a raster version of the soil series map with the classified TWI map to create a new raster grid, where the value of each grid cell was a value that represented one of the unique combinations of soil series and TWI category that occurred. With the TWI grid grouped into three classes (low, medium, and high) and 18 different soil series, there was a potential for as many as 54 different FACETA terrain types, which was how many resulted in this case (Fig. 4.44). Each terrain type

was considered a unit that could be modeled in FACETA with one set of model parameters. Determining parameters for these terrain types is discussed in Chapter 6.

Conclusions: Landscape Terrain Types

Terrain types for FACETA were defined through a combination of soil and topographic characteristics. Soil series as defined in the Denton County soil survey provided by the Natural Resource Conservation Service (2010) within the USDA were used as the basis for partitioning the study area map by soil characteristics. The TWI topographic characteristic was used to partition the map. A number of issues behind developing the TWI map were considered and analyzed. Two different sources of elevation data–LiDAR-derived and contour-derived–were obtained, with the contour-derived DEMs in two grid sizes of 10-m and 29-m. The LiDAR dataset was converted into DEMs of three different resolutions, 5-m, 10-m, and 29-m. After removing the depressions from all the DEMs, the DEMs were each processed using two different flow direction algorithms, the SDF D8 and the BDF D∞. Alternative methods or algorithms for making a depressionless DEM were not examined in this study. These 10 different DEMs were then processed through the steps required to produce the TWI grid and analyzed at various steps for quality in the application of FACETA terrain type definition.

Problems were detected in slope grids calculated from the contour-derived DEMs in the form of striping artifacts. The striping artifacts existed in all four contour DEMs, but the artifacts were more apparent in the 10-m grid than the 29-m grid and were more apparent in the D∞ processed grid than the D8 processed grid. Another difference between the contour-derived slope grids and the LiDAR-derived slope grids was that the increased accuracy of LiDAR yielded slope maps with more topographical changes as

well, although this was more apparent in the 10-m grid than the 29-m grid. Between the different grid resolutions, the smaller grid size allowed for more of the microtopographical changes to be detected.

Flow accumulation grids were compared with location and shape of surface water features. Generally, accuracy increased with the finer grid resolutions, the LiDAR-derived grids were more accurate than contour-derived grids, and D∞ processed grids more accurately than D8 grids. However, the 29-m LiDAR-derived D8 map was less accurate than the 29-m contour-derived D8 map. An unexplainable problem was detected in the D∞ processed grids where a number of cells located in high accumulation areas or around the perimeter of the watershed did not have defined values. Between the increased accuracy of the bi-directional flow algorithm over the single directional algorithm and the missing data problem resulting from the D∞ algorithm, a potential future improvement might be to use an MDF algorithm.

The striping artifacts that first became apparent in the contour-derived slope grids were enhanced through calculation of TWI grids. Even after reclassifying TWI grids into just three categories, the artificial lines were still apparent, and would have therefore become part of the terrain type delineation. Without using a filter to clean out the striping artifacts, the contour-derived DEMs were determined inappropriate. Since LiDAR was not available for many places, a new version of contour-derived DEM was added to the analysis. The 10-m DEM was resampled to 29 m, and the resampling acted as a filter. While successfully removing the artifacts, the resampling process only made inaccuracies in the original DEM worse, and this contour-derived DEM was determined to be unacceptable. Both of the finer grid resolution DEMs resulted in a great deal of

patchiness (i.e., individual pixels or patches of low TWI values isolated within the floodplain or channels of higher TWI values in the hills). The 5-m grids were patchier than the 10-m grids, and the D8 flow direction algorithm produced less patchiness in the flats and bottomlands while the D∞ algorithm was less dendritic in the hilly areas. Since patches were still apparent in all finer resolution grids, even after reclassifying the TWI grid, these grids also resulted in a patchy terrain type map. The patchiness did not correspond to changes in terrain or vegetation cover on the ground, and the smaller grid sizes were determined to be less appropriate than the 29-m grids. The two LiDAR-derived 29-m grids were relatively similar to each other; however, the D∞ processed 29-m grid was patchier than the D8 processed map in flat areas and had more isolated pixels of low TWI values scattered within the wetlands. The D∞ processed grid also contained missing data cells in areas of high accumulation. Because of its better representation of flat, bottomland areas, the D8 29-m grid was determined to be more appropriate than the D∞ 29-m grid.

The study area map was partitioned through all combinations of soil series and TWI categories to create the FACETA terrain type map. The TWI map was reclassified into three categories–high, medium, and low–using the 20% and 80% TWI values as the break points. Break points were determined after comparing possibilities with topographic and vegetation features on the ground; however, they should be considered landscape model parameters that can be further calibrated for fit. Each soil series was determined to have statistically different distribution TWI values from the others, and soils grouped by vegetation cover types had distinct TWI distributions. Combining soil series together with TWI categories, FACETA terrain types were further separated.

CHAPTER 5

FACETA BIOLOGICAL PARAMETERS

Forest gap models such as FACETA model the growth of individual trees grouped in plots, with the trees individually responding to climatic conditions, available resources, and competition. The modeling approach to growth in FACETA as with many gap models is that each individual tree can grow each year up to some maximum, optimal growth increment that is a function of species and the tree's diameter. The optimal annual growth is then decremented when environmental conditions are less than optimal, for example when soil nutrients or sunlight are reduced by competing trees, temperatures are warmer or colder than the species' optimum range, or soil conditions are too dry or too wet. The different tree species simulated in FACETA have different optimal growth rates and respond differently to these conditions through a number of model input parameters that must be provided to describe the life history, growth, and stress tolerances for each species. Details of these parameters, how they are derived, and the values used in FACETA are discussed below.

Methods: FACETA Biological Parameters

One objective of this research was to set up FACETA for a watershed within the Eastern Cross Timbers ecoregion with parameters based as much as possible on measured data. Selecting and parameterizing tree species for FACETA involves determining an appropriate set of species to model and determining the necessary model parameters for those species. Model parameters are calibrated and tested for sensitivity. An appropriate set of species includes all the important species present as well as representative species for the relevant ecological niches and roles. At the same

time, each species has a required set of model parameter values that must be inputted. Determining or finding parameter values based on quantitative data is not always easy, especially for species that lack commercial importance. One problem is that species characteristics and tolerances are often described qualitatively, but the model requires quantitative, numerical input. There are also potential problems with the model assumptions when determining model parameters. In some cases, the data from a particular species may simply not fit assumptions of the model equations.

The first step in determining the biological parameters was determining the species to be modeled. This was done in a two-step process. First a list of candidate species was determined based on a combination of the species prevalence in the study area, prevalence within the Eastern Cross Timbers ecoregion in general, and the need to have species that represented the different ecological niches. Local tree surveys conducted in the Greenbelt State Park were used to determine species importance within the study area. The second step in species selection was linked to parameter estimation. It was not always possible to estimate a complete set of model parameters for every species with sufficient level of confidence. A subset of candidate species with parameters based on the best available qualitative data was then selected for initial FACETA simulation runs.

FACETA requires a set of parameter values for each modeled species that determines how individuals grow and respond to environmental conditions, competition, and stressors. These parameters fall into three general categories: growth, tolerances, and reproduction. Growth parameters include size and age limits, growth rate, and allometric parameters that describe the relationship between height and diameter.

Parameters for tolerances include responses to drought, flooding, temperature, shade, and soil nutrient deficiency. Reproduction parameters include values for seeding and stump sprouting. Many of the different parameters are linked with each other through the various equations used in the model, and mathematically they can be sensitive to each other. The maximum height parameter is used as a constant in the regression that determines the allometric parameters. The allometric, growth rate, maximum height, and maximum diameter parameters are all used in the equation that determines the optimal annual diameter growth increments for each species. According to the environmental conditions in any year, the tolerance parameters are used to reduce the optimal diameter growth increment to produce the realized modeled diameter growth increment. Larger trees in the model can have critical advantages in competition, so the ability for a species to grow determines its success, and a lack of growth of any individual species will lead to mortality. The growth parameters are also used in the algorithms that determine mortality. Ideally, all of the model parameters would be based on data collected from each of the species; however, some practical and philosophical questions on modeling assumptions and data measurements have to be addressed to achieve this. FACETA model parameters and the process of determining values for them are discussed in the following sections.

Generally, growth parameters for the modeled tree species are estimated through a combination of measurements and surveys of published literature in forestry and ecology. Parameters for maximum height, diameter, and age were estimated from several sources of silvics information, including manuals and databases from the U.S. Forest Service (USFS), U.S. Department of Agriculture (USDA), a non-profit run

database of the nation's largest trees, and local measurements. Modeling philosophy in this case typically has these maximum parameters set to ideal maximums, but because the various model parameters can be sensitive to each other, estimating maximum parameters becomes a bit of a balance between the ideal maximums and values that fit with the other parameters that may be based on local growth patterns. Growth parameters used in modeling the geometry of tree species were all estimated from local measurements. Growth parameters for growth rates were estimated from three tiers of sources: growth rings measured locally from trunk cross sections or tree cores, growth rings measured from tree cores that were not local and were available through a tree ring database run by the National Climatic Data Center, and a combination of qualitative and quantitative information published from some of the same sources used in estimating the maximum age and size parameters. The tolerance parameters were all estimated from a variety of published information sources such as the USFS and USDA, much of it qualitative in nature butt some also quantitative. Reproduction parameters were researched for the modeled tree species, but model runs made for this research were done without using the two reproduction parameters, one for seeding and one for sprouting. Specific details for each of these model parameters are provided in the following sections.

Results: FACETA Biological Parameters

The results from estimating the biological parameters for FACETA, along with descriptions and assumptions behind these parameters, are described in the following sections. Some of the parameters have dependencies on others, and the first four sections – species selection, maximum age and size, allometry, and growth rate – are

ordered based on those dependencies. Selecting species is described first, and then the maximum size and age parameters for those species are described. The allometric parameters depend on maximum height, and the growth rate depends on the allometric and maximum size parameters. The reproduction and tolerance parameters, which are discussed last, only depend on the species.

Species Selection

Tree species simulated in FACETA for the Greenbelt were selected based on a combination of factors including the prevalence of the species within the study area, the availability of data on the species to determine model parameters, and the goal of having a collection of species representative of the various ecological niches and roles. Species prevalence and having a full representation of the niches in the modeled study area should ideally dictate species selection for the model. However, quite a bit of data must be available in order to determine meaningful model parameters for any species. Species model parameters included maximum height, diameter, age, a parameter for growth rate, parameters for the allometric relationships between height and diameter, tolerances for temperature range, dry soil (drought), saturated soil (flood), shade, nutrient availability and deficiency, and seeding and sprouting capacities. Some plausible values for parameters such as maximum height and age were not difficult to find in forestry literature and silvics manuals, at least for the tree species that were commercially important. However, there are some species where very little information could be found in the published literature. For example, *Forestiera acuminata* (swamp privet) was the most dominant species found in the lowest lying parts of the Greenbelt.

However, swamp privet probably is short-lived, grows as a shrub more than a tree, and has no commercial value. Therefore, little literature or data exist on the species.

For all species, information and data for determining parameters such as flood and drought tolerances were even more difficult to find. Information that did exist on these tolerances was typically qualitative and not quantitative. Determining flood tolerance of mature trees required long-term ecological observations, which was available for many species but in a qualitative form. Flood tolerance for a species might be categorized as *moderately tolerant*, which may be further described as being able to survive in flooded conditions for a few months during the growing season but with high mortality if flooding persists. However, these categories can be somewhat broad and contain varying degrees of tolerances if they were quantified to a finer scale. One example of this involved two bottomland species considered in this research. *Fraxinus pennsylvanica* and *Acer negundo* were both described as moderately tolerant to flooding in the USGS guide to bottomland hardwood restoration (Allen, Keeland, Stanturf, Clewell, & Keenedy, 2001). From personal observations within the Greenbelt, both *F. pennsylvanica* and *A. negundo* grew in the floodplain, but *F. pennsylvanica* was more likely to be found in low areas and sloughs than *A. negundo*, which seemed to prefer higher and sandier positions. Based on these observations, *F. pennsylvanica* should have a higher model parameter value for flood tolerance than *A. negundo*, but there was no available quantitative data on which to base those differences in parameter values. Often in situations like this, the modeler uses the relative differences known between the species to assign different parameter values and then uses the model output to adjust or calibrate the parameter values, but that is not the ideal way to

assign parameter values. Ideally, parameter values are based on data collected from the same biological or physical processes they represent in the model.

Another problem with using forestry resources for determining parameter values is that the information found from different sources on any tree species does not always agree. For example, resources from three different offices within the USFS gave a range of 30-m to 52-m for the maximum height of *Quercus macrocarpa* (bur oak). The result was that determining a list of species to model became a struggle between the ecological importance and prevalence of the species, having a set of species that was a good representation of the study area and its ecological niches, and the ability to find enough quality data to parameterize the model for the species. Determining a species list to be modeled thus was split into two steps. The first step was to develop a list of desired candidate species and to gather as much information as possible on each for parameter estimation. The remainder of this chapter describes that process. The second step was to reduce the candidate list to a subset of species with the most reliable set of parameters for initial FACETA simulation runs. As more information was gained about candidate species and problems with the model and species parameters were resolved through model testing and calibration, more species could be included in the simulation.

The landscape modeled here was within the Cross Timbers Level III ecoregion, and included parts of both the Eastern Cross Timbers and the Grand Prairie Level IV ecoregions. This area historically comprised upland forests, bottomland forest including wetlands, and upland areas that have historically developed as grasslands rather than forests. Any forest model of the Eastern Cross Timbers must include the characteristic

tree of the ecoregion, *Quercus stellata*, or the post oak. Other upland species of the Eastern Cross Timbers included *Quercus marilandica* (blackjack oak), *Carya texana* (black hickory), *Juniperus virginiana* (eastern red cedar), and *Prosopis glandulosa* (honey mesquite; Griffith, Bryce, Omernik, Rogers, & Harrison, 2007). However, upland Eastern Cross Timbers consisted primarily of post oak with some blackjack oak, especially in areas with very poor soils. Riparian species in the Eastern Cross Timbers included *Carya illinoinensis* (pecan), *Salix nigra* (black willow), *Populus deltoides* (eastern cottonwood), and *Acer negundo* (boxelder). The Grand Prairie ecoregion was historically mostly upland prairie grasslands, but the riparian areas in the Grand Prairie included *Ulmus spp.* (elms), pecan, *Celtis spp.* (hackberry), and *Quercus macrocarpa* (bur oak). The Society of American Foresters has a classification system that describes different forest types occurring in different conditions and seral stages, and while none of the forest type descriptions matched the Greenbelt bottomland exactly, Type 93, Sugarberry–American Elm–Green Ash, were the closest. Type 93 occurred in bottomlands throughout the Southeast from east Texas to the Atlantic and north to southern Illinois (Eyre, 1980). Denton County is a little to the west of that range, and the Greenbelt bottomland was more of a Sugarberry-*Cedar Elm*-Green Ash forest, but the Type 93 description still applied well. Common associates of Type 93 also common in the Greenbelt included cedar elm, boxelder, eastern cottonwood, red mulberry, and honeylocust. Variants found within Type 93 included stands of green ash on moist flats and sloughs, and stands of sugarberry on fronts and new land, both of which were found in the Greenbelt as well. The three species were all shade tolerant, as was cedar elm. Type 93 is considered a long-term seral stage. Generally, within the bottomland

hardwood forests that develop in alluvial floodplains of streams there were different species that tended to occupy different topographic positions (e.g., sandy high fronts versus low-lying clayey sloughs; Hodges, 1997). The Greenbelt State Park at the center of the modeled landscape contained a mix of bottomland topographic positions and soil conditions, as well as varying stages of reforestation, forest age, and development (Rijal, 2011). While the Greenbelt State Park contained only small areas of upland forest and upland prairie, the modeled landscape surrounding the State Park was historically composed of both these vegetation cover types. The area east of the Greenbelt was primarily upland Eastern Cross Timbers, and to the west it was primarily upland Grand Prairie with some riparian areas for tributary streams of the Elm Fork Trinity River. The modeled species should contain representatives of both upland and bottomland species for both ecoregions, and species within the different topographic positions and seral stages found in the bottomland of the Greenbelt. Since FACETA was not equipped to model grassland plants, slow growing stands of the most drought tolerant species that were also tolerant to heavy clay soils represented parts of the landscape where grassland communities would likely grow.

Species prevalence was determined from two studies conducted in the Greenbelt with a time difference of nearly one decade. These were Rijal (2011) and Barry and Kroll (1999). In Rijal's (2011) study, tree surveys were conducted at various topographic positions within the floodplain, including both young regenerating and older growth forest. Table 5.1 lists the species with the 15 highest importance values across all bottomland plots found in this study. Upland plots were essentially composed of four species (Table 5.2), greatly dominated by *Quercus stellata* (post oak), with a few other

species only present in small size or number. The other three species of significant importance in the upland plots were *Ulmus alata* (winged elm), *U. crassifolia* (cedar elm), and *Q. marilandica* (blackjack oak). Barry and Kroll (1999) focused on an area of the Greenbelt that contained the oldest patches of bottomland forest, and the resulting list of species by importance value was similar. Both studies found the same three species at the top of the list, although in different order and proportions. Barry and Kroll found *Celtis spp*. to have a much higher importance value than the other two species and *Fraxinus pennsylvanica* (green ash) a much lower importance. The Rijal (2011) study found the three species to have roughly equal importance values. Barry and Kroll (1999) also identified two different species of *Celtis* (hackberry), *C. laevigata* and *C. occidentalis*, while Rijal (2011) only identified *C. laevigata*. Hackberry species can be difficult to distinguish, and there was not complete agreement over the classification of some of the varieties. For example, netleaf hackberry, which was present in the Greenbelt study area in small numbers primarily as a small upland tree, has been classified both as its own species (*Celtis reticulata*) and as a variety of *C. laevigata* (var. *reticulata*). Classification of the *Celtis* taxon has generally been described as being complex and needing revision (Diggs, Lipscomb, and O'Kennon, 1999). However, North Texas is outside and to the south of the historic range of *C. occidentalis* (sometimes called northern hackberry), whereas it is in the latitudinal heart of the historic range of *C. laevigata*. The ranges of the two species overlap, and the historic range of *C. occidentalis* extends southward into Oklahoma, so it is possible that both species exist in the Greenbelt. There is little difference between the two species ecologically or in life histories, and for the purpose of FACETA modeling in this research, all

hackberries were assumed to be *C. laevigata.* Another notable difference between the two studies was that Barry and Kroll (1999) found the presence of some species not found by Rijal (2011) such as *Juglans nigra* and *Q. shumardii*, although with low importance values. It is not clear if the differences between the two studies are because of forest age or other reasons.

Table 5.1

Greenbelt Bottomland Species by Importance Value (IV-300)

Species	Common Name	IV-300	Relative Density (%)	Relative Basal Area (%)	Relative Frequency
Fraxinus pennsylvanica	Green ash	50.0	16.5	22.0	11.6
Ulmus crassifolia	Cedar elm	45.2	16.2	19.4	9.6
Celtis laevigata	Sugarberry	44.2	21.1	10.5	12.6
Forestiera acuminata	Swamp privet	27.3	15.1	5.3	7.0
Acer negundo	Boxelder	23.8	9.7	7.1	7.0
Snag[1]		20.6	5.4	4.2	11.1
Populus deltoides	Eastern cottonwood	17.7	1.3	13.9	2.5
Ulmus americana	American elm	15.5	2.6	5.8	7.0
Morus rubra	Red mulberry	12.2	3.7	1.4	7.0
Quercus macrocarpa	Bur oak	8.3	0.5	4.8	3.0
Maclura pomifera	Bois d'Arc	7.4	1.0	1.4	5.0
Gleditsia triacanthos	Honeylocust	7.0	3.0	0.5	3.5

(table continues)

Table 5.1 *(continued)*

Species	Common Name	IV-300	Relative Density (%)	Relative Basal Area (%)	Relative Frequency
Gleditsia triacanthos	Honeylocust	7.0	3.0	0.5	3.5
Carya illinoinensis	Pecan	4.9	1.1	1.8	2.0
Salix nigra	Black willow	2.5	0.4	0.6	1.5
Sapindus saponaria	Western soapberry	2.3	0.6	0.2	1.5
Sideroxylon lanuginosum	Chittamwood	2.3	0.2	0.5	1.5

Note: Tree species found in the Greenbelt bottomland areas in 2007-08 with the 15 highest importance values. Data were collected by Rijal (2011) from 30 plots across different topographic positions within the floodplain. The plots were each 625 m^2. Density was a measure of the number of stems, basal area was a measure of total cross-sectional area of the stems, and frequency was a measure of how frequently the species occurred in different plots. The relative form of these three metrics was a conversion of the absolute field measurements to a relative, 100-point scale, with each species measured relative to the other species present. Importance Value 300 (IV-300) was the sum of the three relative scores. [1]Snags were standing dead trees, which were not identified by species in this study.

Table 5.2

Greenbelt Upland Species by Importance Value (IV-200)

Species	Common Name	IV-200	Relative Density (%)	Relative Basal Area (%)
Quercus stellata	Post oak	80.1	21.3	58.7
Ulmus alata	Winged elm	41.5	34.0	7.5
Snag[1]		27.2	18.0	9.2
Ulmus crassifolia	Cedar elm	25.7	14.7	11.0
Quercus marilandica	Blackjack oak	17.0	6.0	11.0
Crataegus spp.	Hawthorn	3.3	2.0	1.3
Juniperus virginiana	Eastern redcedar	2.5	2.0	1.3

(table continues)

Table 5.2 *(continued)*

Species	Common Name	IV-200	Relative Density (%)	Relative Basal Area (%)
Sideroxylon lanuginosum	Chittamwood	1.3	0.7	0.7
Gleditsia triacanthos	Honeylocust	0.8	0.7	0.1
Celtis laevigata	Sugarberry	0.7	0.7	0.1

Note: Tree species found in the Greenbelt upland areas. The data were collected from only two 625-m^2 plots in 2007. Relative frequency diminishes real differences between species if the survey involves a small number of plots, so it was not used here. IV-200 is the sum of relative basal area and relative density. Blackjack oak, while not dominant in this survey, can occur as the dominant species in patches of the Eastern Cross Timbers with poor soil quality. Eastern redcedar has become more dominant, and in fact, it is considered invasive within parts of the ecoregion, but only two individuals were found in this survey. The increase in eastern redcedar is widely thought to be due to fire suppression. Both winged elm and cedar elm were more dominant in this survey than would be expected in typical Eastern Cross Timbers upland, but this might be due to the close proximity of these survey sites to bottomland of the Elm Fork.

Between the general ecoregion and forest type descriptions and the local surveys of trees from within the Greenbelt, the list of species desired to be modeled was formed. Each of the species considered in this research, their prevalence in the Greenbelt, ecological roles and niches, and potential benefits or difficulties in choosing them for simulation is briefly described in the following paragraphs. These species were the candidates for the Greenbelt FACETA model, and they were all investigated for their importance and feasibility to model and parameterize, but not all of the species ended up in the final model.

Acer negundo (boxelder) is the only maple species native to the North Texas area. In two surveys of the Greenbelt, boxelder had low importance value in the old growth portions of the forest but had the fifth highest importance value of all species within bottomland plots generally. It is a small to medium sized tree, typically about 15 m in height, and less than 50 cm in diameter. Its average lifespan is 60 years and usually lives less than 100 years (Burns & Honkala, 1990). It is categorized as

moderately tolerant to shade, flooding and drought, and is generally thought of having a wide range of tolerances to environmental conditions and soils types. Boxelder is a colonizing or pioneer species and can expand rapidly into open alluvial plains and old fields. Considered a bottomland species, it can also occupy drier upland sites and tends to favor deep, well-drained soils within the floodplain. Boxelder is a species with no commercial value, and there is accordingly little information about potential yields. Its growth rings can be somewhat nondescript, and there is no available source of growth ring data.

Carya illinoinensis (pecan) is the very commercially important hickory tree that produces the pecan nut. It is the largest of the hickory species, is one of the largest and longest-lived species found in North Texas, and happens to be the official state tree of Texas. While numerous pecan seedlings were noted in both of the Greenbelt surveys, very few mature pecan trees were found. In Barry and Kroll's (1990) survey, the number of mature pecans was so small that the importance value for the species was zero. In the Rijal (2011) study, pecans made up about 1% of the total number of individuals. While most of the trees in Rijal's study were small to mid-size, some trees had a diameter at breast height (DBH) exceeding 100 cm. Pecan is classified as intolerant to shade. It is a bottomland species favoring well-drained, sandy, and loamy soils, but it can also grow in heavier soils. Problems with modeling pecan include a small local data set of measurements and no available source of growth ring data.

Celtis laevigata (sugarberry) is a very common species in the Greenbelt, having the highest importance value in the Barry and Kroll (1999) study. While *C. laevigata* had the third highest importance in value in the Rijal (2011) study, the value was only

slightly less than the two higher ranked species, *Fraxinus pennsylvanica* and *Ulmus crassifolia.* It is a medium-sized tree and can grow very rapidly. This species is tolerant to shade, moderately tolerant to flood and drought, and a climax species for this forest type. Primarily a bottomland tree, it can occasionally be found in uplands, although with a stunted growth form. It can be difficult to distinguish between sugarberry and its similar and closely related species *Celtis occidentalis* and *Celtis laevigata* var. *reticulata* in the field. Being of little commercial importance, there is not a large amount of published data on sugarberry and no available source of growth ring data.

Forestiera acuminata, or swamp privet, is one of the only native tree species that can tolerate completely wet conditions. While not mentioned in Barry and Kroll's (1999) study, swamp privet ranked fourth in importance in value in Rijal's (2011) study and dominated in the low flats and sloughs. It was absent in upland sites. The species is tolerant to shade, and it is a common associate and likely successor to the shade intolerant black willow. Swamp privet's growth form is typically more shrub-like than like a tree, usually having multiple stems coming up from the base, with the stems bending and growing laterally. This type of growth form is not currently implemented in FACETA, and it is a poor fit for the model's growth assumptions. The tree is unimportant commercially, has very little published data, and has no growth ring data.

Fraxinus pennsylvanica (green ash) was one of the most important species in both Greenbelt surveys. Green ash thrives in moist soils and is tolerant to flooding, but it is also hardy in dry soils. It is moderately shade tolerant, a fast grower, and is considered a climax species for the forest type. Considerable published information is

available on the species, and an excellent data set of growth rings sampled from the Greenbelt in a previous University of North Texas student' s research is available.

Morus rubra (red mulberry) is a fast growing, small to medium sized tree found to be fairly abundant in the Greenbelt understory in the Rijal (2011) survey but appeared only rarely in the Barry and Kroll (1999) study. It is known to hybridize with the Asian imported white mulberry (*Morus alba*), and the species appears on some states' threatened or species of concern lists. Generally, the species is not that abundant, and it is thought to occur only as scattered individuals (Burns & Honkala, 1990). However, some parts of the Greenbelt understory were thick with mulberries, and occasionally there were individuals of substantial size. There is little published data on the species and no available sources of growth data.

Populus deltoides (eastern cottonwood) was the tree with the largest growth potential – height, diameter, and rate – in the Greenbelt. Cottonwood was not present in the Barry and Kroll (1999) study but was fairly important in the Rijal (2011) study, often appearing as very large trees. It is considered a pioneer species and is intolerant to shade, moderately tolerant to flooding, fast growing, and short-lived. It favors high banks and well-drained soils in the floodplain. There is some publicly available tree ring data through a dendrochronology database, but it is collected in South Dakota, which is at the limit of the species' range.

Quercus macrocarpa (bur oak) was potentially one of the largest in diameter and longest-lived species found within the Greenbelt. Bur oak showed up as a minor component in both Greenbelt studies, infrequently but often as large individuals. Seedlings too small to be included in these surveys were not uncommon in the

Greenbelt. Bur oak can be found in both uplands and bottomlands within its range, and it is one of the most important trees of the northern American prairie. It is considered very drought tolerant, weakly tolerant to shade, slow growing, and while it is considered intolerant to flooding, it is common in bottomlands; individuals do survive through periodic floods in the Greenbelt floodplain. As with cottonwood, there is some tree ring data available through dendrochronology resources for bur oak, but these data were sampled from locations near the western limit of the species' range and not close to this study area.

Quercus marilandica (blackjack oak) is a small to medium size tree. Blackjack oaks along with *Quercus stellata* (post oak) are only found on upland sites. The Barry and Kroll (1999) Greenbelt study focused exclusively on bottomland sites and subsequently found none of these two oak species. While the Rijal (2011) study also focused on bottomland sites, the surveys from the study did include two upland sites. Blackjack oak was absent in one of these two sites but made up a significant proportion of the other site with the second largest basal area and importance value. It was notable that the site with no blackjack oak had sandy loam soil with sites on a low slope. The soil in the other site was on top of a ridge and had a considerably coarser texture that was very rocky. The species has a reputation for thriving on dry ridges and sites with poor soil. Generally, blackjack oak is considered the second most important tree species in Eastern Cross Timbers upland sites after post oaks. It is a very slow growing tree, and while it often is small or even shrubby, it can grow to diameters exceeding 60 cm, heights close to 20 m, and can live in excess of 200 years. It is intolerant to shade and flood, has a high tolerance to drought and poor soil nutrients, and is tolerant

to periodic fires. It can dominate on some sites, typically where soil conditions are very poor. Dendrochronologists avoid this species because of its notoriously hard wood. Additionally, the center of the trunk often has heart rot, so there are no sources for tree ring data.

Quercus stellata (post oak) is the characteristic tree of the uplands of the Eastern Cross Timbers. In North Texas, it does not typically grow very tall, typically staying under 15 m, but it can reach heights exceeding 30 m and diameters of 100 cm. Post oak only showed up in the two upland sites in the Greenbelt surveys, but it dominated in both surveys, particularly in the basal area. It is intolerant to shade, flooding, and soils with poor drainage or clayey textures. Post oak is found together with blackjack oak in sites with dry, poor soils, as both species tolerate these conditions; however, post oak is a little more tolerant to drought and a little less tolerant to poor soil nutrients. It is slow growing but faster than blackjack oak, and it can live longer than 300 years. Post oak is a favored species by some dendrochronologists, and a number of tree ring data sets are available, including datasets collected in North Texas.

Salix nigra (black willow) is the largest North American willow species, and the only one native to North Texas. It was not found in the Barry and Kroll (1999) surveys and only constituted a minor component in the Rijal (2011) surveys; however, there were areas in the Greenbelt area where black willow dominated. Black willow is one of the first species that grows from new sand bars, often together with cottonwood. It is commonly found in sloughs and low-lying areas in the bottomland, and it is common in ditches and disturbed places where water collects in urban areas. Together with swamp privet, it is the most flood tolerant woody species in North Texas, and it has a high

moisture requirement for seed germination and establishment. It is intolerant to shade, short lived, a fast grower, and considered a pioneer species. There is limited published data and no available sources of tree ring data for black willow.

Ulmus alata (winged elm) is a small to medium sized tree able to grow in a wide range of soil and moisture conditions. This tree was absent in the Barry and Kroll (1999) surveys. In the Rijal (2011) surveys, winged elm had high importance values in the two upland sites and appeared as a minor component in the bottomland sites. Correspondingly, the species was described as being a minor component in both the post oak-blackjack oak and the sugarberry-American elm-green ash forest types. In dry upland sites, it stays small, has stunted growth, but can grow to decent size on better sites. It is tolerant to shade but not as much as other elm species. The winged elm is classified as tolerant to flooding, although it is not known to grow in standing water. From personal experience, it is far more common in upland sites than in bottomland sites. It is easy to misidentify cedar elm (*Ulmus crassifolia*) in the field as winged elm. While the two species each have distinguishing characteristics (winged elms grow corky wings on the stems and cedar elms have smaller leaves that are scabrous), cedar elms can also grow wings. Leaf size is highly variable among individuals, and winged elms leaves are slightly scabrous. In some cases, the only way to tell with certainty which of these species a tree belongs to is to identify it during the couple of weeks that it is flowering. Information is available on winged elm, but it is sometimes contradictory or incomplete. No sources of growth ring data are available.

Ulmus americana (American elm) is the largest of elm species in North Texas. American elm was not observed by Barry and Kroll (1999), but it was a significant

component in the Rijal (2011) surveys. A limited number of large, older trees were found in the Greenbelt surveys, but a number of smaller young trees were also identified. Due to its susceptibility to Dutch elm disease, large American elm trees have diminished in importance in U.S. forests (Burns & Honkala, 1990). This is a possible explanation why large American elm trees are not as common in the Greenbelt forest. American elm is tolerant to a range of conditions. It is most common in bottomlands on flats and terraces, but it is not common in swamps. American elm is considered moderately shade tolerant and a climax species. American elm is a well-described species, but it has not been of interest in dendrochronology.

Ulmus crassifolia (cedar elm) was one of the most common species in the Greenbelt. Found throughout the bottomland, it grew in sloughs, on flats, and fronts. It also grew in the uplands, although it was rather small and stunted in the Cross Timbers uplands. Cedar elm can grow in a range of soil conditions and can dominate in poorly drained heavy clay soils. Published data on cedar elm is limited, and growth data are difficult to determine as cedar elm exhibits very irregular radial growth and the cross sections can range from circular to square, or can be deeply scalloped. Growth rings are very indistinct. At times, it can grow corky wings and resemble winged elm.

The species described above were all candidates for FACETA modeling and parameters were researched as far possible. However, either because of limited information and data, or because a species did not fit well in the model's assumptions, not all of these species could be successfully modeled in FACETA. Other species were considered for different reasons for the Greenbelt FACETA model. *Gleditsia triacanthos* (honeylocust) and *Maclura pomifera* (bois d'arc) were both considered because of their

prevalence in the Greenbelt. *Juniperus virginiana* (eastern red cedar) was considered because of its importance as an invader in the Cross Timbers uplands, while *Prosopis glandulosa* (honey mesquite) was considered because of its importance as an invader in the prairie. However, model parameters were not pursued for these species.

Maximum Age, Diameter, and Height Parameters

Species-specific growth parameters include maximum age (AGEMAX), maximum height (HMAX), and maximum diameter (DMAX). It might seem these would be easy parameters to find values for, and indeed, a number of forestry and silvics resources give numbers for these maximums. However, the different sources do not always agree with one another, and information about species that have little or no commercial value is often incomplete or unknown. To some extent, it is not really possible to know these maximum values with certainty, and the best that can be done is to find information on the tallest, widest, or oldest tree of its species recorded. Another complication is that the size that individual trees from any species can reach can vary greatly across the native range of that species. The meaning of the term diameter, as well as height in some cases, is also somewhat ambiguous. Standard forestry practice for measuring diameter is to measures the perimeter around the trunk at *breast height*, and then to divide that length by Π (3.14). This measurement is the diameter at breast height (DBH). The assumption or rationale behind calling this measurement the diameter is that the trunk of a tree is essentially symmetric and circular. That assumption holds well for many trees of many species, but not for all trees or species. FACETA also relies on an assumption of symmetric trunk growth. This symmetry assumption does not cause an issue with modeling tree growth, forest development, or for finding a value for the

parameter DMAX, but it does become an issue for collecting and analyzing data when determining the growth rate parameter since in reality many data points will come from asymmetrical trees. The height of the DBH measurement was initially defined in American forestry practices as 4.5 feet, or 1.37 m, above the ground. Now the common standard used is 1.4 m above the ground, and in some countries, the convention is 1.3 m. If there is a branch or burl growth at breast height, then the tree should be measured at the thinnest point below that level. In cases of trees growing on sloping land, some standards measure from the base of the tree on the high side of the slope while others measure from the midpoint between the high and low sides. The procedure for measuring trees growing on sloping land becomes significant on steep slopes with trees that have a pronounced broadening at the base of the trunk. Trees that are themselves growing at a slant or in odd forms can present challenges to measure according to a uniform standard. For the Greenbelt FACETA model, slanted tree growth was primarily a problem for the shrub-like species *Forestiera acuminata*. The height of a tree was typically measured as the height above the ground from the top of the crown, which is a straightforward definition. However, for a slant-growing species like *F. acuminate*, this method may be problematic, and it might be more appropriate to measure the length of the stem, at least for determining allometric relationships. Growth patterns such as slant-growing or asymmetrical stems that do not conform well to model assumptions were referred to as non-conforming growth (Fig. 5.1). In this research, when referring to measured data, the term DBH meant the perimeter of the trunk divided by 3.14 and measured at 1.37 m above the ground, or as close below that as possible to avoid lateral growths. The measurement itself was typically made with *DBH*

tape, a forestry measuring tape with a scale that has already been divided by 3.14. Within the model world of FACETA, DBH is defined as the diameter of a symmetric tree trunk at 1.37 above the ground. For both real-world measurements and within FACETA, the height is defined as the vertical distance from the ground to the top of the crown.

Figure 5.1. Non-conforming growth in Greenbelt area trees. FACETA makes assumptions about growth forms and symmetry of trees, but many tree species do not conform well to these assumptions. (A and B) *Maclura pomifera* often grows multiple stems with a twisting, irregular form, or as a single, asymmetrical, lobed main stem branching out at low height. (C) *Forestiera acuminata* typically grows laterally and often even back towards the ground. (D) *Quercus stellata* can grow as two or three main stems. It is often unclear if multiples trees merged into each other, or if one tree split into multiple main stems. (E) *Celtis laevigata* is one of a number of Greenbelt area tree species that can exhibit asymmetrical radial growth of the main stem. These kinds of non-conformities can cause problems interpreting DBH and height measurements, interpreting height/DBH allometry, collecting and analyzing growth ring data, and may affect the assumptions for leaf area allometry.

Size limit parameters DMAX and HMAX are both used in FACETA's growth algorithms. Together with the growth rate parameter, G, they are used in the

incremental optimal diameter growth equation, the primary equation driving the growth of trees. This equation outputs for each species the optimal amount of new annual diameter growth as a function of the current diameter. Optimal growth increment can only be achieved if all environmental conditions are optimal. Stressor equations in FACETA, for example for drought or temperature, decrease annual modeled growth increments from the optimum depending on the environmental conditions and on each species tolerance parameters. Another growth equation that uses HMAX defines the allometric relationship between height and DBH. Both the optimal growth equation and height/DBH allometric equation are discussed in more detail in the following section. In addition to being used in growth algorithms, some parameters are also used in the tree mortality algorithms. FACETA uses a probabilistic, age-related background mortality based on the assumption that only a certain percentage of any population will be able to reach its maximum age. In any simulation year, all individuals of a species face the same probability of this background mortality, and the higher the AGEMAX parameter value is for a species, the lower its annual background mortality probability will be. Mortality also occurs in FACETA when trees do not grow significantly for some number of years. A lack of sufficient growth can occur when the environmental stressors are too great or if a tree reaches its maximum size. Once a tree reaches DMAX for its species, the tree will no longer grow and the no-growth component of mortality will follow.

The limit parameters AGEMAX, HMAX, and DMAX are intended to represent true maximums that would occur under optimal conditions. Realized growth will always be reduced from this maximum through the stressor equations. Being able to find values for these maximums can depend on how common, desired, or commercially important

the species is. Considering how little old growth forest remains in the eastern United States, it is possible there are no remaining examples of true maximums for some of these native eastern species. Observing and measuring the width or height of a tree is much more common and far simpler than measuring a tree's age, so it is likely observed maximums for DBH and height reflect the truer potential maximums for a species than those for age. To find values for these parameters, the approach taken is to find the largest cited values from credible sources while at the same time maintaining consistency by limiting the number of sources. The large variation in size that some species can exhibit across their range raises a question about this parameterization approach.

The Greenbelt FACETA species that is probably most different in size across its range is *Quercus stellata*, or post oak. Post oaks require aerated soils and suffer in inundated soil. In the Greenbelt area, they grow on the sandy uplands of the Cross Timbers, and in the hot and dry summers in that part of Texas, sandy soil becomes very dry. The post oaks growing wild in the Cross Timbers typically do not exceed 12 m in height. They will grow taller if they receive more water, so the post oaks growing in residential properties within the study area may reach 15 m. In the wetter part of post oak's range, it can achieve heights greater than 30 m. For example, the National Register of Big Trees, a national database of individual large trees, lists a post oak in Mississippi that exceeds 32 m. The question then is should HMAX be the maximum height across the species' entire range, or should HMAX be limited to values that are realistic within the modeled area. The same question applies to DBH. It would be ideal to be able to set model parameters to an overall potential maximum and let the modeled

weather, soil moisture, and growth and stress relationships determine the modeled output size. One potential problem from doing this is ending up with unrealistic output, such as 30-m tall post oaks in Texas. It turns out that this particular problem is avoided if the height/DBH data for the allometric parameters and the growth ring data for the growth rate parameters are collected locally. The locally collected data has a stronger influence on the model parameters than the potential maximums.

Possibly a larger concern or potential problem in using the maximums from across the entire range of species occurs when species with significantly different ranges are included in the same model. In this case, the maximum parameters from those different species might be incomparable. For example, *Ulmus crassifolia*, or cedar elm, has a smaller and more southwestern range than the other candidate species for the Greenbelt FACETA model. Its range lies mostly in Texas and northern Mexico, and extends on its eastern side to northern Louisiana, southern Arkansas, and the northwestern edge of Mississippi. For all the Greenbelt FACETA candidate trees, the largest growth is typically realized in the wetter, eastern parts of their range. A commonly cited maximum height for cedar elm is 30 m, the same as post oak. However, it seems plausible if not probable that cedar elms would achieve taller growth if their range extended further east. Considering cedar elms in the Greenbelt bottomlands grow twice as tall as upland post oaks, using 30 m for the maximum height parameter for both of these species is incomparable. The modeling philosophy is that you seed the model with the species' optimal potential and let stress and competition within the model reduce the realized growth from the optimal. However, if parameters for the optimal potentials for different species are derived from places with different

climates or environmental conditions, then the question rises of whether those parameters reflect a true optimal potential or they simply reflect the realized maximums the species were able to attain under those different environmental conditions. This concern is somewhat alleviated by using local measurements for the other growth parameters, which brings the realized growth of the modeled trees more in line with the trees growing in the area.

The question of how to exactly deal with the maximum parameters for species that vary greatly over their ranges is not fully addressed in this modeling philosophy. In this research, commonly cited maximums regardless of species range were typically used for the maximum parameters, but only to the extent that those maximums were still compatible with local measurements. The allometric and growth rate parameters were estimated from measurements taken locally within the modeled area, and these parameters caused the modeled growth to be influenced by the local growth patterns. In some cases, using maximum values that are out of line with local measurements can lead to undesirable outputs in the growth model, so using the largest of the referenced maximums is not always the best choice.

Resources offered through the USDA, USFS, National Registry of Big Trees (NRBT), and local measurements were used to determine the maximum parameters. Three of the sources used are offered through the USDA Forest Service: Silvics of North America (Burns & Russell, 1990), the Climate Change Tree Atlas (Prasad & Iverson, 2007-ongoing), and the USDA Fire Effects Information System (FEIS; USDA, 2014a). Silvics of North America is an agricultural handbook offered in print and online that describes the silvical characteristics of many North American tree species. This

manual is focused towards applications in forestry, and subsequently, commercially important trees have more comprehensive and complete descriptions. The Climate Change Tree Atlas is an online spatial database describing many species of the Eastern United States with the emphasis being the impact of climate change on these species. The database also describes many silvical and ecological characteristics of the species. The USDA FEIS online database provides information regarding fire effects on various plants, animals, and lichens. It includes a great amount of silvical and ecological information on tree species. The Natural Resources Conservation Service (NRCS), another agency housed within the USDA, offers the PLANTS Database (USDA, 2014b), an online resource describing biological and ecological characteristics of many native and imported plant species. While all four resources are from the USDA and three are from the USFS, the information they contain often overlaps and agree; however, they do not always agree. In some cases, the sources from the USFS cite maximums that come from notable or record-breaking trees. The numbers given are often for *average*, *typical*, or *mature* trees, but the NRCS PLANTS Database only reports typical or average values. The NRBT (American Forests, 2013) is a non-governmental resource. Operated by the non-profit, conservation organization, American Forests, the register allows people from around the country to submit information – circumference, height, and sometimes a photograph – of trees that are particularly large examples for their species. The trees are scored through a combination of the circumference and height, and the *Big Tree Champions* are declared for each species based on those scores. An interesting result of this scoring system is that many champions win that honor based on the circumference, while the height can often be far from record breaking. This register

is by its nature a source of maximum growth potential, but it probably should be used with caution for determining these maximum parameters. Species identification and measurements are done by people who nominate trees to be added to the register, the circumference measurements are sometimes made on trees with split or multiple stems or exhibiting other non-conforming growth patterns, and in some cases, these trees just seem to be extreme outliers in size (Fig. 5.2). Table 5-3 summarizes the maximum size and age values from these five sources as well as from local measurements.

Figure 5.2. National Register of Big Trees champions. Photographs are submitted for many of the champions in the National Register of Big Trees. (A) A very large blackjack oak (*Quercus marilandica*) growing in Illinois, with a circumference of 125 in., equating to a DBH of 101 cm, and a height of 23 m. (B) This post oak (*Quercus stellata*) in Georgia became a champion by virtue of its circumference (245 in.), but the trunk is split. (C) This black willow (*Salix nigra*) in Michigan has a massive trunk and limbs, but has a modest height of a little over 20 m. (D) An American elm (*Ulmus americana*) growing in Louisiana, this tree is close to 34 m tall and has a measured circumference of 324 in. The large circumference, equated to a DBH of 2.6 m, reflects the tree's very broad, fluted base, and it should not be calculated as a DBH. (E) Another post oak, this one growing in Mississippi, has an amazing height, circumference, and crown, and it would tower over post oaks growing in Texas. Images are all from the NRBT (American Forests, 2013).

Table 5.3

Maximum Age, Diameter, and Height for Greenbelt FACETA Trees

Species	AGEMAX (years)		DMAX (cm)		HMAX (m)	
Acer negundo	Silvics: n/a	FEIS: 100	Silvics: 120	FEIS: 92	Silvics: 23	FEIS: 21
	PLANTS: Short	NRBT: n/a	PLANTS: n/a	NRBT: 210	PLANTS: 18	NRBT: 23
	CCTA: 100	Denton: n/a	CCTA: n/a	Denton: 67	CCTA: 15	Denton: 22
	FACETA: 100		FACETA: 90 - 120		FACETA: 23	
Carya illinoinensis	Silvics: n/a	FEIS: Long	Silvics: 210	FEIS: 210	Silvics: 55	FEIS: 45
	PLANTS: Long	NRBT: n/a	PLANTS: n/a	NRBT: 216	PLANTS: 43	NRBT: 41.5
	CCTA: 300	Denton: n/a	CCTA: n/a	Denton: 102	CCTA: 55	Denton: 32
	FACETA: 300		FACETA: 210		FACETA: 43 - 55	
Celtis laevigata	Silvics: 150	FEIS: n/a	Silvics: 46	FEIS: 46	Silvics: 30	FEIS: 30
	PLANTS: Mod.	NRBT: n/a	PLANTS: n/a	NRBT: 244	PLANTS: 24	NRBT: 28
	CCTA: 150	Denton: n/a	CCTA: 122	Denton: 76	CCTA: 24	Denton: 26
	FACETA: 150		FACETA: 75-120		FACETA: 30	
Forestiera acuminata	Silvics: n/a	FEIS: n/a	Silvics: n/a	FEIS: n/a	Silvics: n/a	FEIS: n/a
	PLANTS: Long	NRBT: n/a	PLANTS: n/a	NRBT: 25	PLANTS: 10	NRBT: 14
	CCTA: n/a	Denton: n/a	CCTA: n/a	Denton: 16	CCTA: n/a	Denton: 11
	FACETA: 40		FACETA: 25		FACETA: 14	
Fraxinus pennsylvanica	Silvics: n/a	FEIS: n/a	Silvics: 76	FEIS: 146	Silvics: 37	FEIS: 44
	PLANTS: Short	NRBT: n/a	PLANTS: n/a	NRBT: 219	PLANTS: 24	NRBT: 30
	CCTA: 150	Denton: n/a	CCTA: n/a	Denton: 100	CCTA: 17	Denton: 38
	FACETA: 150		FACETA: 100-140		FACETA: 40	
Morus rubra	Silvics: n/a	FEIS: 125	Silvics: 76	FEIS: 181	Silvics: 21	FEIS: 22
	PLANTS: Mod.	NRBT: n/a	PLANTS: n/a	NRBT: 222	PLANTS: 21	NRBT: 17
	CCTA: 125	Denton: n/a	CCTA: n/a	Denton: 37	CCTA: 21	Denton: 17
	FACETA: 125		FACETA: 100		FACETA: 22	
Populus deltoides	Silvics: n/a	FEIS: 200	Silvics: 180	FEIS: 183	Silvics: 58	FEIS: 58
	PLANTS: Short	NRBT: n/a	PLANTS: n/a	NRBT: 364	PLANTS: 58	NRBT: 27
	CCTA: 200	Denton: n/a	CCTA: 160	Denton: 118	CCTA: 50	Denton: 34
	FACETA: 200		FACETA: 160-180		FACETA: 50 - 58	

(table continues)

Table 5.3 *(continued)*

Species	AGEMAX (YEARS)		DMAX (cm)		HMAX (m)	
Quercus macrocarpa	Silvics: 300	FEIS: 440	Silvics: 213	FEIS: 260	Silvics: 52	FEIS: 40
	PLANTS: Long	NRBT: n/a	PLANTS: n/a	NRBT: 239	PLANTS: 30	NRBT: 30
	CCTA: 400	Denton: n/a	CCTA: n/a	Denton: 92	CCTA: 30	Denton: 32
	FACETA: 400		FACETA: 210		FACETA: 32 - 52	
Quercus marilandica	Silvics: n/a	FEIS: 230	Silvics: n/a	FEIS: n/a	Silvics: n/a	FEIS: 15
	PLANTS: Long	NRBT: n/a	PLANTS: n/a	NRBT: 101	PLANTS: 8	NRBT: 23
	CCTA: 230	Denton: n/a	CCTA: n/a	Denton: 64	CCTA: 15	Denton: 14
	FACETA: 230		FACETA: 100		FACETA: 15-23	
Quercus stellata	Silvics: n/a	FEIS: n/a	Silvics: 122	FEIS: 122	Silvics: 30	FEIS: 30
	PLANTS: Long	NRBT: n/a	PLANTS: n/a	NRBT: 183	PLANTS: 18	NRBT: 32
	CCTA: 400	Denton: n/a	CCTA: 135	Denton: 92	CCTA: 18	Denton: 16
	FACETA: 400		FACETA: 135		FACETA: 18 - 30	
Salix nigra	Silvics: n/a	FEIS: n/a	Silvics: 122	FEIS: n/a	Silvics: 43	FEIS: 42
	PLANTS: Short	NRBT: n/a	PLANTS: n/a	NRBT: 325	PLANTS: 30	NRBT: 20
	CCTA: 85	Denton: n/a	CCTA: n/a	Denton: 66	CCTA: 40	Denton: 22
	FACETA: 85		FACETA: 120		FACETA: 30 - 43	
Ulmus alata	Silvics: n/a	FEIS: n/a	Silvics: 61	FEIS: n/a	Silvics: 30	FEIS: n/a
	PLANTS: Short	NRBT: n/a	PLANTS: n/a	NRBT: 146	PLANTS: 20	NRBT: 27
	CCTA: 125	Denton: n/a	CCTA: 74	Denton: 61	CCTA: 24	Denton: 12
	FACETA: 125		FACETA: 74		FACETA: 20 - 30	
Ulmus americana	Silvics: 300	FEIS: 300	Silvics: 152	FEIS: 152	Silvics: 38	FEIS: 36
	PLANTS: Mod.	NRBT: n/a	PLANTS: n/a	NRBT: 262	PLANTS: 37	NRBT: 34
	CCTA: 300	Denton: n/a	CCTA: 152	Denton: 74	CCTA: 38	Denton: 28
	FACETA: 300		FACETA: 152		FACETA: 38	
Ulmus crassifolia	Silvics: n/a	FEIS: n/a	Silvics: 90	FEIS: n/a	Silvics: 30	FEIS: n/a
	PLANTS: Short	NRBT: n/a	PLANTS: n/a	NRBT: 126	PLANTS: 27	NRBT: 37
	CCTA: 125	Denton: n/a	CCTA: n/a	Denton: 64	CCTA: 24	Denton: 28
	FACETA: 125		FACETA: 90		FACETA: 30	

Note: Maximum age (AGEMAX), DBH (DMAX), and height (HMAX) parameters are derived from forestry and ecology resources, measurements of trees in the modeled area, and the NRBT. The sources in the table are coded as follows: Silvics = Silvics of North America, PLANTS = The PLANTS Database, CCTA = Climate Change Tree Atlas, FEIS = Fire Effects Information System, NRBT = National Register of Big Trees, and Denton = trees measured in Denton County both in and out of the Greenbelt Park. The values listed by FACETA are the initial model parameters used.

The initial FACETA parameter values are chosen from the range of possible values from these sources. In general, model parameters need to be tested for sensitivity, calibrated, and validated. This process is particularly important when the

model output is easier to measure than the model's input parameters. The maximum height, diameter, and age parameters are easier to measure than most of the other parameters needed in FACETA, but they still need to be tested for sensitivity and validated to ensure realistic results. Most of the model input parameters are linked to each other through multiple equations or algorithms, and in some cases, a particular parameter value may work well for one component of the model but not for another.

Allometric Growth Parameters

The three species-specific parameters in FACETA that define the geometric relationships between height, DBH, and leaf area are the diameter/height allometric coefficients, b_2 and b_3, and the height to base of crown ratio *Hc*. Another allometric growth parameter *lifeform* requires an input value in FACETA. Lifeform is used in one of FACETA's predecessor models, ZELIG. The different lifeforms are defined primarily by genus, e.g., *Thuja*, *Pinus,* and *Acer* were three of the available values, with the idea that each lifeform group has an average or representative pattern in its allometric relationships. In the model, each lifeform is linked to a set of regression coefficients used in various equations for trunk tapering, diameter to sapwood, and leaf area to sapwood allometric relationships. This approach to tree allometry and the specific equations in ZELIG were developed for species growing in the Pacific Northwest, and lifeform was not implemented in FACETA. However, the approach could potentially be implemented in the future. To do so would require determining appropriate equations to represent the allometric relationships and collecting sufficient allometric data from each lifeform group to do the necessary regression analysis. The success of this kind of approach would depend on the consistency of the relationships within each lifeform

group and the ability to generalize those allometric relationships. While it is not used in the model calculations, a value for the lifeform parameter is still required in the FACETA species input file, so as a convention, it is set to that of generic deciduous tree.

The height to base of crown parameter *Hc* is input as the ratio of the height of the base of the crown to the total tree height. FACETA actually uses the compliment of this value to determine the crown ratio or the ratio of the thickness of the crown to the tree height. This ratio is subsequently used in the calculation of total leaf area of the tree. The crown ratio turns out to be an important parameter because leaf area is calculated as a function of a tree's DBH and the species' *Hc* parameter. Leaf area is then used in calculating volumetric growth, and the volumetric growth equation is quite sensitive to changes in *Hc*. One advantage in the *Hc* parameter is that the measurements needed to estimate the parameter are relatively easy to make. Using a clinometer, it only requires measuring the angles to the base of a tree, to the base of its crown, and to the top of the tree. *Hc* can then be calculated from these angles.

For this research preliminary data were collected for three candidate species–*Quercus stellata* (post oak), *Ulmus crassifolia* (cedar elm), and *Celtis laevigata* (sugarberry)–to estimate the *Hc* parameter (Table 5.4, Fig. 5.3). All were measured in Denton County close to the study area watershed, and trees with any obvious signs of past pruning were avoided. For measurement purposes, the base of the crown was defined as the lowest point on the tree where branches with leaves were growing from the trunk. Leaves growing directly from the trunk were not included as part of the crown, and if a branch growing from the trunk grew upwards before leaves appeared from it, the lowest point on the branch with leaves was used to define the base of the crown.

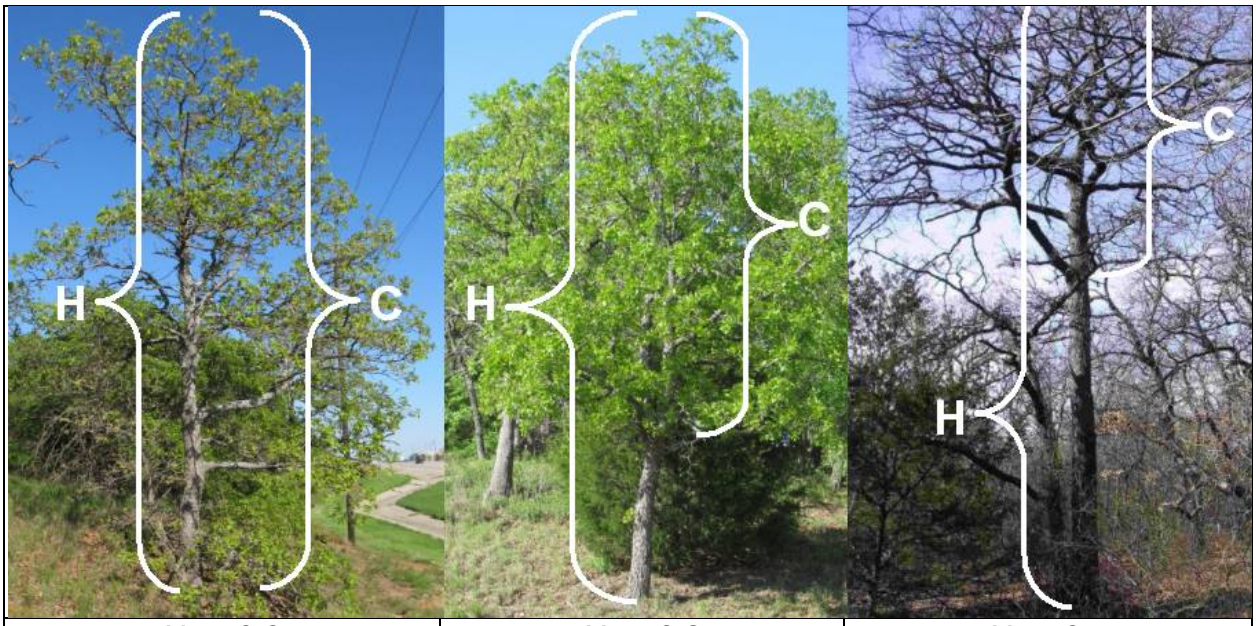

Hc = 0.0	*Hc* = 0.3	*Hc* = 0.5

Figure 5.3. Variation in crown to height ratio for *Quercus stellata.* Post oaks growing in the Cross Timbers ecoregion often have branches and leaves growing from the trunk close to the ground, resulting in a small height to base of crown ratio. Within the species there is still quite a bit of variation. From these images, the *Hc* parameter is calculated as the unlabeled height to the base of the crown divided by the total tree height H. *Left*: This tree has branches with leaves growing from the trunk down to the ground, resulting in a height to base of crown ratio of 0. *Center*: This tree has a height to base of crown ratio very close to the median value for post oaks of 0.29. *Right*: This image did not capture the full height of the tree, and the proportions are a little misleading. The height to base of crown ratio of this tree is approximately 0.5.

Table 5.4

Height to Crown Ratio for Selected Candidate Species

Species	N	Average	Minimum	First Quartile	Median	Third Quartile	Maximum
Post oak	61	0.30	0.00	0.21	0.29	0.37	0.62
Cedar elm - All	14	0.34	0.21	0.28	0.34	0.41	0.47
- In the open	8	0.29	0.21	*n/a*	*n/a*	*n/a*	0.40
- With competition	6	0.42	0.33	*n/a*	*n/a*	*n/a*	0.47
Sugarberry - All	15	0.44	0.28	0.38	0.46	0.50	0.65
- In the open	4	0.39	0.28	*n/a*	*n/a*	*n/a*	0.48
- With competition	11	0.46	0.34	*n/a*	*n/a*	*n/a*	0.65

Note: The results from data collected to estimate the height to crown parameter *Hc* for three FACETA candidate species: *Quercus stellata*, *Ulmus crassifolia*, and *Celtis laevigata*. Of the three, *Q. stellata* (post oak) had the smallest average *Hc*, but it also had the largest variation and range. *C. laevigata* (sugarberry) had the highest average *Hc*, and *U. crassifolia* (cedar elm) had the smallest variation and range in values. Quartiles were not calculated for the *in the open*

and *with competition* subgroups of cedar elm and sugarberry as the datasets were very small, and for post oak, the trees were not differentiated into those subgroups.

The crown ratios of the trees were measured using two different methods: (a) using a clinometer as previously described and (b) taking a digital photograph of the tree and measuring the tree using a digital screen caliper on a computer.

Many of the trees were measured using both methods, and when compared, the differences between the measurement methods were small. The advantage of using a digital photograph was that because of the ability to zoom into the image on a computer, the measurement was often more accurate. Determining which tree that branches and leaves are growing from can be difficult at times when trees are growing close together; zooming in on a digital photograph can really help in the differentiation. The disadvantage of using a photograph was that the image had to be taken from a distance far enough away that the angle to the top of the tree did not distort the measurement, and the camera required a clear view of the tree from that distance. For these reasons, the photo method was not possible when making the measurements within a forest, and a clinometer had to be used. Using binoculars in conjunction with the clinometer improved the accuracy.

The post oak dataset contained 61 trees measured from three groups in different locations and conditions of Denton County. The group in the driest location was located on a rocky sandstone hill covered with a thicket of small, tightly spaced post oaks. The second group was a grove of post oaks located within a residential neighborhood but in an area that was not irrigated or landscaped. This grove was located in a topographic dip on the side of a slope, had deep sandy loam soil, and was likely representative of some of the best possible conditions for post oaks growing naturally in the area. The

trees were densely spaced but were also large. The third group was of post oaks growing out in the open without any competition and within a residential neighborhood that sat on deep sand to sandy loam soil. The objective was to get measurements from different conditions and get a full range of possibilities for post oak crown development; crown ratios between the three groups were not compared.

However, an interesting followup question not addressed here is whether the crown ratios differ between these different conditions. The average value of *Hc* calculated from the post oaks was 0.30, and the values ranged from 0.00 to 0.62. The datasets for the other two species were much smaller. All of the cedar elms and sugarberries were measured within the same flat area close to a small, intermittent stream within a 500-year floodplain. The area was not properly described as a bottomland as the stream and its floodplain were too small, but it was a topographically moist location sitting on a clay loam to silty clay soil. About one third of these sugarberry and cedar elm trees were growing away from other trees without any canopy competition, and the other two thirds were growing closely next to other trees with canopies growing into each other. The average *Hc* from 15 sugarberries was 0.44, and the values ranged from 0.28 to 0.65.The average *Hc* from 14 cedar elms was 0.34, and the values ranged from 0.28 to 0.47.

While these datasets were not sufficiently large to draw many conclusions, there were some possible trends. Of the three species, post oak tended to have the smallest *Hc* but also the largest variation and range. Sugarberry had the highest average *Hc*, and cedar elm had the smallest variation and range in values. For both cedar elm and sugarberry, the individuals growing in the open without competition for light had smaller

average *Hc* values than those growing with close canopy competition; however, the individual datasets were too small to draw conclusions on. Sugarberry growing in the bottomland forest grew tall and had a relatively high *Hc*, but sugarberry trees growing in the uplands were short and scraggly, often having crowns that reached close to the ground. However, this personal observation was not addressed in the dataset. Observation of branches low to the ground also extended to other species, such as blackjack oak, cedar elm, and winged elm, when found growing in the upland positions. It seems at least plausible that *Hc* can depend as much on topographic position as it does on other factors. While the comparison between upland and bottomland trees was not possible from this dataset, this interesting question should be examined.

Some of the difficulties in determining and using the *Hc* parameter became apparent from initial measurements and observations. While *Hc* appeared to depend in part on species, there was variation within any species. In addition, *Hc* can change for an individual tree as it grows over its lifetime. Factors other than species can impact height and crown development. Competition for light from other trees can be a significant factor in height and crown development. Trees growing close together in the bottomland forests seemed to grow taller and have a higher *Hc* than trees of the same species growing without competition in the open. It is possible that competition impacts height and crown development differently for different species. For example, post oaks growing in dense upland stands seemed to have a lower average *Hc* than post oaks in the open. Another potential issue with using the *Hc* parameter was that for different species, the relationship between *Hc* and leaf area was likely to be different. For example, in the Greenbelt upland forests *Hc* tended to be smaller than in the Greenbelt

bottomlands, as the post oaks and blackjack oak often grew branches close to the ground. In comparison, the bottom of the crown of a large green ash in the bottomland may have been 15 m above ground. In the model, this difference equated to a larger crown ratio for the upland species, which resulted in a larger calculated leaf area and more rapid growth. However, there was more light penetration through a post oak canopy than through the crown of a large green ash tree, implying thinner or less dense crowns for post oaks. Additionally, many trees can have lopsided or one-side crowns, a condition common with post oaks. This sort of irregularity could be factored into the measurement, but that would make the measurement more complex.

FACETA uses the same assumptions for calculating leaf area from DBH and *Hc* for all species and does not consider foliage density or other differences in the productivity of the crown. The *Hc* parameter is the only component in the model that can distinguish the leaf area allometries of different species, and that together with the simplicity of the measurement makes it a useful parameter. It could be more adaptable to different species if the parameter were calibrated to an efficiency or productivity factor rather than just the crown ratio; however, the measurements needed to estimate such a parameter would be considerably more complex than for *Hc*. In the optimal growth equation calculation, the *Hc* parameter's role overlaps with another species-specific parameter, the growth rate *G*. Total leaf area calculation is in part a function of the *Hc* of each species, and *G* represents the optimal volumetric growth as a function of leaf area. Therefore, these two parameters are mutually sensitive to each other through the optimal growth equation. The output of this equation can be changed in similar ways by either changing *Hc* or by changing *G*. Estimating and calibrating two parameters that

are so sensitive to each other is considerably more difficult than it is for one, especially when the measurements and estimations for the parameters are either difficult to make or highly variable. Because of these various issues, no further attempt to determine species values for *Hc* was made at this time, and instead, this research focused on determining values of *G* for each species. For now, the parameter value of *Hc* was set to be the same in the model for all species.

Other growth parameters are height/DBH allometric coefficients and growth rate. Of these two, it is simpler to make measurements for the allometric coefficients. In general, the quantitative relationships between different tree dimensions and other properties, for example between height and diameter or between diameter and leaf area, are referred to as tree allometry. The FACETA allometric parameters b_2 and b_3 are the coefficients in an exponential model derived from the measurements of heights and diameters of individual trees. The height/DBH model is:

$$H = H_0 + \left(H_{\max} - H_0\right)\left(1 - \exp\left(b_2 D\right)\right)^{b_3} \quad (5.1)$$

In the model, H_0 is breast height, or 1.37 m; H_{max} is the maximum height parameter HMAX; and D is the DBH of the tree. This model assumes that height is a function of DBH and only models the growth of trees exceeding breast height. The parameter b_2 is a negative number, so as the diameter of the tree increases, the entire exponential term approaches 1 and the overall model value approaches HMAX. Note that the maximum diameter parameter is not included in this model, and depending on the data used to fit the regression model, a tree might have to attain unrealistically large diameters before coming even close to HMAX in height. Making measurements for the height to diameter allometry regression model only requires measuring the heights and DBHs of trees from

each of the species. All of the trees measured for the allometric parameters in this research were either located in the Greenbelt State Park or nearby within Denton County. The Greenbelt tree surveys conducted in Rijal (2011) were included in this analysis. In the Rijal study, all trees with DBH greater than 5 cm were measured within square 25-m x 25-m plots. The plot locations were selected through a stratified random selection method to include plots on different soil types, topographic positions, and at different seral or developmental stages. Because all trees within the plots were measured, this dataset included individuals growing asymmetrically, at a slant, or with the top broken off, which all resulted in a departure from the idealized height to DBH allometry. The range of sizes in the dataset was limited to those trees found within the Greenbelt in these randomly sited plots. For some species like green ash and cedar elm, that probably included some of the largest individuals in the area, but for other species such as post oak and winged elm, there were much larger individuals growing outside of the Greenbelt Park. In addition to the Rijal dataset, trees from some species were specifically sought out in a non-random fashion for measurement. These targeted measurements were made both within and outside of the Greenbelt Park. The trees were selected to include the full range of heights and diameters in the dataset, and those with broken trunks or any significant non-conforming geometry were avoided in these measurements. Individuals from the species *Populus deltoides*, *Quercus stellata*, *Quercus marilandica,* and *Salix nigra* were specifically sought out for measurement within the Greenbelt Park, and *Carya illinoinensis*, *Quercus stellata*, *Quercus marilandica*, *Salix nigra,* and *Ulmus alata* were also sought out for measurement outside of the Greenbelt Park. Trees growing in the *unnatural* setting outside of a forest were

sometimes measured in order to include larger individuals. These trees were growing in places like parks, old fields, college campuses, and residential lots. In all the measurements, height was measured using a clinometer for the taller trees or with a measuring pole for shorter trees. DBH was measured using DBH tape at 1.37 m above the ground or as close as possible to avoid burls, limbs, or split trunks. The measurements, together with the HMAX parameter for each species, were then used in a nonlinear regression to solve for the allometric coefficients. Multiple values of HMAX taken from the forestry references were used in the regression to compare the differences in the height to DBH regression curves. HMAX was the asymptotic maximum height in the regression equation and therefore influenced the overall height of the curve's rate of increase; however, the regression was performed on the measured data points. In general, the regression was not particularly sensitive to HMAX and the resulting curves differed little, and typically only differed perceptibly for large DBH values. The resulting error terms, for example the residual sum of squares, from the regressions using different HMAX values were also very similar. If only the allometric regression curve was considered, then the larger HMAX often seemed to yield the best fit to the data. However, using an HMAX value that was much larger than the tree heights used in the regression could cause difficulty with the volumetric growth equation, which is explained in more detail in the discussion on the growth rate parameter. In these cases, the smaller HMAX were considered. The results of the nonlinear regression analysis along with a brief discussion for each of the Greenbelt FACETA candidate species follow.

Acer negundo (boxelder) measurements were all made within the Greenbelt bottomlands (Fig. 5.4). Although boxelder was found throughout the Greenbelt bottomlands, most of these trees were concentrated in just a few locations. The input parameter HMAX was set to 23 m, which was the largest cited height in the sources used. One of the trees from the Greenbelt dataset measured just a little less than 23 m, and thus the true potential maximum height for boxelder may be higher.

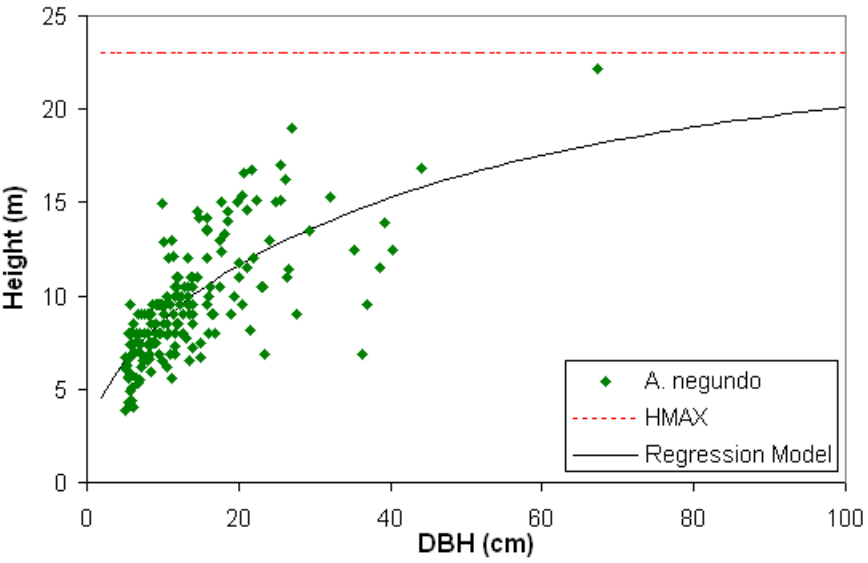

Regression coefficients: b_2 = -0.01461, b_3 = 0.54255
Residual Standard Error = 2.139 on 182 Degrees of Freedom
Residual Sum of Squares = 832.8

Figure 5.4. *Acer negundo* height/DBH allometry. Results of nonlinear regression performed on height/DBH measurements of boxelder trees.

The height of boxelder varies considerably throughout the DBH range, and the variation increases with increasing DBH. Boxelder is a weak tree that breaks easily, which may be a factor in some of this height variation.

Carya illinoinensis (pecan) were measured both inside and outside the Greenbelt Park (Fig. 5.5). All of the smaller trees, those with DBH of 20 cm or less, were

measured in the Greenbelt Park. There were some larger pecan trees inside the park, but they were not included in this survey. The largest pecan trees found in the study area often grew along smaller streams in deep, well-aerated soil.

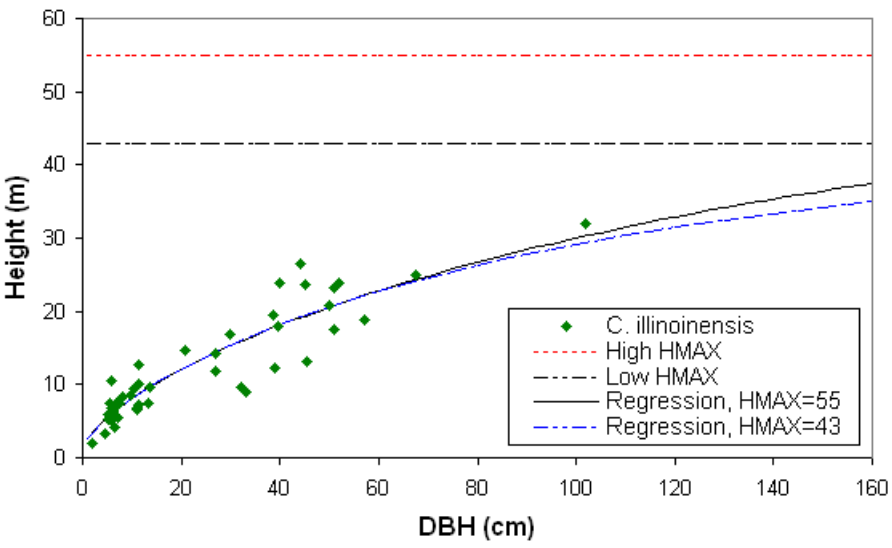

Regression coefficients

HMAX=55: b_2 = -0.00526 b_3 = 0.70190

HMAX=43: b_2 = -0.00857 b_3 = 0.73351

Residual Standard Error on 47 Degrees of Freedom

HMAX=55: 2.922 HMAX=43: 2.944

Residual Sum of Squares

HMAX=55: 401.3 HMAX=43: 407.4

Figure 5.5. Carya illinoinensis height/DBH allometry. Results of nonlinear regression performed on height/DBH measurements of pecan trees.

All larger trees in this dataset were measured near a smaller stream at the site of a former pecan orchard. Pecan is a species where larger cited maximum heights may not be appropriate. The highest reference value for the maximum height parameter was 55 m, a number far greater than the height of any trees in this dataset and greater than any pecans, or trees of any other species for that matter, observed in the study area. Setting the HMAX value in the regression curve to one of the lower reference values

such as 43 m yielded a regression curve that was imperceptibly different for DBHs less than 100 cm, and the resulting error terms were slightly larger. However, the higher HMAX may have yielded an unrealistic growth equation in this case. If the allometric height and HMAX differed too greatly, then the resulting growth equation could either output unreasonably large DBH increments or positive DBH increments even when the tree far exceeded its maximum diameter. This is explained in more detail in the discussion on the volumetric growth equation.

Celtis laevigata (sugarberry) were measured in the Greenbelt Park (Fig. 5.6). The maximum height parameter was set to 30 m, the highest cited value from the references used in estimating HMAX and appeared to fit well to sugarberry growth in the Greenbelt.

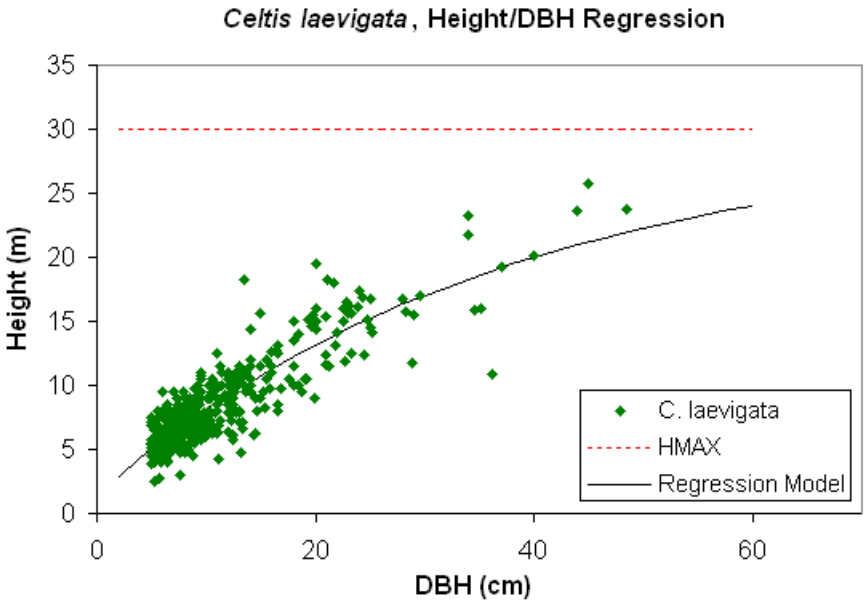

Regression coefficients: b_2 = -0.02567, b_3 = 0.97264
Residual Standard Error = 1.771 on 402 Degrees of Freedom
Residual Sum of Squares = 1260

Figure 5.6. *Celtis laevigata* height/DBH allometry. Results of nonlinear regression performed on height/DBH measurements of sugarberry trees.

Because the regression curve underestimated the height of trees with the largest DBHs in this dataset, regression was also performed with a larger HMAX value of 35 m. The resulting regression curve differed only slightly at the highest DBHs, had a slightly smaller error term, but still underestimated all trees with the largest DBHs. It was likely an artificially high HMAX would cause problems with the growth equation.

Forestiera acuminata (swamp privet) were measured inside the Greenbelt Park (Fig. 5.7). The maximum height parameter was set to 14 m, considerably higher than any measured heights but plausibly attainable. The swamp privet data were variable and did not fit tightly about the regression curve; however, the curve followed the general height and DBH pattern well, and the error was not bad. The swamp privet's main stems rarely grow straight up for long; rather they typically bend and grow at a slant, sideways, or even back down towards the ground. Smaller offshoot stems grow straight up giving the plant additional overall height. The growth pattern assumed in FACETA's height/DBH model, as well as in the calculations for growth, volume, and biomass was that of a single main stem growing more or less straight up. Swamp privet was fundamentally a poor fit for this assumption. As with all the tree height measurements used in this research, the swamp privet heights were measured as the height above the ground to the highest leaves. For swamp privet, it might be more appropriate, at least in the context of the height to DBH allometry, volume, or biomass calculations, to measure the length of the stem rather than the height. Swamp privet's sideways growth pattern together with FACETA not being coded to simulate multiple-stemmed trees made the species a poor choice for modeling, and the lack of reliable

information on the species' life history (Table 5.3) added to the difficulty of modeling it successfully.

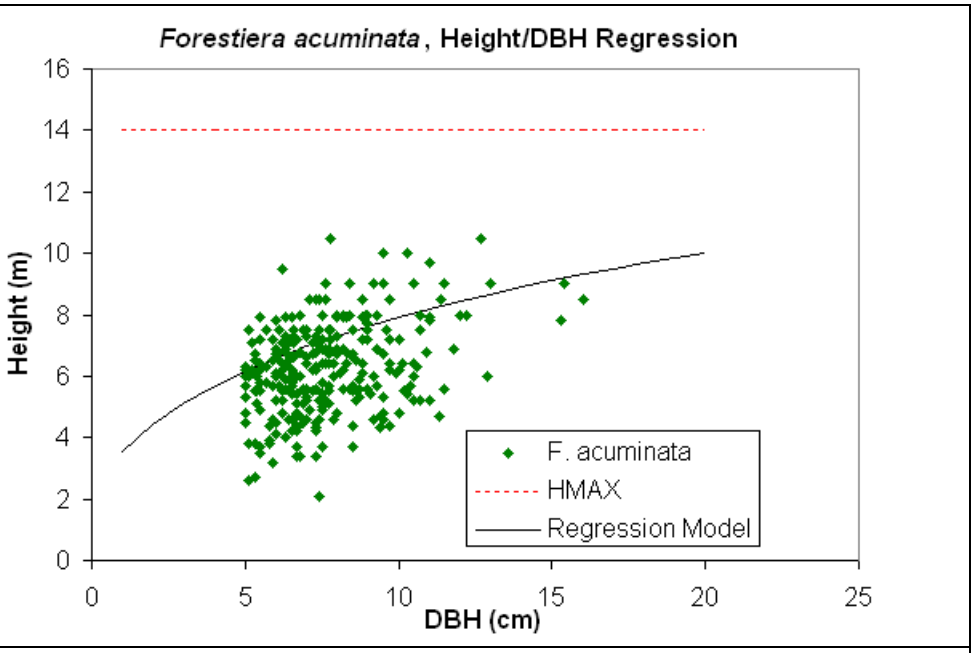

Regression coefficients: b_2 = -0.03187, b_3 = 0.50631
Residual Standard Error = 1.38 on 284 Degrees of Freedom
Residual Sum of Squares = 540.7

Figure 5.7. Forestiera acuminata height/DBH allometry. Results of nonlinear regression performed on height/DBH measurements of swamp privet trees.

Fraxinus pennsylvanica (green ash) were measured in the Greenbelt bottomland (Fig. 5.8). The maximum height parameter was set to 40 m. One tree came close to this height, but 40 m appeared to be an appropriate HMAX for the growth pattern reflected in the dataset. There was a good fit of the model to the data with little error for DBH smaller than 25 cm, but the heights varied much more at larger DBHs. Green ash typically grows a fairly straight trunk, and they were some of the tallest trees in the Greenbelt bottomland. One particular outlying point had a DBH of approximately 70 cm and height of about 12 m. This tree most likely had been uprooted and started to fall over or had its top broken off. Without being able to confirm such, the tree remained part of the height to DBH regression dataset. As a check to see if outliers such as this

made much difference in the result, the nonlinear regression was also performed with the outlying data point removed, but the resulting curve was essentially unaffected. A similar check on the influence of outliers was performed with some of the other height/DBH datasets. In no case did it change the result significantly.

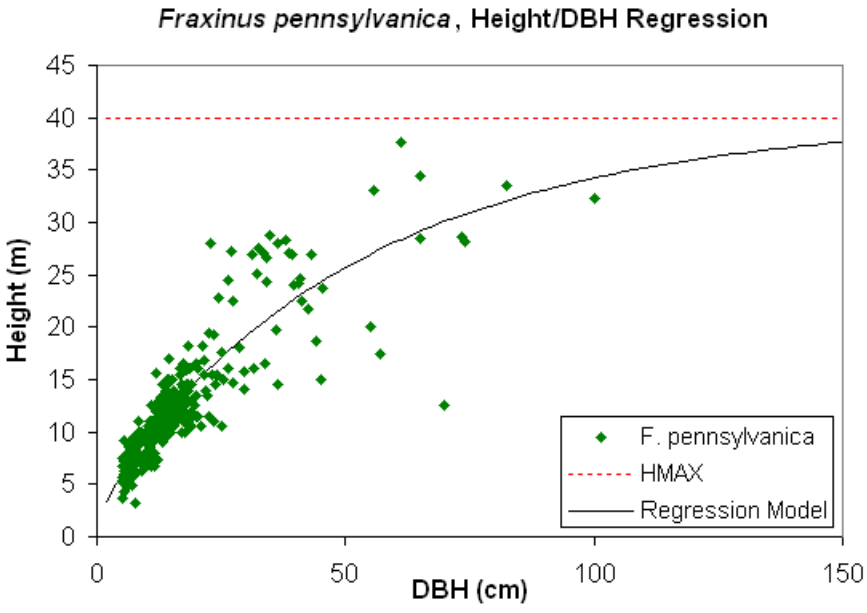

Regression coefficients: b_2 = -0.01788, b_3 = 0.88020
Residual Standard Error = 2.795 on 313 Degrees of Freedom
Residual Sum of Squares = 2445

Figure 5.8. Fraxinus pennsylvanica height/DBH allometry. Results of nonlinear regression performed on height/DBH measurements of green ash trees.

Morus rubra (red mulberry) were all measured in the Greenbelt bottomland (Fig. 5.9). Most of the individuals measured were small trees with DBH less than 20 cm. Red mulberry trees grow as an understory tree, and large individuals were not very common in the Greenbelt. There were mulberry trees in the Greenbelt with DBHs around 50 cm to 60 cm, but none of the larger trees were measured for this dataset. The maximum height parameter was set to 22 m in the regression, much taller than any measured heights, but this was reasonable considering how small the DBH of most trees in the

data was. The model was a good fit to the data; there were no apparent trends in the error. However, the dataset would improve with the addition of a few larger individuals.

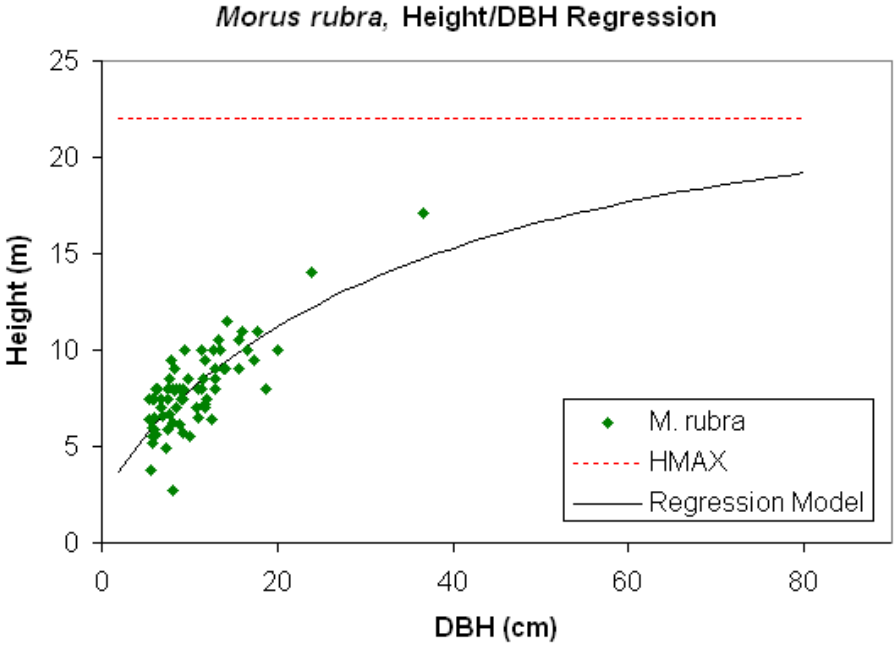

Regression coefficients: b_2 = -0.02059, b_3 = 0.68250
Residual Standard Error = 1.366 on 69 Degrees of Freedom
Residual Sum of Squares = 128.7

Figure 5.9. *Morus rubra* height/DBH allometry. Results of nonlinear regression performed on height/DBH measurements of mulberry trees.

Populus deltoides (eastern cottonwood) in this dataset were not as tall as expected given eastern cottonwood's reputation as one of the tallest species east of the Rocky Mountains (Fig. 5.10). Trees in this dataset were measured within the Greenbelt bottomland, some from randomly assigned plots and some selected specifically for their size. However, because of bias introduced by the selecting organism being shorter than 2 m, the trees measured specifically because of size were chosen based on DBH rather than height. The maximum height parameter used in the regression was 58 m, much taller than the cottonwoods in this dataset. Using a smaller HMAX of 50 m, which was the smallest of the reference heights but still considerably taller than the trees in this

dataset, had little effect in the resulting regression model other than slightly decreasing the error term. It was possible this sample of cottonwoods did not well represent the species' height potential, but this was the sample measured in the study area. Even the smallest referenced maximum height appeared too large for the growth patterns based on these measurements.

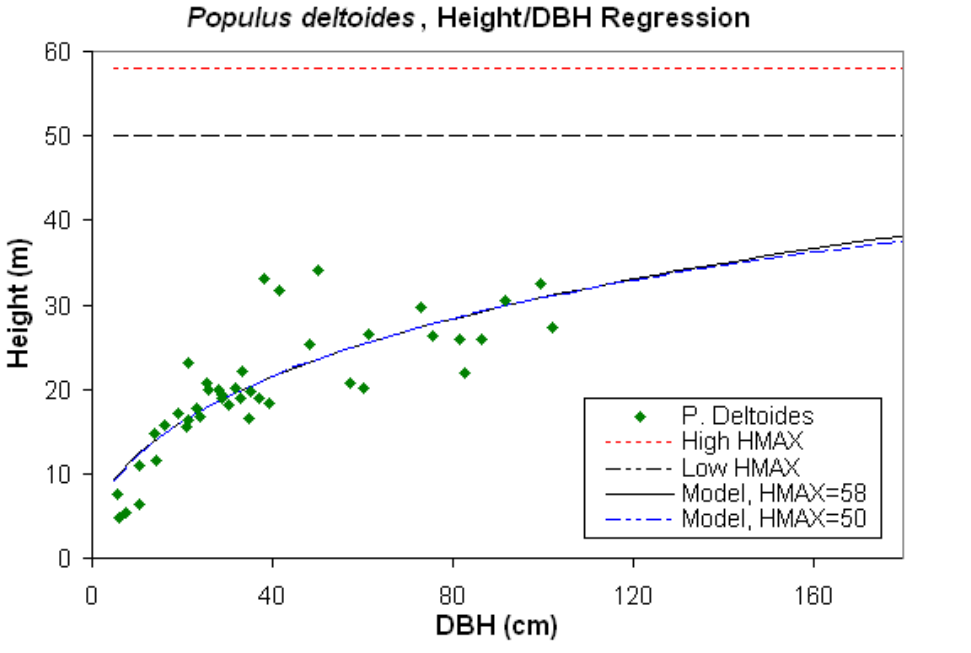

Regression coefficients
HMAX=58: b_2 = -0.002729 b_3 = 0.455932
HMAX=50: b_2 = -0.004287 b_3 = 0.475318
Residual Standard Error on 40 Degrees of Freedom
HMAX=58: 4.188 HMAX=50: 4.164
Residual Sum of Squares
HMAX=58: 701.6 HMAX=50: 693.6

Figure 5.10. Populus deltoides height/DBH allometry. Results of nonlinear regression performed on height/DBH measurements of cottonwood trees.

Containing only 11 trees, the set of *Quercus macrocarpa* (bur oak) height and DBH measurements was small (Fig. 5.11). These trees were measured in the Greenbelt. Though young seedlings were seen frequently, larger bur oaks worthy of measuring were not very common in the Greenbelt bottomland. Bur oak is considered

adaptable to both upland and bottomland positions; however, it grew naturally in the uplands of the Cross Timbers ecoregion. The largest HMAX parameter of 52 m was much higher than any of these trees were tall, and probably much taller than bur oaks growing in the western part of the species' range. The 53-m maximum height was cited for a particular tree growing in the Ohio Valley, while 30 m was the more often cited maximum height for typical trees. Even with a relatively small sample size, two trees exceeded 30 m, and one came very close to that height. Generally, the size of bur oak can vary quite a lot across its range, and it is another species where multiple HMAX values need to be considered. An HMAX of 40 m appeared to fit well to the pattern of this dataset.

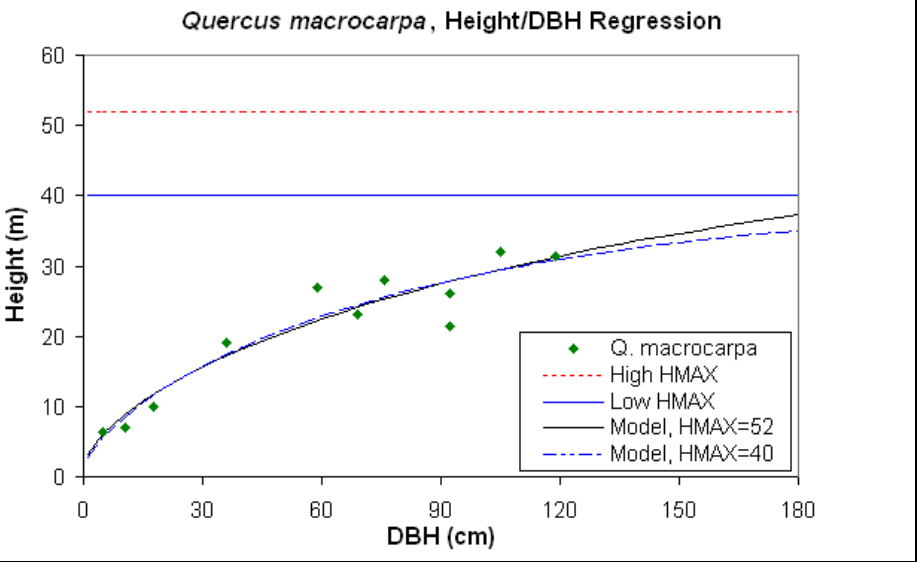

Regression coefficients

HMAX=52: b_2 = -0.00481 b_3 = 0.632286

HMAX=40: b_2 = -0.00975 b_3 = 0.720277

Residual Standard Error on 9 Degrees of Freedom

HMAX=52: 3.156 HMAX=40: 3.089

Residual Sum of Squares

HMAX=52: 89.6 HMAX=40: 85.9

Figure 5.11. *Quercus macrocarpa* height/DBH allometry. Results of nonlinear regression performed on height/DBH measurements of bur oak trees.

Quercus marilandica (blackjack oak) measurements contained a large range of sizes from trees measured in variety of conditions, from densely packed oak thickets on dry hills with thin, rocky soil, to open areas on irrigated residential properties with deep, sandy soil (Fig. 5.12). A third of the trees were measured inside the Greenbelt Park. The maximum height parameter is set much higher than any of the measured trees, but smaller values of HMAX yielded regression models with slightly larger error terms.

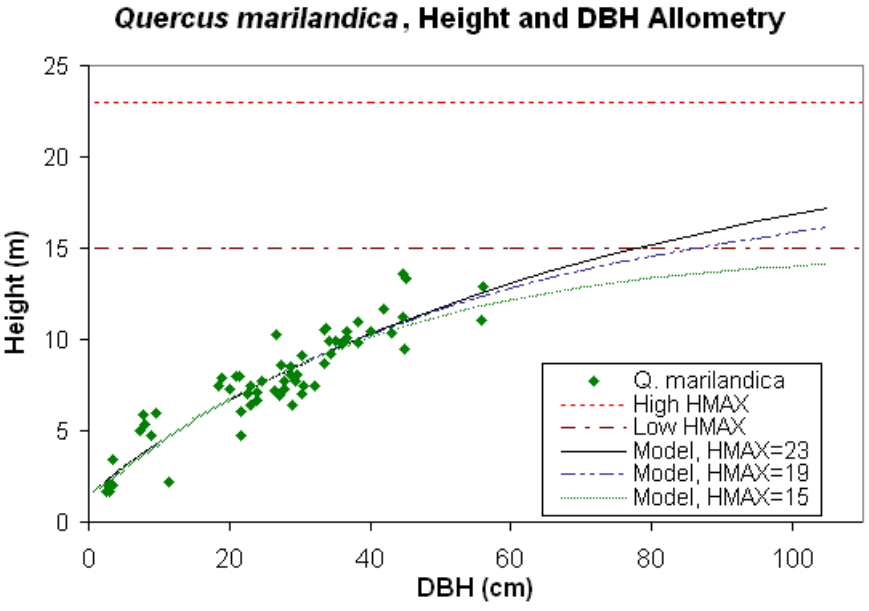

Regression coefficients

HMAX=23: b_2 = -0.01159 b_3 = 0.89007

HMAX=19: b_2 = -0.01673 b_3 = 0.94826

HMAX=15: b_2 = -0.02756 b_3 = 1.07262

Residual Standard Error on 62 Degrees of Freedom

HMAX=23: 1.135 HMAX=19: 1.141 HMAX=15: 1.164

Residual Sum of Squares

HMAX=23: 79.8 HMAX=19: 80.7 HMAX=15: 84.0

Figure 5.12. Quercus marilandica height/DBH allometry. Results of nonlinear regression performed on height/DBH measurements of blackjack oak trees.

None of the regression models' trajectories will take trees close to an HMAX of 23 m, and the pattern of the data indicates a height trajectory that could surpass an HMAX of

15 m. The variation in height for different DBHs is small when compared to many of the other FACETA candidate species, and all three models fit the data well.

Like its close associate species *Quercus marilandica*, *Q. stellata* (post oak) measured for this research included a broad range of sizes from trees growing across a broad range of conditions (Fig. 5.13). About half of these trees were measured inside the Greenbelt Park. Post oak is one species with the greatest variation in height growth across its range, and the post oaks growing in Texas tend to be on the shortest end of the height range. However, the regression models and error terms generated using the different HMAX values were nearly identical for trees with DBH less than 100 cm, and all the error terms were very close as well. As with blackjack oak, the largest referenced HMAX appeared too tall to fit the data collected in the study area, while the smallest appeared too short. The most appropriate choice probably lay between the two.

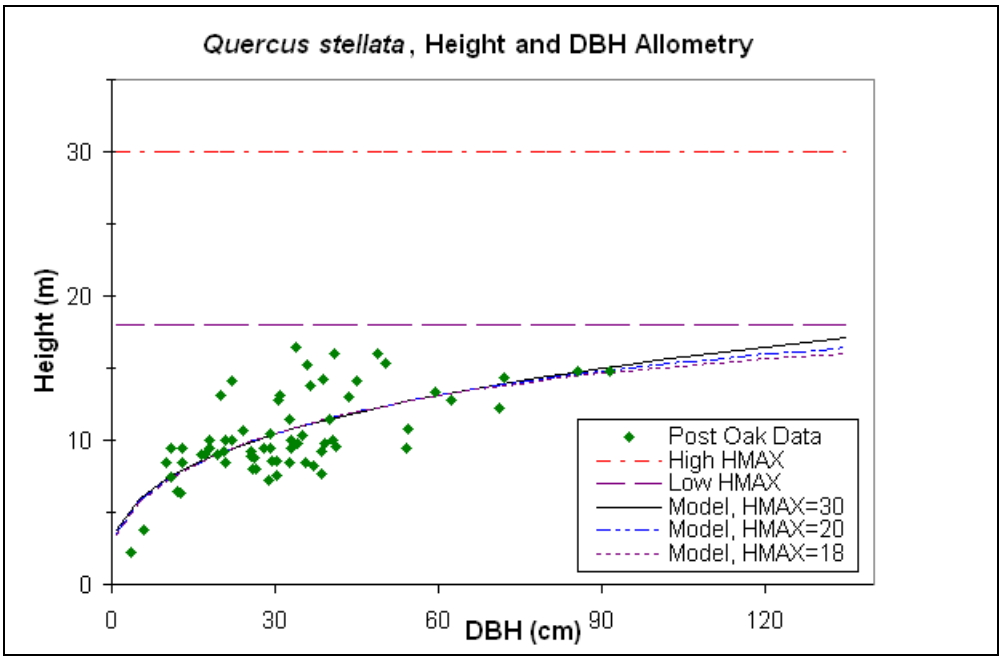

Regression coefficients

HMAX=30: b_2 = -0.00178 b_3 = 0.38954

HMAX=20: b_2 = -0.00693 b_3 = 0.42872

HMAX=18: b_2 = -0.01037 b_3 = 0.45541

Residual Standard Error on 65 Degrees of Freedom

HMAX=30: 2.145 HMAX=20: 2.141 HMAX=18: 2.139

Residual Sum of Squares

HMAX=30: 299.1 HMAX=20: 297.9 HMAX=18: 297.4

Figure 5.13. *Quercus stellata* height/DBH allometry. Results of nonlinear regression performed on height/DBH measurements of post oak trees.

Seeds from *Salix nigra* (black willow) require wet conditions almost immediately after falling in order to geminate, and the species is very intolerant to shade. Some of the best places to find black willows are in wetlands or in roadside ditches. Some trees in this dataset were measured within the Greenbelt, but most were measured outside the park boundary (Fig. 5.14). Black willow's growth pattern did not conform well to FACETA's assumptions. The trunk is often split at the base into multiple trunks that are twisted and irregularly shaped, and it frequently leans and grows laterally out over water in the tree's thirst for light. Black willow is also susceptible to a number of infestations, and the wood is weak and brittle, so larger trees commonly have broken tops.

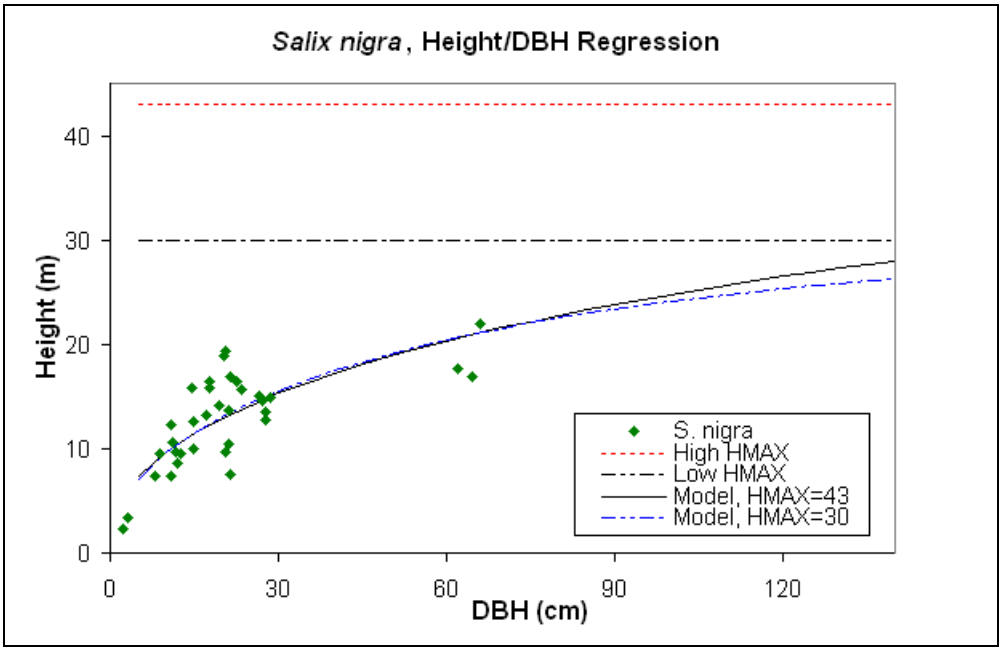

Regression coefficients
HMAX=43: b_2 = -0.003578, b_3 = 0.479056
HMAX=30: b_2 = -0.010641, b_3 = 0.542547
Residual Standard Error on 35 Degrees of Freedom
HMAX=43: 2.91 HMAX=30: 2.856
Residual Sum of Squares
HMAX=43: 296 HMAX=30: 285

Figure 5.14. *Salix nigra* height/DBH allometry. Results of nonlinear regression performed on height/DBH measurements of black willow trees.

In addition, the black willows sampled in the study area appeared to have shorter growth tendencies than the largest reference maximum would require, and multiple HMAX values had to be considered.

Most *Ulmus alata* (winged elm) were measured in the rocky Greenbelt upland hills, where it grew under and between the dominant post oaks and did not typically achieve large heights or diameters (Fig. 5.15). The two trees from this data with DBH greater than 30 cm were also measured in an upland location, but in a residential neighborhood where competition had been thinned and extra water more than likely added over the years. One winged elm was identified and measured from a Greenbelt bottomland survey that included more than 1000 trees. Sometimes winged elm is considered a bottomland species as well as, but that did not seem to be the case in the Greenbelt study area. The reference maximum height values, which ranged from 20 m to 30 m, also did not seem to align with the winged elm in this dataset. Either the winged elm in the study area was somewhat different from those in the eastern part of its range, or the species was confused with *Ulmus crassifolia* (cedar elm) in areas where their ranges intersected. The ranges of the two species only overlapped in relatively small areas including eastern Texas, southern Arkansas, and northern Louisiana. The two species can share many characteristics, and it can be difficult to identify between the two.

Regardless of the source of the discrepancy, HMAX for winged elm had to be set to the lowest referenced values to fit local growth patterns.

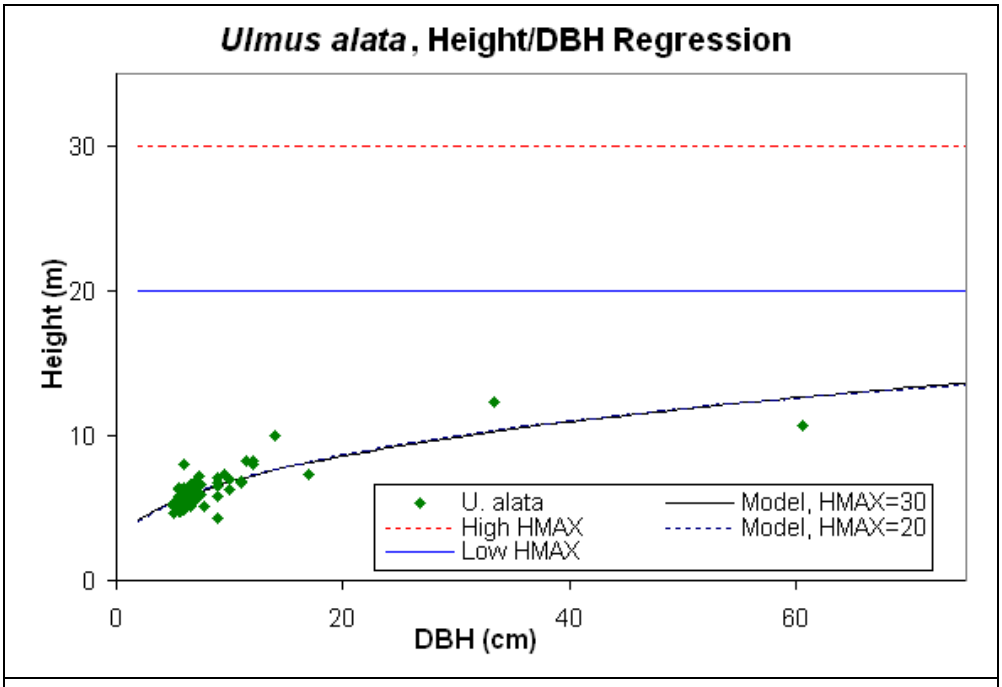

Regression coefficients
HMAX=30: b_2 = -0.00187 b_3 = 0.41640
HMAX=20: b_2 = -0.00637 b_3 = 0.440187
Residual Standard Error on 53 Degrees of Freedom
HMAX=30: 0.889 HMAX=20: 0.885
Residual Sum of Squares
HMAX=30: 41.98 HMAX=20: 41.53

Figure 5.15. Ulmus alata height/DBH allometry. Results of nonlinear regression performed on height/DBH measurements of winged elm trees.

Ulmus americana (American elm) were measured in the Greenbelt bottomlands (Fig. 5.16). Both the HMAX value of 38 m and the regression model appeared to fit the data's growth trend well. Large American elms were difficult to find in the study area, at least in part to the fungal disease Ascomycota (Dutch elm disease) that killed the majority of American elms throughout their range since the 1930s. This dataset only included four trees with DBH greater than 50 cm. The data benefited from relatively small variation in the heights and produced a well-fitting regression curve.

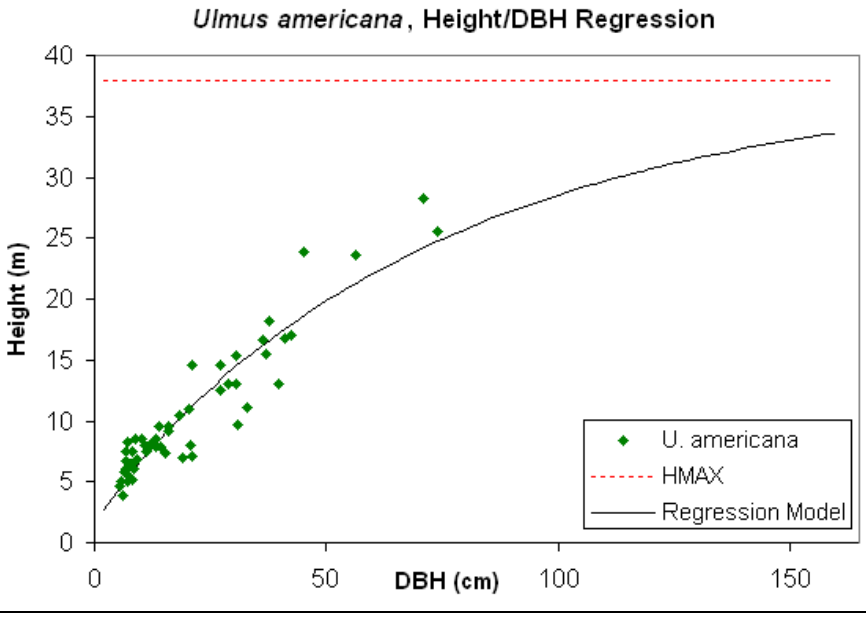

Regression coefficients: b_2 = -0.01269, b_3 = 0.90654
Residual Standard Error = 2.052 on 49 Degrees of Freedom
Residual Sum of Squares = 206.3

Figure 5.16. *Ulmus americana* height/DBH allometry. Results of nonlinear regression performed on height/DBH measurements of American elm trees.

The dataset for *Ulmus crassifolia* (cedar elm) contained a large number of trees and range of sizes (Fig. 5.17). The variation in heights was substantial, especially for DBHs greater than 20 cm. The HMAX value of 36 was actually higher than the forestry or silvics reference sources, but the NRBT had a cedar elm listed as 37 m. In this case, the highest for maximum height from the forestry references, which was 30 m, appeared too small for the data. While the models were nearly identical for DBH less than 50 cm and the error terms were nearly identical, the appearance from the growth pattern in the data was that a tree from this group could eventually exceed a height of 30 m. The Cedar elm range lies mostly within Texas, and it is not an important forestry species, which may account for an underestimation in its maximum height.

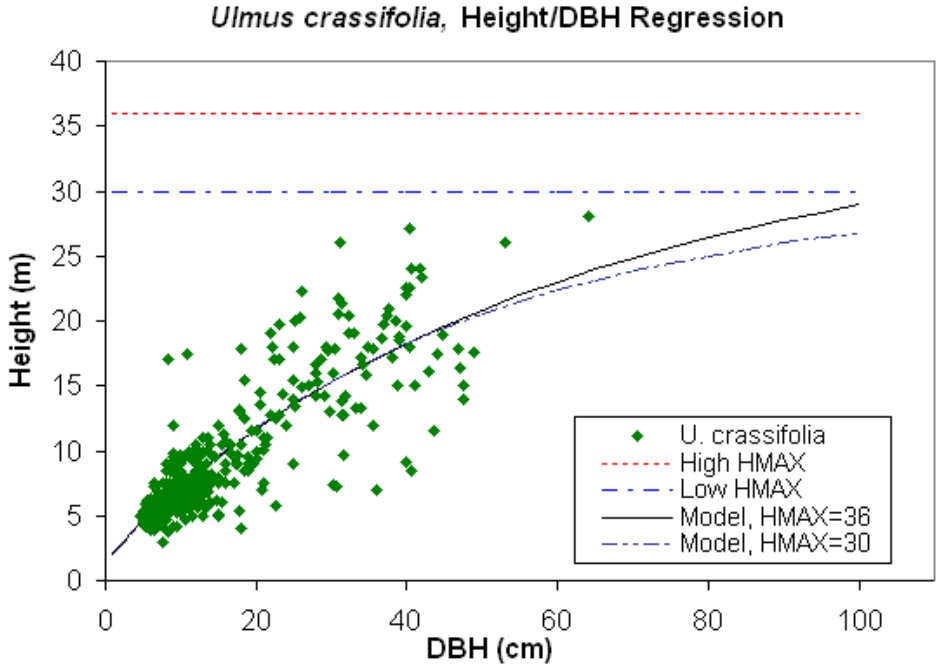

Regression coefficients

HMAX=36: b_2 = -0.01491 b_3 = 0.89509

HMAX=30: b_2 = -0.02144 b_3 = 0.96163

Residual Standard Error on 342 Degrees of Freedom

HMAX=36: 2.791 HMAX=30: 2.792

Residual Sum of Squares

HMAX=36: 2665 HMAX=30: 2667

Figure 5.17. *Ulmus crassifolia* height/DBH allometry. Results of nonlinear regression performed on height/DBH measurements of cedar elm trees.

Allometric parameters are used by FACETA to define the height to diameter relationship for each modeled trees species. These parameters can be estimated by measuring the heights and diameters of a number of trees of different sizes, and then performing a nonlinear regression on this data. While seemingly simple, there are a few considerations related to measurement, model assumptions, and the mutual sensitivity between the model parameters. The model assumes a straight, cylindrical trunk, and the allometric parameters are linked through model equations to the maximum height, growth rate, and maximum diameter parameters. Information for many of the tree species on characteristics such as maximum size, particularly the commercially less

important species, can be missing or conflicting. To estimate the allometric parameters, a reasonable maximum height parameter that is not too out of line with the data used in the nonlinear regression must first be determined. The height/DBH data for the different candidate tree species had varying degrees of fit to the regression curve; however, the basic shape of the model fit well for all the species. FACETA has another allometric parameter, the ratio of the crown to the overall height of the tree. The appeal of this parameter is that it is easy to measure for, and other than the allometric coefficients, it is the only species parameter describing tree geometry. However, this parameter is also mutually sensitive with the other growth parameters, and its function is somewhat duplicated by the growth rate parameter. In addition, many tree species have a great amount of variability in this height to crown ratio. It was determined therefore not to use the height to crown parameter at this time, and this parameter was kept as a fixed value for all species.

Growth Rate

The growth rate parameter *G* is more difficult to measure and collect data for than the allometric coefficients. *G* represents the optimal or maximum amount of annual volume (cubic centimeters) of wood growth per unit of leaf area (square meter). Optimal growth refers to completely uninhibited growth that would be achieved under optimal conditions without any deficiencies in resources. The growth equation that uses *G* outputs an optimal annual volumetric growth increment based on the tree's diameter, height, and leaf area at the start of the growing season, and the specie's growth rate. Under the FACETA assumptions, the rate of change of volume over time is given by the equation:

$$\frac{dV}{dt} = GL\left[1 - \frac{DH}{D_{\max} H_{\max}}\right]. \quad (5.2)$$

The growth rate parameter *G* is expressed in cubic centimeters of wood per square meter of leaf area per year, *L* is the total leaf area of the tree in square meters, D_{max} and H_{max} are the maximum DBH and height parameters, and *D* and *H* are the modeled DBH and height, all in centimeters. As the product *DH* approaches the product of the maximum diameter and height parameters, the volumetric growth rate goes to zero. Another allometric relationship and assumption used by FACETA is that leaf area is proportional to the basal area of the tree:

$$L = 0.16 * D^2 (1 - Hc). \quad (5.3)$$

In this equation, *D* is the DBH, so D^2 approximates the basal area, 1 – *Hc* is the proportion of the tree trunk occupied by the crown, and 0.16 is a regression coefficient that was first used in one of the early predecessors to FACETA. The regression coefficient could easily be modified in the model if data showed that an improvement could be achieved. As a potential future refinement to the model, the regression coefficient could be combined together with the crown ratio to become a species-specific leaf area coefficient and estimate the parameter from measurements made with species in the modeled region. The underlying assumption of this growth model is that the growth rate of small, young trees starts slow and is limited by the leaf area. As the tree grows, gains diameter and subsequently leaf area, then the growth rate increases. The growth rate eventually peaks, and as the product of the height and diameter approaches the product of the maximums, the growth rate starts to decline until it reaches zero. The rationale behind the peak and decline of the growth rate is that the

tree eventually reaches a size at which most of the energy assimilated is used in the maintenance of the plant. From equation 5.2, it is clear why the growth equation is very sensitive to changes in *Hc.* However, as discussed earlier, *Hc* was set to the same value for all species, and species differences in growth rate were controlled only by the parameter *G*. Measuring and collecting data in order to estimate *G* could presumably be done directly by measuring both leaf area and annual volumetric growth, but these measurements would be difficult to make at all and even more difficult to make accurately. An indirect way to measure for *G* involves solving the growth equation for a different output, the diameter growth increments. Equations 5.1, 5.2, and 5.3 can be combined, manipulated algebraically, and the entire expression can be rewritten as an annual rate of change of diameter as a function of DBH, where *G* is still a parameter. *G* could then be fitted to data of diameter growth. This process is discussed in detail later.

Mathematical assumptions and simplifications are used in the derivation of this growth model, allowing for the indirect method of measuring for an estimate of *G*. These assumptions can give rise to some subtle issues to be careful about in parameter estimation for *G*, *HMAX*, and the allometric coefficients b_2 and b_3. One such simplification is that the volume of the trunk is estimated as a square column, where the width of the column is the DBH (Fig. 5.18). This same assumption is used for basal area in the leaf area calculation (equation 5.3). While this might seem like a crude simplification, any geometric shape used to represent an organism in a model will be a crude simplification. Additionally, there are in fact tree species, for example cedar elm, which will sometimes grow an almost square or rectangular shaped trunk.

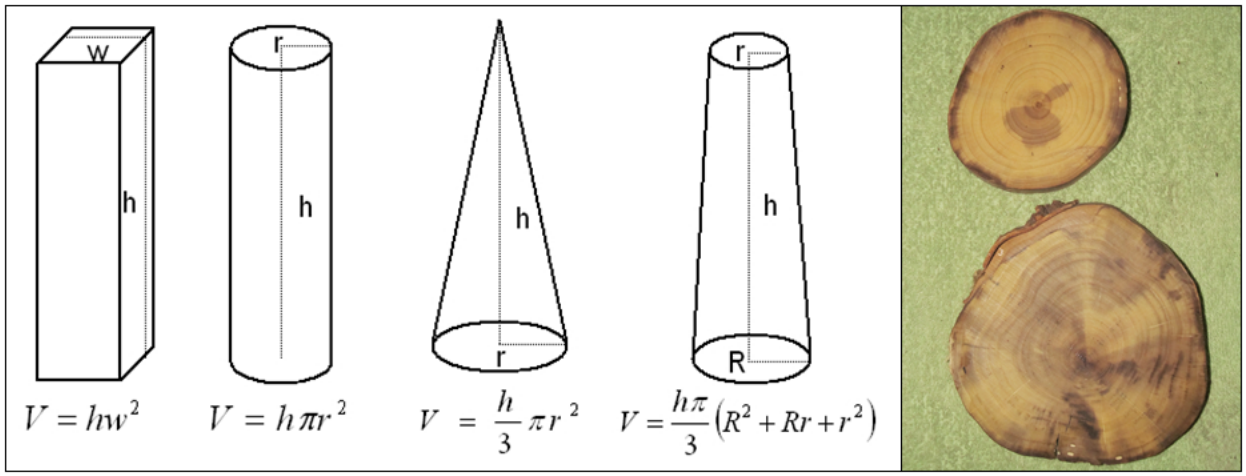

Figure 5.18. Different models of trunk volume. Left: Any model of tree growth requires some assumptions and simplifications to be able to calculate the modeled dimensions such as height, diameter, leaf area or volume. FACETA uses the assumption that trunk volume can be estimated as the volume of a square column. Other possible assumptions include cylinders, cones, and frustums of cones. Right: These two cross sections came from the trunk of the same sugarberry tree, with the larger cross section from about 1 meter above the ground and the smaller section 3 meters above that. The entire tree was approximately 7 meters tall. The difference in size between the two cross sections illustrates the kind of tapering typical of the trunks of many tree species.

Many species, green ash for example, have trunks that are more consistently circular in shape (hence the term *diameter* at breast height); in those cases, estimating the volume as a cylinder is more appropriate. However, the volume of the square column and the volume of the cylinder differ only by a factor of (4 – π). The problem with both the column and cylinder models is that a tree trunk is widest at its base and tends to taper and become smaller higher up on the trunk. It might be that using a cone to model the volume is better. The difference in volume between a cone and a square column is much larger. They differ by a factor of (4 – $\pi/3$), or approximately 2.95. This assumes that the radius used to calculate the volume is at the base of the cone rather than at breast height, and that the width of the column is twice the radius. If the radius of the cone is measured at breast height, then the volumes differ by a little less. A cone may not be the best model as it probably overestimates the tapering angle of most trunks, and in turn underestimates the volume.

Some models are more sophisticated, and tapering equations have been applied to estimating trunk volume (e.g., using a paraboloid). When trunk volume is measured in the field, the trunk is estimated as a string of frustums of right circular cones. The diameter is measured along a series of locations along the trunk, each segment's volume is calculated as a frustum, and the volumes are added together. A frustum of a cone may be a more accurate model than a square column, cylinder, or a cone, and it still provides relatively simple geometry. However, even this kind of modest increase in fidelity can add substantial complexity to the model's calculations, with its assumptions, or in determining parameters. For example, using a single frustum to represent the trunk would require defining and modeling the relationship between the DBH and the height and the diameters of both the base and top of the frustum.

Two sugarberry cross sections provided an example in the differences in volumes between these four simple models (Fig. 5.18). These two cross sections came from the same small sugarberry that was growing with a single, straight trunk, with relatively symmetric radial growth. The larger cross section came from approximately 1 meter above the ground, a little below breast height, and the smaller cross section was at about 4 meters above the ground. The total height of the tree was approximately 7 meters. The radii of the two slices, as calculated by the circumference divided by 2π, were 7.6 cm and 5.3 cm, respectively. Assuming the diameter of the larger cross section, which calculated to 15.2 cm, was the DBH of the tree, then three of the simplified volume models would calculate to approximately as follows: 161,700 cm^3 for the square column, 127,000 cm^3 for the cylinder, and 76,400 cm^3 for the frustum of a cone. In order to calculate the frustum volume, it was assumed that the slant or tapering

angle of the trunk stayed constant throughout its length. In this particular example, the volume of the square column was more than double the volume of the frustum. In order to calculate the volume of the cone model, some assumption had to change since the extended height of the cone formed by these two cross sections would be nearly 11 meters tall, and this tree's height was only 7 meters. If it was assumed the cone was 7 meters in height and the diameter of the larger cross section was the DBH, then the volume was approximately 64,700 cm^3, which was about 15% less than the frustum volume. In order to achieve the overestimated volume given by the square column model, the value assigned to *G* would need to be about twice as large as the actual volume of wood grown per unit of leaf area compared to directly measuring volumetric growth rate.

The average annual volumetric growth of this sugarberry provided perspective of what that might mean for values of *G*. This tree had 20 annual growth rings in the lower slice, so assuming it was 20 years old, the average annual volumetric growth rate estimated from the different volume models would range from a high of 8085 cm^3/year for the square column to a low of 3235 cm^3/year for the cone. There are two important differences between these average annual growth rate examples and the parameter *G*. The first is that *G* is the *optimal* or maximal growth rate, while the annual average is not necessarily representative of optimal conditions or even the optimal year for the life of this tree. The second difference is that *G* was the annual volume of new wood growth *per square meter of leaf area*. Annual average of volumetric growth could be more directly comparable to *G* if the amount of leaf area on the tree were known. The tree was cut down during the winter season with no leaves on it, so there was no way of

knowing what the actual leaf area was. Using the leaf area equation (5.3) to estimate it, this sugarberry would have had about 11 m^2 of leaf area during its last year. Additionally, according to the leaf area model, the leaf area on this tree would not have exceeded 1 m^2 until its 10th year. This discrepancy in the size of the estimated parameter *G* and the actual volumetric growth rate became transparent when using the indirect method of measuring for *G* specifically because the indirect method measured diameter growth rather than volume growth. It should be mentioned that city workers replacing underground sewer lines cut down the sugarberry tree used in this example to gain access to their dig site, and the cross sections were removed from the already felled tree. In fact, because this research involved looking at the cross sections of many trees, the following blanket disclaimer was made: No trees were cut down or otherwise injured for this research. All of the cross sections used in this research came from trees that had already been felled by other people, such as property owners or city workers, for reasons having nothing to do with this or any other academic research.

Other assumptions behind the growth equation that can complicate estimating *G* include that the modeled height and DBH follow the height/DBH curve defined by the allometric regression coefficients, combined with the assumption that the volumetric growth will continue until the product *DH* equals the product *DmaxHmax*. Since the modeled height *H* at any time is always less than *HMAX*, which is the asymptotic maximum height, the only way for *DH* to be equal to or greater than *DmaxHmax* is for *D* to be greater than *DMAX*. A situation that needs to be avoided is having *HMAX* set too large as compared with the trajectory from the DBH/height data used to estimate the allometric coefficients. One potential problem that could result is that trees may have

the potential to realize unrealistic diameter growth. The model is growing trees towards the product of their optimal height and diameter, and if a tree's height trajectory keeps it far below its optimal height, then the tree can put on that extra product in diameter. While the modeling philosophy of setting the optimal growth parameters to the true potential maximum makes sense as a philosophy, in practical terms the HMAX parameter used needs at least to align with the maximum height implied by the data used in the allometric regression. *DMAX* is also part of this product and impacts the growth curve. Increasing either of the two maximum size parameters has the effect of increasing the optimal volume and growth curve. However, *HMAX* is in some ways the more complicating parameter because the allometric coefficients are also linked to *HMAX*. Some examples of how the relationships between *HMAX*, *DMAX*, *G*, *Hc,* and the allometric coefficients impact the volumetric growth equation are shown in Fig. 5.19.

The idea behind the indirect way of measuring for *G* is that data of diameter growth increments vs. diameter can be collected. With the equation expressed in the form of the optimal change in diameter as a function of diameter, and with the four other parameters determined, the value of *G* is then fitted so that the area under the curve includes all of the diameter growth increments from the data. The hope is that the largest growth increments in the dataset are representative of the true maximum potential diameter growth. It helps to have data across a wide range of diameters, but large diameter growth increments at any DBH will push the entire growth curve up.

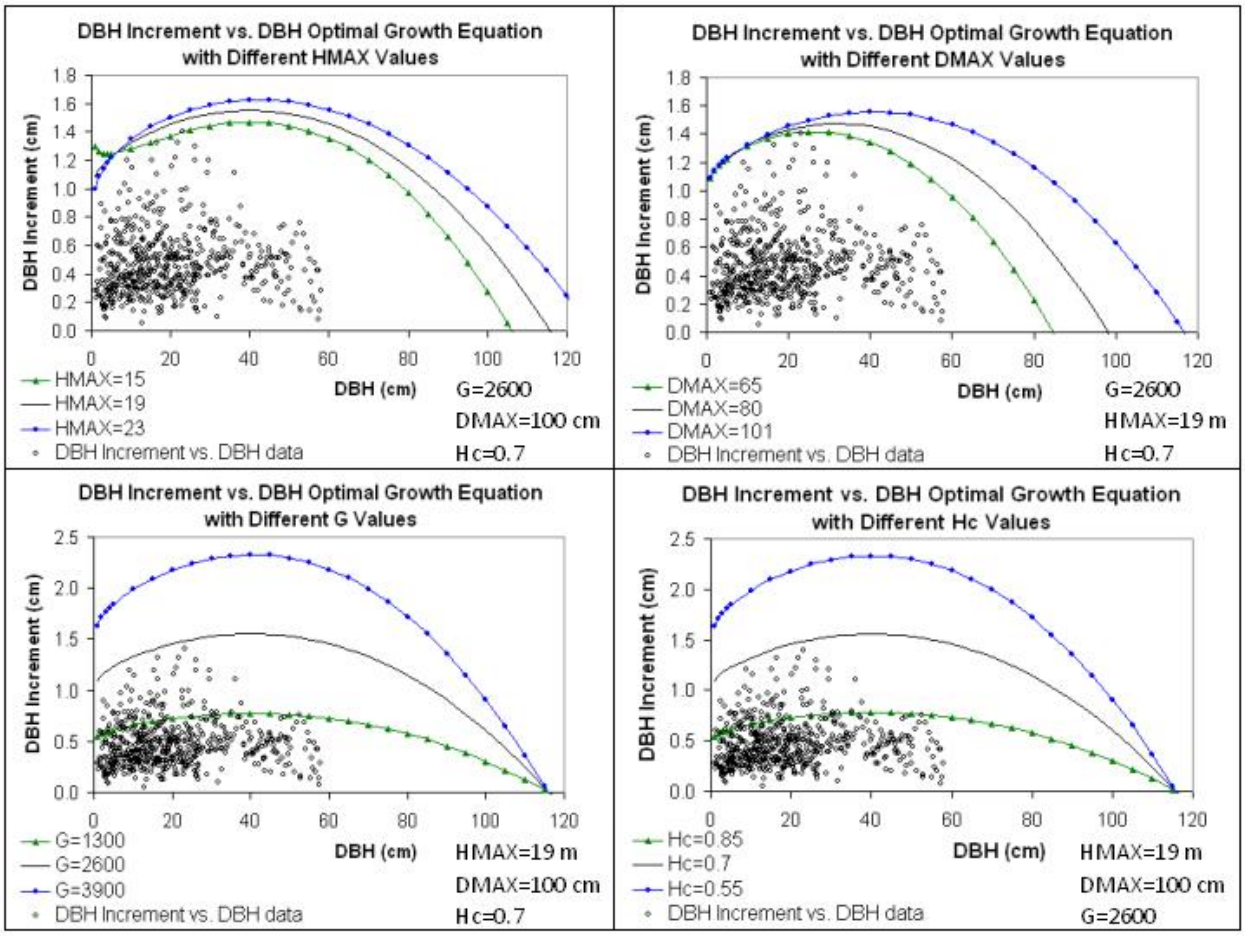

Figure 5.19. Optimal growth equation with varying parameters. The optimal volumetric growth equation can be solved for an optimal DBH growth increment as a function of DBH. All of the following parameters impact this equation: *HMAX*, *DMAX*, *G*, b_2, b_3, and *Hc*. The graphs show examples of the different optimal growth equations that result when one of these parameters is changed and the others are held fixed. *Top-left: DMAX* is changed and the other parameters are fixed. Under the assumption that the other parameters are correct, all three of these curves have a *G* value that properly fits them to the data. *Top-right: HMAX* is changed, and subsequently b_2 and b_3 change since these regression coefficients depend in part on *HMAX*; the other three parameters are fixed. Under the assumption that the other parameters are correct, all three curves are properly fitted to the data. *Bottom-left*: *G* is changed. *Bottom-right*: *Hc* is changed. For both of these bottom two sets of graphs, the only properly fitted curves for these data are the ones resulting from the *G*=2600, *Hc*=0.7 parameter pair. From these curves, it is clear how the effect of *G* and *Hc* overlap.

The data used in the examples in Figure 5.19 were of blackjack oak. Note that the growth curve continued past the maximum diameter parameter. It was apparent from the bottom two graphs how much the roles of *Hc* and *G* overlapped, which is why *Hc* was held fixed for all species and *G* was used alone to differentiate the growth rates

of species. Leaf area allometry for now was assumed the same for all species. It was notable that all three of the *Hc* values used in the curves were likely too large for blackjack oak. Blackjack oak was not measured for *Hc*, but of the three species that were measured, the largest median value was 0.46 and the median value for post oak was 0.29. However, the decision had been made to set the *Hc* value to be the same for all species, and that value was set to an old FACET holdover value of 0.7. The origins of the *Hc* value of 0.7 may have come from species growing in the Pacific Northwest, but that was speculative.

The best way to measure for *G* might be to install dendrometer bands on trees across a range of different sizes and record their annual diameter growth over a period of years. A dendrometer band actually measures changes in the perimeter of the trunk, which is after all how diameter is measured. This method requires quite a lot of investment in both materials and time, and dendrometer band data were not available for any of the Greenbelt candidate species. A set of dendrometer data for *Fagus grandifolia*, or American beach, that was collected in East Texas by a team of researchers from Rice University was available (Paul Harcombe, personal communication). This dataset, while not used directly in this research, was extremely helpful as a reference and guide to this approach of estimating *G*. Two alternatives to dendrometer bands are measuring growth rings from cores removed with an increment borer and measuring them from cross sections cut from trunks. Both methods have associated problems and costs. Coring trees is difficult work, and the increment borers are expensive and can break or become stuck, especially in certain tough-wooded species. The quality of the core depends a little on luck. Trees can have very

asymmetrical radial growth. For the purpose of *G* estimation, which requires finding examples of optimal growth, cores that contain relatively small rings are of no value.

Estimating *G* requires measurements of the diameter increments together with the diameters at which that grow occurred. In order to determine a diameter, the core must reach all the way to the center of the tree. Some trees are too large for the increment borer to reach the center, and the center can be missed for asymmetrical trees. Even with symmetrical trees, the borer can miss the center if it is not started in just the right spot and direction. Another problem can be trees with heart rot, a common condition in species like blackjack oak. A work around for some of these problems is to measure the DBH around the outside with DBH tape, measure the growth rings in the core starting from the outside, and subtract from the DBH to estimate the previous year's DBH. There is not really a good work around for radial asymmetry other than to guess an outside spot on the trunk that will yield rings closest to the average growth of the tree.

There is of course some variation in the size of growth rings between any two cores from the same tree. In some species, there can be a lot of variation. Asymmetric trees can have rings that are twice as wide in one part of the trunk as they are in another. A way to minimize problems with the variation in growth rings is to remove four orthogonal cores and then calculate average growth ring widths across the four cores. This also helps to reduce problems of missing and false rings since there is access to the growth rings from multiple parts of the trunk, but it also greatly increases the labor involved for each tree.

In general dendrochronology practice, two cores are typically removed. After a core is removed it must be mounted, sanded, and scanned or photographed with a high-resolution device before the growth rings can be measured. Sometimes a core removed from a tree, once sanded and mounted, will prove to be of little value because of asymmetries, rot, insect damage, or it is simply too difficult to distinguish or measure the rings. Standard procedure in dendrochronology requires that the cores are crossdated, which is the procedure where cores from different trees and from different locations are compared, and the growth rings produced during different years are matched by their relative widths. This procedure assures the correct year assignment for each ring, and without crossdating, matching of growth rings to years cannot be trusted. For estimating *G*, crossdating is not so important. The year that any ring is produced is not needed to estimate *G*, rather only the diameter and the ring width. Crossdating would still be useful to help avoid counting false or double rings or missing very small or faint rings, but it is not necessary. Measuring false or double rings would result in the error that a single year's growth would be measured as two, which would impact *G* by underestimating its value. However, with a sufficiently large dataset, a few such double ring errors would likely be negated by other large growth rings measured correctly. Missing a small ring likely will not impact *G* estimation since the small rings are not going to contribute to the optimal growth parameter. The biggest risk of error to *G* by not crossdating the growth rings comes in with certain species that have very indistinguishable growth rings where multiple years of good growth might mistakenly be counted as a single year. Cottonwood is a good example of such a species. It is a rapid grower and puts on large annual growth rings under most conditions. Thus, the lines

distinguishing the annual rings can be very difficult to see. Extra care and high magnification must be used when measuring cottonwood growth rings.

The biggest problem with using cross sections is that a tree must be cut down to reveal the cross section, an activity that was strictly prohibited for the purpose of this study. Cross sections from trees that had been cut down for other reasons were used. The advantages of using cross section are that each growth ring is fully viewed, any asymmetries are revealed, and with the full rings visible, it is easier to identify false or missing rings. Dendrochronologists typically measure tree growth using tree cores from increment borers. Some public dendrochronology databases are available with the International Tree-Ring Data Bank (ITRDB), managed by the National Oceanic and Atmospheric Administration's National Climatic Data Center, being the most extensive (National Climate Data Center [NCDC], 2015). Post oak happens to be a species favored by dendrochronologists, and a number of post oak datasets are available from the ITRDB, including ones collected from North Texas and Oklahoma. Most of the Greenbelt candidate species, however, were not represented in the ITRDB. Some datasets of bur oak and one of eastern cottonwood were available, but these were primarily taken from the northwestern part of their range (e.g., in South Dakota), and it was questionable how similar the growth patterns were from such climatically different parts of the species' range. The most relevant dataset available was from a set of green ash cores that were collected, processed, measured, and crossdated by Komperod (2009) from trees growing within the Greenbelt bottomland. Green ash tended to grow symmetrically, had rings that were relatively easy to see, and happened to be a good species for coring. Post oak and green ash were the two most important upland and

bottomland species, respectively, of all the Greenbelt FACETA candidates. Additionally, these two species almost represented opposite ends of the growth rate spectrum of the candidate species. The only candidate species considered a slower grower than post oak was blackjack oak, and by some accounts possibly winged elm. Only two candidate species, black willow and cottonwood, grew distinctly faster than green ash. The growth rate of boxelder may also have exceeded that of green ash. Between the Greenbelt green ash core data and the publicly available post oak data, increment borer cores were a reliable starting point for estimating *G*.

Before estimating *G* for any of the candidate species, it was useful to characterize their growth rates more qualitatively. The same forestry, ecology, and botany sources were referenced as with the maximum growth parameters. Not all of these sources consistently discussed growth rates for each species. The USDA (2014b) PLANTS database ranked growth rate qualitatively as slow, moderate, or rapid. This kind of information was useful only to the degree that it could help with relative rankings of growth rates between the species; it could not help estimate the number. The Silvics Manual from the USFS (USDA, 2014a) was consistent in providing some growth rate information for each of the species described in the manual, and often it even included quantitative rate information. Unfortunately, the way growth rate was described, it was not always consistent between species. Some species were only described qualitatively, while some were described by annual growth in height, some by average annual DBH growth, and some by average height or DBH achieved after a certain number of years. Some species with commercially important wood may have had stand-level productivity quantified (e.g., volume of wood per acre), but FACETA requires

individual growth rates. Growth rates were rarely described quantitatively in a way that was easily transferable to FACETA parameterization. The older version of the USFS Climate Change Tree Atlas (Burns & Honkala, 1990), which featured ecological information on 80 different North American tree species, had tables available for each of the species displaying quartiles of growth rate measured across many plots. The growth rates were given in units of square centimeters per year. One obvious interpretation was that these growth rates were of basal areas of individual trees, and if that interpretation were correct, then the data could actually be directly interpreted to estimate a growth rate parameter. That interpretation, however, was not believed to be correct, as the numbers seem too large. Unfortunately, the tables were not accompanied by an explanation. They also seemed to have disappeared from the new version of the Climate Change Tree Atlas, although they still exist as files that can be downloaded from the USFS website. Even with the uncertainty of the interpretation of these data, they were still included for consideration of growth rates because the numbers were still possibly valuable in interpreting relative differences between the species. Table 5.5 summarizes some of the growth rate information from these three sources.

Table 5.5

Growth Rate Information for Greenbelt FACETA Trees

Species	USDA PLANTS Database	USFS Silvics Manual	USFS Climate Change Tree Atlas – Diameter Growth (cm^2/yr)		
			Mdn	Max	Rank (of 80)
Populus deltoides	Rapid	• Fastest growing commercial species • On one site DBH averaged 29 cm by 5 years	54.1	400.4	1

(table continues)

Table 5.5 *(continued)*

Species	USDA PLANTS Database	USFS Silvics Manual	USFS Climate Change Tree Atlas – Diameter Growth (cm^2/yr) Species		
			Mdn	Max	Rank (of 80)
Salix nigra	Rapid	• In natural stands in Mississippi Valley after 10 years trees average 15 m tall and 14 cm DBH • After 40 years they averaged 31 m tall and 49 cm DBH	34.8	491.6	4
Fraxinus pennsylvanica	Rapid	• DBH averaged 20-30 cm after 21 years	16.8	275.7	30
Acer negundo	Rapid	• Rapid growth in first 15 to 20 years, up to 2.5 cm DBH/year • On poor sites DBH growth of 5 mm/year	19.0	232.8	24
Celtis laevigata	Moderate	• Moderate to fast growth • Average 10 year DBH growth greater than 6 cm	20.7	203.8	29
Ulmus americana	Rapid	• Poor on droughty sands • Medium on wetter sites and good on well-drained flats in first bottoms	16.3	317.0	32
Morus rubra	Moderate	• Rapid growing • Very little is known about growth and development	n/a	n/a	n/a
Ulmus crassifolia	Rapid	• Grows rapidly • "The annual growth rings are very indistinct. Thus there may be considerable error in estimating the average annual growth rate."	n/a	n/a	n/a
Carya illinoinensis	Slow	• DBH growth over 10 years ranges from 5-7 cm	n/a	n/a	n/a
Forestiera acuminata	Moderate	n/a	n/a	n/a	n/a
Quercus macrocarpa	Slow	• Slow growing • Annual DBH growth less than 2.5 to 6.4 mm/yr in Iowa upland sites • In better site in Kansas DBH growth averaged 2.5 cm in 3.8 years	15.1	516.0	38
Ulmus alata	Moderate	• Diameter growth in natural stands averaged 50-64 mm in 10 years	6.6	222.5	70

(table continues)

Table 5.5 *(continued)*

Species	USDA PLANTS Database	USFS Silvics Manual	USFS Climate Change Tree Atlas – Diameter Growth (cm^2/yr) Species		
			Mdn	Max	Rank (of 80)
Quercus stellata	Slow	• Slow growing • Diameter growth doubled after thinning	11.9	188.5	51
Quercus marilandica	Slow	n/a	9.2	100.3	63

Note: Greenbelt FACETA candidate species growth rates were characterized both qualitatively and quantitatively in various forestry and botanical references. Growth rate characterizations from three of these references are included in the table. The species are listed in order assumed for FACETA of highest growth rate to lowest growth rate.

Green ash.

The estimation of the growth rate parameter *G* for the different candidate species is discussed in the same order the problem was approached; thus, the order of the species is not alphabetic or linked to the magnitude of the growth rate or necessarily the importance of the species. The most relevant and reliable dataset available was from the increment borer cores of green ash growing in the Greenbelt, which made green ash a good species to start with. Before estimating *G*, the parameters *DMAX*, *HMAX*, and its corresponding allometric coefficients needed to be set. Green ash's parameter value for *HMAX* was not in dispute. While the range of maximum heights cited in Table 5.3 was large, the local data and two good references had maximum heights centered around 40 m, which fit the pattern of the local height/DBH data well. The value of *DMAX* for green ash was a little less clear and may need to be adjusted with *G*. The cores used for this analysis had already been processed, measured, and crossdated, and the growth ring measurements were arranged in the standard data format used by dendrochronology software. The data were reformatted and imported into a

spreadsheet, after which the annual growth increments were added together to calculate diameters. The diameter increments were plotted as pairs with the diameter. The data included 62 cores taken from 31 trees located in two different plots within the Greenbelt. This process revealed the first potential problem with using dendrochronology data.

The two quantities needed for *G* estimation are the diameter and the diameter increment. In dendrochronology, two important things are the radial growth increment and the year in which it occurred. While possibly measured by the dendrochronologists when coring the tree, the outer DBH of the tree was not indicated anywhere in the standard format used in the analysis or dissemination of the data. Likewise, the data did not indicate which cores, if any, did not make it to the center of the tree. Additionally, the data did not indicate whether center rings were excluded because they were too indistinct to measure or because the center of the tree was rotted out. Sometimes parts of a core may be excluded because of problems with crossdating, and the data from the reliable part of the core are reported by themselves, but this was not indicated in the disseminated data.

The files were laid out to give the history of growth going back in time, one yearly radial increment at a time. If it was known a core reached the tree's center and all the rings were included in the measurements, then the data in the file could be flipped or transposed to give the growth history going forward in time. The radial increments could then be doubled to yield diameter increments and added together one year at a time to yield a progression of the tree's diameter and new diameter growth over time. Without knowing whether the core reached the center, annual diameter growth increments could

still be calculated and increments added to yield what might be interpreted as diameters. However, if the center part of the tree's growth rings was missing, then the calculated diameter total was too low. If this happened in the estimation of *G,* it essentially caused a shift to the left towards smaller diameters of the diameter growth increment data, and it may have resulted in causing an overestimation of *G* (Fig. 5.20).

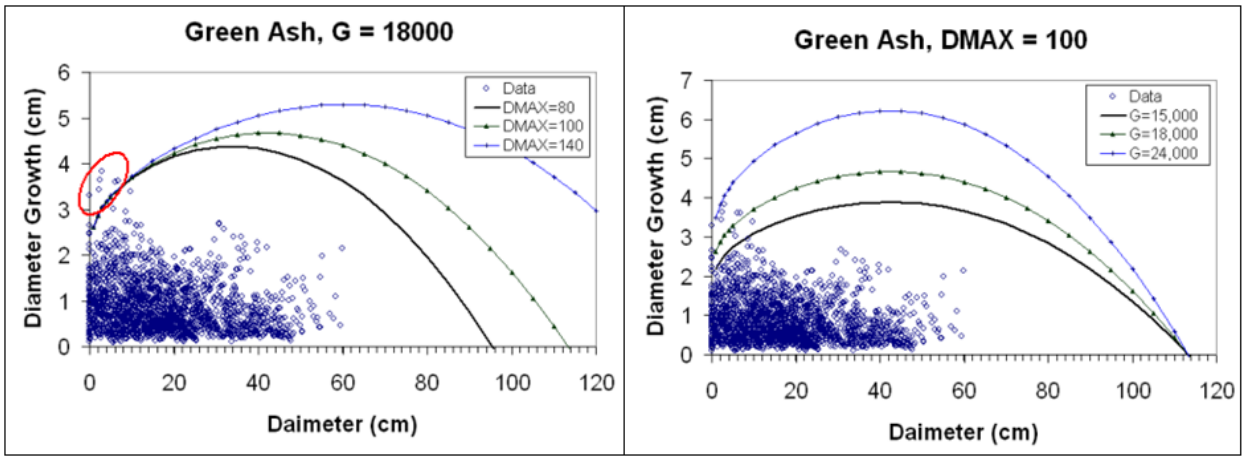

Figure 5.20. Green ash *G* estimation. The green ash growth data were measured from tree cores collected with increment borers from within the Greenbelt (Komperod, 2009). The data included 62 cores taken from 31 trees. *Left*: Growth equation with different possible values of *DMAX*, ranging from 80 cm to 140 cm. *G* was set to 18,000 cm^3/m^2. Before seeing the impact of *DMAX* on the growth equation, the assumption was to set *DMAX* to 140 cm, but *DMAX* of 80 cm yielded a better fitting growth curve for this data. The data points at the top-left (circled) were not included under any of the curves. Some of these large measured increment growths occurring on trees with apparently very small DBH may have come from a core without the center of the trunk included. If so, that would have caused these points to shift left. *Right*: *DMAX* was fixed at 100 cm, and *G* ranged from 15,000 to 24,000 cm^3/m^2. In order to include all points under the curve, *G* had to be set as high as 24,000, but G=15,000 yielded a curve that included the vast majority of data points and looked generally to fit this data better.

After adding the diameter increments and arranging the data as diameter/diameter increment pairs, the data were plotted on a graph together with the optimal growth equation. In order to fit *G* to the data, it was assumed all other parameters had been estimated and set. The value of *G* was then increased or decreased until the data points were all under the growth equation curve. The green ash growth curves used three different *DMAX* values: 80 cm, 100 cm, and 140 cm (Fig. 5.20). Before seeing how *DMAX* impacted the growth equation, the assumption was to

set *DMAX* to 140 cm, a value that was smaller than the largest value cited in Table 5.3. One green ash in the Greenbelt dataset measured 100 cm DBH. The philosophy behind the maximum growth parameters was to use true maximums. However, *DMAX* of 80 cm yielded the better fitting growth curve for this data, which raised the question of whether the data represented optimal growth. This green ash data came from two plots of green ash trees growing in relatively close proximity. The data did not indicate any trees larger than 60 cm in diameter. It was likely there were examples of faster growth than what was captured in this dataset. One thing that was unclear about this method was whether *all* of the data points should be under the curve or just the majority. In the green ash data, few points with high diameter increments occurred at small DBH values and were not under all of the growth curves (circled area in Fig. 5.20). Since these points were so high and up against the y-axis, *G* would have to be increased to approximately 24,000 cm^3/m^2 to include them under the curve, which would have resulted in an unrealistically high curve. Additionally, it was possible these high diameter increment data points were not located at the correct DBH coordinate due to errors made when estimating DBH from an incomplete core. It was not known how many cores in this dataset were incomplete, but it was known there were some. Given that, including those few points was not necessary or even appropriate. Between this curve fitting exercise, the allometric regression, and the locally collected data, the starting point for green ash growth parameters were *G*=18000, *HMAX*=40, and *DMAX*=100. However, it is possible this estimate for *G* was inflated from calculating diameters on incomplete cores.

Post oak.

Through the ITRDB, post oak was another species for which a relatively large set of tree core data was available to this study. Many of the post oak tree cores in the data bank were collected in the same North Texas region as the Greenbelt study area. After graphing the post oak core data, the same issue became even more apparent. That is, some cores included in the G estimation process were likely incomplete at the center, resulting in calculated total diameters that are smaller than the trees' actual diameters (Fig. 5.21). It was unlikely that any of the post oaks from this tree core dataset grew more than 0.5 cm of diameter in their first year.

Another issue with using dendrochronology data for *G* estimation became apparent after adding the growth ring data from another post oak tree to the dataset, a tree grown on a residential property that had recently been cut down. Dendrochronologists are not particularly interested in optimal growth. In fact, the standard approach in dendrochronology is to sample from sites that will maximize the signal of whatever stressor is being investigated (e.g., water stress). In other words, sites are selected by their nature, not by environments that produce optimal growth; thus, the growth rings typically reflect some environmental stressor. The nature of estimating *G* requires finding examples of a species' optimal growth potential, which means finding samples growing on sites with conditions offering minimal stress and abundant resources.

The core data used from the ITRDB contained 36 cores taken from 31 trees growing near Fort Worth, TX (Stahle & Edmondson, 2014). When the data were graphed with the growth equation (Fig. 5.21), even small values of *G* dwarfed most of

the data, and the only thing that forced *G* to be increased was the data points with high diameter increments occurring at small diameters (i.e., those same data points were likely shifted to the left). The data from the one post oak growing on a residential property looked much different. For convenience, because it had been growing in a subdivision called Live Oak, it was referred to as "LO1." The general growth pattern of LO1 included much larger growth increments than the tree core data, and there was a very distinctive pattern of increasing growth rates followed by decreasing rates after a peak. With the exception of the growth increments in the smallest diameter range, the data from this one tree made a greater impact on *G* than all tree cores combined.

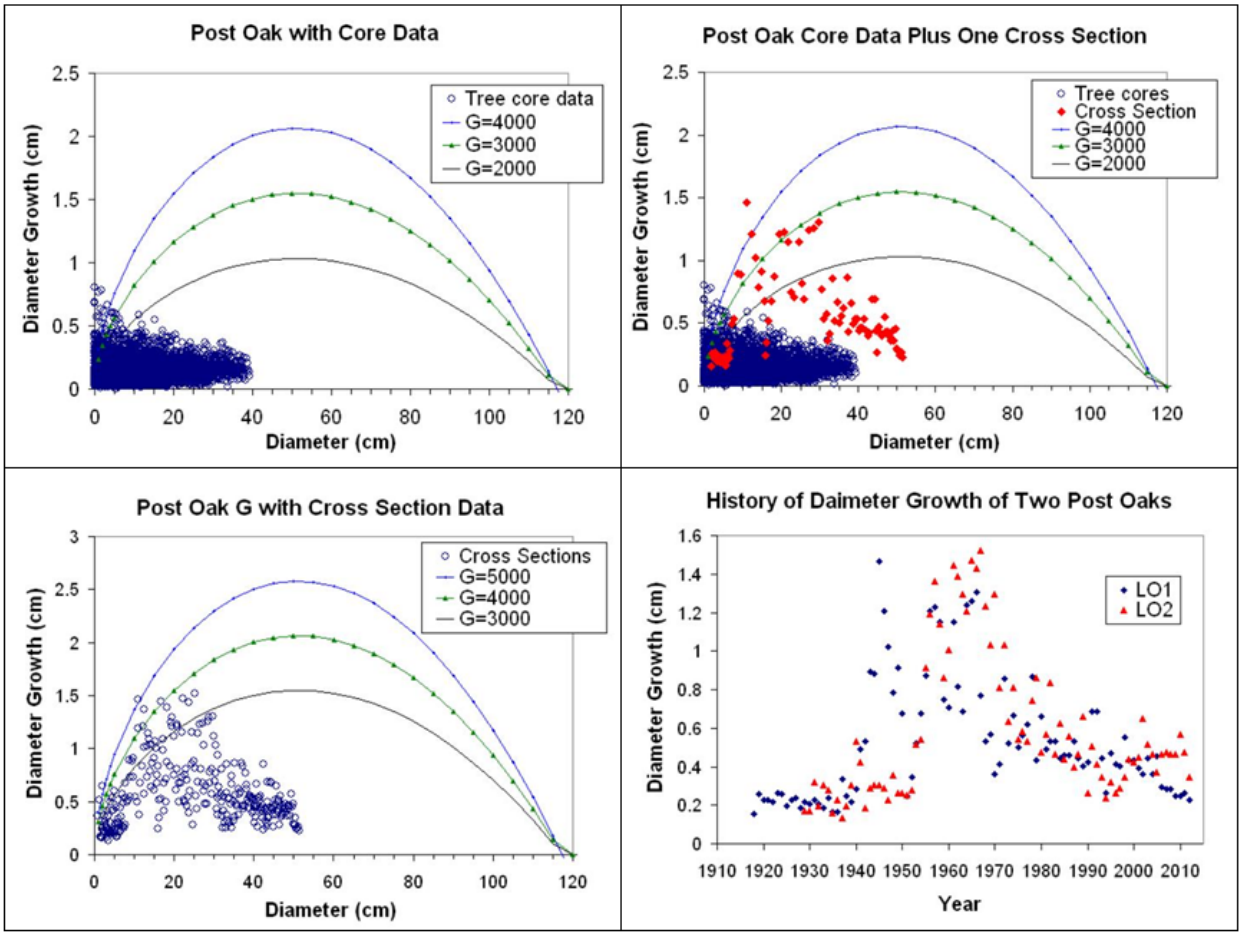

Figure 5.21. Post oak *G* estimation. Post oak *G* estimation was done with data taken from increment borer tree cores and from tree trunk cross sections. The other parameters in the growth equations were *HMAX*=18 m and *DMAX*=100 cm. The tree cores were taken from natural settings of the Cross Timbers

ecoregion for dendrochronological analysis, and they were most likely from a dry rocky hill and in relatively dense woodland. The measurements from the cross sections came from only four trees that probably started their lives in natural settings of the Cross Timbers ecoregion, but then spent the last several decades growing in a residential neighborhood. The time series of growth of two of these cross sections indicated the impact that development of the neighborhood had on the trees' growth. *Top-left*: *G* estimation using only tree cores. The total number of cores was 36 coming from 31 trees. *Top-right*: Adding data from one cross section greatly changed the appropriate value of *G*. *Bottom-left*: *G* estimation with four cross sections. *Bottom-right*: Time series of diameter growth from that same cross section plus another one that grew close by. Around 1940, the growth rate of both trees increased. The years are approximate since the samples were not crossdated.

Approximately one year after measuring LO1, another large post oak growing in the same neighborhood became available for measurement. This tree, referred to as LO2, was blown over in a storm. After measuring its growth rings, a remarkably similar pattern of growth to LO1 was discovered (Fig. 5.21). Eight post oak cross sections were collected for growth ring measurement, all which had been growing in residential neighborhoods. Of those eight, only four were used to estimate *G*, as the growth rings on the other four were too small to contribute to the estimation of the optimal growth rate. In this case, too small simply meant they were generally smaller than the growth rings on the other four cross sections. As a result of the *G* and allometry analysis, the starting points for post oak growth model parameters were *G*=5000, *HMAX*=18, and *DMAX*=100.

Because of the discovery of this particular post oak cross section and the impact it had on the estimation of *G*, it was realized that random selection was not the best approach for measuring the optimal growth rate parameter. Since *G* is supposed to reflect optimal growth, it should be estimated from samples that have grown in as optimal of conditions as possible. Residential properties often offer conditions better than in the natural forest, at least for the upland forests and species like post oak, so collecting felled tree trunks from residential curbsides became a new strategy for *G* measurements. With an increasing collection of cross sections, some of the advantages

of using them over tree cores became more apparent. Ultimately, it was not possible to collect cross sections for all of the Greenbelt FACETA species. Some species, such as black willow, swamp privet, red mulberry, and even green ash, do not commonly grow in people's yards or in city parks, and conveniently finding a felled log of one of these species is a matter of luck.

Post oaks LO1 and LO2 presented an incredibly interesting example of growth history that needed to be investigated a little further. The backstory of LO1 was that it was growing in a residential neighborhood, and it was cut down during the winter of 2012-2013. There were two surprising facts about this tree. It was much younger than its size might have implied. The DBH measured a little over 54 cm, quite large for post oak, and a post oak of this size could easily be over 200 years old. However, this tree was only around 100 years old when it was cut down. The second surprising fact was the incredible increase in the growth rate that occurred right about 1940. A few growth rings on the very inside of the trunk were not counted or measured because they were very difficult to discern. Growth ring measurement started on approximately the 10th growth ring. For the first 25 measured growth rings, the diameter increments averaged 2.2 mm, and none exceeded 3 mm (growth period A in Fig. 5.22). The growth over the next 50 years was very robust (growth period B) with an average diameter increment of 7.2 mm. The highest diameter growth increment of nearly 15 mm occurred in the mid-1940s. By the 1990s, the diameter growth increments slowed down again, averaging about 3.6 mm during approximately the tree's last 20 years (growth period C). The neighborhood, house, and block the tree came from was probably developed sometime

between the late 1950s and early 1960s, making the growth spurt starting in 1940 even more interesting.

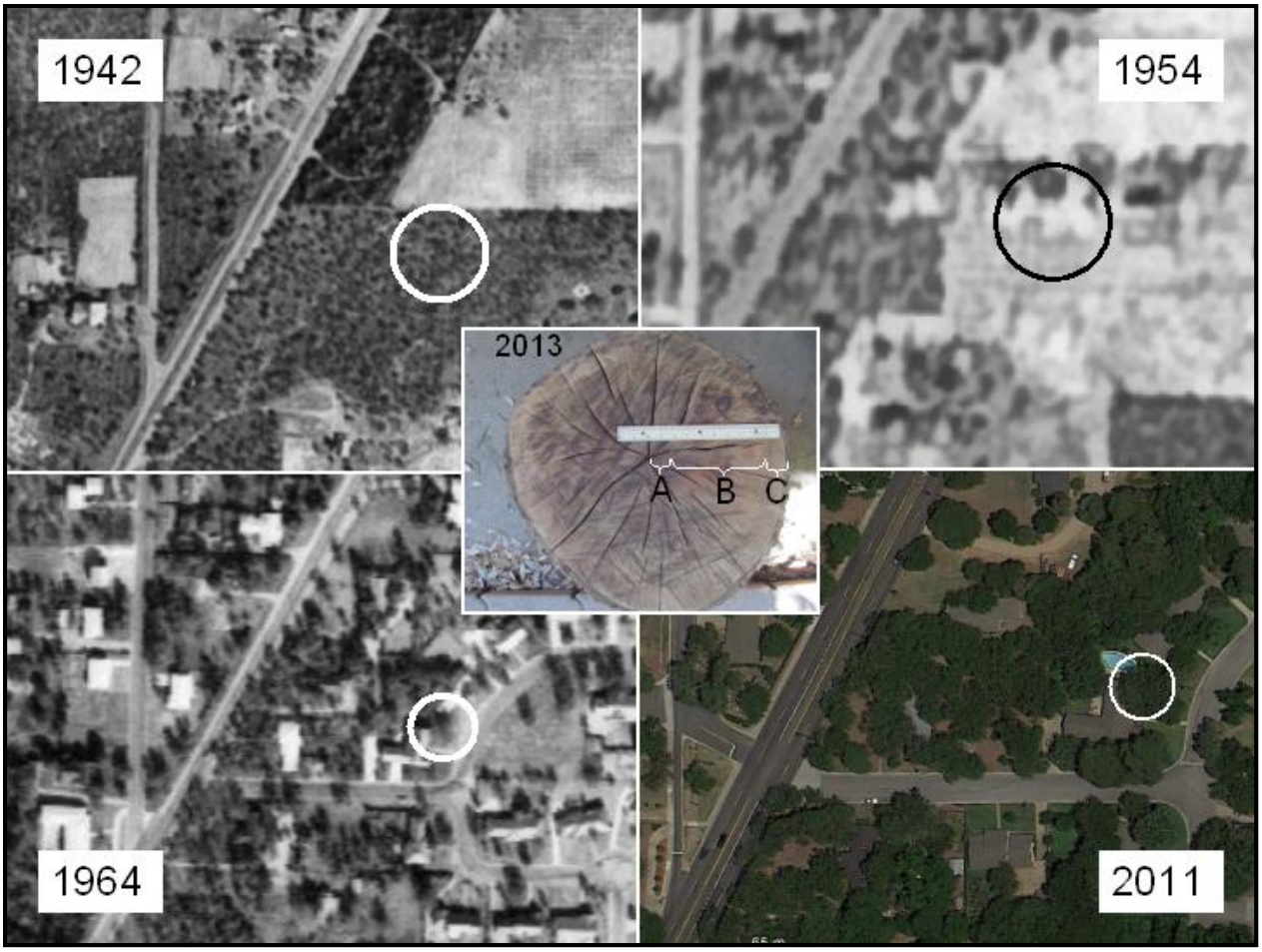

Figure 5.22. One post oak's history. History of the 100-year-old post oak, LO1. *Top-left*: In 1942, the area around LO1 had been recently thinned. *Top-right*: By 1954, the area had been cleared for development. *Bottom-left*: By 1964, the neighborhood had been built. *Bottom-right*: By 2011, LO1 was approximately 100 years old and apparently growing too close to the house. *Center*: A cross section of LO1. The ruler in the image for size perspective is a standard 12 inch/30 cm ruler. The labels A, B, and C indicate the three periods of different growth rates – slow, rapid, slow – in LO1's history.

After a little investigation of some historical aerial photos, a likely explanation was found (Fig. 5.22). The land this neighborhood sits on contained some of the last remaining larger tracks of the upland Cross Timber post oak forest within the city of Denton before the neighborhood was developed. There was some agriculture within the area, but much of the land was largely unsuitable for crops because of the extremely

sandy soil found through much of the area, which was probably why the tracks of forest remained. The sandy soil in this area was the most likely explanation for an early nickname given to the neighborhood after it was developed: “Idiot’s Hill.” While the house where this tree was growing was not built until around 1960, development related activities might have started much earlier. In an aerial photograph from 1942, it seemed clear that the area this tree was growing in had been recently thinned of trees. The location of LO1 is inside the circle on the image. From the wider view provided by the full aerial photograph (Fig. 5.22 only shows a zoomed-in shot of the tree’s immediate surroundings), it can be seen that many of the forested patches are darker and thicker looking, like the patch growing along the road on the north (top) side of the image. In comparison, the patch with the circled tree is much thinner. It is not possible to know from the image when the thinning occurred, but within a few years after such a thinning, the remaining trees should have spread and filled out more to give a thicker appearance again. At the time of the 1942 image, LO1 had a DBH of approximately 9 cm. By 1954, most of the other trees from the thinned patch had also been removed, and a number of tracks of land had been cleared completely for streets and blocks of houses to go up. The resolution of the 1954 image is unfortunately poor, but LO1 is still visible in a little cluster of about four other oak trees. At this point, LO1 had grown to a DBH of approximately 18 cm. By 1964, the house had been built, and LO1 was now part of someone’s yard. It was likely that LO1 started receiving extra water from lawn irrigation once the house was built. By 1964, the DBH had reached 28 cm.

The proposed hypothesis for the cause of LO1’s growth spurt was the reduced competition, with the primary factor being the additional light it received after the

surrounding trees were removed. If this hypothesis were correct, then it would be an indication of just how strong of a limiting factor light is for post oak. The reduced competition for water is undoubtedly also a factor. Another important question raised by LO1's growth history is what caused the growth rate to decline. One possible answer is that the tree was following the exact kind of growth trajectory that is assumed by the FACETA growth equation, which is that after reaching a certain size the tree's energy primarily goes into maintenance, and growth rate slows down. Another possible explanation also has to do with light. Four tall pine trees were planted after development of the neighborhood that grew just to the south and southwest of the LO1. These pine trees can be seen in the 2011 image, clearly taller than the post oak. It is not known how the pine trees' growth correlated to the post oak's growth decline, but certainly by 2011 they would have blocked much of the direct sunlight from the post oak.

The growth history of LO2 is remarkably similar to LO1. LO2 was uprooted during a strong storm, and it revealed a root system that had mostly rotted away. This raises a third possible explanation to the decline in growth rate – root rot from too much lawn watering. From the graph in Figure 5-21 it appears that LO2's growth trajectory lags a little behind LO1's. This may be a real lag, or it is also possible that ring counting errors are a factor. The outer growth rings of LO2 were very difficult to see, and it is possible some were missed which would underestimate the tree's age. Crossdating on the growth rings of the two trees was also not done.

Blackjack oak.

Only cross sections were collected for blackjack oak, and this species ended up with the largest collection of cross sections with approximately 15. Of those, nine were

measured and included in the estimation of *G* (Fig. 5.23). The growth rings on the samples collected but not included were too small to change the *G* estimation and were discarded. Blackjack oak growth rings tend to be easy to distinguish and are relatively easy to measure, at least when they are not too small. Some of the samples that were not used had rings that were very small and more difficult to distinguish. Blackjack oak is one of, if not the slowest growing tree species from the candidate list, so getting a good estimate for its *G* helped provide a lower bound for estimates on the growth parameters for the other species. Between the allometric regression and *G* estimation, the starting values for blackjack oak model parameters were *G*=2600, *HMAX*=18, and *DMAX*=100.

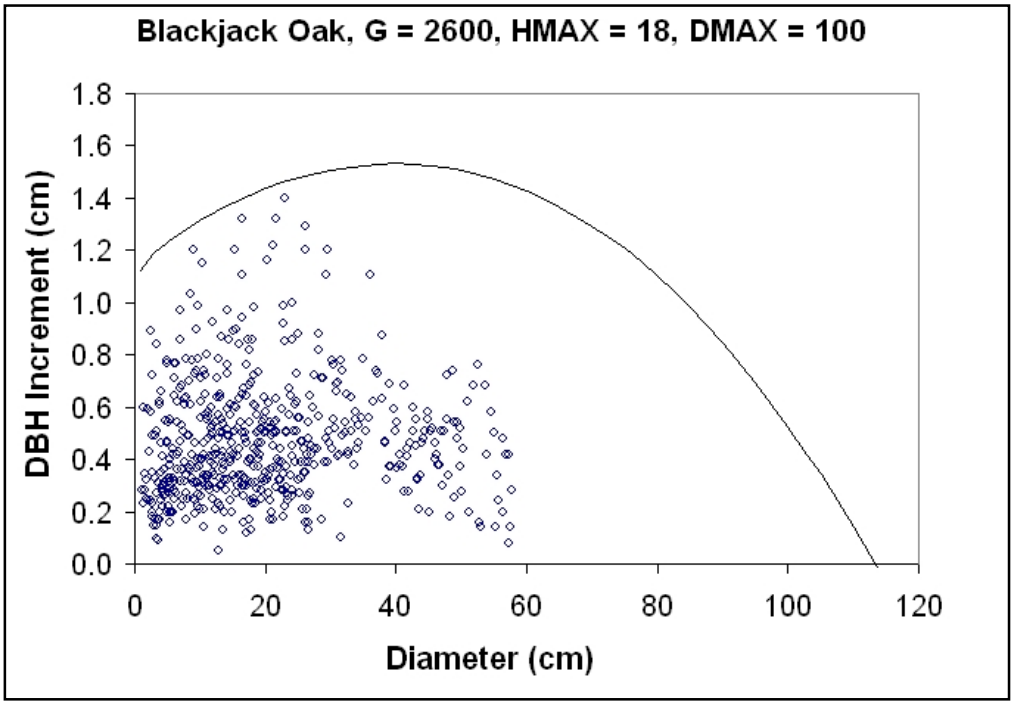

Figure 5.23. Blackjack oak *G* estimation. *G* for blackjack oak was estimated from growth rings on nine cross sections of trees that had been growing in residential properties.

Sugarberry.

Thirteen cross sections of sugarberry were examined for *G* estimation, but almost half had small growth rings, and only seven were measured and included in the analysis (Fig. 5.24). This dataset was likely not representative of sugarberry growth as all the samples collected were growing in upland positions, albeit in residential neighborhoods. Many of the largest sugarberry trees in the study area were found in the Greenbelt bottomland. Similar to blackjack oak, sugarberry growth rings tend to be easy to distinguish unless they are too small and become more difficult to see. Starting parameter values for sugarberry were *G*=11000, *HMAX*=30, and *DMAX*=100.

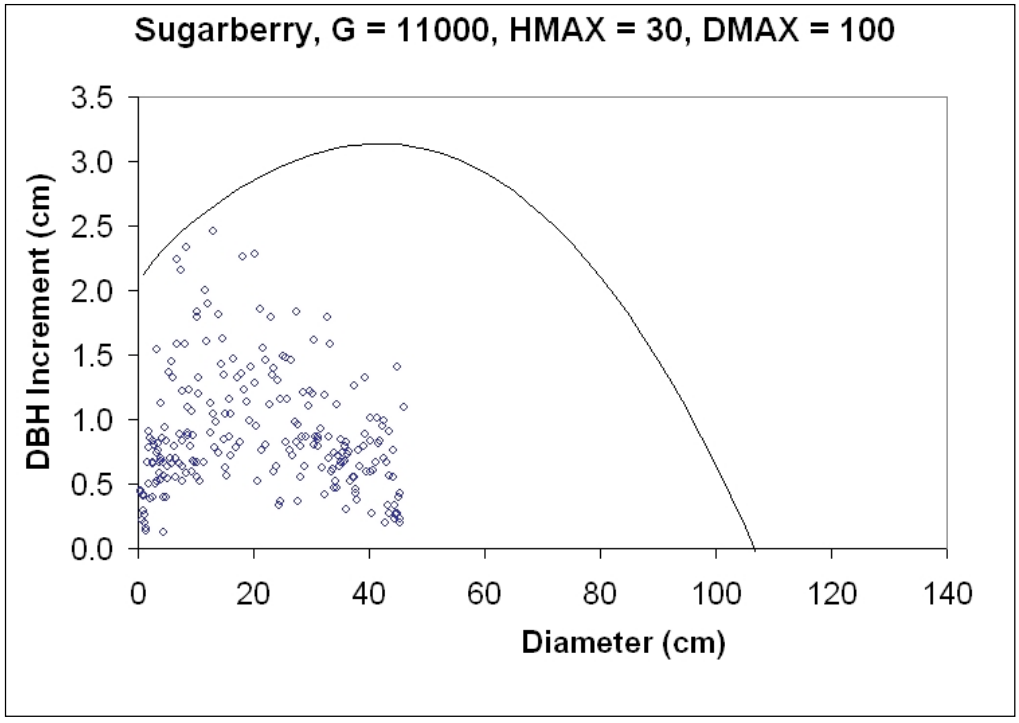

Figure 5.24. Sugarberry *G* estimation. *G* for sugarberry was estimated from growth rings on seven cross sections of trees. All of the samples came from topographically upland positions, albeit on residential properties.

Cottonwood.

Cottonwood ended up with a small sample of four cross sections, all of which grew on residential properties in topographically upland positions. Even with the small sample size, the *G* estimate still ended up larger then the next largest sample set discussed yet, green ash. However, given that the green ash data set contained 30 trees, the *G* value for cottonwood was likely underestimated and would be improved with a better dataset. Cottonwood growth rings, while large, can also be very hard to distinguish. Measuring these samples took a great amount of care and high magnification, and having the full cross section available to view was very helpful. Initial parameter values for cottonwood were *G*=25000, *HMAX*=50, and *DMAX*=160.

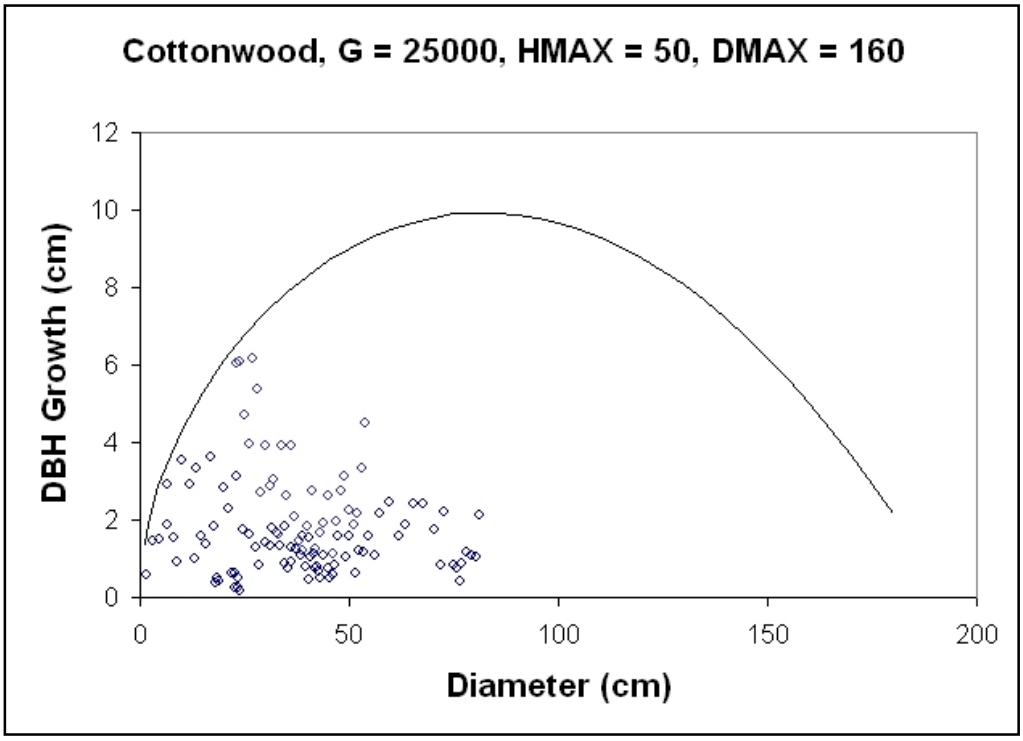

Figure 5.25. Cottonwood *G* estimation. Only four cottonwood cross section samples were included in the specie's *G* estimation. All of the samples came from residential properties located in topographically upland positions.

American elm and boxelder.

These two species ended up with micro sample sizes of one cross section each. While one data point is better than zero, unless that tree exhibits robust growth rates, the only value the one data point brings to the estimation of *G* is to provide a lower limit of values. Both of these trees had been growing in upland residential sites before being cut down. The boxelder exhibited very rapid growth; in 16 years, it grew to a DBH of approximately 25 cm. Even with a sample size of one boxelder, *G* estimate was a plausible value in that it fit roughly in with the sugarberry growth rate. According to some of the silvical information available on boxelder, it grows rapidly when it is young but then slows down considerably. It would be helpful to obtain samples from older boxelder trees to see how well their growth pattern fit FACETA assumptions. The *G* estimate for the American elm was too low. American elm is known to have poor growth rates on dry sites, and this tree was growing in an upland, sandy soil location.

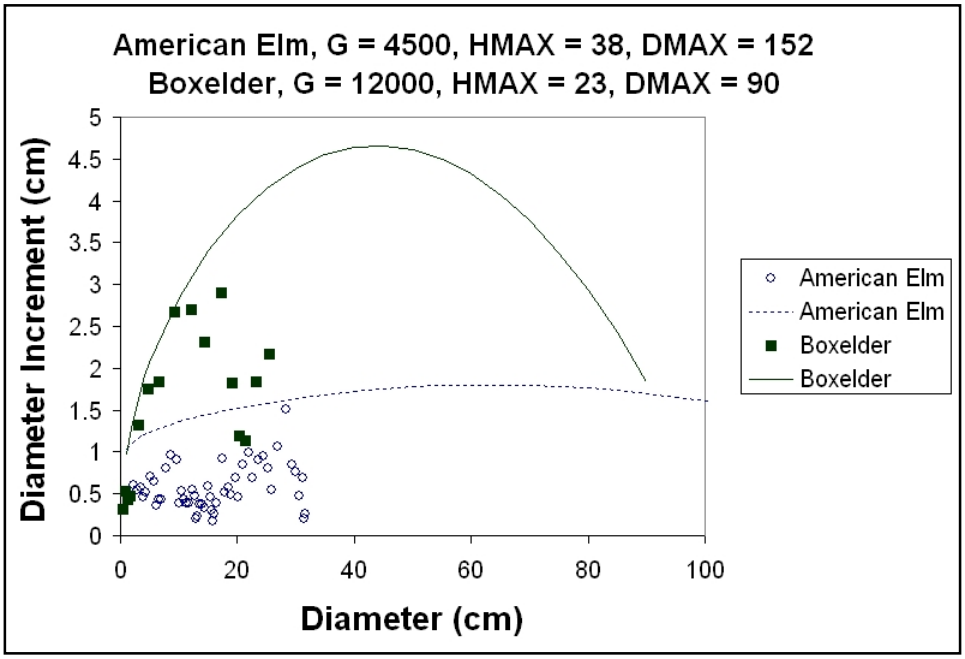

Figure 5.26. American Elm and Boxelder *G* estimation. American elm and boxelder only had one cross section sample each to estimate *G*. The result for boxelder seemed reasonable, but for the American elm, it was too low. This particular tree was growing on a sandy, upland site.

Of these two trees, the rings on the American elm were relatively easy to discern and measure, while the rings on the boxelder were more difficult. The boxelder rings were not as difficult to distinguish as the cottonwood samples, but having the entire cross section was still useful in determining ring boundaries. From this analysis the starting parameter values for American elm were *G*=4500, *HMAX*=38, and *DMAX*=152, and for boxelder they were *G*=12000, *HMAX*=23, and *DMAX*=90. However, by no estimates does American elm grow slower than post oak (*G* = 5000), and the *G* value determined from this one tree was not an acceptable starting FACETA parameter. A *G* value for American elm needs to be estimated by other means.

All Other Species

No growth rings were successfully measured or data obtained for the other candidate species. Some growth ring datasets were available through the ITRDB for two of the candidate species, bur oak and cottonwood (NCDC, 2015). The bur oak data, sampled in South Dakota, had the same problems as the post oak tree core data from the ITRDB in that growth rings were overall small with the exception of some graphing as if they occurred at a DBH of zero. The growth increments were no doubt calculated from data reported from incomplete cores. The dataset was deemed unhelpful for estimating *G*, and the ITRDB cottonwood data was not even examined. More than 10 samples of cedar elm cross sections were collected, but all proved too difficult to measure the rings with enough confidence, and none was used. Cedar elm is notorious for having rings that are difficult to tell apart. Three old stumps of black willow were found, photographed, and growth ring measurements attempted, but they were too deteriorated to measure successfully. The American elm sample that was measured fell

short of providing a reasonable *G* estimate. No samples of mulberry, pecan, swamp privet, or winged elm were obtained. Without data, the best alternative for estimating *G* was to use published sources, the best available qualitative data, and assign values of *G* according to the relative differences in growth rates for the species. Estimates from blackjack oak, post oak, sugarberry, green ash, and cottonwood, going from low to high growth rate, were used as anchor points to rank and assign values to the unknown species. Information used in the ranking and parameter estimation of these species is summarized in Table 5.5. It should be noted that there is a much greater level of uncertainty in the estimates not based on measured growth rings. The results of the growth curves from the *G* estimations are shown in Figure 5.27, and parameter values are given in Table 5.6. As with any model parameters, these initial values will be calibrated and improved with testing. Since all of the growth parameters are mutually sensitive, changes to any one of them may require changing others.

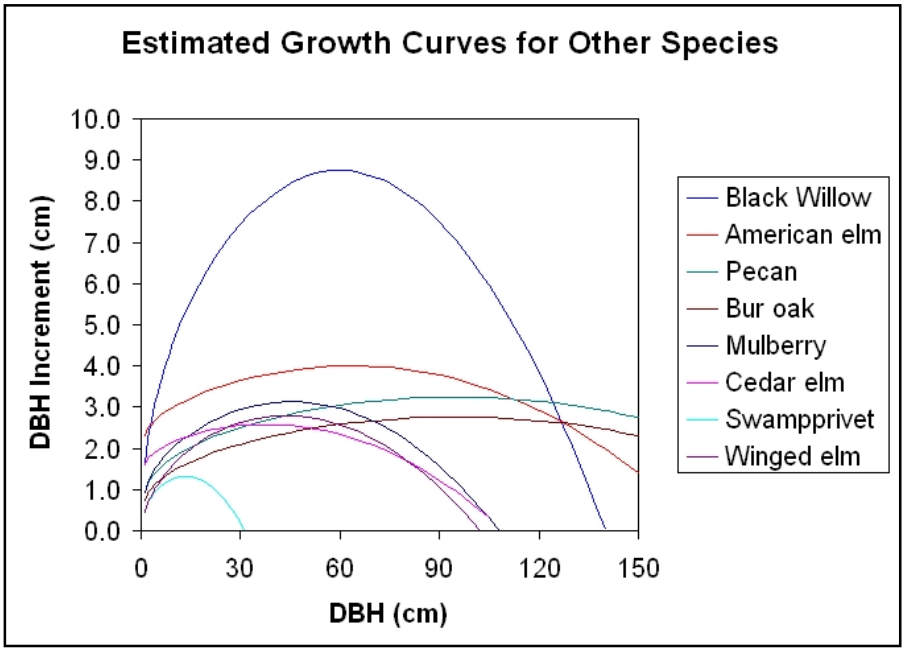

Figure 5.27. G estimation for other species. The growth curves are from the estimated *G* parameters for the candidate tree species for which no useful growth ring data was obtained. These *G* values were estimated based on relative ranking in growth rates between these species and the other species where

G was based on measured growth. There is a large amount of uncertainty in these estimates and for some species, for example swamp privet, the estimate is only a little more than a guess.

Table 5.6

Initial Species Growth Parameter Estimates

Species	Common Name	G	HMAX	DMAX
Populus deltoides	Cottonwood	25000	50	160
Salix nigra	Black willow	21500	30	122
Fraxinus pennsylvanica	Green ash	18000	40	100
Acer negundo	Boxelder	12000	23	90
Celtis laevigata	Sugarberry	11000	30	100
Ulmus americana	American elm	10000	38	152
Morus rubra	Red mulberry	8000	22	100
Ulmus crassifolia	Cedar elm	8000	36	90
Carya illinoinensis	Pecan	7000	43	210
Forestiera acuminata	Swamp privet	6000	14	25
Quercus macrocarpa	Bur oak	6000	40	210
Ulmus alata	Winged elm	5000	20	74
Quercus stellata	Post oak	5000	18	100
Quercus marilandica	Blackjack oak	2600	18	100

Note: The growth parameter estimates for the FACETA candidate tree species. The shaded rows indicate species for which the growth rate parameter *G* is based on tree ring measurements, while those in the unshaded rows are based on relative rankings. The table is listed in the assumed descending order of growth rates. Relative rankings are based on the same information that was used to generate Table 5-5.

To summarize some of the results in estimating values for the optimal growth parameter, while the equation is in units of volume of wood, it can be modified into an equation based in diameter and diameter increments. Between the three different methods of measuring diameter growth, dendrometer data are likely the most accurate because it really is measuring the characteristic that is interpreted as diameter, the circumference. No dendrometer data were available for this study for the candidate species so the other two methods were explored. Measuring growth from tree cores was considered first, but using cross sections was found to be a better method. Advantages of cross sections included being able to see the entire ring, which helped to eliminate errors and avoided measuring in areas with asymmetric growth rings. The

primary disadvantage was that using cross sections required destroying the tree, and this was avoided by only using cross sections taken from felled trees that had been discarded as waste. The main disadvantage of core data was it was not known whether the rings were measured from incomplete cores. When incomplete cores were treated as complete in this procedure for estimating *G*, the parameter value was inflated. There were also numerous difficulties in extracting usable cores. Another useful finding was that individual trees exhibiting rapid growth or that had been growing under good environmental conditions were helpful in estimating *G*. Trees growing on dry rocky slopes or with dense competition probably did not provide examples of optimal growth.

Regeneration: Seeding and Sprouting

Regeneration in FACETA is modeled through a process where a number of new seedlings are determined annually for each species, and then a proportion of these are probabilistically made available for establishment. These potential new recruits are subjected through an environmental filtering process, where the filtering is done as a multiplier determined by conditions of soil moisture, fertility, light, and temperature. If seedlings make it through this filtering, they become trees. There is a species parameter available in FACETA, called SEED, which assigns rank differences between the species. Differences in seeding rates and rates of establishment definitely exist between species, and there is some information available for some species, often qualitative in nature. For example, the USDA (2014b) PLANTS database describes seed abundance in terms of *high* or *low*, and provides descriptions of seedling spread rate, such as *slow*. Other silvics reference sources may provide additional information such as number of seeds per pound, age range at which trees produce seed, or

methods of dispersal, but this information is difficult to convert into a model parameter. Since the SEED parameter is just a ranking, it is possible to use the kinds of qualitative descriptions found in the PLANTS database to rank the different species. However, the focus of this study was modeling site conditions. A value for this parameter was required for each species in the species parameter input file in order to run the model. A switch in the species parameter input file that negates the SEED parameter. With it negated, regardless of the value entered into the input file all species have the same number of expected seedlings in any year. Since each species has its own set of environmental tolerance parameters, annual differences in establishment between species still occurs through the environmental filtering process. Rather than introducing seeding advantages or disadvantages to any of the modeled species, the SEED parameter was negated in this research. With this parameter negated, site conditions were the sole determining factor in establishment success.

Another mechanism for regeneration encoded into FACETA is vegetative reproduction through stump sprouting. This is another characteristic where information can be found for some species, but it is almost entirely qualitative. Sources may provide information on whether or not a species has the ability to reproduce vegetatively, or some provide descriptors such as a species being a *prolific* stump sprouter. This capability is controlled by two input parameters required for each species. One parameter is the number of sprouts per stump expected to grow into mature trees, and the other is a maximum size limit of trees that can produce sprouts. Values for these input parameters are also required to run the model, but setting either or both parameters to zero turns off the capability. As with the seeding parameter, the decision

was made to negate this parameter and allow site conditions alone drive the regeneration dynamics between species.

Tolerances for Temperature, Drought, Flood, Shade, Nutrient

FACETA requires species parameters that define the range of tolerances and responses to various environmental and physical conditions. There are parameters for each species that describe tolerances to temperature range, drought, flooding or saturated soil, shade, and deficiencies in soil nutrients. In general, each tolerance parameter yields a tolerance curve. The curve produces a number between 0 and 1 depending on some metric of that environmental condition over a growing year, and the tolerance curve values is used as a multiplier to the optimal growth increment. In some cases, for example with the two soil moisture related tolerances, the values of the tolerance curves are combined into a single multiplier by taking the minimum of the two.

Temperature tolerance is modeled with a parabolic function with the input based on the concept of growing degree days (GDD). GDD is based on the notion that trees require a minimum temperature to grow. Every day during the growing season when the temperature exceeds the minimum limit, it counts towards the year's GDD by the number of degrees that the temperature exceeds the limit. FACETA requires two input parameters for temperature tolerance, a minimum (DDMIN) and a maximum (DDMAX). These two values are the x-intercepts of the tolerance parabola, so any simulation year with the total number of GDD outside this range results in zero growth. These parameters are typically estimated by using the native range of the species and taking the average GDD occurring at the northernmost extent of the range for DDMIN and southernmost extent for DDMAX. A problem arises with this approach whenever

modeling a species close to its temperature range. A potential solution to this problem is using upper and lower limits for the average number of GDD occurring at the southern and northern extents, respectively. For example, rather than taking the average GDD over a 30-year history as the parameter, the minimum number over the 30 years is used if it is from the northern extent and the maximum number over the 30 years is used if it is from the southern extent. This approach requires more effort than finding the average, but, if taken, then average temperature years at the extent of the species range can still result in positive growth. This issue is not a problem if the species modeled are not near the edge of their range. In this study, the temperature tolerance parameters were determined in the traditional manner of finding the northern and southern averages for the number of GDD occurring in a typical growing season. This was accomplished using a species range map and temperature records or even climographs of the southern and northern extents of the range. In the case where two species' ranges essentially overlapped, the same values are used. Having said that it, must be noted that there were problems in the underlying assumption and approach to modeling and determining parameters for the temperature tolerances. It is not apparent that high temperatures are a limit to the ranges of any of the tree species native to the southeastern United States, or any of those considered for FACETA. Many have their ranges bounded on the south by the Gulf of Mexico, and the limiting factor on the western side of their ranges is much more likely to be precipitation than temperature. However, using the traditional assumptions on temperature tolerances, Table 5.7 lists these parameter values for the FACETA candidate species.

Table 5.7

Temperature Tolerance Parameters for Candidate Species

Species	Common Name	DDMIN	DDMAX
Acer negundo	Boxelder	890	5500
Carya illinoinensis	Pecan	2390	5500
Celtis laevigata	Sugarberry	2680	6220
Forestiera acuminata	Swamp privet	2390	5500
Fraxinus pennsylvanica	Green ash	890	5500
Morus rubra	Red mulberry	1950	5500
Populus deltoides	Cottonwood	1950	5500
Quercus macrocarpa	Bur oak	1950	5500
Quercus marilandica	Blackjack oak	2510	5560
Quercus stellata	Post oak	2680	6010
Salix nigra	Black willow	1950	6220
Ulmus alata	Winged elm	2680	6010
Ulmus americana	American elm	1950	5500
Ulmus crassifolia	Cedar elm	2680	6220

Note: The minimum (DDMIN) and maximum (DDMAX) temperature parameters are derived by estimated that average number of GDD that occur at northern extent (for DDMIN) and southern extent (for DDMAX) of the species range.

Drought tolerance itself is not a new feature for FACETA; however, the way it is implemented has changed. Predecessors to FACETA used relative rankings of 1 through 5, with 5 being the most tolerant. The parameter in FACETA is a value that represents the proportion of days in the growing season that the species can tolerate being in dry soil. In this case, dry soil is defined as having no extractable water, which is when the soil moisture level drops below wilting point. Any such day is called a *dry day*, and the total number of dry days is divided by the length of the growing season. As this number approaches a specie's drought tolerance parameter, the specie's tolerance curve decreases as a square root function. This approach certainly is a refinement over FACETA's predecessor in that it is tallying a drought index daily; however, there are still some limitations. For example, the annual drought index does not take into account when in the growing season dry days occur or how they are distributed. It surely seems

reasonable that 10 consecutive dry days would be more injurious to a tree than 10 days scattered throughout the growing season. However, the model's drought index treats these two scenarios the same. Another limitation to the approach is that although the parameter is based on quantifiable value – the proportion of dry days in the growing season the species can tolerate – there is little to no available data on which to base the parameter. The best that can be accomplished with the model's current drought tolerance implementation and the information and data available is to rank the species by relative drought tolerance, group them when possible, and assign initial values for the tolerance parameter based on those rankings. Relative rankings are based on the same type of descriptive or qualitative information that is often only what is available for determining qualitative model parameters (descriptions such as *low* drought tolerance or *high* moisture requirement). As with some of the previously discussed information available for tree species, details can often be either unavailable or conflicting. Table 5.8 gives examples of common descriptions regarding drought tolerances of the candidate species. Three example sources are used in this table: the USFS Climate Change Tree Atlas (Prasad et al., 2007-ongoing), the USFS Fire Effects Information System (USDA, 2014a), and the USDA (2014a) PLANTS database. The PLANTS database in particular has contained information that seems contradictory to other sources or personal observations. The advantage of this database is that it contains information on a very large number of species, including every one of the FACETA candidate species. Examples of suspect information from the PLANTS database in Table 5.8 include giving the same low tolerance rating to drought for sugarberry, pecan, and swamp privet. Both sugarberry and pecan can survive in dry sites whereas swamp

privet does not. Additionally, the PLANTS database ranks both green ash and cottonwood as more drought tolerant than sugarberry, which from personal observations in the North Texas area seems incorrect. Both green ash and cottonwood are noted for having considerable variation in drought tolerance across their ranges, and it is quite possible that the individuals from these species in the North Texas region are of the less tolerant variety.

Table 5.8.

Drought Tolerance Descriptions for Candidate Species

Species Common Name	CCTA Drought Comments	FEIS Drought Comments	PLANTS Drought Rating	Dry Day Limit Parameter
Post oak	Extremely resistant to drought	Drought resistant; Seedlings resistant to drought	High	0.60
Blackjack oak	Dry site intolerant	Semi-xeric species; Typically occurs on dry sites; Often survives more xeric sites than post oak but during severe drought in Oklahoma had higher mortality than post oak	High	0.60
Winged elm	n/a	n/a	Low	0.45
Bur oak	Extremely resistant to drought	Endured drought very well over a 7 year period	High	0.40
Cedar elm	n/a	n/a	Medium	0.35
Boxelder	Resistant to drought	Tolerant once established	High	0.35
Sugarberry	n/a	n/a	Low	0.35
Green ash	n/a	Varies across the species' range; In South Dakota 63% survival over 5 years of drought	Medium	0.35
Red mulberry	n/a	n/a	Medium	0.35
Pecan	n/a	n/a	Low	0.30
American elm	n/a	n/a	Medium	0.30

(table continues)

Species Common Name	CCTA Drought Comments	FEIS Drought Comments	PLANTS Drought Rating	Dry Day Limit Parameter

Table 5.8 *(continued)*

Species Common Name	CCTA Drought Comments	FEIS Drought Comments	PLANTS Drought Rating	
Cottonwood	n/a	Drought tolerant; Significant geographic variation in drought resistance	Medium	0.25
Black willow	Wet required	Not drought tolerant; Entire stands may die when water tables lower	Low	0.15
Swamp privet	n/a	n/a	Low	0.15

Note: Drought tolerance descriptions can be found for many species from various botanical or silvics sources; however, the information available is rarely quantitative and sometimes contradictory. This table summarizes drought tolerance descriptions from three such sources: The USFS Climate Change Tree Atlas = CCTA, the USFS Fire Effects Information System = FEIS, and the USDA PLANTS database = PLANTS. One advantage to the PLANTS database is that it contains information on most species; however, it also offers the vaguest descriptions and can often contradict other sources or observations. In some cases a simple rating system is used, in which case a one-word descriptor appears in the table (e.g., High). In other cases, the sources offer more verbal descriptions, in which case the table paraphrases the information from the source. If the table states *n/a*, then no specific information about drought tolerance was found from the source. The table is listed in order from what is assumed to be most drought tolerant to least for the Greenbelt FACETA model.

Final ranking and drought parameter estimation was based on both the information from the various botanical resources and on familiarity with tree responses to dry conditions in the North Texas area. For example, bur oak was frequently described as being drought tolerant or even extremely drought tolerant, but the species did not occur on the direst sites in North Texas where post oak and blackjack oak do occur. However, both winged elm and cedar elm associated with the post oak on these dry sites. The conclusion drawn was that winged elm and cedar elm are very close to bur oak in drought tolerance. Since winged elm appeared on some of the driest of these sites, albeit as a small scrubby tree, it was ranked just above bur oak in drought tolerance, while cedar elm was ranked just under bur oak. There are actually two

required drought tolerance parameters in FACETA for each species, one for trees and one for seedlings. Mature trees and seedlings are treated differently in the model when considering access to and requirements for soil moisture. Seedlings' access to soil moisture is limited to the first 20 cm of soil depth whereas trees have access to the moisture from the entire column. However, without better data on which to base these parameters, there was no reason to assume the limit for trees was different from that for seedlings. Since trees have access to more of the soil moisture than seedlings, even with the same parameter value seedlings will be more impacted during dry periods. These initial parameter estimates were tested and calibrated, and as with all model parameters, they should be altered as more information is gained. Figure 5.28 shows graphs of the drought tolerance curves using these parameter estimates.

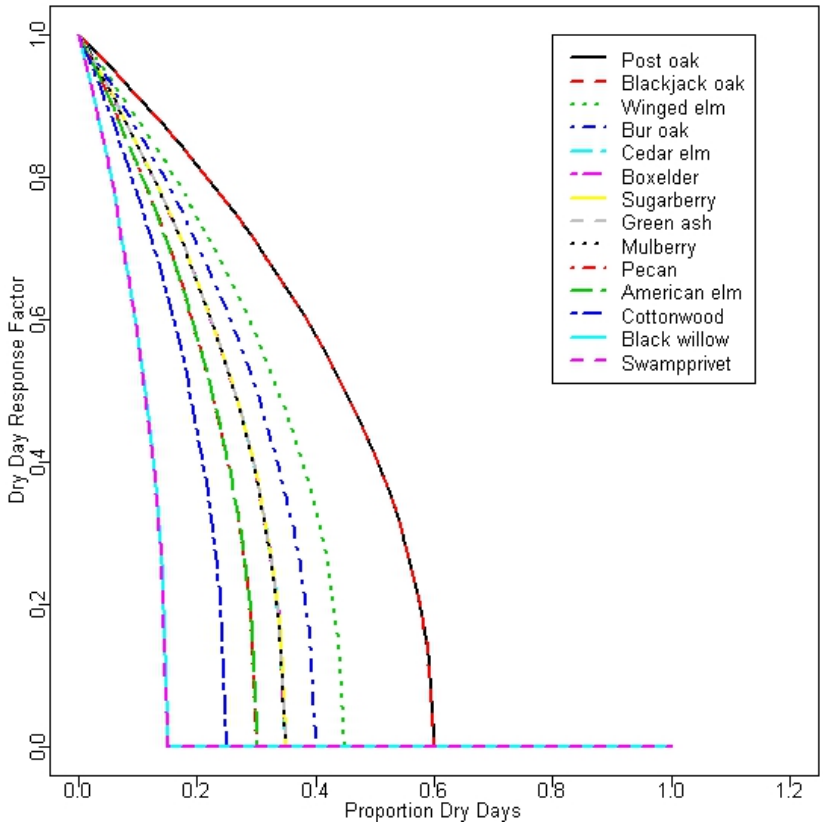

Figure 5.28. Dry day response curves for candidate species. Dry day tolerance response curves for FACETA candidate species using the parameters listed in Table 5.8. The model parameter is the proportion of dry days at which the graph intersects the x-axis, which equates to growth response factor of 0 or no growth.

Flood tolerance is a new addition to FACETA. While it is referred to as flood tolerance, it functions more like anaerobic tolerance combined with a minimum moisture limit. Similar to the temperature tolerance, the curve is parabolic, and there are two required parameters, which are the two x-intercepts of the parabola. Similar to the drought tolerance, both the parameters and the index that determines the tree response are expressed as a proportion of days in the growing season. In this case, the days being counted are *wet days*, which are defined as being days when the soil moisture exceeds field capacity. Soil water that is in excess of field capacity is also called *gravitational water*, and is water that percolates down towards the groundwater. This excess water takes up soil pore space that would otherwise be occupied by air, so it is anaerobic stress. Table 5.9 lists some of the common descriptions regarding flood tolerances of the candidate species and lists initial parameter values. The sources used for this table included USFS Climate Change Tree Atlas (Prasad et al., 2007-ongoing), USDA Fire Effects Information System (2014a), and the USDA (2014b) PLANTS database along with a handbook produced in collaboration between the US Geological Survey (USGS, n.d.) and the USFS (USDA, 2014a) on bottomland hardwood restoration. The parameter was allowed to exceed 1 to allow for positive growth of swamp-tolerant species, or it could be below 0 to allow for positive growth of xeric species. As with the drought tolerance parameter, FACETA allows for different parameter values for seedlings and trees. At this time without better data on which to base the parameters, the values for seedlings and trees were set the same for most

species. Figure 5.29 shows graphs of the flood tolerance response curves using the parameters in Table 5.9.

Table 5.9.

Flood Tolerance Descriptions for Candidate Species

Species Common Name	FEIS or CCTA Flood Comments	USGS Flood Tolerance	PLANTS Moisture Use	PLANTS Anaerobic Tolerance	Wet Day Parameter Low / High
Swamp privet	n/a	T	High	High	0.1 / 1.5
Black willow	FEIS: Develops best in stagnant water; thrives in saturated soil	T	High	High	0.1 / 1.5
Green ash	CCTA: Extremely tolerant of flooding	MT	Medium	Medium	0.0 / 0.95
Cedar elm	n/a	MT	Medium	None	0.0 / 0.8
American elm	CCTA: Tolerates dormant season flooding but not growing season flooding FEIS: Found in bottomlands but not typically in deep swamps	MT	High	Low	0.0 / 0.8
Sugarberry	FEIS: Cannot tolerate prolonged flooding; Found on moist soils and slough margins but not deep swamps	MT	High	Medium	0.0 / 0.8
Cottonwood	FEIS: Moderately tolerant to water-logged soils; tolerant to short-term inundation	WT to MT	High	High	0.0 / 0.8
Boxelder	FEIS: Can withstand short periods of flooding	MT	Medium	Medium	0.0 / 0.75
Red mulberry	CCTA: Moderately tolerant at least for one growing season	WT to I	Medium	Medium	0.0 / 0.75
Pecan	FEIS: Most common on well-drained soils not subject to prolonged flooding	WT	High	None	0.0 / 0.5
Winged elm	n/a	WT to I	Medium	Low	0.0 / 0.35
Bur oak	FEIS: Tolerant to some inundation but not to prolonged flooding CCTA: Intolerant to flooding	I	Medium	None	0.0 / 0.35

(table continues)

Table 5.9 *(continued)*

Species Common Name	FEIS or CCTA Flood Comments	USGS Flood Tolerance	PLANTS Moisture Use	PLANTS Anaerobic Tolerance	Wet Day Parameter Low / High
Blackjack oak	FEIS: Excessive soil moisture and inundation cause severe stress and often high mortality in seedlings; Typically occurs on dry sites	n/a	Low	None	-0.1 / 0.3
Post oak	CCTA: Very intolerant of flooding	n/a	Medium	Low	-0.1 / 0.25

Note: Flood tolerance descriptions can be found for many species from various botanical or silvics sources; however, the information available is rarely quantitative and sometimes contradictory. This table summarizes flood tolerance descriptions from four such sources: the USFS Climate Change Tree Atlas = CCTA, the USFS Fire Effects Information System = FEIS, the USGS Guide to Bottomland Hardwood Restoration = USGS, and the USDA PLANTS database = PLANTS. In some cases, a simple rating system is used, in which case a one-word descriptor appears in the table (e.g., High). In the case of the USGS ratings, the codes are tied to specific meanings: T = tolerant to long-term flooding, MT = tolerant to several months of flooding, WT = tolerant to a few weeks of flooding, and I = tolerant for at most a few days. In other cases, sources offer more verbal descriptions, in which case the table paraphrases the information from the source. Information in both the CCTA and FEIS on flood tolerance is spotty, so these two sources are combined into one column. If the table states n/a, then no specific information about flood tolerance was found from the source. The table is listed in order from what is assumed to be most flood tolerant to least for the Greenbelt FACETA model.

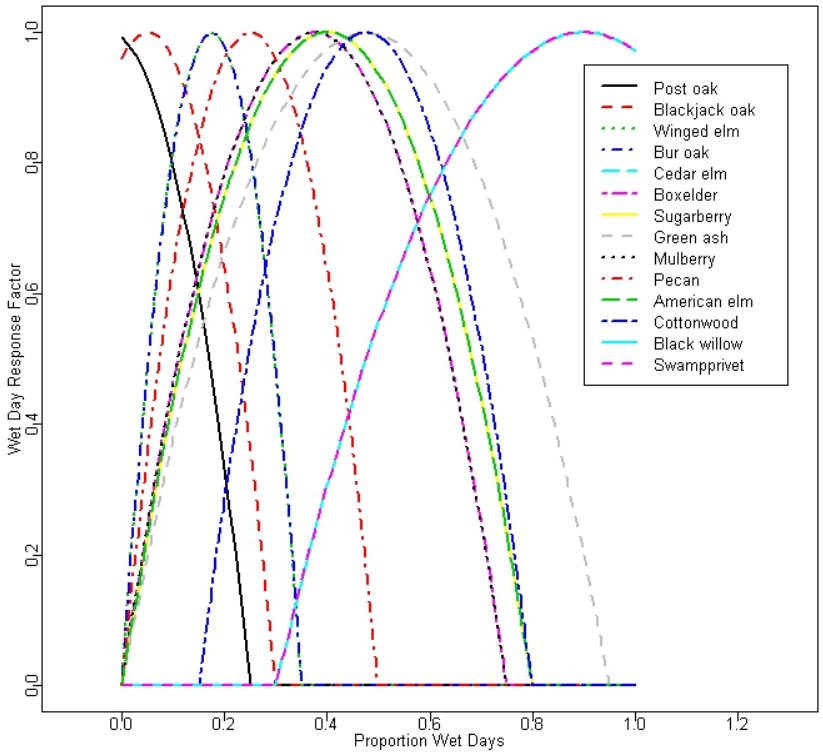

Figure 5-29: Wet day response curves for candidate species. Wet day tolerance response curves for FACETA candidate species using the parameters listed in Table 5-8. The model parameters are the values at which the parabolic graph intersects the x-axis, which equates to growth response factor of 0, or

no growth. If a parameter value is either less than zero or greater than 1, then this species can still grow in either xeric (for 0) or swamp (for 1) conditions.

Shade tolerance is implemented in FACETA in a relatively simple manner, and is unchanged from its predecessor. Each species is assigned a value from 1 (very intolerant) to 5 (very tolerant), and a different tolerance curve based on the percentage of full sun received is assigned to each class. Sunlight is reduced from 100% in FACETA through a light attenuation model that diminishes sunlight as it passes through the canopy. This is one way that competition between individual trees is simulated. Taller trees get more sunlight. For this parameter, it is more important to know the relative differences in shade tolerances between the species rather than some quantifiable characteristic. While this approach is a little arbitrary, shade tolerance is a very difficult characteristic to measure so this approach is about the best option. Through observations and tree surveys, it is not too difficult to determine which species are or are not tolerant to shade. This is the only silvics characteristic for which the various sources consulted are mostly in agreement. Examples of shade tolerance characterizations are given in Table 5.10. The sources used for this table again include USFS Climate Change Tree Atlas (Prasad et al., 2007-ongoing), the USGS (n.d.) bottomland hardwood restoration handbook, and the USDA (2014b) PLANTS database.

Tolerance to soil nutrient stress is also modeled in a somewhat simple fashion. Every soil type is given a fertility parameter expressed as a potential annual productivity rate. As trees grow within a plot, potential productivity is used, and species susceptible to nutrient stress will have their growth rate diminished. This is another way to simulate competition dynamics. Similar to shade tolerance, the parameter is based on classes. The classes are rated from 1 (nutrient demanding) to 3 (nutrient stress tolerant).

Table 5.10

Shade Tolerance Descriptions for Candidate Species

Species Common Name	CCTA	USGS Tolerance Description	PLANTS Shade Tolerance	Shade Tolerance Parameter
Sugarberry	Tolerant	T to VT	Tolerant	5
Red mulberry	Tolerant	T to VT	Tolerant	5
Swamp privet	n/a	T	Tolerant	5
Winged elm	Tolerant	T	Tolerant	4
Boxelder	Tolerant	MT to T	Tolerant	3
American elm	Intermediate	MT to T	Intermediate	3
Cedar elm	Intermediate	MT to T	Intermediate	3
Green ash	Tolerant, but varies through its range	Adult = I; Seedling = MT to T	Tolerant	3
Bur oak	Intermediate	WT	Intermediate	3
Pecan	Intolerant	I to MT	Intolerant	2
Post oak	Intolerant	n/a	Intolerant	2
Blackjack oak	Intolerant	n/a	Intolerant	2
Cottonwood	Very intolerant	VI	Intolerant	1
Black willow	Very intolerant	VI	Intolerant	1

Note: Shade tolerance descriptions can be found for many species from various botanical or silvics sources and is always qualitative, but different sources tend to agree more on this silvics characteristic. This table summarizes shade tolerance descriptions from three sources: the US Forest Service Climate Change Tree Atlas = CCTA, the USGS Guide to Bottomland Hardwood Restoration = USGS, and the USDA PLANTS Database = PLANTS. The characterizations tend to be simple rankings such as “tolerant” or “intermediate”. In the case of the USGS ratings, the codes are tied to specific meanings: VT = species is able to survive and thrive in the deep shade of a closed canopy forest, T = species is able to survive and grow in the shade, but growth may be slowed if shade is deep, MT = species will survive in moderate shade, but growth and seed production may be reduced, WT = species will grow with partial shading for a portion of the day but requires some direct sunlight for normal growth, and I = species requires open conditions and full sunlight for normal growth. No definition is given in the handbook for “VI”, but interpolating from the description of “I” it must be assumed that “VI = Very Intolerant” means something to the effect of the species does not grow at all in the shade. If the table states “n/a” then no specific information about shade tolerance was found from the source. The table is listed in order from what is assumed to be most shade tolerant to least for the Greenbelt FACETA model.

Only the USDA (2014b) PLANTS database provided information on fertility demands with any consistency at all. Many sources have within the species descriptions statements such as *thrives in rich soils*, but these descriptions vary greatly and are difficult to apply to estimating model parameters. Nutrient stress tolerance is another

characteristic that is very difficult to measure. Table 5.11 lists the nutrient stress tolerances for the candidate species.

Table 5.11

Nutrient Tolerance for Candidate Species

Species Common Name	PLANTS Fertility Requirement	Nutrient Stress Parameter
Blackjack oak	Low	3
Post oak	Medium	3
Red mulberry	Low	3
Winged elm	Medium	2
Sugarberry	Medium	2
Cedar elm	Medium	2
Bur oak	Medium	2
Boxelder	Medium	2
American elm	Medium	2
Green ash	Medium	2
Cottonwood	Medium	2
Black willow	Medium	2
Swamp privet	Medium	2
Pecan	High	1

Note: Beyond descriptions of types of soils that a species may favor, nutrient stress tolerance descriptions are difficult to find and likely impossible to quantify. This table lists the nutrient or fertility requirements for the species from only one source, the USDA PLANTS Database = PLANTS. The characterizations are simple rankings of *high*, *medium,* and *low*. The table is listed in order from what is assumed to be most nutrient stress tolerant to least for the Greenbelt FACETA model.

Of all species parameters, the ones for tolerances to environmental stress are the most difficult to measure for or quantify. Typical methods used across the board for modeling these responses and determining parameters is by ranking the species and assigning response curves based on rank. The wet-day and dry-day response methods incorporated into FACETA represent an effort to base the response more on the biological response to the physical moisture conditions being modeled in the soil. However, because of how response and parameters work, there are still limitations. Wet-days or dry-days within the growing season are not differentiated by when they

occur or how they are distributed. Data to base the parameter values on are limited at best. Considering the definition of a dry day is that the moisture level has been reduced to the wilting point, few plant species could withstand very many dry days within the growing season. However, because response curves tend to drop with a very steep slope as they approach the parameter values, setting parameter values too low (or high in the case of the smaller of the wet-day parameters) results in little or no growth and high mortality. The parameters may require a little buffer space to prevent this.

Of all the tolerance parameters, temperature range is the most straightforward and easiest to quantify a parameter value for given the model's assumptions. Potential problems with assumptions occur if a species being modeled is close to the edge of its temperature range, in which case growth will be too restricted because of the steep decline of the response curve. In this case, a little buffer could be built in by using lower (from the north end of the range) and upper limits (from the south end of the range) rather than averages of the annual GDD.

Shade and nutrient stress responses and parameters are fairly easy to determine since the parameters are simple rankings. Collaborating information to base those rankings is easy to find for shade tolerance as it is an easy characteristic to observe. However, there is very little good information for the nutrient parameter. Additionally, the responses for these stressors are a bit arbitrary, but probably the best approach available without a better way to quantify both the stress tolerance and stress response.

All tolerance parameters, as well as all of the other species parameters, are calibrated as the model is developed, and because of the mutual sensitivity between them, all calibration can be an exceedingly challenging task.

Conclusions: FACETA Biological Parameter

To develop a model that is representative of a particular ecoregion, it must contain species that represent it and all of its important ecological niches. If the model is trying to capture the effects of topography and terrain attributes, then the species used in the model must allow validation of the model and possess terrain sensitive characteristics. If the model is representing a particular location, area, or watershed within the ecoregion, then species prevalence in that location must be consider in selecting the species for the model. There are also model concerns in selecting modeled species, in that it can be difficult to find adequate, non-contradictory information to model many species. Some species have little commercial value and are somewhat ignored, while other species may be well known and studied but can possess huge variations in characteristics, from growth potential to drought resistance, across their range. A species like winged elm can have so much differing or conflicting information about them from different sources that it can seem like different species are being discussed. Perhaps some of these different sources are really discussing different species, or maybe different varieties, and certainly different populations. This raises the question of what is meant by a species, and how that understanding is translated into a forest model like FACETA. Different populations adapt to the environmental conditions they live in, and can develop greatly varying characteristics and phenotypes. If building a forest model for Texas, should post oak growth parameters be based on observations of Texas post oak or should they include the much larger post oaks that grow in places like Mississippi? Could a post oak taken from the population in North Texas grow as large as one from the southeast if given more optimal conditions? These questions

arose through this research, though they were not satisfactorily answered. There is also the problem that some species just do not fit well to the model's assumptions of growth patterns and forms. All of these issues complicated developing a list of species to be modeled.

The issue of differences in characteristics across a specie's range is particularly clear in determining the maximum parameters. Proposed limits on heights and diameters for some species can vary wildly. In a way, these maximum values are not knowable since a potential cannot be really understood unless it is realized. The philosophy behind parameters such as maximum height in these kinds of models is to set the value to the idealized maximum potential and then let environmental conditions and competition control the realized growth. There are two potential problems with that approach. Numerous model parameters interact with each other through model equations and mutual sensitivity can be high. If interacting model parameters are dramatically out of alignment with each other, it can result in unrealistic outcomes from the model assumptions. Another problem with the maximal approach is that in many cases, models such as these are not simulating the actual biophysical processes taking place; rather, they often simulate the effects of those biophysical processes. For example, instead of simulating the actual reduction in photosynthesis because of shade, it is much simpler to group species into tolerance classes and then penalize growth accordingly when shade is present. Modeling responses to stressors in this way can work quite well; however, success depends on getting the relative rankings correct.

Changes made in FACETA to the species parameters and response to both drought and anaerobic stress is an example of an attempt to base the model more on

measurable, physical responses, by making the growth penalty a function of the proportion of the growing season during which the stressor occurred. However, even a small enhancement in the realism in the model requires a large amount of knowledge to use properly. How do trees respond if seasonal soil moisture levels exceed field capacity during half of the growing season? Does it make a difference it this occurs because every other day during the growing season the soil moisture exceeded that level versus a scenario where the soil is soaked for three months continuously? The answers obviously depend on the species. Relative difference between species' responses is often fairly well understood, but the difficulty lies in quantifying those relative differences. In the case of FACETA, the model was enhanced to make the soil moisture responses more real, but in the end the data available to parameterize those responses was too limited to do any better than rank the species, then assign best guess parameter values based on those. One problem with drought response is that FACETA does not treat species differently underground. Root geometry and root depth do not change with species. While a number of factors impact a plant's susceptibility or tolerance to drought, one factor at least for some species is the root geometry. Honey mesquite, a common invader in dry sites, has been said to grow a tap root up to 60 feet deep. On the other hand, most tree species grow most if not all of their roots in the upper layers of the soil. Modeling species response based on a physical property such as access or lack thereof to soil water at depth rather than assigning ranks between the species provides more realism. However, that does not change the problem of parameterizing a species to respond to a stressor once one occurs.

Using actual tree measurements to determine the allometric and growth rate parameters is an example of trying to make model parameters based more on data than just intuition. The techniques generally seemed to work well, but there are still some limitations and problems. Different species fit the assumptions of the model to varying degrees. For example, with the allometric growth equation relating height and diameter, the shrubby swamp privet does not seem to follow the rule at all whereas the height/DBH data points used in the blackjack oak regression look almost as if they were generated by the regression curve. One of the problems of measuring for the growth rate parameter *G* is determining just how to do it. The parameter is given in units of volume of new wood per unit leaf area per year. Direct measurements for such a parameter are difficult at best. In this case, using the assumptions behind the model equations – assumptions regarding the relationships between leaf area and diameter and between diameter and volume – the parameter can be measured for by measuring diameter growth increments. This is seemingly simple enough, but how are diameter increments measured? Some tree species can have very irregular geometries with lobed, twisted, fluted, or angular trunk shapes where the question arises of what is even meant by diameter. It is typically assumed or interpreted that diameter means the circumference divided by pi, and that a diameter increment is twice the width of a tree growth ring. For this study, it was found that the best way to measure for diameter increments, short of using dendrometer bands in a long-term study, was to measure growth rings using cross sections. Using cross sections reduced uncertainty about asymmetric growth rings, rings that were difficult to see or false rings, and the diameter of the tree at the time any particular growth increment occurred. Since the objective of

measuring for the growth rate parameter was find examples of optimal growth, using trees growing in optimal conditions such as residential yards was concluded to not only be acceptable but the best approach.

While there are methods for measuring growth rate and allometric parameters, many of the biological parameters do not such methods. For parameters such as the various tolerances, typically the best that can be done is to determine the relative parameterization between species accurately. In some cases, a parameter might be easy to measure for (e.g., height to crown ratio), but variation might be so great that the measurements become difficult to interpret.

CHAPTER 6

FACETA ENVIRONMENTAL PARAMETERS

The environmental parameters required by FACETA can be grouped into three categories: climate averages used to drive the random weather generator, soil conditions used to model the soil water balance, and landscape and terrain parameters used in the insulation and hydrological components of the model. A weather generator is used in the model to provide simulated daily high and low temperatures and daily rainfall amounts. Input parameters are required for each month, which are calculated from local daily weather records as well as from monthly averages. The soil water balance model and weather generator are linked. The generated rainfall is used as input into a soil moisture model, where daily moisture dynamics are simulated through a water budget calculated for each soil layer that includes infiltration through layers, percolation away from the root zone, and evapotranspiration to the atmosphere. Soil parameters include depth, infiltration rate, how much water the soil can hold, and how much water the soil must have for it to be available to plants. Landscape and terrain input parameters include topographic measurements of slope, aspect, and elevation. Terrain type parameters are also derived from the topographic wetness index (TWI) and soil type groups. Slope and aspect are used to model insulation. Elevation is used in the model to simulate changes in temperature and precipitation that can occur in mountainous regions. While these three parameters are used by FACETA and are required in the input file, they were not focused on in this research. Rather the hydrologically centered parameters derived from the TWI and soil type terrain types were the landscape parameters of interest.

Methods: FACETA Environmental Parameters

Environmental parameters were estimated through different methods for the three categories. The weather and climate parameters were determined from historical records. Monthly solar radiation parameters were obtained from already aggregated historical monthly averages, but all the other weather-related parameters were determined from a history of daily records. Soil parameters for the modeled soil series were estimated using layer depths, textures, and organic content of the typical pedon for each soil series as described in the Denton County soil survey (Ford & Pauls, 1980). Soil parameters for selected locations were also determined from layer depths, textures, and organic content measured from soil core samples taken from within the Greenbelt. The two sets of parameters were estimated to compare results from the two sources to help determine the reliability of using a county survey in the gap model application. The terrain type parameters were determined from the distribution of values of the different raster grids calculated from the digital elevation model (DEM). Specific details for the environmental model parameters are provided in the following sections.

Results: Climate and Weather Parameters

A major change in FACETA was to convert its weather simulator from a monthly to a daily time step. Like most models of its kind, FACET produced monthly high and low temperatures and monthly rainfall totals based on probability distributions. Monthly results were then aggregated across the growing season to determine annual tree growth response. Because the objective of this research was to introduce the hydrologic effect of topography and to develop a more detailed method to simulate tree response to soil moisture conditions, the rainfall simulator was converted to a daily model.

Daily weather records from the City of Denton spanning the years 1913 to 2013 were obtained from the Utah Climate Center's database (Utah Climate Center, 2013). The records included the high and low temperatures and precipitation totals for each day. The data were used to describe the climate from annual, monthly, and daily perspectives. At each level, only complete data sets were used in the analysis. For a given day, the temperature record was considered complete if both the high and low temperature record existed, and precipitation record was considered complete if both that day's and the previous day's precipitation records existed. For either monthly temperature or precipitation analysis, a month's records were considered complete if there was a complete record for every day of the month. For the annual analysis, a single year was considered complete if there were at least 365 days of complete data for that year. Incomplete months or years were not included in the analysis. Temperature and precipitation were treated separately in terms of *completeness*. For example, if the temperature sensor for the weather station was down one day but the rain gauge was functional, that day's data were included in the precipitation analysis but not for temperature. After eliminating incomplete months and years from the 100 years of weather data collected, there were 78 years of complete precipitation data and 65 years of complete temperature data. For any of the 12 months of the year for both temperature and precipitation, there were at least 88 complete records. The parameters for FACETA's weather generator were determined from this data using the daily weather records for each month separately.

Prior to making the big change from monthly to daily rainfall simulation, a smaller change was made to the way monthly temperatures were simulated. It is common to

use a normal distribution to model the monthly high and low temperatures, which was the method in FACET. In a literature review, it was noted that in many climates some months have more of a skewed temperature distribution. The monthly temperature averages were analyzed from the historical records for normal distributions using exploratory data analysis, chi square goodness of fit, and Shapiro-Wilks tests. Both skewness and kurtosis were calculated (Table 6.1). Most months' average temperature distribution could not be concluded to be significantly different from normal, but three were. All months showed a small degree of being peaked according to Geary's kurtosis, and most months had some amount of skew to the left or right. Of note, these calculations were done on the set of average monthly temperatures. The results were a little different when performed on the average low or average high monthly temperatures. For example, the average low temperatures for April were significantly different from normal but neither the average high nor the average April temperatures were. To make the temperature distribution options more flexible, a skewness coefficient was added to FACETA's monthly temperature model.

While kurtosis was calculated, no model changes were made to incorporate it. Results from the exploratory data analysis are listed in Table 6.1, and examples of graphs from that analysis for one winter and one summer month are illustrated in Fig. 6.1. Both months had slightly skewed temperature distributions (July skewed right and December skewed right). Generally winter months, December through February, have a notable left skew, and summer months, June through August, have right skews.

Table 6.1

Results of Average Monthly Temperature Analysis

Month	Chi-square GOF (X^2), *p* value	Shapiro-Wilks (SW), *p* value	Skewness	Kurtosis (Geary's)	Conclusion (Using α =0.10 for normality tests)
January	0.16	0.09	-0.43	0.78	Can reject the distribution is normal based on SW; skewed left and slightly peaked; there are outliers at low values
February	0.72	0.33	-0.36	0.78	Cannot reject the distribution is normal; slightly skewed left and peaked; there are outliers at low values
March	0.02	0.56	-0.16	0.81	Cannot reject normal based on SW; X^2 result in conflict with SW; small left skew, peak around the mean
April	0.24	0.30	0.28	0.80	Cannot reject the distribution is normal; skewed right and a little peaked; there are outlier at the high end
May	0.08	0.96	0.02	0.78	Cannot reject normal based on SW; X^2 result in conflict with SW; slightly peaked; there are outliers at both high and low ends
June	0.11	0.03	0.47	0.81	Reject normal based on SW; peaked and skewed a bit to right; there are outliers
July	0.06	0.07	0.55	0.77	Reject normal from both tests; peaked and slightly skewed right; outliers to the right
August	0.68	0.48	0.32	0.81	Cannot reject normal; a little right skewed and peaked; outlier on each end
September	0.63	0.77	0.18	0.80	Cannot reject normal; slightly peaked
October	0.38	0.16	-0.20	0.76	Cannot reject the distribution is normal; slight left skew and peak
November	0.28	0.63	-0.19	0.81	Cannot reject normal; slight left skew and peak
December	0.44	0.36	-0.38	0.79	Cannot reject normal; left skew and peak

Note: Distributions of monthly temperature averages were analyzed from historical weather records using exploratory data analysis and testing for normality, skewness, and kurtosis. Normal temperature distributions are often assumed in weather models such as the one used in FACETA. However, some of monthly distributions were found to be different from normal. FACETA was modified to include a skewness coefficient.

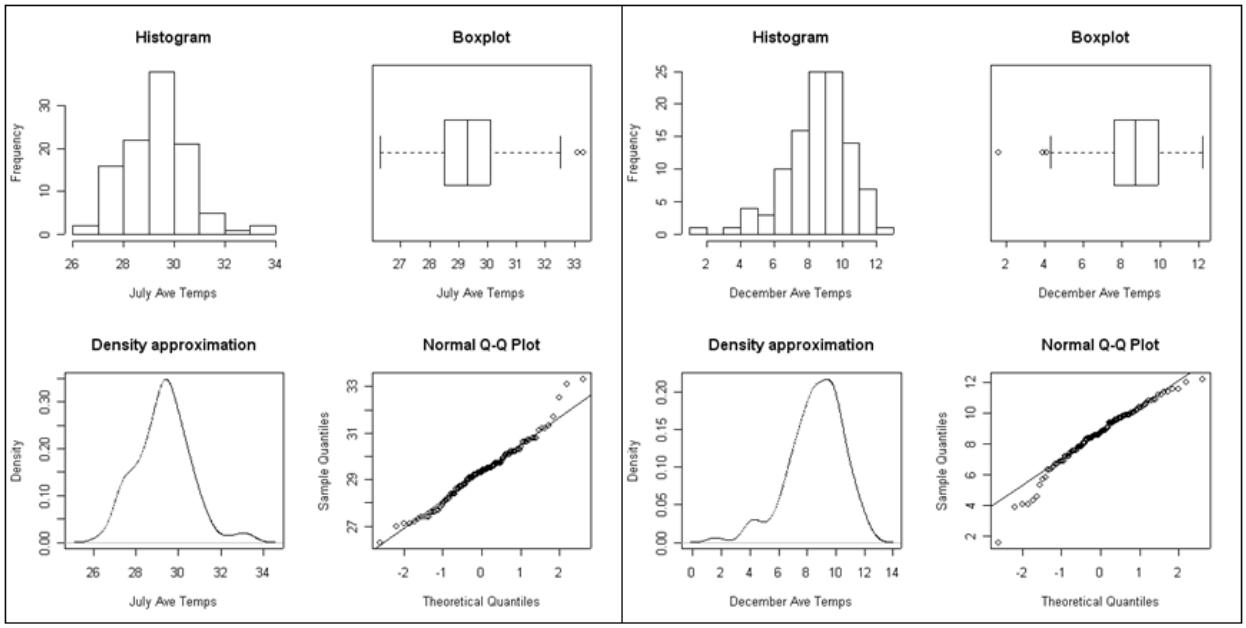

Figure 6.1. Average monthly temperature distributions for July and December. Distributions of monthly temperature averages were analyzed from historical weather records using exploratory data analysis and testing for normality, skewness, and kurtosis. Normal temperature distributions are often assumed in weather models such as the one used in FACETA. However, some monthly distributions were found to be different from normal. FACETA was modified to include a skewness coefficient. Graphs from the analysis are shown here for two months, one winter and one summer, as examples of months with distributions different from normal. The graphs on the left with the slight right skew are from July, and the graphs on the right with the left skew are from December.

This pattern intuitively at least can be explained by the unusually cold or hot days experienced during those months' respective seasons. Some of the months' distributions were not significantly different from normal or exhibited little skewness.

The precipitation component of FACETA's weather simulator was converted into a full daily model; however, the temperature component at the time was a hybrid between monthly and daily. The model produced daily temperatures, but the random temperature simulator only generated one high and one low temperature for each month. These simulated monthly temperatures were converted to daily by linear interpolation between the days in the middle of each month. This could have the unwanted effect of temperatures steadily increasing or decreasing, depending on the season, from one day to the next. Because of how the temperature component interacts

with tree growth in the model, which only depended on the accumulation of total number of growing degree days (GDD) in a growing season, potentially the growing season in the model could start too early or end too late. The FACETA temperature model uses a monthly based random number generator to draw high and low temperatures for each month from distributions that are skewed from normal. The temperature inputs needed were average high, average low, the standard deviation, and skewness for each month. The standard deviation was calculated from the average monthly temperatures rather than from the average high or low monthly temperatures. Results for these parameters are given in Table 6.2.

Table 6.2

FACETA Monthly Temperature Parameters

Temp	Jan	Feb	Mar	Apr	May	Jun	Jul	Aug	Sep	Oct	Nov	Dec
Min	.6	2.7	6.7	11.3	16.3	20.8	22.7	22.4	18.5	12.6	6.3	1.9
Max	13.2	15.8	20.1	24.7	28.3	32.8	35.4	35.5	31.5	26.0	19.4	14.3
StDev	2.5	2.3	2.2	1.6	1.3	1.3	1.3	1.5	1.6	1.5	1.9	1.9
Skew	-.43	-.36	-.16	.28	.02	.47	.55	.32	.18	-.20	-.19	-.38

Note: FACETA requires temperature inputs for average monthly lows (Min), average monthly highs (Max), standard deviation (StDev), and skewness (Skew). The temperature statistics were calculated from a 100-year history of daily weather records from the City of Denton, where monthly statistics were only calculated using months with a complete record. Temperatures are in degrees Celsius.

One component of FACETA's weather model that was not altered was the solar radiation model. This component was still simulated in monthly time steps using daily averages for each month as parameter inputs. In the model, each day of a month received the same amount of radiation. Data for these parameters were obtained from the Renewable Resource Data Center, operated by the National Renewable Energy Laboratory (NREL, 2006). The monthly model parameters were calculated from daily averages collected for each month spanning from 1961 to 1990. The data were collected in Fort Worth, TX, approximately 40 miles southwest of the study area

watershed. Solar radiation was measured using 14 flat plate collectors with a fixed tilt of zero degrees, i.e. oriented horizontally. The daily averages were averaged across the 14 collectors, and then averaged over all the days in each month. This was done for each month over the 30-year period. The daily average for each month was averaged again across the 30-year record. Results from these calculations were used as the model input parameters for the solar radiation model (Table 6.3).

Table 6.3

Average Monthly Total Radiation

Jan	Feb	Mar	Apr	May	Jun	Jul	Aug	Sep	Oct	Nov	Dec
247.5	318.3	406.1	481.2	537.7	594.5	603.7	548.0	447.7	363.4	270.7	229.1

Note: The FACETA solar radiation model is a simple model that average monthly totals as input parameters. Solar radiation data had been collected daily over a 30-year period in Fort Worth, TX, and obtained through the National Renewable Energy Laboratory's Renewable Resource Data Center (NREL, 2006). The daily values were totaled for each month, and monthly averages calculated over the 30-year history. The numbers are in units of calories/cm^2/day.

Changes to the precipitation component of the weather simulator required a completely different approach than what was implemented in FACET. Monthly precipitation distributions were straightforward to model as compared to daily. With daily rainfall, depending on the climate, there was no rain most days, and days when it did rain, the amount could vary from a sprinkle to a deluge. Most rainy days received a small to average amount of rain, some rainy days were soakers but not extreme events, and rare events occurred with large amounts of precipitate in a single day. Capturing this pattern accurately can be difficult in random weather simulators. Many daily rainfall simulators fail to model rare extreme events adequately. Most also fail to sum up the precipitation so that the daily rainfall simulator produces annual averages in the way that is hoped.

A number of different modeling approaches have simulated daily rainfall. The one implemented into FACETA is a two-stage approach. A first order Markov model is used to determine which days are rainy and which are dry in a month. The assumption behind using a Markov model is that the likelihood of rain falling in any given day will depend on whether or not it rained the previous day. This is not a novel approach and has been implemented in many situations; however, one noted problem using this approach is that it can fail to capture drought periods in semiarid climates appropriately. Using a higher order Markov chain has been proposed as a potential remedy; at this stage of FACETA development, the first order model is being implemented.

Parameters for the Markov model are conditional transition probabilities for days in each month, with the probabilities being the chance of rain on any given day conditioned on whether the previous day was rainy or not. With this approach, it is common to treat each month as having different probabilities; rainfall patterns are certainly seasonal in many places. To estimate these parameters, a 100-year history of daily weather records was grouped into the different months. Any month with an incomplete record was omitted, and proportions of days were calculated where a rainy day was followed by no rain or a rainy day was followed by rain. A complete rainfall record for any month was interpreted to be a complete set of every day's rainfall total plus the rainfall total of the last day of the preceding month. These proportions were then averaged across all 100 years, and these averages were used as the transition probability parameters (Table 6.4).

Table 6.4

FACETA Precipitation Parameters

Precipitation	Jan	Feb	Mar	Apr	May	Jun	Jul	Aug	Sep	Oct	Nov	Dec
P(wet|wet)	0.45	0.43	0.40	0.40	0.43	0.40	0.32	0.34	0.39	0.42	0.42	0.44
P(wet|dry)	0.20	0.21	0.21	0.21	0.24	0.18	0.12	0.14	0.14	0.16	0.16	0.17
Average rain on wet days	0.59	0.75	0.80	1.16	1.33	1.19	1.07	1.06	1.29	1.38	0.88	0.78
SD rain on wet days	0.91	1.29	1.30	1.67	1.89	1.51	1.58	1.43	2.00	2.23	1.36	1.19
Proportion of rainy days	0.27	0.28	0.26	0.27	0.30	0.23	0.16	0.18	0.20	0.22	0.22	0.24

Note: Transition probabilities for the Markov model that determines which days are rainy or not are estimated from the proportions of wet days followed by wet days and the proportion of dry days followed by wet days. This is done for each month independently. P(wet|wet) is the probability that it will rain conditioned on if it rained the previous day, and P(wet|dry) is the probability that it will rain if it was dry the previous day. The average amount and standard deviation on the rainy days were used to define the gamma distribution that the random weather simulator drew from to determine the rainfall amounts on rainy days. The average rainfall amounts are in centimeters.

The second part of the precipitation model determines the amount of rainfall that occurs on a rainy day. FACETA assumes a gamma distribution to model this daily amount of rainfall. The parameters required for the gamma distribution are *shape* and *scale*, which can be estimated using the mean and variance of daily rainfall as determined from the days there is rain. FACETA therefore has been set up so the input parameters for the gamma distribution are the average and standard deviation of the total rainfall amount calculated only from days there was rain. Estimating these values from the daily rainfall records is simply a matter of calculating the average and standard deviation of rainfall amount after omitting the days with no rain. Another parameter required but not used in the random weather generation is the average proportion of days for each month that it rains, which is used to verify that the Markov model produces the correct stable distribution of rainy days.

Unlike some of the biological parameters, the estimation of the parameters used in the weather model was based on a solid set of empirical data of 100 years of daily weather records. The modeled weather outputs were compared with the weather history. The results of these comparisons said more about the assumptions behind the weather simulator as well as the simulator's numerical implementation than about the ability to measure for parameter estimation.

Results: Soil Parameters

Soil parameters for FACETA were derived from two sources: all the modeled soil types from the USDA soil survey for Denton County and plots and soil types from field measurements taken by Rijal (2011) from the Greenbelt. In the Rijal study, soil cores were taken to a depth of around 2 m and analyzed for texture as well as other physical and chemical properties. Soil parameters derived from the field data were compared to the county's soil survey, and FACETA simulations were performed using both.

In the FACETA soil moisture model, water is input at the surface through the rainfall simulation and infiltrated into the top layer of soil. Each layer of soil works like a tipping bucket in that water flows into the top of the layer until it is *full*, at which point the water starts to pour down into the next layer. The full point for each layer is its field capacity. If the water infiltrates down through the last layer, then it is lost to groundwater percolation. Water is also pulled back up through layers of soil by evapotranspiration, unless the level of water in a layer is at or below wilting point when water can no longer be drawn upward. Evapotranspiration also works through the layers. Soil depth available to tree roots is different between seedlings and established trees. Seedling can only draw water from the first 20 cm of soil, whereas trees can reach water

throughout all layers. The assumptions and treatment of root geometry and depth are the same regardless of species. The parameters needed for each soil type for the soil moisture routine included the fast flow fraction of water flowing through macropores from the surface, the dry surface infiltration rate, the saturated surface infiltration rate, the maximum available porosity of the soil, the number of layers, the depth of each layer, the field capacity and wilting point of each layer, and the saturated hydraulic conductivity of each layer.

The Denton County soil survey (Ford & Pauls, 1980) produced by the Soil Conservation Service is an example of an Order II level survey. The higher the order number, the more detailed and accurate the information. It would be very costly to directly measure all parameters for more than a limited number of soils. However, there was enough information in the Order II level soil surveys to estimate these parameters. Given the small scale of these soil surveys, it was not clear how close the survey's description for any soil series were to the conditions on the ground in any specific location. In addition, the soil surveys did not provide the level of detailed measurements required for FACETA parameters. In order to use the soil survey parameters such as field capacity and wilting point, they had to be estimated from the description of soil texture. Therefore, parameters determined from the soil surveys were estimates of estimates. The soil parameters determined from the soil cores taken from the study site were also indirectly estimated (e.g., field capacity was still estimated from soil texture). The difference and the point of comparison was how close the descriptions in the county soil survey were to the descriptions from on-site samples.

To determine the model soil parameters from the county soil survey, the description of the typical pedon for each modeled soil series was used (Ford & Pauls, 1980). The soil survey provided descriptions of layers including depths, representative values or ranges of values for proportions of sand, silt and clay of each layer, ranges for saturated hydraulic conductivity, percent organic content, and percent gravel. These values where then used to estimate field capacity, wilting point, and maximum available porosity using an available hydrology model called SPAW, for Soil – Plant – Atmosphere – Water. One component of this model was a calculator that estimated hydraulic characteristics from soil texture and a few other variables. Other available input variables in the SPAW calculator were percent organic matter, salinity, percent gravel, and compaction level. Outputs included wilting point, field capacity, maximum available porosity, and saturated hydraulic conductivity. Percentages of sand, silt, clay, organic matter, and gravel were estimated from the soil survey information and input into the SPAW calculator. Output from the calculator on saturate hydraulic conductivity typically did not agree with the ranges stated in the soil survey, so this parameter was selected from within the soil survey range. However, since the soil survey did not list values for wilting point or field capacity, the SPAW calculator values were used for these parameters. Clearly, there was a considerable amount of estimation and room for error in determining the required FACETA soil parameters. The data from the field soil cores included number of layers, depth of layers, representative proportions of sand, silt and clay for each layer, and percent organic matter. The soil model parameters estimated from these field samples were also estimated using the SPAW calculator, the only difference being that field samples analyzed were taken from the study site.

Additional soil parameters required were dry infiltration rate at the surface, fast flow fraction, and soil fertility. Fast flow fraction, which is a function of available macropores, was not considered since no reliable data were available upon which to base this parameter value. Dry infiltration rate at the surface was estimated based on the surface layer texture using the values implemented in the EPA's Soil and Water Assessment Tool (SWAT). Soil fertility was estimated using the range productivity values given in the soil survey for each soil series. Layers in the model did not necessarily coincide with discernible physical layers in the soil. The model has some requirements in determining depths of the top layers because of how seedlings can extract water and how solar evaporation from the soil work. Seedlings can only extract water from the first 20 cm of soil, so a modeled layer must end at that depth. Solar evaporation (as opposed to transpiration) in the model only affects the uppermost layer of soil. Based on a study of the impact of soil texture on the depth to which bare soil evaporation reaches (Wythers, Lauenroth, & Paruelo, 1999), the depths of the first layer were determined according to the soil texture class. For many of the soil series, the depth of the second layer was set to reach the 20-cm seedling root limit, except for soils with physical layer differences occurring prior to that depth. In those cases, the top three layers made up the soil accessible to seedlings.

Another factor to consider with soil depth is the total depth of all layers. Setting it too deeply in the model can lead to unrealistic water availability for some species. Unlike seedlings, water is accessible to established trees from all the layers of soil regardless of depth or species. Some species of trees grow tap roots or deep root systems; however, many species only grow roots in the upper parts of the soil. FACETA

soil parameters estimated from some of the soil series described in the soil survey as well as from the field soil cores are shown in Table 6.5. Because of the large number of soil series in the study area, the table only presents a few representative examples of the Greenbelt soils. Additionally, for the sake of brevity the table only lists the parameters for the top three soil layers.

Table 6.5

Soil Parameters from Selected Soil Series and Field Core Samples

Soil Parameter	Ovan Clay	Kaufman Clay	Birome Sandy Loam	Plot #9
Fertility (Mg/ha/yr)	18.75	18.75	11.25	11.25
Dry surface infiltration rate (cm/hr)	2.54	2.54	10.16	6.00
Saturated surface infiltration rate (cm/hr)	0.16	0.07	1.78	3.30
Layer 1 Depth (cm)	0-15.0	0-15.0	0-7.0	0-7.0
Layer 1 FC (cm)	6.20	7.04	1.17	1.41
Layer 1 WP (cm)	4.31	5.27	0.64	0.50
Layer 1 SHC (cm/hr)	0.16	0.07	1.78	3.30
Layer 1 AP (%)	50	55	39	44
Layer 2 Depth (cm)	15-20	15-20	7-20	7-20
Layer 2 FC (cm)	2.07	2.33	2.17	2.63
Layer 2 WP (cm)	1.44	1.75	1.20	0.94
Layer 2 SHC (cm/hr)	0.16	0.11	1.78	3.30
Layer 2 AP (%)	50	56	39	44
Layer 3 Depth (cm)	20-38.5	20-35.6	20-30	20-30
Layer 3 FC (cm)	7.64	7.29	2.84	2.02
Layer 3 WP (cm)	5.31	5.46	1.77	0.72
Layer 3 SHC (cm/hr)	0.16	0.11	0.30	3.30
Layer 3 AP (%)	50	56	41	44

Note: Soil parameters were estimated both from soil series descriptions and from measurements made on soil core samples taken from the study site. Ovan clay was the most prominent bottomland soil in the Greenbelt, and Kaufman clay was another prominent bottomland soil with even heavier clay content. Birome sandy loam was one of the more important soil series in the area that was associated with upland post oak development. Plot #9 soil core was taken from the slope of Wildcat Hill in a location that according to the soil survey map was in the Birome Sandy Loam. Significant differences between these two sets of parameters included higher dry and lower wet surface infiltration rates for the soil series. Parameters estimated from the soil series also differed by having lower field capacity (FC) and higher wilting point (WP) for the top two layers, which resulted in significantly less available water. Saturated hydraulic conductivity (SHC) was estimated lower from the soil series, and substantially lower for deeper layers. Estimates of available porosity (AP) were similar from both sources but slightly lower from the soil series. These differences in estimates essentially stemmed from the soil series indicating sandier soil at the upper layers and higher clay content at deeper layers than the field core indicated.

From the examples presented in Table 6.5, Ovan Clay and Kaufman Clay were two of the most prominent bottomland soils in the Greenbelt. Both were heavy clay soils, with Kaufman being the heavier soil. Birome Sandy Loam was one of the more important soil series in the area that was associated with upland post oak development. The soil core taken from Plot #9 was located on the slope of Wildcat Hill in a spot, which according to the soil survey map, was in the Birome Sandy Loam. While the parameters were similar between the estimates from the soil survey and the soil core, and they were much more similar to each other than to either of these two bottomland soils, there were some differences. Significant differences between these two sets of parameters included higher dry and lower wet surface infiltration rates for the soil series. Parameters estimated from the soil series also differed by having lower field capacity and higher wilting point for the top two layers, which resulted in significantly less available water in those layers for tree to draw from. Saturated hydraulic conductivity was estimated lower from the soil series and substantially lower for deeper layers. For most series layers, saturated hydraulic conductivity was given as a range of values with significant differences between the high and low ends of the ranges. Estimates of available porosity were similar from both sources but slightly lower from the soil series. These differences in estimates essentially stemmed from the soil series indicating sandier soil at the upper layers and higher clay content at deeper layers than the field core indicated.

Results: Landscape and Terrain Parameters

The landscape and terrain parameters required by FACETA include elevation, slope, aspect, and the two new parameters devised for FACETA, *flow accumulation* and

a parameter called the *run-on coefficient*. Given the relatively small change in elevation across the Greenbelt study area (less than 100 m difference between the highest and lowest points), and the subtropical latitude, the choice of elevation and aspect parameters potential taken from the study area were assumed to not greatly impact the model output. In FACETA's current implementation slope, as with aspect, is only used in the insulation component of the model. Slope, aspect, and elevation are all required inputs; however, differences in their effects were not investigated, at least not as direct inputs. Slope still plays a role in the input by being a part of the TWI. The parameters estimated for the terrain types, which are based on TWI classes and soil series, also use the distribution of slopes from each terrain type.

The two new parameters work together as one, but incorporating them into the model separately provides a little more flexibility. Flow accumulation is input as an integer and is intended to represent the typical upslope catchment area for a terrain type. It should be noted that the FACETA parameter flow accumulation is not necessarily the same thing as the geographic information systems (GIS) calculation by the same name, but it is based upon the GIS operation. The run-on coefficient is simply a multiplier applied to the flow accumulation. In its current implementation the run-on coefficient cannot be a negative value (i.e., a run-off coefficient), but it can be 0. For any rainfall event an additional amount of water that is equal to the product of the flow accumulation, run-on coefficient, and precipitation total. While these two parameters are implemented in order to capture the hydrological similarity resulting from surface and subsurface flow, incorporating the extra moisture into the rainfall total is a simple solution to avoid developing a more complicated hydrological model.

The flow accumulation parameter for any particular terrain type depends upon the TWI class of that terrain type. For the lowest TWI class, both the flow accumulation and run-on coefficient are set to 0, so no extra added moisture is added to this group. For the medium TWI group, the flow accumulation is set to be one fourth of the median flow accumulation value from across that soil series. The run-on coefficient is set to *c(1-MaxSlp)*, where *MaxSlp* is the maximum slope (expressed as the tangent of the slope angle) from that soil series. *C* is a scalar multiplier between 0 and 1 used in model calibration. The highest TWI class is given the flow accumulation value equal to the median flow accumulation from across the soil series, and the run-on coefficient is *c.* This scheme might seem somewhat arbitrary, but it allows differentiation of the three TWI class for every soil series through varying amounts of moisture, and it incorporates the characteristics of both flow accumulation and slope as determined from the soil series' distributions of values into the added moisture. Table 6.6 shows examples for these terrain parameters from two of the Greenbelt soil series, the upland Birome Sandy Loam, and the bottomland Ovan Clay.

Table 6.6

Terrain Parameters for Ovan and Birome Soils

Soil Type	TWI Group	Flow Accumulation Parameter	Run-on Coefficient	Extra Moisture Factor for Terrain Type
Ovan Clay	Low	0	0	0
Median FA=3	Medium	0.75	0.78c	0.585c
Max Slope = 0.22	High	3	3c	3c
Birome Sandy Loam	Low	0	0	0
Median FA=1	Medium	0.25	0.64c	0.16c
Max Slope=0.36	High	1	c	1c

Note: The terrain parameters flow accumulation and run-on coefficient for each terrain type from the distributions.

One problem devising a systematic algorithm for determining these parameters was that the process of testing different options resulted in too much extra moisture for the medium TWI group. Retrospectively, it became clear the medium group should be moisture-neutral, and the low TWI group if anything should be subject to a moisture penalty. Allowing a negative value for the run-on coefficient would have provided more flexibility in the set up. It would also have allowed the ability to make the low TWI class drier while keeping the medium TWI group neutral and enhancing the moisture level of the high TWI group, but that was not how the run-on coefficient was implemented in FACETA. To avoid the problem of too much simulated moisture, the soil types could have been divided into two TWI groups instead of three, with one moisture neutral and one moisture-enhanced, but three terrain groups aligned better with the variety of topographic positions that existed on the ground (e.g., depressions, flats, or slopes).

Conclusions: FACETA Environmental Parameters

FACETA environmental parameters include climatic statistics used to drive the weather model, soil parameters, and the new hydrologically based terrain parameters. An advantage of finding parameters for the weather model as compared to the biological parameters is that the parameters are nothing more than climatic statistics and can be determined from a statistically significant history of weather records. In this case, a history of 100 years of daily weather records was used. The data the parameters were based on were solid, so the question that was investigated was how good the assumptions were behind the weather simulator. The modeled weather output was compared with the weather history from which the parameters were derived.

Soil parameters were determined primarily from the USDA county soil survey, which gave physical descriptions of representative samples of the different soil series (Ford & Pauls, 1980). Two issues were raised. The descriptions in the soil survey were not necessarily the same physical parameters needed by FACETA. For example, the soil survey did not give information on field capacity or wilting point. These values could be estimated from other properties such as soil texture, but those estimates were based on regression relationships. Although soil texture may have been measured directly, the model parameter was based on estimates that involved assumptions regarding the regression relationships. Another issue was whether the soil series was too course-scaled to use for model parameters. These questions were investigated by comparing parameters estimated from the soil survey with ones that were estimated from the study site. Initial evaluation identified differences in the parameter values. It remains to be tested how much the model parameter differences impact the model output.

FACETA's new terrain parameters were implemented to simulate topographically based hydrologic similarity and differences. Their implementation within the model was simple in that it worked to add additional water whenever the model simulated rainfall. Devising a systematic approach to accomplish these similarities and differences using model parameters was tricky. The goal was to allow the average conditions across each terrain type impact how much, if any, extra moisture was added. In retrospect, the model would be more flexible towards this end if the run-on parameter could also be used as a moisture penalty or run-off parameter. That was not the case in its current implementation, but it is always the case for models like FACETA to change and evolve as they are tested, improved, and the assumptions behind them reconsidered.

CHAPTER 7

FACETA RESULTS

Methods

FACETA simulation runs were executed using various terrain types and tested and analyzed for validity. Model output was examined at three levels: weather and climate, soil moisture dynamics, and forest simulation. In the early stages of model development and parameter calibration, it was best to reduce and simplify where possible. Complexity could be added as the model was verified, corrections were made as needed, and model parameters were fine-tuned. For the initial simulations, species were limited to only those species with the best set of model parameters. The species selected represented some of the different ecological roles in order to draw conclusions on model output, and this could be accomplished with as few as three species. Initial simulations with FACETA included six of the candidate species: cottonwood, post oak, blackjack oak, green ash, sugarberry, and black willow. All of these species with the exception of black willow had growth rate parameters based on tree ring measurements, which was the primary reason they were included in the model. Species with incomplete or conflicting silvics information were left off the list, as well as species such as swamp privet that did not fit well into the model's growth assumptions. Although no tree rings were measured for it, black willow was included to represent the truly swamp tree role. Post oak and blackjack oak provide the best two representatives of the upland forests, and green ash and sugarberry were two of the three best representatives of the Greenbelt bottomland forest. Cottonwood was the fastest grower and the one that was most considered a pioneer species. Sugarberry was also a good,

although probably not the best species from the list to represent those that could grow in a variety of positions. Cedar elm might have been the best species for the generalist role, except at the time there were too many uncertainties in its species parameters. Figure 7.1 shows the input file for the species parameters. All parameters in this file that were used, as well as some that were not were discussed in Chapter 5.

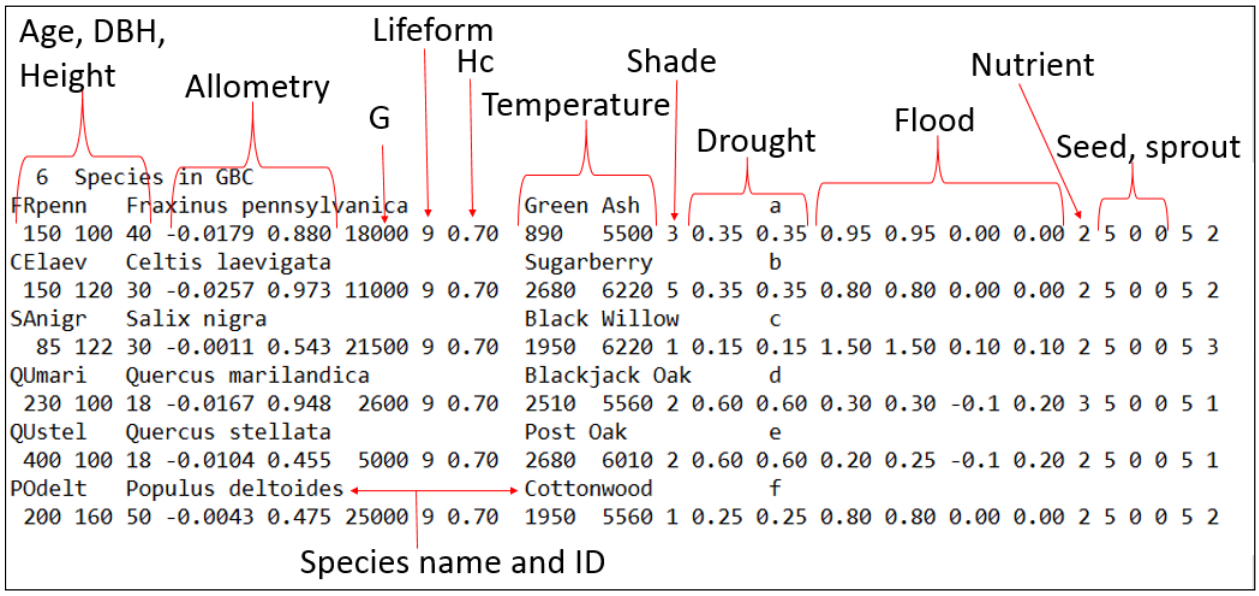

Figure 7.1. FACETA species input file. FACETA input file for species parameters. The last two parameters/columns in the file, hurricane susceptibility and forest type, were not discussed in the previous sections because they were not used. All the other parameters were described in Chapter 5.

Comparisons of soil types and terrain types for early simulations were limited to the two most common soils on opposite ends of the soil spectrum: Birome sandy loam and Ovan clay. Also included in the early runs were the soil parameters estimated from the soil core sample in Plot #9, which according to the soil survey map belonged to the Birome sandy loam series (Ford & Pauls, 1980). This research study was initially limited to these two contrasting terrain cases in order to provide more focus on the new terrain parameters themselves. Figure 7.2 shows the FACETA input file for the soil parameters. The soil input file contains the parameters for all of the modeled soil types. At the top of the parameter list for each soil type are the number of layers, soil fertility, fast flow

fraction, and dry and wet surface infiltration rates. Underneath those are the parameters for each soil layer, including its depth, field capacity, wilting point, and saturated hydraulic conductivity.

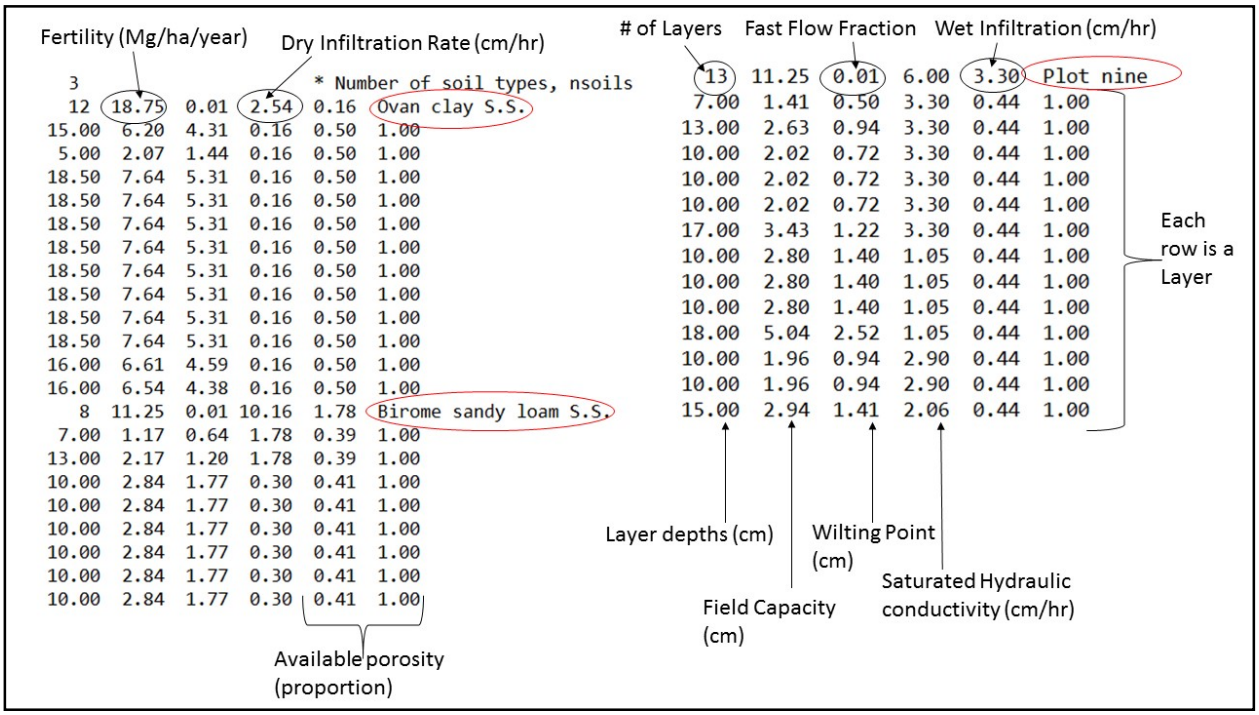

Figure 7.2. FACETA soil parameter input file. Input file for FACETA soil parameters containing parameters for three soils: Ovan clay soil series, Birome sandy loam soil series, and Plot #9 soil core. The actual input file had all of the simulated soil types arranged in one column; the parameters were rearranged for this figure for display purposes.

There were several other input files required for FACETA, with eight files in its current version. The exact number and configuration of input files needed has changed as the model has evolved, and some involve simulation control functions such as defining the plot size, selecting output to be printed, and setting global constants or initial conditions. Two other input files that needed to be described were the climate file and the terrain file (Fig. 7.3 and Fig. 7.4). The climate file had inputs for the solar radiation model, such as longitude and latitude, and the monthly solar radiation averages. It also contained the inputs for the weather generator, such as the wet/dry

conditional transition probabilities used in the rainfall occurrence in the Markov chain model, the daily rainfall statistics used to estimate the shape and scale parameters of the rainfall-amount gamma distribution model, and the monthly temperature statistics. The terrain input file contained the new flow accumulation and run-on coefficient parameters, as well as the parameters for slope, aspect, and soil type. Some parameters in these files were not discussed because they were not used in this study. For example, any parameters involving hurricanes, lapse rates, ponding, or berm heights were incorporated into FACETA for use in other scenarios, and these were bypassed or negated in this application.

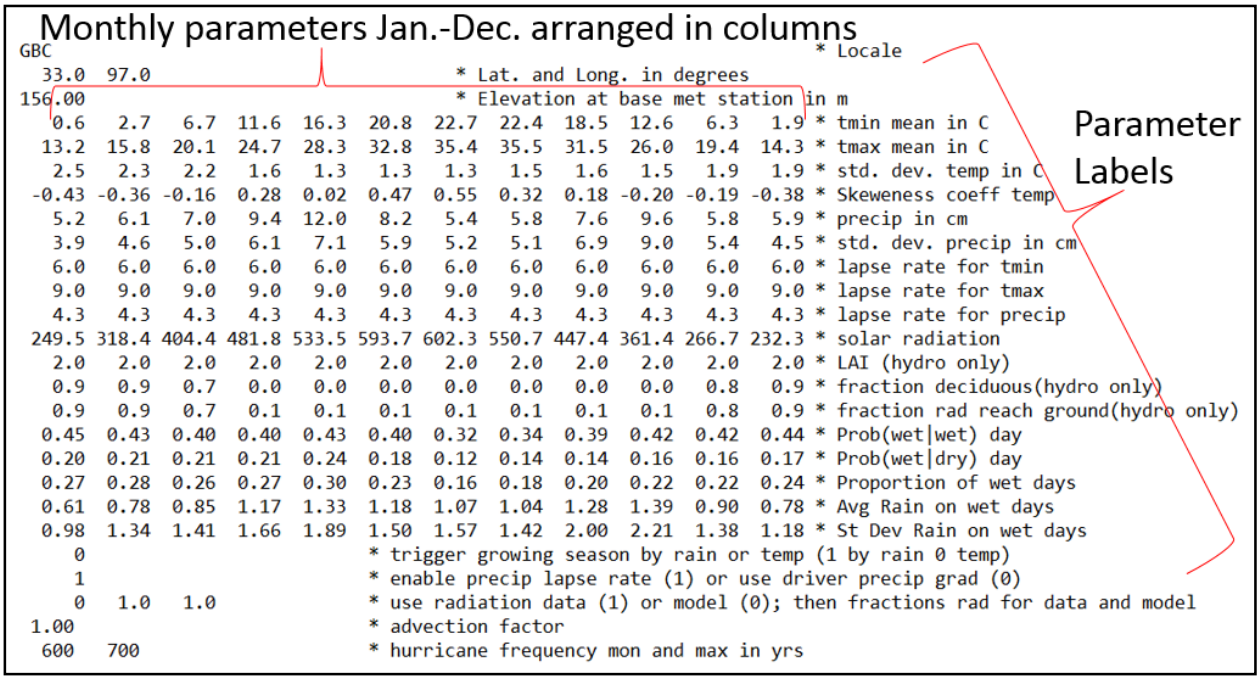


```
GBC                                                          * Locale
  33.0  97.0                          * Lat. and Long. in degrees
156.00                                * Elevation at base met station in m
   0.6   2.7   6.7  11.6  16.3  20.8  22.7  22.4  18.5  12.6   6.3   1.9 * tmin mean in C
  13.2  15.8  20.1  24.7  28.3  32.8  35.4  35.5  31.5  26.0  19.4  14.3 * tmax mean in C
   2.5   2.3   2.2   1.6   1.3   1.3   1.3   1.5   1.6   1.5   1.9   1.9 * std. dev. temp in C
 -0.43 -0.36 -0.16  0.28  0.02  0.47  0.55  0.32  0.18 -0.20 -0.19 -0.38 * Skeweness coeff temp
   5.2   6.1   7.0   9.4  12.0   8.2   5.4   5.8   7.6   9.6   5.8   5.9 * precip in cm
   3.9   4.6   5.0   6.1   7.1   5.9   5.2   5.1   6.9   9.0   5.4   4.5 * std. dev. precip in cm
   6.0   6.0   6.0   6.0   6.0   6.0   6.0   6.0   6.0   6.0   6.0   6.0 * lapse rate for tmin
   9.0   9.0   9.0   9.0   9.0   9.0   9.0   9.0   9.0   9.0   9.0   9.0 * lapse rate for tmax
   4.3   4.3   4.3   4.3   4.3   4.3   4.3   4.3   4.3   4.3   4.3   4.3 * lapse rate for precip
 249.5 318.4 404.4 481.8 533.5 593.7 602.3 550.7 447.4 361.4 266.7 232.3 * solar radiation
   2.0   2.0   2.0   2.0   2.0   2.0   2.0   2.0   2.0   2.0   2.0   2.0 * LAI (hydro only)
   0.9   0.9   0.7   0.0   0.0   0.0   0.0   0.0   0.0   0.0   0.8   0.9 * fraction deciduous(hydro only)
   0.9   0.9   0.7   0.1   0.1   0.1   0.1   0.1   0.1   0.1   0.8   0.9 * fraction rad reach ground(hydro only)
  0.45  0.43  0.40  0.40  0.43  0.40  0.32  0.34  0.39  0.42  0.42  0.44 * Prob(wet|wet) day
  0.20  0.21  0.21  0.21  0.24  0.18  0.12  0.14  0.14  0.16  0.16  0.17 * Prob(wet|dry) day
  0.27  0.28  0.26  0.27  0.30  0.23  0.16  0.18  0.20  0.22  0.22  0.24 * Proportion of wet days
  0.61  0.78  0.85  1.17  1.33  1.18  1.07  1.04  1.28  1.39  0.90  0.78 * Avg Rain on wet days
  0.98  1.34  1.41  1.66  1.89  1.50  1.57  1.42  2.00  2.21  1.38  1.18 * St Dev Rain on wet days
     0                        * trigger growing season by rain or temp (1 by rain 0 temp)
     1                        * enable precip lapse rate (1) or use driver precip grad (0)
     0   1.0   1.0            * use radiation data (1) or model (0); then fractions rad for data and model
  1.00                        * advection factor
   600   700                  * hurricane frequency mon and max in yrs
```

Figure 7.3. FACETA climate and weather input file. FACETA climate parameter input file. This file contained weather and climate statistics that were used to parameterize the solar radiation, temperature, and rainfall models. The parameters were estimated and entered into the model for each month. Each column in the input file are the parameters for one of the months from January through December. Labels for each row of parameters are on the file on the left side.

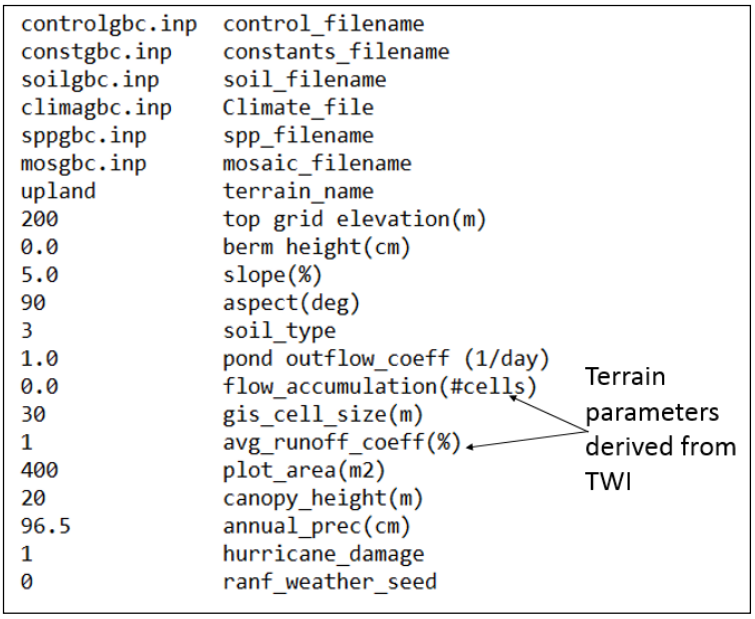

Figure 7.4. FACETA terrain input file. Along with some other parameters, this file was used to input slope, elevation, aspect, and the two new terrain parameters, flow accumulation and run-on coefficient. It contained the random number seed that allowed initiation of different realizations of modeled weather series (the same random seed will produce the same string of weather). Labels for the different parameters are on the file in the left column.

Results: Weather and Climate

A common problem found in daily weather simulation is that model output statistics do not always match well with the climate data at various timescales. With that in mind, the FACETA weather output was analyzed at three different timescales: daily, monthly, and annual. A single 100-year realization of simulated weather was used to compare with the 100-year historical record. One of the input parameters was a random weather seed, which could be changed for each simulation run to produce a different series of weather. While each of these realizations was different from each other, since they were all generated by the same probabilistic number generators they were statistically equivalent. To confirm this, a number of simulation runs using different random seeds were compared, and the results were relatively consistent. Each random seed produced a unique series of weather that was distinguishable from all other runs,

but statistically the differences were minor. As an example, the totals of annual precipitation for two runs using different random seeds are presented in Figure 7-5. Each of these runs was for a 100-year period.

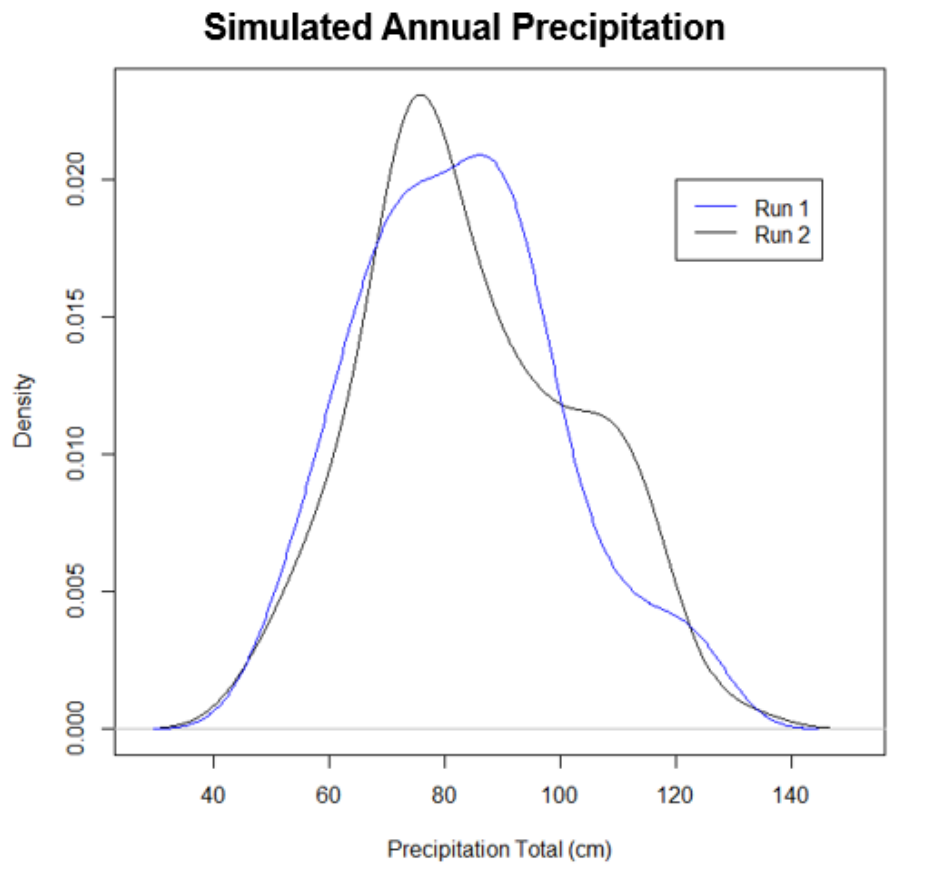

Run 1
Minimum = 48.28
Median = 82.35
Maximum = 126.00
Mean = 82.84
SD = 17.57

Run 2
Minimum =47.50
Median = 81.08
Maximum = 131.70
Mean = 84.61
SD = 18.32

Fail to reject Run 1 and Run 2 are from the same distribution, Mann-Whitney U test, p=.55

Figure 7.5. Annual precipitation totals from different simulation runs. Different realizations of simulated weather generated using different random number seeds were compared for statistical difference. At the annual timescale, the results were statistically equivalent. Different simulation runs also matched well at the monthly timescale. The graphs used in this example were the kernel densities estimated from the histograms.

Precipitation results were analyzed separately from temperature, and temperature results were only analyzed at the annual scale and only through the total growing degree days (GDD). Precipitation was parameterized at the monthly scale but using daily data. The output of the precipitation model was in daily time steps, and precipitation at the daily timescale was examined first.

The daily precipitation model used the two-step approach with the Markov chain model determining the sequence of rainy and dry days for each month. On wet days, the total amount of rain received was drawn from a gamma distribution. Wet day referred to a day that any amount of precipitation was generated, and dry day meant there was no precipitation. The Markov model parameters were the conditional transition probabilities estimated from proportions of wet days following wet days and wet days following dry days for each month over a long history of records. The transition probabilities were estimated for each month of the year separately. Similarly, the shape and scale parameters defining the gamma distribution were estimated from the mean and variance of the amounts of rain received on wet days for each month separately. Therefore, the simulated daily rainfall pattern for each of the months was examined independently. Resulting precipitation across all months was analyzed at the annual scale. On the daily time scale, the simulated weather was analyzed through the distributions of rainfall amounts occurring on wet days for each month and comparing those distributions with real weather history. The sequence of wet and dry days could have been considered a daily process, but it was analyzed at the monthly scale.

Due to the nature of the distributions of daily rainfall amounts, it was somewhat difficult to do a visual comparison. However, histograms and estimated kernel densities for both real and simulated weather were graphed and were compared (Fig. 7.6). Differences for some months were apparent in the graphs, but they were subtle. Generally, the distributions of simulated and real daily rain amounts compared fairly well. Using a Mann-Whitney U test to compare the distributions of real versus simulated daily rain totals, seven of the months were rejected as coming from the same

distribution (α=0.05). The two months selected as examples for closer examination included one of the worst fits and one of the better fits, February and June, respectively. Comparisons of these two months are presented in Figure 7.6 and Table 7.1.

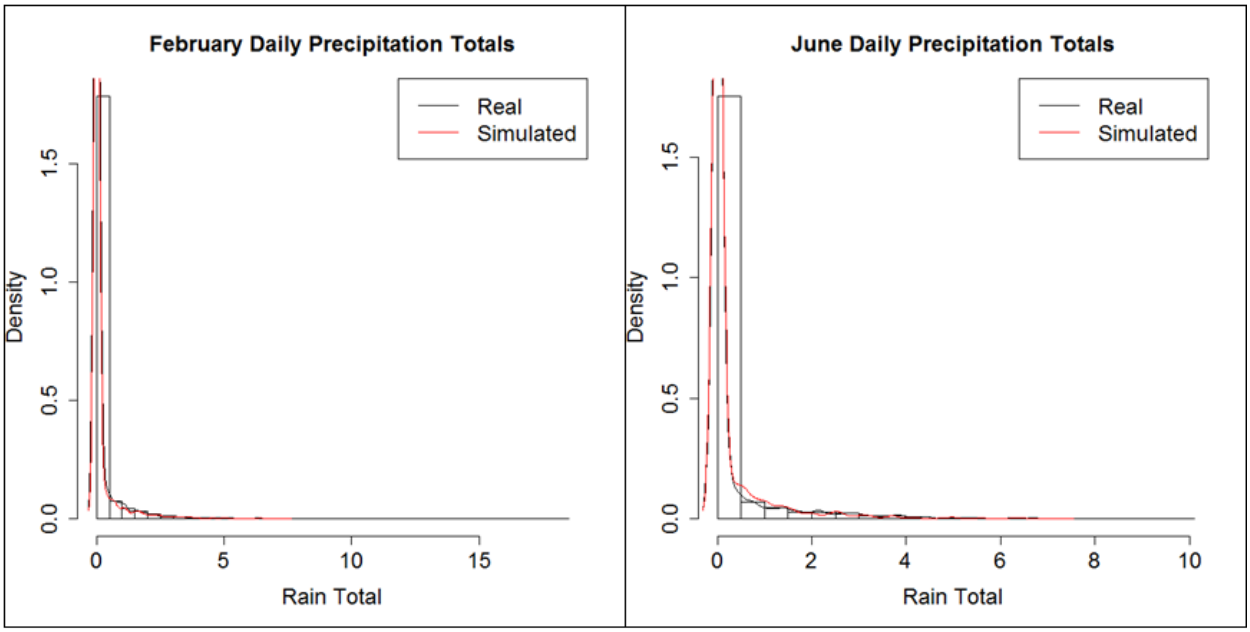

Figure 7.6. Daily simulated and real rainfall amounts for February and June. The graphs show the estimated kernel densities from the real daily precipitation amounts (black) and the simulated amounts (red). The histogram was graphed from the real rainfall data. The FACETA rainfall generator captured daily rainfall patterns well in June, but not as well in February. Simulated February daily rainfall was less than real February daily rainfall. Rainfall totals are in centimeters. The number of simulation years is 100; thus, the number of February days is N=2800. The weather history used spanned 100 years, but records during that time were not complete. Only one record of precipitation was missing during the month of February. Because of leap year (which is not accounted for in FACETA), N=2824 for the real weather data. The simulated and rainfall daily rainfall amounts were much closer for the month of June. The real weather data had a slightly longer tail, but the distributions were too close to be differentiated by the Mann-Whitney U test. In June, N=3000 for simulated rain and N=2970 for real rain.

A comparison of the higher percentiles and maximum values showed that the simulator substantially underestimated large rainfall events in February. Comparing the means showed that the total amount of simulated rainfall in February was also underestimated; however, the mean on simulated wet days was higher than the mean on real wet days. Therefore, the real February weather had on average more wet days with smaller amounts than simulated February weather, but the real weather also had much larger extreme rain events. Subtle differences were seen in the graphs of

estimated kernel densities, but primarily visible in the graph was the extended tail of the real weather as compared to simulated (Fig. 7.6). Results from the Mann-Whitney U test rejected that the real and simulated daily February rainfall amounts came from the same distribution ($p<10^{-8}$).

Table 7.1

Simulated and Real Daily Rainfall Summaries for February and June

Test	February	June
Simulated	Min 1st Med 3rd Max 0.00 0.00 0.00 0.00 7.32 90th percentile = 0.39 95th percentile = 1.15 Mean = 0.18 Mean on wet days = 0.84 *SD* on wet days = 1.19	Min 1st Med 3rd Max 0.00 0.00 0.00 0.00 7.25 90th percentile = 0.79 95th percentile = 1.62 Mean = 0.26 Mean on wet days = 1.09 *SD* on wet days = 1.29
Real	Min 1st Med 3rd Max 0.00 0.00 0.00 0.01 18.06 90th percentile = 0.56 95th percentile = 1.39 Mean = 0.22 Mean on wet days = 0.78 *SD* on wet days = 1.34	Min 1st Med 3rd Max 0.00 0.00 0.00 0.00 9.80 90th percentile = 0.76 95th percentile = 2.05 Mean = 0.27 Mean on wet days = 1.18 *SD* on wet days = 1.49
Mann-Whitney U Test	Reject the simulated and real daily rainfall totals come from the same distribution, $p<10^{-8}$	Reject that the simulated and real daily rainfall totals come from the same distribution, $p=.74$

Note: Daily rainfall summary statistics for February and June, for both real weather data and the FACETA weather simulator. The June simulation is very close to the real June rainfall amounts, but the February simulations fall short. The mean and standard deviation calculated only from wet days from the real weather data are the input parameters for the gamma distribution that models the daily rainfall amounts.

In June, the distributions between the simulated and real amounts were much closer. The tails compared much better for June, but the model slightly underestimated the highest rainfall. The means were very close, indicating the total amounts for June compared well. The average amount of rain on real June wet days was a little higher than simulated, and the largest daily amounts were also a little higher, but overall the

simulated and real June daily rain compared well. The Mann-Whitney U test failed to determine that they came from different distributions (p = .74).

Although the simulated and real daily rainfall amounts did not test statistically as coming from the same distribution for all months, the daily rainfall generator appeared to capture the general characteristics of daily rainfall amounts well for most months (Table 7.2). For most months, the simulator followed the highs, percentiles, and means for daily rain amounts well. The graphs for the estimated kernel densities appeared similar, with the only apparent difference in some months being the length of the tails. For some months, for example April, the model was remarkably good. Some months had a small difference in the overall means, in which case there were also differences in the total amount of rain for that month. The largest such difference was in February at 0.04 cm. The difference in the daily mean implied a difference in total rainfall of 1.2 cm for February. Otherwise, it was unclear at this scale how the statistical differences in the daily rainfall amount distributions affected monthly and annual time scales.

The daily rainfall totals were evaluated for sensitivity to gamma distribution input parameters, the mean and standard deviation of the rain amounts on wet days. Small changes in these values did not substantially alter the rainfall output. Changes of approximately 10% to either of these parameters resulted in roughly the same amount of change in the output to the same statistic. The most noticeable impact from either of these changes was to the maximum value as a result of changing the input standard deviation parameter. An increase of 10% to the parameter resulted in an increase of approximately 30% to the maximum daily rainfall amount over 100 years of simulation.

General characteristics of the distributions of simulated amounts were not very sensitive to changes in the gamma distribution parameters.

Table 7.2

Simulated and Real Daily Rainfall Summaries

Month	Simulated 90^{th}, 95^{th}, 100^{th} percentiles Mean (μ), Wet day mean (μ_R), Wet day *SD* (σ_R)	Real 90^{th}, 95^{th}, 100^{th} percentiles Mean (μ), Wet day mean (μ_R), Wet day *SD* (σ_R)	Mann-Whitney U, $\alpha = 0.05$
January	$90^{th} = 0.37$, $95^{th} = 0.99$, Max. = 7.96 $\mu = 0.16$, $\mu_W = 0.69$, $\sigma_W = 1.00$	$90^{th} = 0.41$, $95^{th} = 1.09$, Max. = 9.47 $\mu = 0.16$, $\mu_W = 0.61$, $\sigma_W = 0.98$	Reject same, p=.0009
February	90^{th} =0.39, 95^{th} =1.15, Max.=7.32 $\mu = 0.18$, $\mu_W = 0.84$, $\sigma_W = 1.19$	$90^{th} = 0.56$, $95^{th} = 1.39$, Max. = 18.06 $\mu = 0.22$, $\mu_W = 0.78$, $\sigma_W = 1.34$	Reject same, $p=10^{-8}$
March	$90^{th} = 0.54$, $95^{th} = 1.61$, Max. = 16.55 $\mu = 0.25$, $\mu_W = 1.05$, $\sigma_W = 1.64$	$90^{th} = 0.56$, $95^{th} = 1.47$, Max. = 12.90 $\mu = 0.22$, $\mu_W = 0.85$, $\sigma_W = 1.42$	Fail to reject, p=.058
April	$90^{th} = 0.86$, $95^{th} = 2.10$, Max. = 20.70 $\mu = 0.31$, $\mu_W = 1.23$, $\sigma_W = 1.74$	$90^{th} = 0.97$, $95^{th} = 2.16$, Max. = 20.52 $\mu = 0.31$, $\mu_W = 1.17$, $\sigma_W = 1.66$	Fail to reject, p=.246
May	$90^{th} = 1.17$, $95^{th} = 2.73$, Max. = 20.30 $\mu = 0.41$, $\mu_W = 1.50$, $\sigma_W = 2.08$	$90^{th} = 1.32$, $95^{th} = 2.54$, Max. = 18.54 $\mu = 0.40$, $\mu_W = 1.33$, $\sigma_W = 1.89$	Fail to reject, p=.052
June	$90^{th} = 0.79$, $95^{th} = 1.62$, Max. = 7.25 $\mu = 0.26$, $\mu_W = 1.09$, $\sigma_W = 1.29$	$90^{th} = 0.76$, $95^{th} = 2.05$, Max. = 9.80 $\mu = 0.27$, $\mu_W = 1.18$, $\sigma_W = 1.50$	Fail to reject, p=.74
July	$90^{th} = 0.17$, $95^{th} = 0.88$, Max. = 12.10 $\mu = 0.16$, $\mu_W = 1.14$, $\sigma_W = 1.64$	$90^{th} = 0.20$, $95^{th} = 1.14$, Max. = 10.67 $\mu = 0.17$, $\mu_W = 1.07$, $\sigma_W = 1.57$	Reject same, p=.015
August	$90^{th} = 0.36$, $95^{th} = 1.21$, Max. = 12.30 $\mu = 0.18$, $\mu_W = 1.09$, $\sigma_W = 1.43$	$90^{th} = 0.31$, $95^{th} = 1.19$, Max. = 10.26 $\mu = 0.18$, $\mu_W = 1.04$, $\sigma_W = 1.42$	Fail to reject, p=.353
September	$90^{th} = 0.33$, $95^{th} = 1.40$, Max. = 12.02 $\mu = 0.24$, $\mu_W = 1.38$, $\sigma_W = 2.02$	$90^{th} = 0.51$, $95^{th} = 1.58$, Max. = 14.28 $\mu = 0.26$, $\mu_W = 1.28$, $\sigma_W = 2.00$	Reject same, p=.003
October	$90^{th} = 0.52$, $95^{th} = 1.79$, Max. = 17.82 $\mu = 0.28$, $\mu_W = 1.41$, $\sigma_W = 2.14$	$90^{th} = 0.69$, $95^{th} = 2.01$, Max. = 15.88 $\mu = 0.31$, $\mu_W = 1.39$, $\sigma_W = 2.22$	Reject same, p=.025

(table continues)

Table 7.2 *(continued)*

Month	Simulated 90^{th}, 95^{th}, 100^{th} percentiles Mean (μ), Wet day mean (μ_R), Wet day *SD* (σ_R)	Real 90^{th}, 95^{th}, 100^{th} percentiles Mean (μ), Wet day mean (μ_R), Wet day *SD* (σ_R)	Mann-Whitney U, α = 0.05
November	90^{th} = 0.39, 95^{th} = 1.13, Max. = 12.02 μ = 0.19, μ_W = 1.00, σ_W = 1.56	90^{th} = 0.43, 95^{th} = 1.37, Max. = 11.53 μ = 0.20, μ_W = 0.90, σ_W = 1.38	Reject same, *p*=.034
December	90^{th} = 0.37, 95^{th} = 1.10, Max. = 9.13 μ = 0.17, μ_W = 0.83, σ_W = 1.22	90^{th} = 0.42, 95^{th} = 1.23, Max. = 7.52 μ = 0.19, μ_W = 0.78, σ_W = 1.18	Reject same, *p*=.003

Note: Simulated daily rainfall amounts for each month were compared with real daily amounts. While for the majority of the months the data and the simulated amounts did not test as coming from the same distribution (Mann-Whitney U test, α=0.05), in general the simulator does a good job capturing the characteristics of daily rainfall amounts for most months.

Two precipitation characteristics were examined at the monthly time scale, the number or proportion of wet days and the total precipitation amounts for each month. The proportion of wet days was impacted only by the transition probability parameters used in the Markov model, and the total amount of rain per month depended on both the Markov parameters and the gamma distribution parameters as both the frequency of rain and amount per event impacted the monthly totals. For monthly comparisons, the same 100-year series of simulated weather was compared with monthly historical data. The monthly historical data came from the same 100-year dataset, but any months with missing records were excluded from the analysis. The smallest number of years for any of the months was N=93.

The distributions of proportions of wet days were much closer to normal than the daily rainfall amounts and were much easier to compare visually. Histograms of both real and simulated weather were graphed and overlaid with the estimated kernel densities, summary statistics were compared, and Mann-Whitney U test calculated. The graphs from all of the months were similar but with some differences. Four months had

distributions that could be rejected as being the same: January, February, September, and December (Table 7.3).

Table 7.3

Simulated and Real Proportion Wet Days Summaries

Month	Simulated Minimum, Median, and Maximum Mean (μ) and *SD* (σ)	Real Minimum, Median, and Maximum Mean (μ) and *SD* (σ)	Mann-Whitney U, α = 0.05
January	Min. = 0.03, Med. = 0.23, Max. = 0.42 μ = 0.23, σ = 0.09	Min. = 0.00, Med. = 0.27, Max. = 0.65 μ = 0.27, σ = 0.14	Reject same, *p*=.02
February	Min. = 0.03, Med. = 0.21, Max. = 0.46 μ = 0.21, σ = 0.09	Min. = 0.03, Med. = 0.21, Max. = 0.59 μ = 0.28, σ = 0.12	Reject same, *p*=.0001
March	Min. = 0.06, Med. = 0.23, Max. = 0.48 μ = 0.24, σ = 0.09	Min. = 0.07, Med. = 0.26, Max. = 0.52 μ = 0.26, σ = 0.10	Fail to reject, *p*=.058
April	Min. = 0.00, Med. = 0.23, Max. = 0.53 μ = 0.25, σ = 0.10	Min. = 0.03, Med. = 0.23, Max. = 0.67 μ = 0.27, σ = 0.12	Fail to reject, *p*=.68
May	Min. = 0.10, Med. = 0.26, Max. = 0.55 μ = 0.27, σ = 0.10	Min. = 0.03, Med. = 0.29, Max. = 0.61 μ = 0.30, σ = 0.12	Fail to reject, *p*=.06
June	Min. = 0.03, Med. = 0.23, Max. = 0.47 μ = 0.23, σ = 0.10	Min. = 0.03, Med. = 0.23, Max. = 0.57 μ = 0.23, σ = 0.11	Fail to reject, *p*=.47
July	Min. = 0.00, Med. = 0.13, Max. = 0.35 μ = 0.14, σ = 0.07	Min. = 0.00, Med. = 0.16, Max. = 0.42 μ = 0.16, σ = 0.09	Fail to reject, *p*=.17
August	Min. = 0.00, Med. = 0.16, Max. = 0.52 μ = 0.16, σ = 0.09	Min. = 0.00, Med. = 0.16, Max. = 0.52 μ = 0.18, σ = 0.10	Fail to reject, *p*=.22
September	Min. = 0.00, Med. = 0.17, Max. = 0.37 μ = 0.17, σ = 0.08	Min. = 0.03, Med. = 0.20, Max. = 0.50 μ = 0.20, σ = 0.09	Reject same, *p*=.043
October	Min. = 0.03, Med. = 0.19, Max. = 0.52 μ = 0.20, σ = 0.09	Min. = 0.00, Med. = 0.19, Max. = 0.58 μ = 0.22, σ = 0.11	Fail to reject, *p*=.34
November	Min. = 0.00, Med. = 0.20, Max. = 0.40 μ = 0.20, σ = 0.08	Min. = 0.00, Med. = 0.20, Max. = 0.53 μ = 0.22, σ = 0.11	Fail to reject, *p*=.10

(table continues)

Table 7.3 *(continued)*

Month	Simulated Minimum, Median, and Maximum Mean (μ) and *SD* (σ)	Real Minimum, Median, and Maximum Mean (μ) and *SD* (σ)	Mann-Whitney U, α = 0.05
December	Min. = 0.03, Med. = 0.21, Max. = 0.42 μ = 0.21, σ = 0.08	Min. = 0.03, Med. = 0.23, Max. = 0.58 μ = 0.24, σ = 0.11	Reject same, *p*=.03

Note: Simulated and real weather were compared at the monthly timescale through the proportion of wet days for each month. The simulator generally captured the characteristic well; however, it underestimated the mean, variance, and maximum proportion of wet days for almost every month, implying that the simulator produced fewer and less persistent wet periods. The distributions for all but four months were not rejected as being the same. (Mann-Whitney U test, α=0.05).

One commonality between the four months with different distributions was the simulated weather underestimated the maximum, mean, and variance of the proportion of wet days, implying that real weather can result in longer, more persistent wet periods than simulated. The model underestimated proportions of wet days to some degree for all of the months. Considering the North Texas climate, one of the most important factors impacting plant growth is dry periods, which can be particularly prevalent in the summer, and droughts. While it was possible, it was not necessarily the case that an underestimation of wet periods was linked to the model's ability to simulate dry periods or droughts accurately. Droughts are defined by more than just the proportion or number of dry days, but also by their persistence, whether or not wet days are interspersed with dry days, and by the amount of rain on wet days. While not exact fits, the simulated proportions of wet days compared fairly well with the real weather.

As with the daily rain amounts, February was an example of a month where simulated and real proportions of wet days did not compare as well, while for June the comparison was good (Fig. 7.7; Fig. 7.8). However, there was no apparent reason that these two should be linked. Proportions of wet days depended only on the Markov model, while daily rainfall amounts depended only on the gamma distribution.

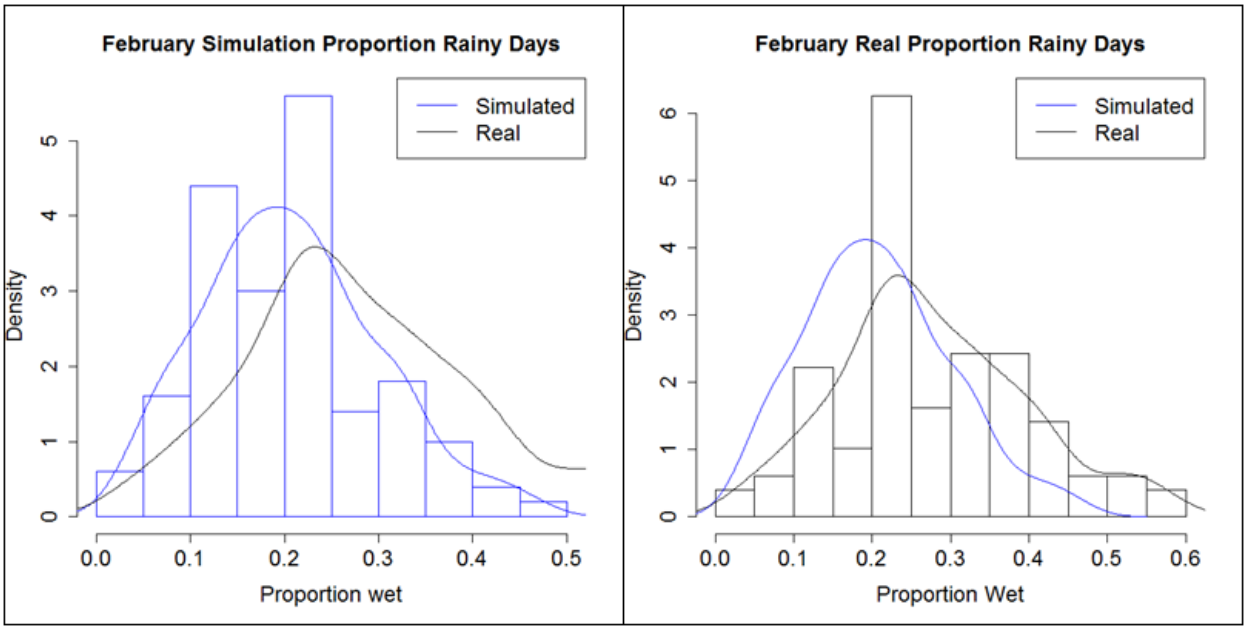

Figure 7.7. Simulated and real proportions of wet days for February. Simulated (left) and real (right) proportions of wet days were compared for each month visually through the graphs of their histograms and estimated kernel densities. The February simulated weather underestimated the proportions of wet days. The histogram on the left is graphed from the simulated weather, and the histogram on the right from the real weather. In both graphs, simulated weather is in blue and real weather in black.

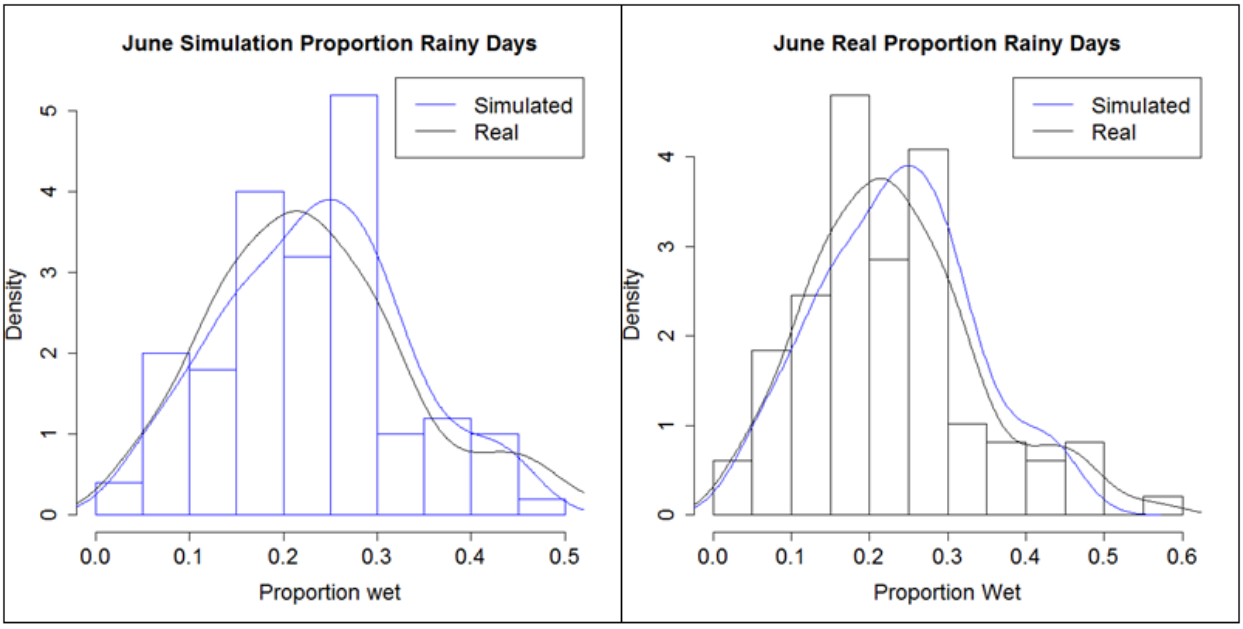

Figure 7.8. Simulated and real proportions of wet days for June. Simulated (left) and real (right) proportions of wet days were compared for each month visually through the graphs of their histograms and estimated kernel densities. The simulation for June was very close in proportions of wet days to the real weather. The histogram on the left was graphed from the simulated weather, and the histogram on the right from the real weather. In both graphs, simulated weather is in blue and real weather in black.

Total rainfall for each month was compared in a similar way as proportions of wet days. In general, simulated and real weather compared very well for monthly rainfall totals. Distributions from all 12 months could not be rejected as being the same (Mann-Whitney U test, α=0.05). Graphs of histograms and kernel densities between real and simulated monthly totals compared well, and means and medians were all fairly close (Table 7.4; Fig. 7.9).

Table 7.4

Simulated and Real Total Monthly Rainfall Summaries

Month	Simulated Minimum, Median, and Maximum Mean (μ) and *SD* (σ)	Real Minimum, Median, and Maximum Mean (μ) and *SD* (σ)	Mann-Whitney U, α = 0.05
January	Min. = 0.19, Med. = 3.70, Max. = 13.61 μ = 4.54, σ = 3.16	Min. = 0.00, Med. = 4.47, Max. = 18.11 μ = 5.20, σ = 3.87	Fail to reject, *p*=.34
February	Min. = 0.01, Med. = 4.43, Max. = 14.58 μ = 5.03, σ = 3.41	Min. = 0.10, Med. = 5.09, Max. = 22.02 μ = 6.08, σ = 4.64	Fail to reject, *p*=.18
March	Min. = 0.12, Med. = 6.50, Max. = 19.51 μ = 7.31, σ = 4.43	Min. = 0.15, Med. = 5.89, Max. = 28.14 μ = 6.98, σ = 5.04	Fail to reject, *p*=.35
April	Min. = 0.00, Med. = 7.32, Max. = 24.65 μ = 8.31, σ = 5.43	Min. = 0.05, Med. = 8.82, Max. = 30.96 μ = 9.43, σ = 6.14	Fail to reject, *p*=.20
May	Min. = 0.97, Med. = 11.17, Max. = 40.50 μ = 12.18, σ = 7.30	Min. = 1.36, Med. = 10.86, Max. = 42.56 μ = 11.97, σ = 7.06	Fail to reject, *p*=.95
June	Min. = 0.01, Med. = 7.49, Max. = 23.86 μ = 8.74, σ = 5.40	Min. = 0.05, Med. = 7.42, Max. = 32.05 μ = 8.22, σ = 5.83	Fail to reject, *p*=.42
July	Min. = 0.00, Med. = 4.01, Max. = 25.20 μ = 4.79, σ = 4.31	Min. = 0.00, Med. = 4.14, Max. = 34.49 μ = 5.40, σ = 5.19	Fail to reject, *p*=.50
August	Min. = 0.00, Med. = 4.89, Max. = 19.07 μ = 5.78, σ = 4.42	Min. = 0.00, Med. = 4.92, Max. = 31.28 μ = 5.80, σ = 5.14	Fail to reject, *p*=.78
September	Min. = 0.00, Med. = 6.81, Max. = 31.22 μ = 8.10, σ = 5.92	Min. = 0.03, Med. = 5.64, Max. = 34.47 μ = 7.61, σ = 6.87	Fail to reject, *p*=.21

(table continues)

Table 7.4 *(continued)*

Month	Simulated Minimum, Median, and Maximum Mean (μ) and *SD* (σ)	Real Minimum, Median, and Maximum Mean (μ) and *SD* (σ)	Mann-Whitney U, α = 0.05
October	Min. = 0.03, Med. = 6.74, Max. = 41.06 μ = 8.97, σ = 7.83	Min. = 0.00, Med. = 7.77, Max. = 59.59 μ = 9.56, σ = 9.04	Fail to reject, *p*=.76
November	Min. = 0.00, Med. = 4.92, Max. = 19.22 μ = 5.76, σ = 4.09	Min. = 0.00, Med. = 4.29, Max. = 30.81 μ = 5.84, σ = 5.39	Fail to reject, *p*=.46
December	Min. = 0.15, Med. = 4.78, Max. = 20.91 μ = 5.72, σ = 4.22	Min. = 0.05, Med. = 4.69, Max. = 21.41 μ = 5.85, σ = 4.47	Fail to reject, *p*=.99

Note: Simulated and real weather were compared at the monthly timescale through the total rainfall for each month. The simulator does a very good job capturing this characteristic. It underestimates extremely large monthly totals, but is very close in its central tendencies. Simulated and real monthly totals from all 12 months could not be rejected as being from the same distribution. (Mann-Whitney U test, α=0.05). Rainfall totals are in cm.

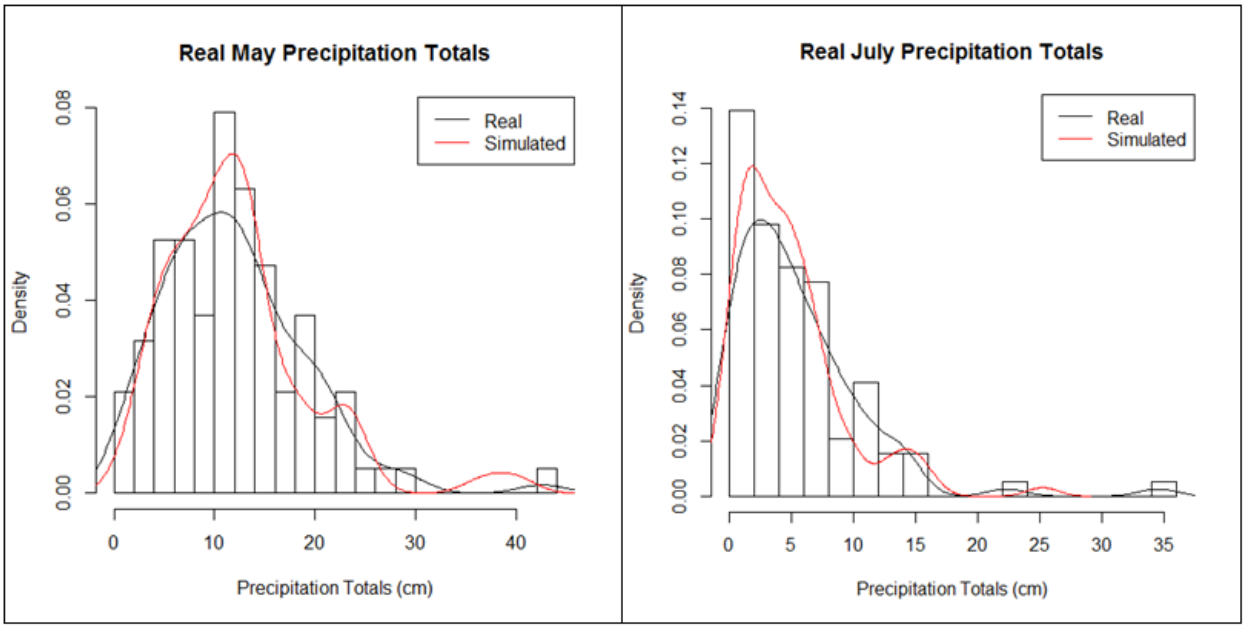

Figure 7.9. Distribution of total rainfall amounts. Distributions of real and simulated monthly totals of rainfall were very close for all 12 months. The real weather distributions had longer tails due to higher maximums and more abnormally high monthly rain totals, but the distributions were otherwise difficult to distinguish. The months of May and July are used here simply as examples.

One way in which the simulated and real weather differed was in the maximum total rainfall. The maximums were greater for every month in the real weather, and in

nine of the months, the maximums were substantially larger. This observation was in agreement with the similar one made with the daily rainfall amounts, in that the model was not as good as real weather at producing abnormally large amounts of rainfall. However, from the perspective of the distribution of monthly rainfall totals, the model produced a very realistic simulated weather that was very close to the climate for which it was parameterized.

Annual precipitation totals were also compared between the model and historical records. As with the monthly totals, the annual total amounts between simulated and real weather compared very well in means and medians, and their distributions were not distinguishable by the Mann-Whitney U test (Fig. 7.10).

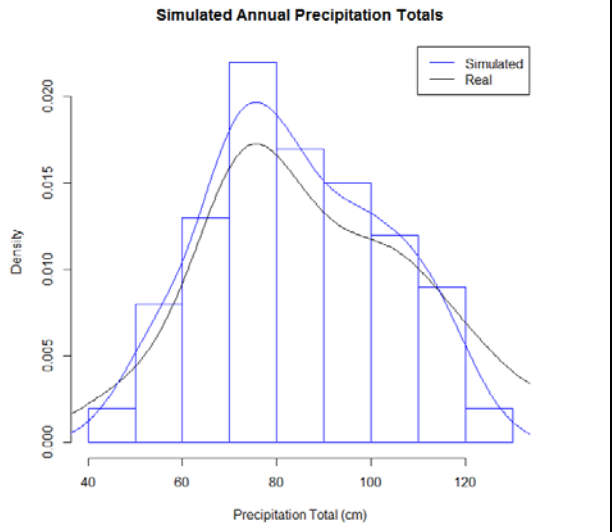

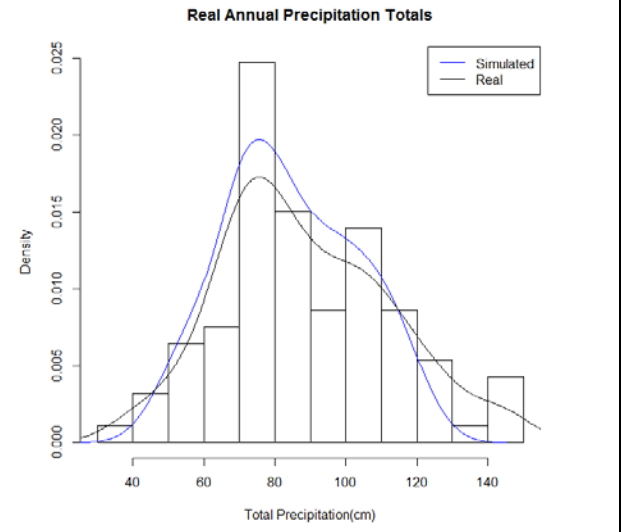

Min. = 38.54, Med. = 84.59, Max. = 145.20 $\mu = 88.50$, $\sigma = 23.92$	Min. = 44.79, Med. = 81.94, Max. = 125.00 $\mu = 84.29$, $\sigma = 18.86$
Mann-Whitney U test result: Fail to reject that the distributions are the same, p = 0.29.	

Figure 7.10. Annual precipitation totals. Annual totals of precipitation for real and simulated weather were compared and the distribution found to be similar. The real weather produced a greater variation in annual totals, including a smaller minimum and a larger maximum. However, the Mann-Whitney U test failed to reject the distributions are the same (*p*=.29).

The primary difference between the simulated and real weather monthly totals was in variability. The real annual precipitation totals had a bigger variance and a wider

range with both a smaller minimum and larger maximum. This pattern was an echo of what was seen at both the daily and monthly timescales. The simulated precipitation amounts and totals were just a bit less variable than real weather. The mean and median values for simulated weather were also a bit smaller by about 5%. However, generally the distribution of the simulated rainfall total appeared to be a good fit overall.

The temperature component of the weather simulator was not examined as closely, and expectations were not high that it would hold up under close scrutiny. Because of time limitations, the temperature component was a hybrid between a daily and monthly model, and thus, individual day-to-day temperatures in the model had an unrealistic increasing or decreasing pattern depending on the season. However, tree growth in the model only depended on the accumulation of GDD during the growing season, and so that was the only output from the temperature model that was analyzed. The model used a well-defined trigger based on temperature progression to indicate both the beginning and end days of the growing season for each modeled year. GDD were summed up only during the growing season. The total was then input into the species temperature tolerance curve to determine temperature stress. If the model produced temperatures resulting in too high or too low of a total number of GDD, then any tree species with temperature tolerance limits set close to that output GDD would struggle to grow.

One problem with comparing temperature output with the real weather data was that unlike the model, nature does not have a well-defined trigger indicating when the growing season starts or stops. Additionally, different species do not respond in the same way to temperature or sunlight triggers that cause them to leaf out in the spring or

drop their leaves in the fall. In mild winters in North Texas, for example, American and winged elm start budding and growing leaves by the second week of February. Post oaks and pecans on the other hand usually do not produce any leaves until well into March. These species tend to keep their leaves until later into the fall than many others, often barring an early freeze all the way through November. A conservative estimate to bind the real growing season in North Texas would be that at maximum it goes from the beginning of February through the end of November, and at a minimum from March through October. Using the same 100-year weather record used in the precipitation comparisons and weather parameterization, GDD were calculated for every day and totaled across every month. Months with any missing temperature records were omitted. Historical GDD monthly totals were calculated using the same assumption the model used for temperature and tree growth, where 5.6° C was the threshold temperature for tree growth to occur. Under this assumption, a GDD was counted for each degree Celsius when the average daily temperature exceeded the 5.6° C threshold. Thus, if the average temperature during a day reached 10°C, then 4.4 GDD were accumulated for that day. To compare the accumulation of GDD for the entire growing season with the model output, three different values were calculated. An upper limit used maximum total GDD for each of the months from across the weather history. The monthly totals from February through November were then summed. The lower limit used the minimum historical monthly GDD totals, which were then summed up from March through October. An average growing season GDD was estimated using the average monthly GDD totals, summing up March through October together with half of the February and November values. With these assumptions, the upper limit for growing

season GDD in North Texas was 7885, the lower limit was 3348, and the average was 4617. These values were compared with the model output from a 100-year simulation run (Fig. 7.11).

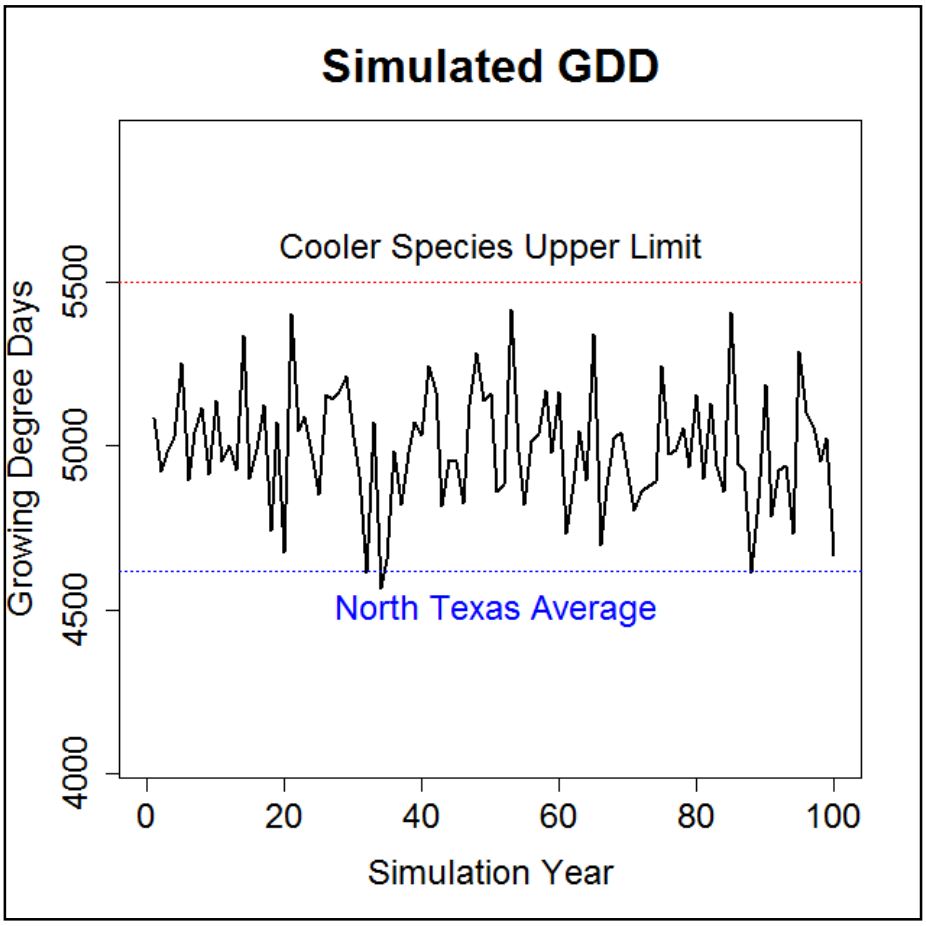

Figure 7.11. Simulated annual GDD output. Modeled output of the growing season accumulation of GDD was compared to average, upper limits, and lower limits for growing season GDD estimated from the 100-year historical weather data. The model output was substantially higher than the average calculated from the real weather history, but it was within the upper and lower limits. The model output came close to upper temperature tolerance limit for some of the cooler-temperature modeled species such as green ash and blackjack oak. The lower temperature tolerance limit for all of the modeled species was well below the simulated output.

The model output of growing season GDD was too high when compared with the North Texas average; however, it fell easily within the upper and lower bounds estimated from the historical record. The simulated average GDD accumulated over the growing season was approximately 5000, about 400 higher than the estimated North

Texas average. Given this output and the species tolerance parameters for temperature, none of the Greenbelt species being modeled were at risk of cold temperature stress. However, several of the Greenbelt species (green ash, cottonwood, and blackjack oak from the shortened list) had upper limits set at around 5500 GDD, which was not much higher than some of the simulation's warmest years were. It was possible this may have caused problems for these species as they competed with others that had higher temperature limits; however, most of the modeled years had GDD outputs well below this limit, and it may not have noticeably impacted them.

To investigate why the simulated temperature output was too high, a quick check of monthly simulated temperature averages was performed and compared with the historical weather records. The simulated temperature averages for every month had a distribution that was statistically indistinguishable from the historical weather data (Mann-Whitney U test, with the smallest p=.22). All 12 sets of maxima and averages were very close between simulated and real weather. The bias in output GDD did not appear to be a result of bias on the modeled monthly temperatures. The modeled growing season did not appear to start too early, but the growing season did appear to end a little too late (Fig. 7.12). The average start of the growing season in the simulated weather was day 76, which was mid-March. By this time in most years, the Greenbelt area tree species had sprouted leaves and had begun photosynthesizing. However, some years freezing temperatures occurred well into March, so this growing season start day in the model was reasonable, although it was little late as an average as since in some years, the growing season did not start until April. The average end day in the modeled growing season was day 331, which was the end of November. In some

simulation years, the growing season did not end until late December, which was later than it should be, but probably enough to explain all of the excess in simulated GDD.

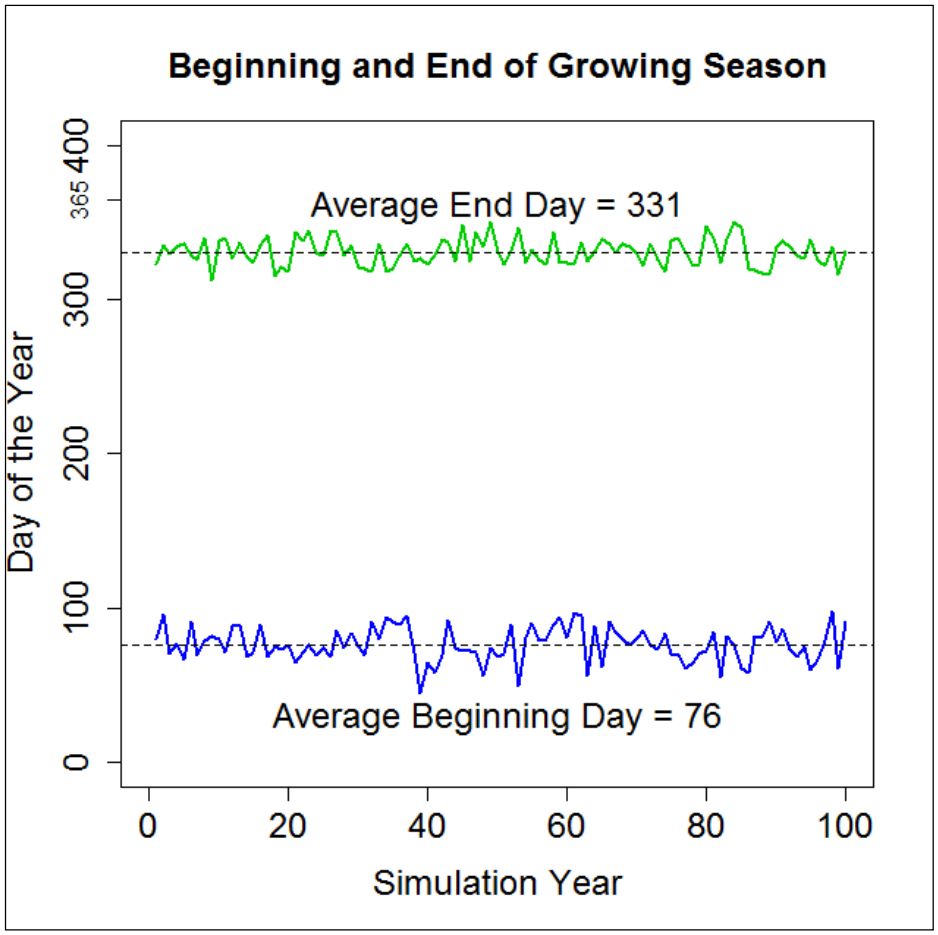

Figure 7.12. Beginning and end of modeled growing season. Average beginning and end of the modeled growing season was examined to determine if it caused high annual GDD output. The average growing season start day was mid-March, and the average end day was in the beginning of December. Both dates were a little later than dates when most of the North Texas deciduous trees typically leaf out or drop leaves, respectively. However, this shift in the growing season was not likely what caused modeled GDD totals to be a little high.

In fact, the entire growing season seemed to be shifted a little to the right in the calendar, which might have been caused from days in the month that were used to interpolate the temperatures between. However, shifting the temperature-based growing season left or right in the calendar would not impact the number of accrued GDD. Part of the explanation to the high model temperatures could be the lack of day-to-day variability in the hybridized daily and monthly temperature model. In real weather,

temperatures can go up and down from one day to the next. Cool fronts during summer months bring temperatures down below normal for days or more. The cooler days accrue a smaller number of GDD. The model allowed for monthly temperatures that were either above or below normal, but since the daily temperatures were interpolated between each pair of consecutive months, there was no fluctuation of the daily temperatures in between. Whether or not this helped explain why the modeled GDD output was too high was only a guess. One impact that most likely attributed to the monthly/daily hybrid temperature was the variation in both beginning and end day of the growing season. In this 100-year simulation, the earliest beginning day was 44, or February 13th, and the latest was day 98, or April 8th. These dates were too early and too late, respectively, for the start of the growing season. Since the daily temperatures for an entire month were determined from a single random draw, a result of an unusually warm February or of an unusually cold March could push the start of the growing season too far left or right.

Overall, the FACETA weather model worked well. The output of precipitation at all three timescales fits pretty well to the historical weather record. One common difference was the variability. At the annual timescale, real annual precipitation totals were slightly more variable, with a lower minimum, a higher maximum, and a higher variance. The average annual total precipitation for real weather was also slightly higher. This same trend held for most of the monthly totals and for most months with the daily rainfall amounts, where the real weather tended to have higher maxima and larger variances. However, overall the simulated precipitation patterns appeared remarkably close to the historical records. One characteristic that was not examined or measured in

the output was droughts or dry spells, which should be done in the future to further verify the precipitation model.

The temperature simulation was not as sophisticated of a model as precipitation; however, since it was only used to determine an accumulation of GDD, it was sufficient for its purposes. The model appeared to produce on average about 400 too many growing season GDD, and the modeled growing season ended on average too late. There was probably too much variation in the start and end dates of the growing season. Whether the high temperature bias negatively impacted modeled tree growth was difficult to predict as the trees responded to a combination of interacting factors. If tree growth became a problem, then the species parameters could be adjusted to provide some buffer, or the assumptions behind the species temperature tolerance parameters could be rethought.

Results: Soil Water Dynamics

Model output of soil moisture dynamics was analyzed for three different soil types: Ovan clay, Birome sandy loam, and Plot #9 (Fig. 7.2). Ovan clay was the most common of the bottomland soils in the study area. It was a deep, high-clay content soil with high levels of organic matter. The soil parameters for this soil were estimated from the county soil survey description of a typical pedon. Birome sandy loam was one of the most common upland soils associated with the post oak forests. It was a moderately deep, sandy soil with clay lenses. Its parameters were estimated from the soils survey description. Plot #9 was located in the Greenbelt in an area that according to the soil survey belonged to the Birome sandy loam soil series. The basic differences in the model parameters were summed up through ordered lists:

1. Depth: Ovan > Plot 9 > Birome
2. Surface dry infiltration rate: Birome > Plot 9 > Ovan
3. Saturated hydraulic conductivity: Plot 9 > Birome > Ovan
4. Water-holding capacity: Ovan > Plot 9 > Birome.

Of course, there were more differences, but these were some of the more important differences for the soil water dynamics. In order to compare the output of the soil water dynamics without potential problems with the forest model, simulation runs were done using a bypass of the tree model (e.g., interception and transpiration) that allowed for testing just the soil water dynamics. The impact trees would have was simulated using constants. At this step, no run-on water was added to simulate the topographical-hydrological impact. The only water input into the soil was from the weather simulator. The output from the three soil scenarios were compared with each other for relative differences.

While there were differences in the output between the three soils, but there were also notable commonalities. Some of the differences in output were a little surprising. A number of different output variables were examined and analyzed. These included:

1. fraction of holding capacity (a measure of how much water was in the soil relative to how much it could hold),
2. extractable water minus potential evapotranspiration (a measure of potential moisture deficit),
3. proportions of wet days and dry days (the metrics used to measure potential stress to trees due to flood or drought respectively), and
4. runoff and deep percolation (two ways that rainwater input was lost from the plot or soil, respectively).

Stress metrics were measured differently for trees and seedlings. For the latter, wet days and dry days were integrated across the top 20 cm of soil, while for trees it was calculated across the entire soil profile. A wet day was defined as a day that the moisture level exceeded field capacity, and a day with no extractable water was defined

as a dry day. The general trend for all three soils was that they were very dry. Fraction of hold capacity was low throughout, generally lower for trees than seedlings. This meant that the upper layers of soil were relatively moister than the deeper layers. Extractable water minus potential evapotranspiration was generally negative, meaning potential deficits. Wet days were low for all three soils, and surprisingly the Ovan clay was slightly lower than the other two soils. There were generally more wet days for seedlings than for trees, which coincided with the fraction of holding capacity results. Runoff and deep percolation were checked to see if water was being lost either through infiltration-saturation excess flow to groundwater. Both Plot 9 and Ovan clay had minimal deep percolation, and the percolation in the Birome soil was not enough to explain the low moisture. Runoff was high for all three soils, ranging from10 cm to 40 cm per year. Results are summarized in Table 7.5, and examples of output graphs are in Fig. 7.13.

Table 7**.**5

Soil Moisture Metrics

	Birome Sandy Loam	Plot 9	Ovan Clay
Fraction of holding capacity	Seedlings: 0.25 Trees: 0.3	Seedlings: 0.45 Trees: 0.25	Seedlings: 0.45 Trees: 0.15
Extractable water minus PET (cm/day)	Seedlings: -0.3 Trees: -0.3	Seedlings: 0.1 Trees: -0.15	Seedlings: 0.35 Trees: -0.1
Proportion Wet Days	Seedlings: 0.1 Trees: 0.02	Seedlings: 0.1 Trees: 0.02	Seedlings: 0.1 Trees: 0.01
Proportion Dry Days	Seedlings: 0.6 Trees: 0.5	Seedlings: 0.3 Trees: 0.6	Seedlings: 0.3 Trees: 0.7
Annual Run Off (cm)	10 – 40	10 – 40	10 – 40

Note: PET=potential evapotranspiration. A number of different metrics of output from the soil moisture model were examined for hospitality to trees or seedlings, and to assess and troubleshoot this component of the model. The results in this table summarize some of these. The values were constantly changing in the model as water was input from rain, lost through evaporation, or moved about in some other way. The values in the table are not specifically averages; rather, they are representative middle values. Fraction of

holding capacity is the proportion of space between wilting point and field capacity that is occupied with water. Extractable water minus PET is a measure of deficit. Proportion of wet days and proportion of dry days are the metrics used to measure water and drought stress to trees. The general trend for all three soils was that soil conditions were too dry, particularly for trees.

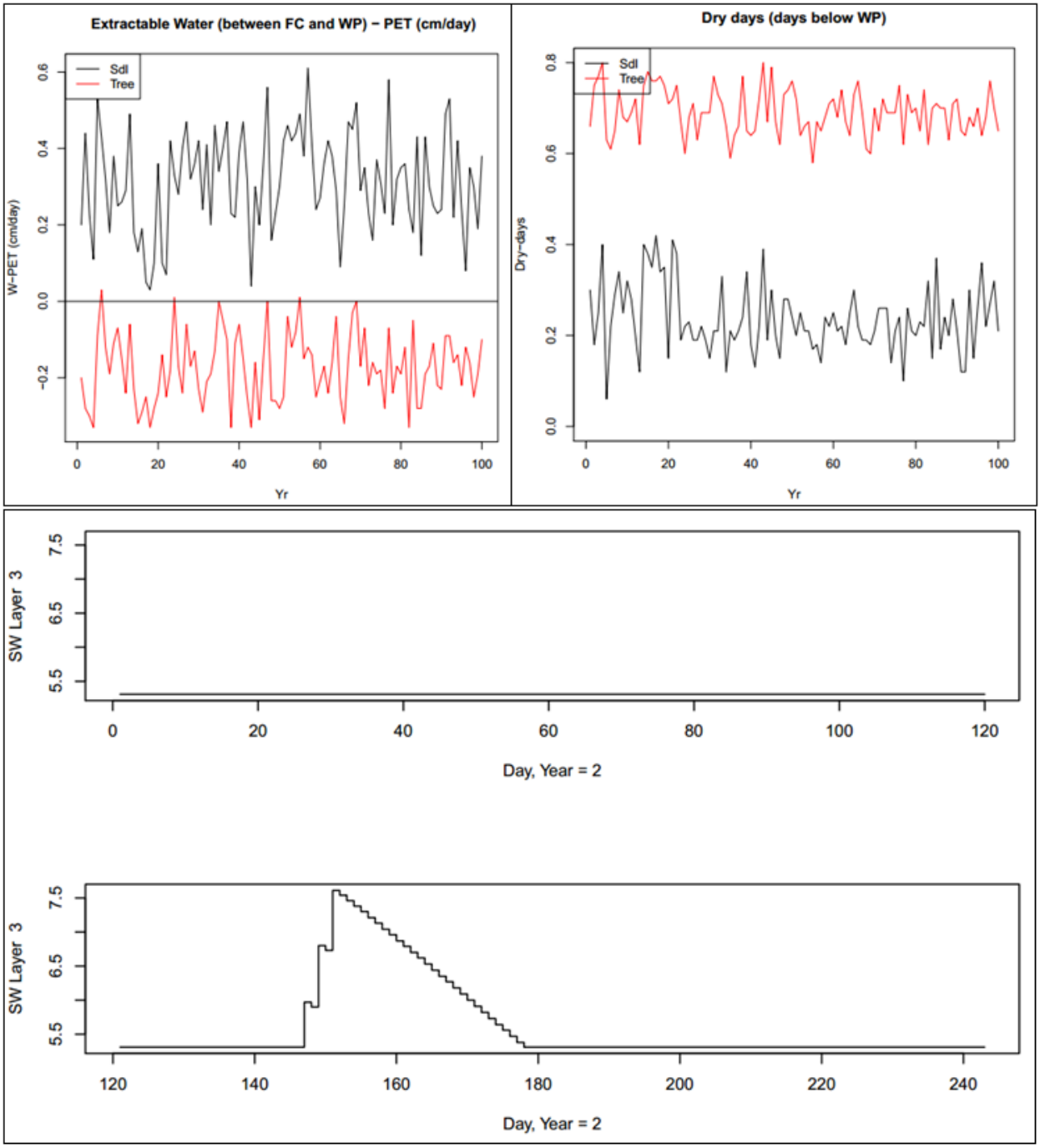

Figure 7.13. Soil moisture outputs. The graphs are examples of several different soil moisture outputs and metrics that were analyzed. These graphs are all from the Ovan clay soil series. Soil moisture output could be examined at daily or annual timescales. Tree stress metrics were calculated from annual averages or totals. Both of these graphs were of annual output over a 100-year simulation. On the top left is annual extractable water (defined to be the water between wilting point and field capacity) minus PET,

with the condition for seedlings graphed in black and for trees in red. This value stayed positive as an annual average for seedlings, which implied there was usually extractable water available in the top 20 cm of soil. Since the values stayed mostly negative for trees, there was a moisture deficit, and any additional water input into the deeper layers was quickly extracted. The graph on the top right is the proportion of dry days, which was the proportion of days during the growing season when soil moisture was at wilting point, for seedlings (black) and trees (red). This metric was used to measure the environmental stress due to lack of moisture. With levels staying between 0.6 and 0.8 for trees, none of the Greenbelt species would be able to grow large. The bottom two graphs show a daily time series of moisture levels in the third layer down during the first 240 days of the second simulation year. Wilting point for this layer was set as an input parameter at 5.31 cm (Fig.7-2), which was where the moisture level stayed most of the time in this layer.

One commonality noticed was that in the deeper layers of all three soils, the moisture level stayed on or close to wilting point through the simulation except for immediately after a rainfall input. This was clearly visible looking at the daily output for the individual soil layers. Shortly after receiving some water input, the moisture level of the soil in the fourth or fifth layer on down would to drop to the wilting point and stay flat lined until the next rainfall provided a little input. A number of changes to the soil input parameters were made to see how they affected these outputs. Possibilities for the low soil moisture included:

1. The soil may have been too deep and the rainfall was not sufficient to fill the deep soil enough to avoid tallying dry days.
2. The hydraulic conductivity was too high causing deep loss.
3. The hydraulic conductivity was too low causing too much runoff.

None of the changes to the input file resulted in an appreciable difference in the low soil moisture levels. A completely different set of soil parameters estimated for a forest in Venezuela were also tested, and results were similar in that soil levels remained low, especially at the deeper layers (M. F. Acevedo, personal communication). It was possible the soil moisture model was accurate, and given the climate of North Texas, the model was simply reflecting the dry soil conditions that existed. However, the conditions seemed too dry for that to be the case. If the model was accurate, then the

model for moisture stress needs to be changed because with these soil conditions, trees could never grow big.

The very odd finding of chronically dry deep layers with moisture in the upper layers, which was accessible to seedlings, could have been due to the assumptions used in the forest and tree growth bypass functioned used to test the soil moisture dynamics. With the bypass turned off and all other parameters set the same, the moisture conditions were reversed, and the drier soil was in the upper layers. However, the soil was still chronically dry throughout. The best estimate for the inverted soil moisture output was that the constants used by the forest bypass assumed a steady forest of mature trees drawing water from deeper layers of soil. Since the soil was dry already, the constant draw of the mature trees assumed by the bypass kept these lower layers completely dry other than immediately after a water input. Without the bypass, the model started tree growth with seedlings that had to be established. The seedlings drew water only from the upper layers. Thus, the seedlings constantly competed for the limited moisture in the upper layers, and it was difficult for any of the seedlings to reach the size required to extend to deeper soil. This result was seen in the forest output, which was examined next.

Results: Terrain Types and Forest Growth

Because of chronically low soil moisture levels seen in the model during the soil moisture testing, forest growth output was suspect. However, examining it still provided insight into the functionality of the model and provided information on how the model could be improved. Three different terrain types were evaluated for forest growth: Birome sandy loam in the medium topographic wetness index (TWI) class (Birome-2),

Ovan clay in the medium TWI class (Ovan-2), and Ovan clay in the high TWI class (Ovan-3). Birome-1 and Ovan-1 were two of the three terrain types with which the soil moisture dynamics were evaluated. Although not discussed in detail, forest growth for those terrain types were evaluated, and in all three of types, growth was limited to a large number of very small trees of the most drought tolerant species, post oak and blackjack oak. While the output was expected given the low moisture levels in the model for those terrain types, it was not realistic for post oak trees or seedlings to grow in the heavy clay soil of the Ovan series. The output indicated the initial assumption that a metric of soil moisture levels would be enough to prevent modeling post oak growth in the bottomland was incorrect. However, the moisture levels output by the model were also not realistic, making it difficult to assess the quality of the forest model output.

Forest growth output was evaluated using two metrics, density and basal area. Density of each species was measured as the number of trees per hectare, and basal area was the amount of cross-sectional area of all tree trunks per hectare. High density meant a large number of trees. The basal area of a tree increased with the square of its radius, so it took a very large number of small trees to produce as much basal area as one large tree. High basal area values generally implied a much smaller number of larger trees. The expected progression of forest development from bare ground in the language of these two metrics was that both started as zero, and then density quickly increased as seedlings started to grow, but basal area stayed very small. As more seedlings started and existing seedlings grew and competed, density continued to increase rapidly while basal area starts increased a little more rapidly. Some of the seedlings managed to out-compete others and gain a size advantage. Those trees

started to grow basal area more rapidly, the outcompeted seedlings started to die off because of stress, and density started to drop. In addition to this general expected behavior, there were species characteristics, as defined by the silvics parameters in the model, which influenced the species composition dynamics as the forest developed. For example, fast growing trees typically won the early competition to become the first large trees, but then shade tolerance typically determined the *second generation* of large trees. Characteristics of drought or saturation tolerance, or tolerance to other soil condition, determined the locations favorable or not favorable to different species.

To get a sense of the types of forest development that can occur in the three modeled terrain types, results of a tree survey conducted in the Greenbelt were displayed. These results were just examples each consisting of a single, 25-m x 25-m plot. The survey within the Birome-2 terrain type was conducted in an area of old post oak forest located close to the bottom of a hillslope on moderately deep, sandy loam soil (Fig. 7.14). The survey found almost exclusively post oak and cedar elm, roughly in the same number as seen in the density graph, but with the post oak being the much larger trees, as seen in the basal area graph.

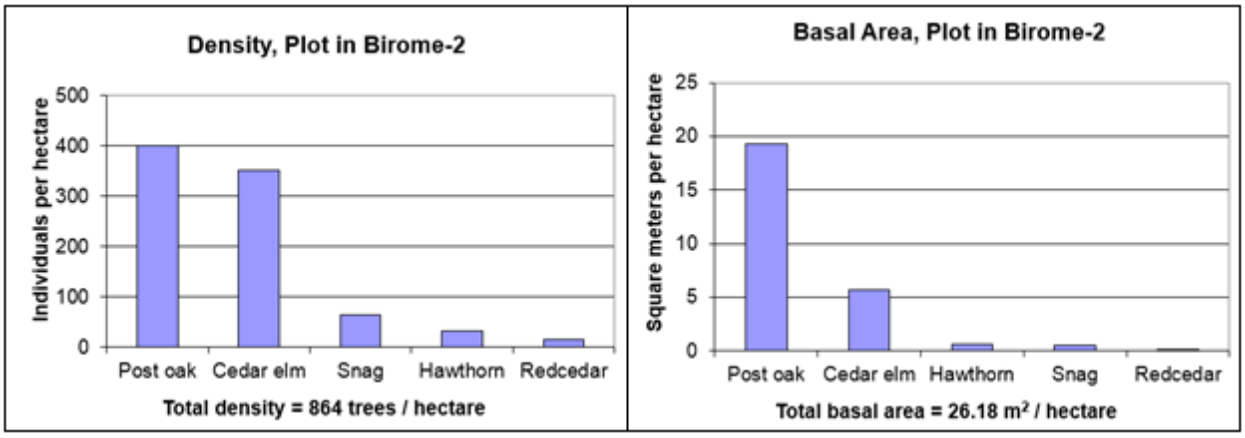

Figure 7.14. Density and basal area in sample Greenbelt plot in Birome-2. In a tree survey conducted within the Greenbelt, density and basal area were measured in different 25-m x 25-m plots. Density was defined as the number of trees per hectare, and basal area was the cross-sectional area per hectare. In a

plot located in an area identified as the Birome-2 terrain type, almost all of the trees were post oak or cedar elm. Post oak had a slightly larger number of trees as shown in the density graph. Additionally, it had much larger trees as shown in the basal area graph. Eastern redcedar and hawthorn were present as 1 and 2 individuals, respectively. A *snag* is a standing dead tree of any species.

Large parts of the Greenbelt bottomland fell into the Ovan-2 terrain type, and green ash, cedar elm, and sugarberry typically dominated these areas. Other species found in this terrain type included red mulberry, boxelder, American elm, swamp privet, and Osage orange. The sample plot surveyed in the Ovan-2 terrain type was in an area in the floodplain flat with approximately 50-year-old forest growth (Fig. 7.15). This particular plot was dominated by cedar elm, which had both the largest number of individuals and the largest trees. Sugarberry was present in large numbers, but all of the trees were small, in the 5-cm to 10-cm DBH size class. Few green ash were in this plot, but the ones present were greater than 50 cm DBH. While these three species were found throughout the Greenbelt bottomland, sugarberry tended to favor the higher and drier land. Green ash was the most adapted of the three species to swampier positions. It was unclear why cedar elm dominated some positions in this plot, but of the three species, it had the broadest range of tolerance to soil moisture conditions.

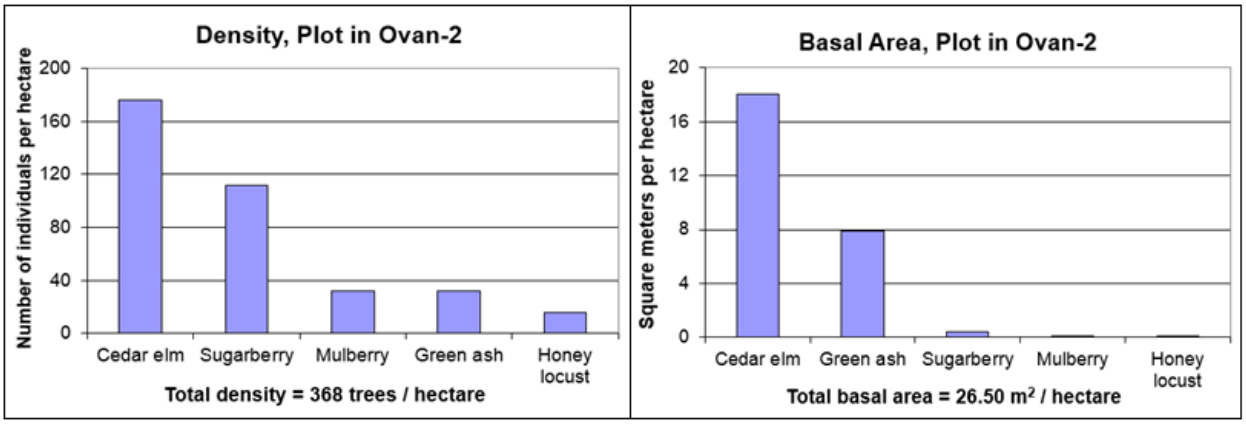

Figure 7.15. Density and basal area in sample Greenbelt plot in Ovan-2. In a tree survey conducted within the Greenbelt, density and basal area were measured in different 25-m x 25-m plots. Density is defined as the number of trees per hectare, and basal area is the cross-sectional area per hectare. A plot identified to be in the Ovan-2 terrain type contained a mix of bottomland species. Like much of the Greenbelt bottomland, this plot was dominated by cedar elm, green ash, and sugarberry. The largest

trees were green ash, sugarberry made up a large number of small trees, but cedar elm made up the largest number of individuals and represented a large range of sizes.

The Ovan-3 sites included the wettest parts of the bottomland such as sloughs and wetlands, as well as parts of the flats. These areas contained the green ash, cedar elm, and sugarberry, but some parts were dominated by swamp privet. Black willow was also more likely in these positions. In a sample plot surveyed in the Ovan-3 terrain type, swamp privet made up more than half the trees (Fig. 7.16). The largest part of the basal area in this plot consisted of standing dead trees or snags. It was important to stress that the survey results presented in these graphs were each of a single 25-m x 25-m plot, so they were considered only as examples of possible forest development in the different conditions rather than some kind of representative average.

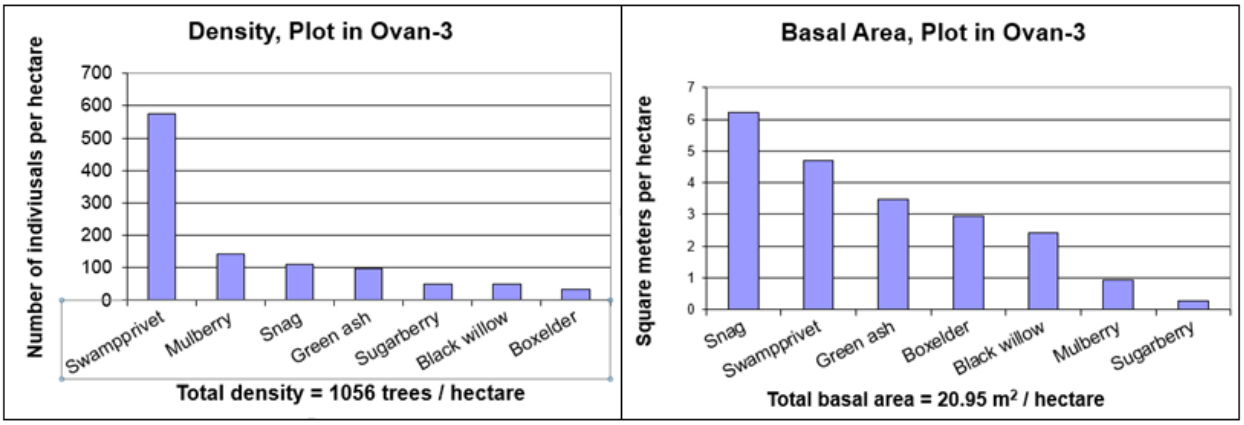

Figure 7.16. Density and basal area in sample Greenbelt plot in Ovan-3. In a tree survey conducted within the Greenbelt, density and basal area were measured in different 25-m x 25-m plots. Density is defined as the number of trees per hectare, and basal area is the cross-sectional area per hectare. In parts of the Greenbelt representing the Ovan-3 class, swamp privet, green ash, and black willow were likely to be the common species. This plot measured in an Ovan-3 area was representative of that combination. A snag is a standing dead tree of any species. The survey result indicated that the largest trees in this plot were snags, and swamp privet made up the largest number of trees.

FACETA simulation runs using the parameters defined by these three terrain types were evaluated for density and basal area of each species present. Because of the model's chronically dry soil conditions, the run-on parameters (described in

Table 6.6) were implemented with the scalar multiplier *c* set equal to 1. In other words, the parameters were implemented in such a way to maximize the parameters' effects on soil moisture; the original intention was for the multiplier to equal less than 1. Numerous runs were performed using different random weather seeds to verify consistency of the results. Each run simulated 300 years. Generally, the output highlighted the problem noted with modeled soil moisture—trees struggled to grow. As the model was designed, seedlings of all species attempted to grow and establish themselves in all simulations. Any species without high drought tolerance parameters set (e.g., green ash and black willow) were almost completely unable to establish themselves with the additional water input from the run-on parameter. Except in the driest of the modeled terrain conditions, once any tree was established, it had a chance to grow big if it could attain a size advantage over the other individuals in its plot.

The most upland of the three terrain types evaluated was Birome-2. This was generally described as a moderately deep, sandy soil that was not in the driest positions, for example on slope sides or hilltops. This terrain position typically developed into a post oak forest but with enough soil moisture to allow some other species. The FACETA simulations on this terrain type resulted in very believable output in terms of species composition, basal area, and density (Fig. 7.17). Both black willow and cottonwood made a brief appearance as established small trees in the simulation, but they were outcompeted by the more drought tolerant post oak and blackjack oak. The densities for both oak species spiked early in the simulation as many new young trees struggled to become dominant big trees. By about 150 years into the simulation, densities dropped as some trees matured and grew, and the small ones died off. This

drop in density coincided with an increase in basal area. The long run projection of a post oak dominated forest, with a total basal area about 30 m^2/ha and a total density of about 400 trees/ha, matched reasonably well with the sample tree survey of the Birome-2 plot (Fig. 7.14).

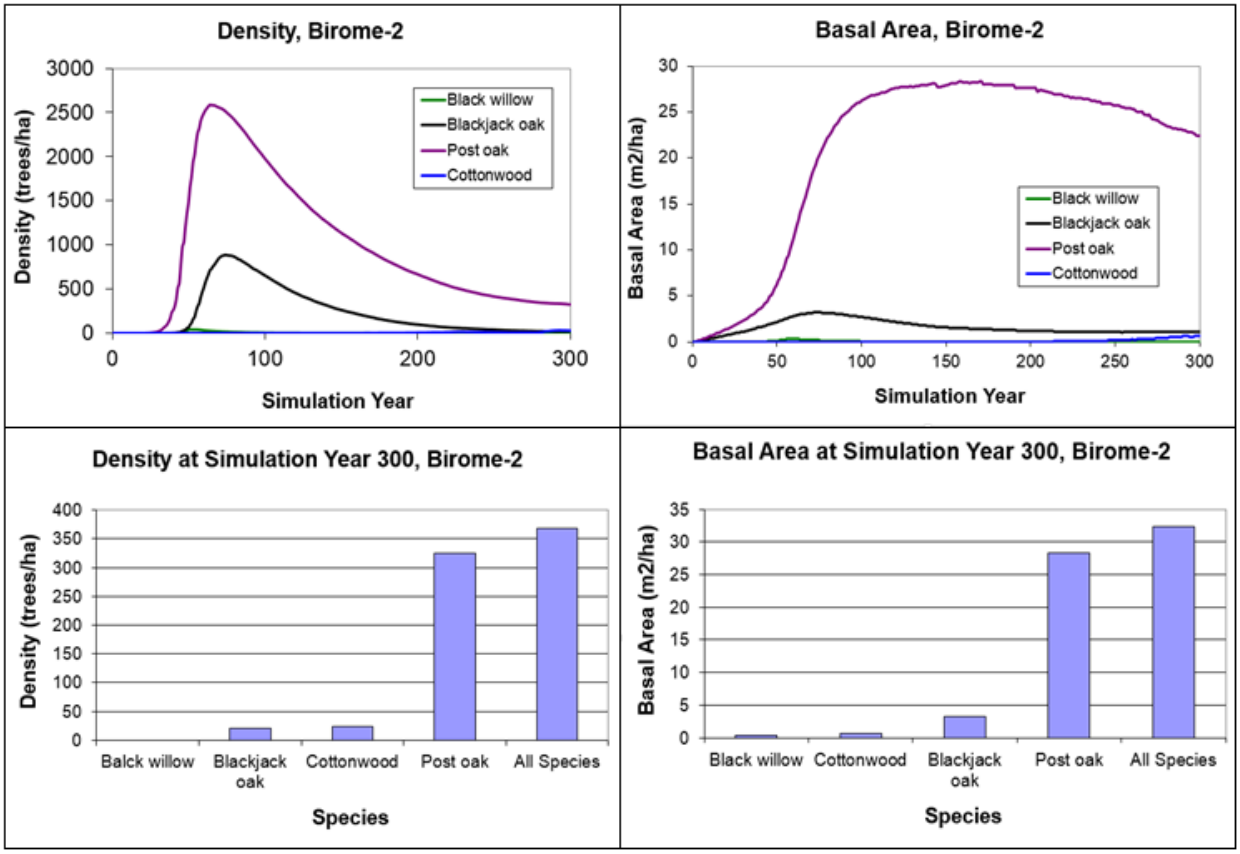

Figure 7.17. FACETA results, Birome-2 terrain class. The FACETA simulations run on the Birome-2 terrain class yielded convincing results. The top two graphs show the modeled trajectory starting from bare ground through 300 years of simulated growth. The bottom two graphs summarize the density and basal area at the end of this 300-year trajectory. Species composition, density, and basal area results at the end of this period agreed fairly well with the forest development that would be expected in this terrain class. The results also agreed well with the sample tree survey conducted in a similar terrain position.

Unfortunately, the FACETA forest results were not as promising for the two Ovan terrain classes. In the Ovan-2 class soil, even with the added moisture input, soil conditions were too dry to allow for growth of any species except the two upland oaks and cottonwood (Fig. 7.18). Cottonwood, which was relatively drought tolerant for a

bottomland species, came into the simulation and eventually co-dominated with post oak in the basal area, but it remained at a very small number of individuals.

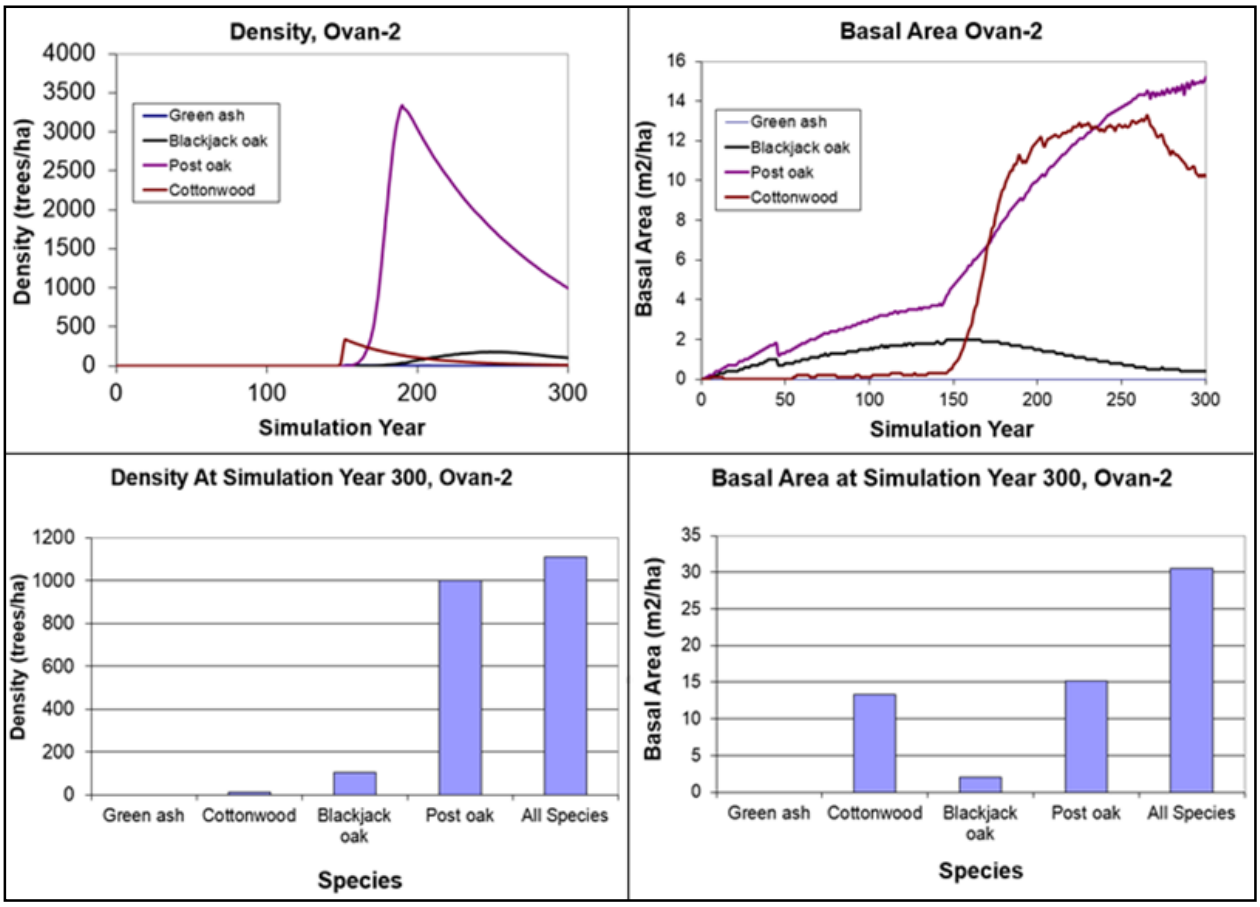

Figure 7.18. FACETA results, Ovan-2 terrain class. FACETA simulation runs in the Ovan-2 terrain class did not yield desired results. The result appeared as an upland post oak forest with a mix of a few very large cottonwoods. Moisture stress in the model prevented many of the bottomland species that would be expected in this position from being established.

The characteristic of rapid growth rate allowed cottonwood to co-dominate in the model. A few green ash trees were established from seedlings, and they grew to tree status in the simulation. However, because of the dry soil conditions, they quickly died off. The other species expected in this terrain type, sugarberry, never managed to establish itself. The final results would actually not be that bad if the modeled position were a sandy upland one, but in reality post oaks would never be able to become established in Ovan clay soil because of the lack of aeration. While occasionally cottonwoods can

become established in upland positions near post oaks, they would only do so as a very minor component and probably only in more topographically favorable positions. From the combination of low density and high basal area, it was clear that the big trees in this simulation were the cottonwoods, and the post oaks were the much smaller but more plentiful trees. Cottonwood thrived best in looser, aerated soils similar to where post oaks grow, but the water demand by cottonwood was much higher. The fact that post oaks thrived in the modeled Ovan-2 position brought into question the original thinking of how to implement flood and aeration stress response into the model. The model could be designed so extra moisture found in the bottomland sites would prevent post oak establishment. Due to issues with soil moisture in the model, extra moisture was not an issue in the Ovan-2 terrain class. However, the soil conditions alone should have prevented post oak development. To capture better this response it is possible that aeration and flood needed to be treated as separate stressors in the model.

The wettest simulated position run was Ovan-3 (Fig. 7.19). Because the scalar multiplier, *c*, applied to the run-on parameter was set to 1, the amount of additional water added to this site in the simulation was by a factor of 3, which was clearly unrealistic; however, moisture conditions were still too low for good establishment of trees. The soil moisture conditions in the different layers and the wet day and dry day calculations for tree stress response were examined. It was clear the additional water added in the simulation was enough to keep the deeper levels of soil accessed by mature trees from becoming dry; however, dry day proportions in the upper, seedling-accessible soil layers were still typically around 0.5.

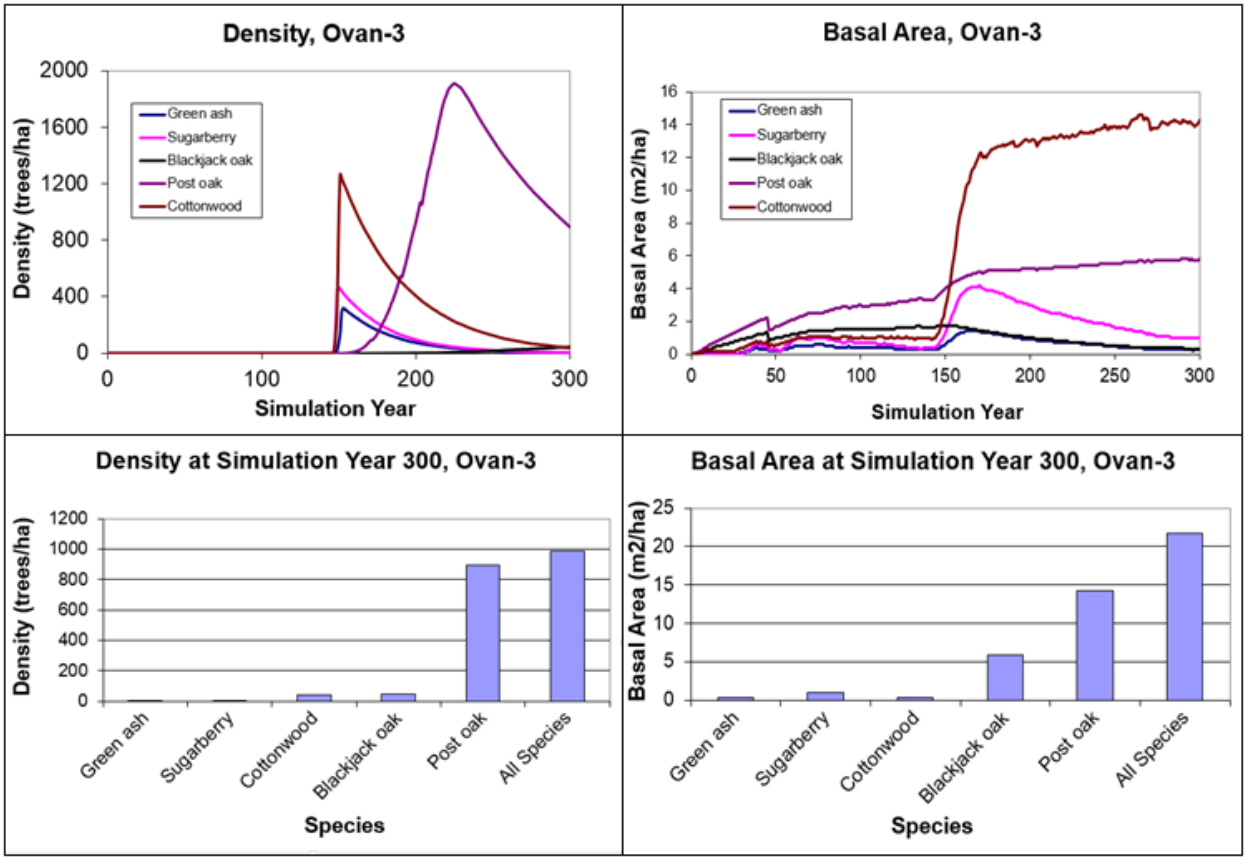

Figure 7.19. FACETA results, Ovan-3 terrain class. The Ovan-3 class in the real world would be areas that in some year could experience flooding for weeks or even months. While not all of Ovan-3 could be classified as a wetland, the class did contain then. The simulation for this class used three times the additional amount of moisture as the weather simulator produced, yet the model output resembled a mix of upland post oak and bottomland forest. At the end of this simulation, cottonwood dominated in size, and post oak dominated in numbers.

It seemed incorrect that bottomland Ovan clay soils would be at wilting point for half of the growing season, especially with so much additional water being simulated. The forest results for this terrain class appeared a little more like a bottomland forest, with all of the species in the simulation making an appearance except for black willow. In reality, black willow seeds need to become wet within just a couple of days after falling from the tree in order to germinate. Thus, black willow is often found growing in ditches and wetlands. In this simulation, the added water failed to make the upper part of the soil moist enough for the modeled black willow to establish. Post oak not only made an appearance again in this bottomland terrain position, but in fact, it was the

species with the highest density. In the end, cottonwood dominated in basal area. This particular composition did not look like any expected forest in the study area, but the problems with proper growth were a result of the model problems with soil moisture.

Conclusions: FACETA Results

FACETA results were somewhat mixed. The precipitation component of the weather model captured month-to-month rainfall patterns. The only notable difference between the real and simulated weather was that for most months, the simulation was unable to capture the full range of variability seen in the real weather. The temperature component of the model was much more simple in structure but still adequate for the way temperature impacted trees in the model. Two problems were noted with the temperature model. The model tended to produce about 10% too many GDD per season as compared to the real weather, and it tended to start and stop the growing season a little late. Of note, at least one random weather seed simulation resulted in years where the growing season both started and stopped in February. This was likely due to a logical counting error in the code for determining growing season, and all growing season and temperature issues with the model could likely be fixed.

The soil moisture component of the model yielded unsatisfactory results. Any terrain type tested without additional simulated run-on water had soil conditions too arid for anything but the growth of tiny post oak and blackjack oak. Running the model with the tree and forest simulation bypassed resulted in soil conditions quite hospitable for seedlings, but with essentially no available water at deeper soil layers accessed by the mature trees. This likely occurred because the forest bypass function assumed a steady draw of moisture from the deeper levels. Running the simulation with the trees included

resulted in thousands of seedlings competing for the very limited moisture in the upper layers. None of the seedlings were able grow enough to reach deeper soils and become large trees. Adding extra moisture in the simulation did finally allow for mature tree growth. The species composition in the output did not match reality for any of the bottomland terrain positions because even with the added moisture, the conditions were dry enough that post oak with its drought tolerance was competitive. This result was unwanted because post oak would be restricted from the bottomland positions due to soil texture alone; therefore, a rethink of the approach used here in how to model aeration stress response became necessary. Overall, the FACETA model appeared to show promise towards this application. The results from Birome-2, for example, were encouraging. The temperature component of the model needs to be examined further and probably adjusted, and the soil moisture conditions need to be investigated more thoroughly. The metrics used for determining soil moisture stress need to be reconsidered, but with some work, FACETA can be adjusted to produce reasonable results for modeling different soil types within the Cross Timbers ecoregion.

CHAPTER 8

CONCLUSIONS

A method for extending a plot-scaled forest model to a watershed-scaled landscape was investigated in this study. The forest model FACETA simulates weather, soil moisture dynamics, and tree growth and competition, but it does not include a spatially distributed hydrological model. Terrain types were defined across the study area watershed through a combination of soil and topographic characteristics. This combination of characteristics was selected based on the understanding of how the different vegetation patterns develop in the Cross Timbers and Prairies ecoregion, and more specifically in the Eastern Cross Timbers ecoregion. FACETA requires numerous inputs describing soil physical properties. In order to simulate the topographic effects on hydrology without developing a spatially explicit hydrology model, an approach using the concept of hydrologic similarity was taken through the use of a topographic wetness index (TWI).

Soil series as defined in the Denton County soil survey provided by the Natural Resource Conservation Service (NRCS; USDA, 2010) together with categories of TWI were used for partitioning the study area map into terrain types. Different issues behind developing the TWI map were considered and analyzed including different sources of elevation data, grid sizes, and grid processing used in the hydrological analysis. Light detection and ranging (LiDAR) derived digital elevation model (DEM) in 5-m, 10-m, and 29-m grid sizes and contour-derived DEMs with 10-m and 29-m resolutions were obtained, depressions were removed to make the DEMs hydrologically correct, and the DEMs were processed using both a single directional flow direction algorithm and a

bi-directional flow algorithm. Ten different DEMs were used to produce TWI grids that were analyzed at multiple steps in the process for their appropriateness in FACETA terrain type definition. Slope, flow accumulation, and TWI grids were all compared.

A difference noted between the contour-derived slope grids and the LiDAR-derived slope grids was LiDAR's ability to detect changes accurately in topography. Especially with the smaller grid sizes, the LiDAR-derived DEMs identified relatively subtle changes in elevation and slope. The small grid, LiDAR-derived DEMs detected microtopographical changes; however, that may not be needed when considering terrain types linked to vegetation covers across a watershed-scaled landscape. The slope grids revealed unfortunate errors contained in the contour-derived DEMs introduced at the time of production. These errors, known as striping artifacts, appeared in some of the grids as artificial parallel lines that crisscrossed the grid. The striping artifacts were more apparent in the 10-m grid than the 29-m grid and more apparent in the bi-directional D∞ processed grid than the single directional D8 processed one.

The different flow accumulation grids were compared with the location and shape of surface water features. Generally, accuracy increased with the finer grid resolutions, the LiDAR-derived grids were more accurate than contour-derived, and the D∞ processed grids were more accurate than D8. However, there was little difference in accuracy between the 29-m LiDAR-derived D8 map and the 29-m contour-derived D8 map. A problem was noted in some cells found in high flow accumulation areas using the D∞. The calculations somehow became undefined, and those grid cells ended up as holes of missing data within the landscape map. Although the D∞ algorithm was more

accurate at locating surface water than D8, since implementation of D∞ resulted in missing data cells, a multi-directional flow (MDF) algorithm should be considered.

The striping artifacts that first became apparent in the contour-derived slope grids became much more prevalent and obvious through the calculation of the TWI grids. The errors were prevalent enough that they showed through even after grouping the TWI values into three categories. The striping artifacts could be removed through filtering techniques, but without such correction, the contour-derived DEMs were determined inadequate for partitioning the landscape into terrain types. Since LiDAR availability was limited in many places, a *filtered* version of the 10-m contour-derived DEM was added to the analysis. The filtering in this case was accomplished through resampling or resizing the DEM grid cells from 10 m to 29 m. This removed the striping artifacts, but it also caused a loss in accuracy, and the contour-derived DEMs were abandoned.

In comparing different grid sizes, the small-grid DEMs were more accurate. However, they were also sensitive to relatively small changes in elevation. Small changes in slope of short distances were detected and seen in the TWI grid. The finer grid resolution DEMs resulted in a great deal of patchiness. Individual pixels or patches of low (i.e., dry) TWI values were left isolated within the floodplain. Likewise, *channels* of higher (wet) TWI values showed up in distinctively upland hilly areas. The 5-m grids were patchier than the 10-m ones, and the D8 flow direction algorithm produced less patchiness in the flats and bottomlands while the D∞ algorithm was less dendritic in the hilly areas. In all four of the finer resolution grids, the patches were still apparent after reclassifying the TWI grid for terrain type definition. They also resulted in a patchy terrain type map. Since this patchiness did not correspond to changes in terrain or

vegetation cover on the ground, the smaller grid sizes were determined to be less appropriate for this application. The two LiDAR-derived 29-m grids were relatively similar to each other; however, the D∞ processed 29-m grid was patchier than the D8 processed map in flat areas and had more isolated pixels of low TWI values scattered within the wetlands. The D∞ processed grid also contained missing data cells in areas of high accumulation. Because of its better representation of flat, bottomland areas, the D8 29-m grid was determined to be best one available for this application.

After comparing different ways to classify TWI cells, a relatively simple approach was used to group cells into three TWI categories of high, medium, and low. The FACETA terrain type map was generated by partitioning the study area through the different combinations of soil series and TWI categories. Initial values for the break points used to classify the TWI grid into groups were determined from the 20^{th} and 80^{th} percentiles. While this particular division produced a satisfactory visual comparison with terrain and vegetation features on the ground, the break points themselves were considered landscape model parameters that needed calibration to every new situation.

Biological parameters needed by FACETA included a list of species and numerous parameters that described their growth rates, geometry, and tolerances to environmental conditions. Allometric parameters used by FACETA defined the height to diameter relationship for each modeled trees species. These parameters were estimated by measuring the heights and diameters of a number of different sized and then performing a nonlinear regression on this data. Other parameters were estimated from qualitative descriptions of species for lack of more qualitative information. Growth rate parameters were estimated from measuring growth rings. However, some

questions regarding model assumptions arose while estimating all required parameters. The model assumed a straight, cylindrical trunk, and the allometric parameters were linked through model equations to the maximum height, growth rate, and maximum diameter parameters. Information for many of the tree species on characteristics such as maximum size, particularly the commercially less important species, were either missing or in conflict. Additionally all of the model parameters were linked together, and there was mutual sensitivity of the different parameters reached throughout the model. Changes in one parameter, for example maximum height, could impact the allometric equation, which could then impact the optimal growth equation, which in turn impacted how successful any species was in the model.

The way the growth rate parameter was estimated in this study represented a new approach. While the growth rate parameter was in units of volume of wood per unit leaf area, under the assumptions used in the model the growth equation was expressed in such a way that the growth parameter was viewed as being in units of diameter growth as a function of the current diameter. It was found that the best way to measure for this parameter, assuming no trees were cut down for the study, was to measure growth rings from trunk cross sections. Using tree cores such as is typically done in dendrochronology could result in a large error in estimating the growth rate parameter. Another interesting outcome of this exercise in measuring growth rings for growth rate estimation was that it was best to measure trees that exhibited something close to optimal growth. This parameter was supposed to represent the full growth potential of a species given optimal conditions, but optimal conditions were not found in places with water stress or too much competition, for example in upland forests in North Texas.

Robust growth of upland species like post oak and blackjack oak was more likely to occur on developed land where competition had been thinned and extra water received.

The environmental tolerance parameters were in many ways the most difficult to quantify. In many cases the information available did not allow for anything more accurate then producing a relative ranking between species. The new wet-day and dry-day response to soil moisture stress incorporated into FACETA was out of an effort to base the response more on the actual physical moisture conditions being modeled in the soil. However, because of the way the response and parameters worked, there are limitations. Wet-days or dry-days within the growing season were not differentiated by when they occurred or how they were distributed, and data available to base the parameter values on was limited at best. Considering that the definition of a dry day was that the moisture level had been reduced to the wilting point, few plant species could withstand very many consecutive dry days within the growing season. All of the environmental stressor response curves were by their mathematical nature very steeply sloped at the edges, so species that experienced conditions close to their tolerance struggled to grow. This problem was accentuated when the model was inaccurate in a physical characteristic such as the number of accrued growing degree days (GDD).

Environmental parameters needed by FACETA included climatic statistics, soil parameters, and the new hydrologically based terrain parameters. Compared to determining biological parameters, finding climatic parameters was very straightforward. A 100-year historical record of daily weather data was employed in this case. Much work had been done on increasing the fidelity of the FACETA weather simulator. Thus, the parameters for it were derived in the most accurate way possible. Soil parameters

on the other hand were more difficult to estimate with confidence. The model used soil parameters that could be measured in theory, such as field capacity or available porosity. However, measuring these parameters across a watershed was far too costly. Therefore, the soil parameters were estimated based on the physical properties described for each soil series in the USDA (2010) Denton County soil survey. One problem with this method was that the soil survey described properties such as soil texture, and organic content, not field capacity or wilting point. However, these values were estimated from properties described in the soil survey. This of course gave more opportunity for error, because the description in the soil survey itself was already an estimation of the actual soil on the ground, and then the model parameters were estimated from that. In order to get a sense of how different model parameters could be estimated from actual field measurement versus a soil survey description, soil parameters were estimated for some soils from measurements done on cores taken from the actual Greenbelt study site. These estimated soil parameters were quite different from the ones gleaned from the soil survey, but it was difficult to assess how much these soil parameter differences impacted model performance due to problems encountered with the FACETA soil moisture model.

FACETA's new terrain parameters were implemented to simulated topographically based, hydrologic conditions within the modeled watershed. The implementation of these topographic and hydrologic parameters was simple, but devising a systematic approach to determining the terrain parameters was not as easy. The goal was to allow the physical properties such as slope and upslope catchment area that were representative of each terrain type to define the parameters. Since the

model did not use an actual spatially distributed hydrological model and slope was only used in the solar radiation component of the model, the approach of devising the terrain parameters seemed convoluted. However, it allowed terrain types with large representative upslope catchment areas to receive more moisture, and those with large representative slope to receive less.

The FACETA model was evaluated after all of the changes and enhancements. The enhanced daily precipitation model performed above expectations, and it was declared a success as a standalone weather generator. Because of problems with the soil moisture component of the model, it was difficult to determine how much it improved the FACETA forest model. The modeled soil moisture levels stayed too low, even in terrain positions that received a large amount of simulated run-on water. While the initial appearance of this issue was a problem with modeled soil moisture, it was not clear this was the problem. The problem might also lie in how the model initiated seedlings and how seedlings and trees were able to extract soil moisture. The forest model did not produce the results in species composition that were expected. The general trends of density and basal area during forest development were simulated pretty well, but due to the soil conditions, only the most drought tolerant species were able to survive in the simulation. The results, however, were promising. As mentioned before, the general patterns of forest development were good, and using a very limited subset of modeled species produced reasonable results in some scenarios. This study confirmed the proof of concept behind this approach. With continued effort, model analysis and improvement, and a higher fidelity of information to base model parameters on, FACETA will become a good landscape forest model.

REFERENCES

Acevedo, M. F., Urban, D. L., & Ablan, M. (1995). Transition and gap models of forest dynamics. *Ecological Applications, 5*(4), 1040-1055.

Acevedo, M. F., Urban, D.L., & Ablan, M. (1996). Landscape scale forest dynamics: GIS, gap and transition models. In M.F. Goodchild et al. (Eds.), *GIS and environmental modeling: Progress and research issues* (pp. 181-185). Fort Collins, CO: GIS World Books.

Acevedo, M. F., Ablan, M., Urban, D.L., & Pamarti, S. (2001). Estimating parameters of forest patch transition models from gap models. *Environmental Modeling & Software, 16*, 649-658.

Acevedo, M. F., Pamarti, S., Alban, M., Urban, D.L., & Mikler, A. (2001). Modeling forest landscapes: Parameter estimation from gap models over heterogeneous terrain. *Simulation, 77*(1-2), 53-68.

Albani, M. & Klinkenberg, B. (2003). A spatial filter for the removal of striping artifacts in digital elevation models. *Photogrammetric Engineering & Remote Sensing, 69*(7), 755-765.

Allen, J. A., Keeland, B. D., Stanturf, J. A., Clewell, A. F., & Kennedy, H. E. (2001). A guide to bottomland hardwood restoration. (U.S. Geological Survey, Biological Resources Division Information and Technology Report USGS/BRD/ITR-2000-0011). Asheville, NC: U.S. Department of Agriculture, Forest Service, Southern Research Station.

American Forests. (2013). National register of big trees. Retrieved from http://www.americanforests.org/bigtrees/bigtrees-search/

Bailey, R. G. (1995). Description of the ecoregions of the United States. Retrieved from http://www.fs.fed.us/land/ecosysmgmt/

Barling, R. D., Moore, I. D., & Grayson, R. B. (1994). A quasi-dynamic wetness index for characterizing the spatial distribution of zones of surface saturation and soil water content. *Water Resources Research, 30*(4), 1029-1044.

Barrett, T. M. (2001). Models of vegetative change for landscape planning: A comparison of FETM, LANDSUM, SIMPPLLE, and VDDT (USDA Forest Service Gen. Tech. Rep. RMRS-GTR-76-WWW). Fort Collins, CO: Natural Resources Research Center.

Barry, D. (2000). *Thresholds in avian communities at multiple scales: Relationships between birds, forests, habitats, and landscapes in the Ray Roberts Greenbelt,*

Denton, Texas. (Unpublished doctoral dissertation). University of North Texas, Denton, TX.

Barry, D. & Kroll, A. (1999). A phytosociological description of a remnant bottomland hardwood forest in Denton County, Texas. *Texas Journal of Science, 51*(4), 309-316.

Bevin, K. J. & Kirkby, M. J. (1979). A physically based, variable contributing area model of basin hydrology. *Hydrological Sciences Bulletin, 24* (1), 43-69.

Beven, K. (1997). TOPMODEL: A critique. *Hydrological Processes, 2*, 1069-1085.

Botkin, D. B., Janak, J. F., & Wallis, J. R. (1972). Some ecological consequences of a computer model of forest growth. *Journal of Ecology, 60* (3), 849-872.

Bugmann, H. (1996). A simplified forest model to study species composition along climate gradients. *Ecology, 77* (7), 2055-2074.

Bugmann, H. 2001. A review of forest gap models. *Climatic Change, 51*, 259-305.

Bugmann, H., & Cramer, W. (1998). Improving the behaviour of forest gap models along drought gradients. *Forest Ecology and Management, 103*, 247-263.

Burns, R. M., & Honkala B. H. (1990). Silvics of North America. Retrieved from http://www.na.fs.fed.us/spfo/pubs/silvics_manual/table_of_contents.htm

Cohen, J. M., Ernst, K. C., Lindblade, K. A., Vulule, J. M., John, C. C., & Wilson, M. L. (2008). Topography-derived wetness indices are associated with household-level malaria risk in two communities in the western Kenyan highlands. *Malaria Journal, 7*, 40.

Cohen, J. M., Ernst, K. C., Lindblade, K. A., Vulule, J. M., John, C. C., & Wilson, M. L. (2010). Local topographic wetness indices predict household malaria risk better than land-use and land-cover in the western Kenyan highlands. *Malaria Journal, 9*, 328.

Diggs, G. M., Barney L. Lipscomb, B. L., & O'Kennon, R. J. (1999). *Shinners & Mahlers illustrated flora of North Central Texas*. Fort Worth, TX: Botanical Research Institute of Texas and Austin College.

Eyre, F. H. (Ed.). (1980). Forest cover types of the United States and Canada. Washington, DC: Society of American Foresters.

Farina, A. (2006). Principles and methods in landscape ecology: towards a science of landscape. Dordrecht, The Netherlands: Springer.

Ford, A. & Pauls, E. (1980). Soil survey of Denton County, Texas. Washington, DC: United States, Soil Conservation Service.

Forman, R. T. T. & Godron, M. (1986). Landscape ecology. New York, NY: Wiley & Sons.

Francaviglia, R. V. (2000). The cast iron forest: A natural and cultural history of the North American Cross Timbers. Austin, TX: University of Texas Press.

Gessler, P. E., Chadwick, O. A., Chamran, F., Althouse, L., & Holmes, K. (2000). Modeling soil-landscape and ecosystem properties using terrain attributes. *Soil Science Society of America Journal, 64*, 2046-2056.

Goodwin, C. N. (2003). Modeling changes in the spatial distribution of soil saturation in urbanizing watersheds. *Proceedings of the 2003 Georgia Water Resources Conference*. Athens, GA: University of Georgia.

Grabs, T., Seibert, J., Bishop, K., & Laudon, H. (2009). Modeling spatial patterns of saturated areas: A comparison of the topographic wetness index and a dynamic distributed model. *Journal of Hydrology, 373*, 15-23.

Grayson, R. B., Western, A. W., Chiew, F. H. S., & Blöschl, G. (1997). Preferred states in spatial soil moisture patterns: Local and nonlocal controls. *Water Resources Research, 33*(12), 2897-2908.

Griffith, G. E., Bryce, S. A., Omernik, J. M., Comstock, J. A., Rogers, A. C., Harrison . . . Bezanson, D. (2004). Ecoregions of Texas. Corvallis, OR: U.S. Environmental Protection Agency.

Griffith, G., Bryce, S., Omernik, J., Rogers, A., & Harrison, B. (2007). Ecoregions of Texas. U.S. Environmental Protection Agency, Corvallis, OR.

Grunwald, S. (2006). What do we really know about the space-time continuum of soil-landscapes. In S. Grunwald (Ed.), *Environmental soil-landscape modeling: Geographic information technologies and pedometrics* (pp. 3-36). Boca Raton, FL: CRC Press.

Hill, R. T. (1887). The topography and geology of the Cross Timbers and surrounding regions in Northern Texas. *The American Journal of Science, 3rd Series, 33*, 291-303.

Hodges, J. D. (1997). Development and ecology of bottomland hardwood sites. *Forest Ecology and Management, 90*, 117-125.

Holcomb, S. S. (2001). *An examination of the riparian bottomland forest in North Central Texas through ecology, history, field study, and computer simulation.* (Unpublished master's thesis). University of North Texas, Denton, TX.

Hsieh, H., Stone, J., Guertin, D. P., & Slack, D. D. (2003). Stochastic daily rainfall generation in southeast Arizona: An example from Walnut Gulch Experimental Watershed. In K. G. Renard, S. A. McElroy, W. J. Gburek, H. E. Canfield, & R. L. Scott (Eds.), *First interagency conference on research in the watersheds* (pp. 139-145). Benson, AZ: U.S. Department of Agriculture, Agricultural Research Service.

Iverson, L. R., Prasad, A. M., & Rebbeck, J. (2004). A comparison of the integrated moisture index and the topographic wetness index as related to two years of soil moisture monitoring in Zaleski State Forest, Ohio. In D. A. Yaussy, D. M. Hix, R. P. Long, & C. P. Goebel (Eds.), *Proceedings, 14th Central Hardwood Forest Conference* (pp. 515-517). Wooster, OH: U.S. Department of Agriculture, Forest Service, Northeastern Research Station.

Kim, S. & Jung, S. (2003). Digital terrain analysis of the dynamic wetness pattern of the Sulmachun watershed. In M. Bruen (Ed.), *Diffuse pollution and basin management* (pp. 10-1 – 10-6). Dublin, Ireland: Proceedings of the 7th International Specialised IWA Conference.

Kirkby, M. J. (1997). TOPMODEL: A personal view. *Hydrological Processes, 2*, 1087-1097.

Komperod, M. (2009). *The impact of climate and flooding on tree ring growth of* Fraxinus pennsylvanica *in North Central Texas*. (Unpublished master's thesis). University of North Texas, Denton, TX.

Kopecký, M. & Čížková, Š. (2010). Using topographic wetness index in vegetation ecology: Does the algorithm matter? *Applied Vegetation Science, 13*, 450-459.

Lanni, C., McDonnell, J. J., & Rigon, R. (2011). On the relative role of upslope and downslope topography for describing water flow path and storage dynamics: A theoretical analysis. *Hydrological Processes, 25*, 3909-3923.

Leemans, R. and Prentice, I. C. (1989). FORSKA: A general forest succession model. Uppsala, Sweden: Institute of Ecological Botany.

Lin, H. S., Kogelmann, W., Walker, C., & Bruns, M. A. (2006). Soil moisture patterns in a forested catchment: A hydropedological perspective. *Geoderma, 131*, 345-368.

Mladenoff, D. J., & Baker, W. L. (1999). Development of forest and landscape modeling approaches. In D. J. Mladenoff & W. L. Baker (Eds.), *Spatial modeling of forest landscape change: Approaches and applications* (pp. 1-13). Cambridge, United Kingdom: Cambridge University Press.

Moore, I. D., Grayson, R. B., & Ladson, A. R. (1991). Digital terrain modeling: A review of hydrological, geomorphological, and biological applications. *Hydrological Processes, 5*, 3-30.

National Climate Data Center. (2015). *Tree ring.* Retrieved from https://222.ncdc.noaa.gov/data-access/paleoclimatology-data/datasets/tree-ring

National Renewable Energy Laboratory (NREL). (2006). Renewable resource data center. Retrieved from http://www.nrel.gov/rredc/

Pan F., Peters-Lidard, C. D., Sale, M. J., & King, A. W. (2004). A comparison of geographical information systems-based algorithms for computing the TOPMODEL topographic index. *Water Resources Research, 40*(6), 1-11. doi:10.1029/2004WR003069.

Pan, F., Stieglitz, M., &. McKane, R. B. (2012). An algorithm for treating flat areas and depressions in digital elevation models using linear interpolation. *Water Resources Research, 48*(2), 1-13. doi:10.1029/2011WR010735

Pei, T., Qin, C-Z., Zhu, A-X., Yang, L., Luo, M., Li, B. and Zhou, C. (2010). Mapping soil organic matter using the topographic wetness index: A comparative study based on different flow-direction algorithms and kriging methods. *Ecological Indicators, 10*(3), 610-619.

Peng, C., Liu, J., Dang, Q., Apps, M. J., & Jiang, H. (2002). TRIPLEX: A generic hybrid model for predicting forest growth and carbon and nitrogen dynamics. *Ecological Modeling, 153*, 109-130.

Piantadosi, J., Boland, J., & Howlett, P. (2009). Generating synthetic rainfall on various timescales–daily, monthly and yearly. *Environmental Modeling and Assessment, 14* (4), 431-438.

Prasad, A. M., Iverson, L. R., Matthews, S., & Peters, M. (2007-ongoing). *A climate change atlas for 134 forest tree species of the Eastern United States* [database]. Delaware, OH: Northern Research Station, USDA Forest Service. Retrieved from http://www.nrs.fs.fed.us/atlas/tree

Rijal, R. (2011). *Soil and forest variation by topography and succession stages in the greenbelt corridor, floodplain of the Elm Fork of the Trinity River, North Texas*. (Unpublished doctoral dissertation). University of North Texas, Denton, TX.

Rodriguez, J., Garcia, L., & Suárez, M. C. G. (2010). Comparison of mathematical algorithms for determining the slope angle in GIS environment. *Aqua-LAC, 2*(2), 78-82.

Ruhe, R. V. (1969). *Quaternary landscapes in Iowa*. Ames, IA: Iowa State University Press.

Sanderson, J., & Harris, L. D. (2000). *Landscape ecology: A top-down approach*. Boca Raton, FL: CRC Press.

Seidl, R., Lexer, M. J., Jäger, D., & Hönninger, K. (2005). Evaluating the accuracy and generality of a hybrid patch model. *Tree Physiology, 25*, 939-951.

Seidl, R., Rammer, W., Scheller, R. M., & Spies, T. A. (2012). An individual-based process model to simulate landscape-scale forest ecosystem dynamics. *Ecological Modeling, 231*, 87-100.

Shifley, S. R., Thompson, F. R., Dijak, W. D., & Fan, Z. 2007. Forecasting landscape-scale, cumulative effects of forest management on vegetation and wildlife habitat: A case study of issues, limitations, and opportunities. *Forest Ecology and Management, 254*, 474–483.

Shugart, H. H. (2002). Forest gap models. In H. A. Mooney & J. G. Canadell (Eds.), *Encyclopedia of global environmental change—The Earth system: Biological and ecological dimensions of global environmental change* (Vol. 2, pp. 316–323). Chichester, United Kingdom: John Wiley & Sons.

Sørensen, R., Zinko, U., & Seibert, J. (2006). On the calculation of the topographic wetness index: Evaluation of different methods based on field observations. *Hydrology and Earth System Sciences, 10*, 101-112.

Srikanthan, R. & McMahon, T. A. (2001). Stochastic generation of annual, monthly and daily climate data: A review. *Hydrology and Earth System Sciences, 5*(4), 653-670.

Stahle, D. W. & Edmondson, J. R. (n.d.). *Fossil hill – QUST – ITRDB TX050*. Retrieved from https://222.ncdc.noaa.gov/cdo/f?p=519:1:0::::P1_STUDY_ID:8555

Tarboton, D. (2012). Terrain analysis using digital elevation models (TauDEM). Retrieved from http://hydrology.usu.edu/taudem/taudem5.0/

Texas Environmental Observatory. (2012). Retrieved from http://www.teo.unt.edu/

Turner, M. G., Gardner, R. H., & O'Neill, R. V. (2001). Landscape ecology in theory and practice: Pattern and process. New York City, NY: Springer-Verlag.

United States Department of Agriculture. (2010). Soil survey geographic (SSURGO) database for Denton County, Texas. Fort Worth, TX: Natural Resource Conservation Service. Retrieved from http://SoilDataMart.nrcs.usda.gov/

United States Environmental Protection Agency (2009). What is a watershed? Retrieved from http://water.epa.gov/type/watersheds/whatis.cfm

United States Geological Survey (n.d.), Seamless data distribution system. Retrieved from http://seamless.usgs.gov/ and http://nationalmap.gov/viewer.html

Urban, D. L. (2000). Using model analysis to design monitoring programs for landscape management and impact assessment. *Ecological Applications, 10*(6), 1820-1832.

Urban, D. L., Acevedo, M. F., & Garman, S. L. (1999). Scaling fine-scale processes to large-scale patterns using models derived from models: Meta-models. In D. J. Mladenoff & W. L. Baker (Eds.), *Spatial modeling of forest landscape change: Approaches and applications* (pp. 70-98). Cambridge, United Kingdom: Cambridge University Press.

Urban, D. L., Miller, C., Halpin, P. N., & Stephenson, N. L. (2000). Forest gradient response in Sierran landscapes: The physical template. *Landscape Ecology, 15*, 603-620.

Urban, D. L., O'Neill, R. V., & Shugart, H. H. (1987). Landscape ecology. *BioScience, 37* (2), 119-127.

United States Department of Agriculture. (2014a). Fire effects information system. Retrieved from http://www.fs.fed.us/database/feis/

United States Department of Agriculture. (2014b). Natural resources conservation service: The PLANTS database. Retrieved from http://plants.usda.gov

Utah Climate Center, Utah State University. 2013. http://climate.usurf.usu.edu/ (last accessed August 5, 2013)

Vaze, J., Teng, J., & Spencer, G. (2010). Impact of DEM accuracy and resolution on topographic indices. *Environmental Modeling & Software, 25*, 1086-1098.

Wang, Q. J. & Nathan, R. J. (2007). A method for coupling daily and monthly time scales in stochastic generation of rainfall series. *Journal of Hydrology, 346*, 122-130.

Wiens, J. A. & Milne, B. T. (1989). Scaling of 'landscapes' in landscape ecology, or, landscape ecology from a beetle's perspective. *Landscape Ecology, 3* (2), 87-96.

Wilks, D. S. & Wilby, R. L. (1999). The weather generation game: A review of stochastic weather models. *Progress in Physical Geography, 23* (3), 329-357.

Wythers, K. R., Lauenroth, W. K., & Paruelo, J. M. (1999). Bar-soli evaporation under semiarid field conditions. *Soil Science Society of America Journal, 62*, 1341-1349.

Yang, X., Young, M. A., Chapman, G. A., & Gray, J. M. (2007). Delineating soil landscape facets from digital elevation models using a compound topographic index in a geographic information system. *Australian Journal of Soil Research, 45*(8), 569-576.

Zhang, J. X., Wu, J. Q., Chang, K., Elliot, W. J., & Dun, S. (2009). Effects of DEM source and resolution on WEPP hydrologic and erosion simulation: A case study of two forest watersheds in Northern Idaho. *Transactions of American Society of Agricultural and Biological Engineers, 52*(2), 447-457.

Zinko, U., Seibert, J., Dynesius, M., & Nilsson, C. (2005). Plant species numbers predicted by a topography-based groundwater flow index. *Ecosystems, 8*, 430-441.